DIVISION OF INFRASTRUCTURE, GEOMATICS & ARCHITECTURE FACULTY OF ENGINEERING
THE FACULTY OF ENGINEERING
DEPARTMENT OF ARCHITECTURE AND THE BUILT ENVIRONMENT

Investigation of A Novel Thermochemical Heat Storage Systems for Building Applications

Norhayati Mat Wajid

B Eng., M Eng.

Thesis submitted to the University of Nottingham for the degree of Doctor of Philosophy

16 September 2016

ABSTRACT

Heating and cooling account nearly 60% of world total energy consumption and highly depending of conventional energy sources generated by fossils fuels. As the scarcity of oil reserves becomes the jargon issues in all part of the world today, researchers have to look into a robust investigation on finding the alternative energy to alleviate the dependency of conventional energy. Furthermore, if the phenomenon of using fossil fuel remain as the primary energy sources, it would affect adversely on the greenhouse gas emission. In 2008, The Climate Change Act by the UK Government had targeted that 34% cut in 1990 greenhouse gas emissions by 2020 and, at least, an 80% cut in emissions by 2050. Therefore, to achieve this target, more low carbon technology needed to realise the future reduction of emission. Renewable energy technologies such as solar, wind, geothermal and such thought to become the solution to reducing the demand for conventional energy. However, their instability considered as problematic for future energy demand. Thus, a more efficient management of energy demand, coupled with efficient energy storage systems is required.

The aim of this study is to develop novel Thermochemical Heat Storage system (THSS) using off-peak power and renewable sources to minimise energy demands from fossil fuels and reducing GHG emissions. Thus, this could be achieved by developed and constructed a unique adsorption heat pipe using a high energy storage density of the nanocomposite Thermochemical material. Other than that, this unique adsorption heat pipe was integrated with a heat-pump circuit for desorption process. In this study, a Novel Thermochemical Heat Storage has been theoretically model, built and tested on a lab scale and a domestic-scale prototype. The chosen Thermochemical Material (Vermiculite + $CaCl_2$) reacting with pure water vapour operates within a closed system. Other than that, result from thermal analysis shown that Vermiculite + $CaCl_2$ could attain higher heat storage capacity of 374 kJ/kg. The heat storage system of this work based on reversible thermochemical reactions, such as

adsorption and desorption of composite Thermochemical materials which exhibits very high energy storage density (up to 364 kWh·m^3 of material storage). The small scale experimental investigation has found this THSS has the maximum adsorption temperature of *45.07°C to 71.12°C with the corresponding Coefficient of Performance (COP) of 0.53 to 1.34. Another investigation on Solar Heat Solar collector (SHSC) has carried out numerically and experimentally. The numerical study predicted that the temperature lift achieved at 42°C of using 10m^2 of the solar collector. Hence, this SHSC has shown the possibility of integrating the TCM (Thermochemical material) with solar thermal energy. Lastly, a domestic scale THSS has revealed that the highest temperature uplift from the adsorption process at 57°C. The economic analysis of a domestic scale THSS has shown that this system will receive payback in 7.5 years with the internal rate of return (IRR) 15.25%. Furthermore, emission analysis demonstrated that this system would reduce 34% of CO_2 in 20 years of its lifespans.*

LIST OF PUBLICATION

Conference Papers

i. **M.W. Norhayati**, Blaise Mempouo, Siddig Omer, Saffa B Riffat, “Review on heat and mass transfer enhancement of thermochemical adsorption pipe systems”, 13th International Conference on Sustainable Energy Technologies (SET2014) 25-28th August 2014, Geneva.

ii. **M.W. Norhayati**, Blaise Mempouo, Siddig Omer, Saffa B Riffat, “Experimental Study on a Novel Thermochemical Energy Storage Pumping Pipe System”. 13th International Conference on Sustainable Energy Technologies (SET2014) 25-28th August 2014, Geneva.

iii. **M.W. Norhayati**, Blaise Mempouo, Siddig Omer, Saffa B Riffat, “Experimental Study of an Adsorption Heat Storage Systems for Building Applications” 14th International Conference on Sustainable Energy Technologies (SET2015), 25th-27th August 2015, Nottingham UK.

iv. Auwwal Dodo, **M.W. Norhayati**, Blaise Mempouo, Siddig Omer, Saffa Riffat. “Experimental Investigation of a Thermochemical Adsorption Pumping Pipe Cooling System” 14th International Conference on Sustainable Energy Technologies (SET2015), 25th-27th August 2015, Nottingham UK

Journals Paper

i. **M.W. Norhayati**, Blaise Mempouo, Siddig Omer, Saffa B Riffat "Experimental Study of an Adsorption Heat Storage Systems for Building Applications" International Journal of Renewable Bioresources, 2016, Vol 4 (2) (http://dx.doi.org/10.7243/2052-6237-4-2).

ii. **M.W. Norhayati**, Blaise Mempouo, Siddig Omer, Saffa B Riffat." Review of Heat & Mass Transfer & Current Advancement for Adsorption Heating/Cooling Systems". International Journal of Low Carbon Technology, 2016 (Accepted manuscript: IJLCT-2015-007.R1)

iii. Y. N. Zhang, R. Z. Wang, Y. J. Zhao, T. X. Li, S. B. Riffat and **M.W. Norhayati** "Development and thermochemical characterizations of vermiculite/$SrBr_2$ composite sorbents for low-temperature heat storage", 2016 (Submitted manuscript in Energy & Environmental Science, The Royal Society of Chemistry).

ACKNOWLEDGEMENTS

Firstly, I would like to express my sincere gratitude to my supervisor, Professor Saffa Riffat, Head of Architecture, Energy and Environment Research Group, the University of Nottingham for his commitment, wide knowledge, his understanding, enthusiasm, encouragement, and continued inspiration towards this Ph.D. journey. Further thanks to Dr. Omer Siddig, my second supervisor for his constructive comments on my works. I would like to offer a sincere appreciation to Dr. Blaise Mempouo & Dr. Auwwal Dodo, Devrim Aydin for the help in the laboratory and field works. I would also extend my thanks to the staff of the Department of Architecture and Built Environment, Faculty of Engineering of the University of Nottingham for providing help, information and experiment facilities required for this project, especially to Mr. David Oliver, Mr. David Taylor, Mr. Jonathan Moss, Mr. Andy Mathews, and Mrs. Zeny Amante-Roberts. Without their help, I would not have been this far. Special thanks to Mrs. Nicola Weston and Dr. Keith Dinsdale in Wolfson Building for their valuable time and technical advice in Material Lab.

I would like to acknowledge Shanghai Jiao Tong University Academics Professor Ruzhu Wang & Professor Yajun Dai, their Ph.D. students, Ms. Dai Enqian, Mr. Huang Tao & Mr. Zhao Yanjie for their help during my visit and excellent collaboration in sharing research information on publishing a research paper.

I wish to express my appreciation to my organisation, Public Works Department of Malaysia for granted a paid study leave. I am also very grateful to Public Service Department of Malaysia for the study scholarship and living allowance in the UK. Without these financial supports, this Ph.D. research would not have been undertaken.

Finally, to my parents Zainab Salleh & Late Allahyarham Mat Wajid Taib, my husband Nazafar Idris and to most precious son and daughter Muhammad Yamin Nazafar & Nur Qisya Rania for their unconditional love, support, and understanding during my hard time

TABLE OF CONTENTS

Abstract i
List of Publication iii
Acknowledgements v
Table of Contents vi
List of Figures xiv
List of Tables xxii
Nomenclatures 1
1. INTRODUCTION 1
1.1 Background 1
1.2 Statement of Problems 4
1.3 Objective and Scope of the Project 6
1.4 Scope of the Project 7
1.5 Novelty and Timeliness 8
1.6 Methodological Approach 9
1.7 Thesis Structure 11
2. LITERATURE REVIEW 15
2.1 Introduction 15
2.2 History of Thermochemical Energy Storage 15
2.3 Investigation of the Thermochemical Energy Storage (TES) 17
2.3.1 Absorption Process 21
2.3.2 Adsorption Process 22
2.3.3 Open TES 24
2.3.4 Closed Thermochemical ES 25

2.4 Adsorbent Materials 28
2.4.1 Silica Gels 28
2.4.2 Zeolites 29
2.4.3 Activated Carbons 30
2.4.4 Metal Oxides 31
2.4.5 Vermiculite 31
2.5 Refrigerant for THSS 33
2.5.1 Water 33
2.5.2 Ammonia 34
2.6 TES Working Pairs Materials 35
2.7 Development of Composite Thermochemical Materials (TCMs) 39
2.8 Selected Studies on Current Thermochemical Heating/Cooling Systems 44
2.9 Mathematical Modelling Simplification on Thermochemical Heating/Cooling systems 51
2.9.1 Thermodynamic Model 51
2.9.2 Lumped Parameter Model 55
2.9.3 Heat and Mass Transfer Model 58
2.10 Heat and Mass Transfer Enhancement of an Adsorption Bed/Reactor 62
2.10.1 Fin Type Adsorbent Tube Module/Heat Exchanger 62
2.10.2 Embedded Adsorbent Bed with Metal Foam 66
2.10.3 Consolidated Adsorbent 68
2.10.4 Adsorbent Coating 70
2.10.5 Adsorbent with Multi Cooling Tubes 73

2.10.6 Summary Heat and mass transfer enhancement techniques.....75

2.11 Conclusions of the Chapter 81

3. METHODOLOGY 83

4. THERMOCHEMICAL MATERIALS SCREENING, SYNTHESISING AND OPTIMISATION.....90

4.1 Introduction 90

4.2 Synthesis of Composite Adsorbent Materials 91

4.3 Experimental Investigation of Temperature Lift – Using Horizontal Glass and Metal Heat Pipe.....93

4.3.1 Data Acquisition 95

4.3.2 Measuring Equipment 95

4.3.3 Experimental Procedure for the Horizontal Rig and Vertical Rig. 96

4.3.4 Materials Preparation 97

4.3.5 Results and Discussion from Temperature Lift Experiments Using Horizontal Glass and Metal Rig 102

4.3.6 Summary of Results from Horizontal Glass and Metal Rig 109

4.4 Adsorption and Desorption Test with Vertical Glass and Metal Rig 110

4.4.1 Results and Discussion for Vertical Rig Test 115

4.4.2 Conclusions from the Temperature Lift and Adsorption/Desorption Investigations Using Horizontal and Vertical Glass and Metal Rigs. 123

4.5 Investigation of Microscopic and Physicochemical Properties of Thermochemical Materials (TCM). 124

4.5.1 Microscope Scanning 124

4.5.2 Electron Beam Microscopic Scanning 127

4.6 Investigation of Pore Size Distribution and Pore Volume of Thermochemical Materials. 147
4.6.1 Experimental Setup and Procedure 149
4.6.2 Result and Discussion of MIP 152
4.7 Thermal Analysis Investigation 157
4.7.1 Introduction 158
4.7.2 Theory 158
4.7.3 Experimental Setup and Procedure 160
4.7.4 Procedure on impregnation of composite material 163
4.7.5 Results and Discussion of DSC analysis 164
4.8 Conclusions in this Chapter 167
5. PERFORMANCE INVESTIGATION OF THERMOCHEMICAL HEAT STORAGE SYSTEM: MODELLING OF THSS-ELEC, THSS-HP & THSS-SOLAR 168
5.1 Introduction 168
5.2 Methodology 169
5.3 EES software 172
5.4 TCM materials and working pairs 173
5.5 Working Refrigerant Gas for the regeneration of THSS 174
5.6 Physical Properties of THSS 174
5.6.1 Adsorption Pipe 174
5.6.2 Evaporator Pipe 175
5.7 Modelling of Transport of Heat and Adsorbate 175
5.8 Adsorption Isotherm 176
5.9 Adsorption rate 177

5.10 Mass Balance of Adsorbate....178
5.11 Heat Balance in the Adsorption Cycle....178
5.11.1 Parameters Adopted in the Simulation....181
5.11.2 Heat Balance in Desorption Cycle....184
5.12 System performance Equation....192
5.13 Numerical result and discussion....193
5.13.1 Adsorption Process....193
5.13.2 Desorption Process....195
5.14 Conclusions of the Chapter....206
6. BUILD UP AND EXPERIMENTAL INVESTIGATION OF A SMALL–SCALE THERMOCHEMICAL HEAT STORAGE SYSTEM (THSS)....208
6.1 Introduction....208
6.2 Equipment and Instrumentations....208
6.2.1 Adsorption Pipe....208
6.2.2 Evaporator Pipe....209
6.2.3 Data Acquisition and Processing Systems....210
6.2.4 Experimental Uncertainty....211
6.3 Methodology of the Investigation....212
6.4....215
6.5 Experimental Procedure....215
6.5.1 Adsorption/Discharge Mode....215
6.5.2 Charging/Desorption Mode....216
6.6 Performance equations....217
6.7 Result and Discussion....218

6.7.1 Temperature variation of Adsorption Test....218

6.7.2 Temperature variation during desorption Test....227

6.7.3 Compressor performance....233

6.8 Overall performance of all test....237

6.9 Validation of the simulation of the adsorbent temperature vs experiment results for VCC 238

6.10 Conclusions of the Chapter....239

7. PERFORMANCE INVESTIGATION OF SOLAR HEAT STORAGE COLLECTOR (SHSC)-THEORETICAL, BUILD –UP AND EXPERIMENTAL TESTING.....241

7.1 Introduction....241

7.2 The Mathematical modelling of SHSC....243

7.3 Option 1: SHSC heat transfer through fan (air to air heat exchange)....244

7.3.1 Analysis for charging process for Option 1....246

7.3.2 Analysis of Discharging Process for Option 1....248

7.3.3 Result and Discussion from the modelling for Option 1....250

7.4 Option 2: SHSC heat transfer through heat pipe and water (air to water heat exchange)....257

7.4.1 Analysis for charging process for Option 2....259

7.4.2 Analysis of Discharging Process for Option 2....259

7.4.3 Result and Discussion from the modelling (Option 2)....260

7.5 Experimental investigation on small-scale prototype of SHSC....262

7.5.1 Material and Method....262

7.5.2 Installation of the prototype systems....265

7.5.3 Measurement procedure....268

7.5.4 Performance equations 270
7.5.5 Experimental Results and Discussion 271
7.6 Conclusions of the Chapter 279
8. DOMESTIC SCALE PROTOTYPE OF THSS: BUILD-UP, EXPERIMENTAL INVESTIGATION, ECONOMIC & ENVIRONMENTAL ANALYSIS 282
8.1 Introduction 282
8.2 Experimental set-up 283
8.2.1 Construction of THSS....285
8.2.2 Construction of Adsorbent & Evaporator cartridge....288
8.2.3 Thermocouple Type and Position 291
8.2.4 Heat Pump 292
8.3 Analysis equations 293
8.3.1 Adsorption process 293
8.3.2 Desorption process 293
8.3.3 Performance 293
8.4 Experimental result and discussions 293
8.4.1 Initial trial issues and piping modification....293
8.4.2 Overall performance....295
8.5 Economic Analysis 297
8.5.1 Impact on energy price with inflation rate of 7% 297
8.5.2 Capital and Running Cost for THSS 298
8.5.3 Payback period, saving and IRR 300
8.6 Environmental analysis 301
8.7 Conclusions of the Chapter 302

9. CONCLUSIONS AND FURTHER WORKS 304
9.1 Introduction 304
9.2 Main conclusion 304
9.2.1 Literature Review (Chapter 2) 304
9.2.2 Thermochemical Material Screening, Synthesizing and Optimization (Chapter 4) 305
9.2.3 Performance investigation of Thermochemical Heat Storage Systems (THSS) with different type of heat source (electric, heat pump circuit using different refrigerant gases of R134a and R1234yf & solar thermal) (Chapter 5) 306
9.2.4 Build up and experimental testing of a small-scale THSS (Chapter 6).....306
9.2.5 Performance investigation of Solar Heat Storage Systems (SHSS) (Chapter 7) 307
9.2.6 Domestic-scale prototype of THSS: building up, experimental investigation, economic & environmental analysis (Chapter 8).....308
9.3 Further Works 308
- Option 1 309
- Option 2 310
REFERENCES.....312
APPENDICES 328

LIST OF FIGURES

Figure 1.1: World energy consumption 2

Figure 1.2: Carbon dioxide emission 2

Figure 1.3: U.K. energy mix 3

Figure 1.4: Trend shift of energy relationship between energy supply and demand..... 4

Figure 2.1: Chemical storage and sorption classification 17

Figure 2.2 Process involved in a thermochemical energy storage cycle 19

Figure 2.3: Classification of chemical and thermochemical storage.....20

Figure 2.4: Adsorption process of water vapour on solids 23

Figure 2.5: Open sorption storage system using a packed bed of solid adsorbent 24

Figure 2.6: Operation principle of a closed thermochemical system 26

Figure 2.7: Different energy storage materials.....37

Figure 2.8: Overview of working pairs tested in prototypes under experimental conditions 40

Figure 2.9: New classification of TCM materials 43

Figure 2.10: View of the solar sorption pilot plant for air-conditioning, flat plate solar collectors, and the thermochemical reactor design. 45

Figure 2.11: Schematic representation of the proposed CO-SAR system.....47

Figure 2.12: (a) adsorber/desorber unit (b) evaporator/condenser unit front view (c) evaporator/condenser unit back view 48

Figure 2.13. Scheme of a double-adsorber heat pump. Phases: a) regeneration b) desorption in bed 2 b') adsorption in bed 1 c) regeneration d) adsorption in bed 2 d') desorption in bed 1. Components: 1& 2) adsorbent beds C) condenser E) evaporator.....52

Figure 2.14: Schematisation of the studied system and the parameters considered for each component and the adsorber.....53

Figure: 2.15: Experimental rig with the different instruments used for measurement. 54

Figure 2.16: A schematic of a two-bed silica gel/water adsorption chiller manufacture by Nishiyodo Kuchouki Co 57

Figure 2.17: Fin type adsorber heat exchanger 63

Figure 2.18: Plate heat exchanger generator design 64

Figure 2.19: Overall (right side) and detailed (left side) view of the A-HEX.....65

Figure 2.20: Composite material of zeolite/foam.....67

Figure 2.21: Consolidated composite block 69

Figure 2.22: Schematic diagram of three types of cellulose fibre membranes (a) Clean fibre membrane (b) Solid desiccant-coated fibre membrane (c) Liquid desiccant-soaking fibre membrane. 71

Figure 2.23: Pictures of the zeolite X coating (a) before and (bed) after the kinetic measurement 72

Figure 2.24: Zeolite SAPO on stainless steel (a) and aluminium (b) 72

Figure 2.25: Adsorption heat pump with multiple cooling tubes 74

Figure 2.26: Adsorption solar tube....75

Figure 3.1: Process flow of THSS research 83

Figure 4.1: Mechanism of adsorption on composite adsorbent 92

Figure 4.2: Schematic of horizontal glass and metal....93

Figure 4.3: Adsorption glass vessel showing aluminium mesh: (a) without adsorbent (b) with adsorbent. Evaporation glass vessel: (c) without wick material (d) with wick material.....94

Figure 4.4: Data Taker DT 500 95

Figure 4.5: A photo showing a thermocouple attached to one of the vessels. 96

Figure 4.6: Procedure on synthesising of composite adsorbent. 99

Figure 4.7: A photo showing silica gel considered for test. 99

Figure 4.8: A photo showing raw vermiculite considered for test. 100

Figure 4.9: A photo showing molecular sieve 10A considered for test. 100

Figure 4.10: A photo showing dry calcium chloride considered as salt solution for impregnation. 101

Figure 4.11: A photo showing of dry magnesium sulphate considered as salt solution for impregnation. 101

Figure 4.12: Photo is showing the tray of impregnated adsorbent material to be dried in the oven. 102

Figure 4.13: The temperature variants of adsorbent and evaporator for silica gel+$CaCl_2$/Water – Test1....103

Figure 4.14: The temperature variants of adsorbent pipe and evaporator pipe for vermiculite+$CaCl_2$/water - Test 2 104

Figure 4.15: The temperature variants of the adsorbent pipe and evaporator pipe for silica gel +$MgSO_4$/water - Test 3 105

Figure 4.16: The temperature variants of adsorbent and evaporator for molecular sieve +CaCl2/water - Test 4 106

Figure 4.17: The temperature variants of adsorbent pipe and evaporator pipe for vermiculite +$MgSO_4$/water – Test 5 107

Figure 4.18: Adsorption temperature for tested TCMs from horizontal metal and glass rig. 108

Figure 4.19: A photo showing the vertical heat pipe for the adsorption and desorption test. 112

Figure 4.20: The multi-chamber perforated cartridge used in the adsorption pipe.....112

Figure 4.21: The schematic of the vertical adsorption heat pipe for the adsorption and desorption test.....113

Figure 4.22: Vertical glass pipe rig. (a) Insulated adsorption pipe for the adsorption test, (b) insulated with ice jacket for desorption test.....114

Figure 4.23: Adsorbent pipe showing cartridge (a) without adsorbent (b) with adsorbent. Evaporation pipe showing water container (c) without wick material (d) with wick mat....114

Figure 4.24: Illustration of temperature variation for adsorption test on vermiculite.....116

Figure 4.25: Illustration of temperature variations of vermiculite+$CaCl_2$/water in a six-hour time frame of the adsorption process.....117

Figure 4.26: Illustration of temperature variation during the adsorption test for silica gel+$CaCl_2$/water - Test 2 118

Figure 4.27: Illustration showing a comparison of temperature variations of two tested working pairs. 119

Figure 4.28: Illustration of the desorption test on vermiculite +$CaCl_2$ /water.....120

Figure 4.29: Illustration of temperature variations during desorption test for silica gel+$CaCl_2$ 121

Figure 4.30: a) prepared saturated pure silica gel in an airtight casing and (b) a single granule through a microscope (500µm scale.).....126

Figure 4.31: (a) prepared saturated silica gel+ $CaCl_2$ in an airtight casing and (b) a broken granule through a microscope (500µm scale.).....126

Figure 4.32: (a) prepared saturated silica gel+ $LiNO_3$ and (b) a single granule through a microscope (500µm scale.) 127

Figure 4.33: A schematic representation of an ESEM 128

Figure 4.34: ESEM images of a water particle on the surface of a silica gel granule and a water particle bonding on two granules 129

Figure 4.35: ESEM images of saturated silica gel+$CaCl_2$ .with (a) a water particle covering the surface of the particle and (b) the crystallised salt covered by a water particle. 130

Figure 4.36: ESEM images of a composite of silica gel+$CaCl_2$ showing $CaCl_2$ crystallisation after the material dried.....130

Figure 4.37: ESEM images & morphology of dry silica gel +$CaCl_2$ 131

Figure 4.38: (a) ESEM images of a silica gel + lithium nitrate chip and (b) enlarged lithium nitrate on the surface of silica gel. 132

Figure 4.39: (a) ESEM images of pores on the surface of silica gel and (b)lithium nitrate on the surface of silica gel. 133

Figure 4.40: (a) ESEM images and morphology of dry silica gel +$LiNO_3$ and (b) X-ray pattern $LiNO_3$. 134

Figure 4.41: ESEM images of vermiculite + $CaCl_2$ 135

Figure 4.42: Morphology of vermiculite + $CaCl_2$. 136

Figure 4.43: ESEM images of silica Gel+$MgSO_4$ 138

Figure 4.44: SEM images of vermiculite +$CaCl_2$ (a) magnified at 2000x, (b) magnified at 250x, (c) (d) magnified at 1000x. 140

Figure 4.45: SEM image showing appearance of $CaCl_2$ in crystallised form on the surface of vermiculite+$CaCl_2$. 141

Figure 4.46: SEM image showing appearance of pore on random section of surface of vermiculite+$CaCl_2$ 141

Figure 4.47: Chemical element morphology of vermiculite +$CaCl_2$. 142

Figure 4.48: Chemical element colour coding scan of vermiculite+$CaCl_2$. 143

Figure 4.49: SEM images at magnification (a) 200x, (b) 3200x, (c) 2000x and 4000x of vermiculite+$MgSO_4$. 144

Figure 4.50: Morphology of random surface section of vermiculite +$MgSO_4$. 145

Figure 4.51: Chemical element colour coding scan of vermiculite+$MgSO_4$. 146

Figure 4.52: Cross-sectional view of penetrometer diagram 149

Figure 4.53: Micrometrics Auto Pore IV 9500 photo 151

Figure 4.54: A schematic of pressure flow inside the systems. 151

Figure 4.55: Pore volume of raw vermiculite and other composite vermiculite adsorbents. 155

Figure 4.56: Pore size distribution of raw vermiculite and other composite vermiculite adsorbents. 155

Figure 4.57: Example heat flow curves and temperature profile from a DSC test. 160

Figure 4.58: Empty specimen pan (a), cap (b&c) and single granule specimen place on the pan (d)....162

Figure 4.59: Single granule of specimen weight using electronic digital scale (a) and clamps (b). 162

Figure 4.60: Inner part of specimen furnace (a), cover of the specimen furnace (b). 163

Figure 4.61: DSC thermograms of composite specimens. Pure silica gel (a), silica gel+$CaCl_2$ (b), silica gel+$LiNO_3$(c), vermiculite+$CaCl_2$(d), and vermiculite+$MgSO_4$(e). 165

Figure 4.62: Heat Storage capacity comparison 166

Figure 5.1: Schematic of THSS-R134a & THSS-R1234yf....171

Figure 5.2: Adsorption pipe and dimension....174

Figure 5.3: Evaporator pipe and Dimension.....175

Figure 5.4: Heat transport of THSS during adsorption. 179

Figure 5.5: Detail of vapour diffusion in the adsorption pipe. 180

Figure 5.6 : Adsorbent pipe model flow 183

Figure 5.7: Desorption via electric heating clamp 184

Figure 5.8: Pressure-enthalpy chart of the heat pump refrigeration cycle. 185

Figure 5.9: Heat transport of THSS-R134a/R1234yf.....187

Figure 5.10: Schematic drawing of THSS-SOLAR.....191

Figure 5.11: The effect of adsorption temperature vs. adsorption uptake and saturation pressure and pressure ratio.....194

Figure 5.12: Effect of heating temperature (T_H) on heating power ($Q_{electric}$), adsorption heat (Q_{ads}), adsorbent bed temperature (T_s) and COP_1.....196

Figure 5.13: Effect of time to adsorbent bed temperature, heating temperature, adsorption heat and COP_1.....197

Figure 5.14: Adsorption heat, condenser heat, COP_2 and COP_{HP} vs. heating temperature (VCC-R134a). 198

Figure 5.15: Effect of mass change to heating power and the COP of the heat pump. ...199

Figure 5.16: Effect of time on adsorption heat (COP_2) and the COP of the heat pump (R134a). 200

Figure 5.17: Effect of heating temperature on adsorption heat and compressor work.....201

Figure 5.18: Effect of mass change on adsorption heat and COP_2.....202

Figure 5.19: Effect of time on COP_2 and COP_{hp}. 203

Figure 5.20: Effect of solar collector size on the COP of the systems. 205

Figure 6.1: Adsorption pipe with Condenser coil R134a circuits 209

Figure 6.2: Evaporator Pipe with evaporator coil (R134a circuits).....210

Figure 6.3: Temperature & pressure sensor position 211

Figure 6.4: Pressure-Enthalpy (P-H) diagram for R134a circuits 213

Figure 6.5: Schematic of THSS-R134a system 213

Figure 6.6: Photo showing the constructed THSS-R134a.....214

Figure 6.7: Temperature Variations of Test 1 218

Figure 6.8: Temperature variation of Test 2.....219

Figure 6.9: Temperature variation of Test 3.....220

Figure 6.10: Temperature variation of Test 4.....221

Figure 6.11: Temperature variation of the 1st cycle on Test 4 222

Figure 6.12: Temperature variation of the 2nd cycle for Test 4 222

Figure 6.13: Temperature variations of Test 5 223

Figure 6.14: The THSS-R134a (fully insulated) 224

Figure 6.15: Comparison of Adsorption temperature for all test 225

Figure 6.16: Temperature variations of adsorption pipe, evaporator pipe, inlet & outlet of the high-pressure loop, inlet & outlet of low-pressure loop of the heat pump for desorption Test1. 228

Figure 6.17: Temperature variations of adsorption pipe, evaporator pipe, inlet & outlet of the high-pressure loop, inlet & outlet of the low-pressure loop of the heat pump (Test 2) 229

Figure 6.18: Temperature variations of Adsorption pipe, Evaporator pipe, inlet & outlet of the high-pressure loop, inlet & outlet of the low-pressure loop of the heat pump (Test 3). 230

Figure 6.19: Temperature variations of Adsorption pipe, Evaporator pipe, inlet & outlet of the high-pressure loop, inlet & outlet of the low-pressure loop of the heat pump (Test 4). 231

Figure 6.20: Temperature variations of Adsorption pipe, Evaporator pipe, inlet & outlet of the high-pressure loop, inlet & outlet of low-pressure loop of the heat pump (Test 5 fully insulate the heat pump circuit). 232

Figure 6.21: The effect of COP with the increase on condenser temperature. 234

Figure 6.22: The effect COP (comp), Heat gain, on the condenser pipe (Qh) versus the evaporator temperature. 234

Figure 6.23: Theoretical versus experimental results of adsorption pipe temperature (Tp) during the adsorption cycle (V-$CaCl_2$) 238

Figure 7.1: The SHSC in discharging cycle (Option 1) 245

Figure 7.2: The SHSC in charging cycle (Option 1) 246

Figure 7.3: Result showing the effect of mass flow rate on collector heat gain and heat transferred to the material for the charging cycle. 251

Figure 7.4: Result showing the effect of charging cycle mass flow rate on inlet–outlet temperatures, charging and collector efficiency. 252

Figure 7.5: Illustrations showing the effect of collector area on inlet–outlet temperature, heat gain from collectors and transferred heat to the adsorbent for the charging cycle 253

Figure 7.6: Illustrations showing the effect of time on inlet–outlet temperature, heat gain from collectors, heat transferred to the absorbent, reaction advancement and charging efficiency for the charging cycle. 254

Figure 7.7: Illustrations showing the effect of mass flow rate on discharging efficiency and heat generation for the discharging cycle. 255

Figure 7.8: Illustrations showing the effect of absolute humidity on discharging efficiency generated heat and temperature lift for the discharging cycle. 256

Figure 7.9: Illustrations showing the effect of time on output temperature, COP & generated heat for the discharging cycle. 257

Figure 7.10 SHSS charging cycle (Option 2) 258

Figure 7.11: SHSS discharge cycle (Option 2) 258

Figure 7.12: Result showing the effect of mass flow rate (m_w) to discharge temperature (T_8), fan-coil outlet temperature (T_{11}), the efficiency of discharge (η_D), reaction advancement (X_d) and COP of the system. 261

Figure 7.13: Result showing the effect of discharge time to discharge temperature, fan-coil outlet temperature, the efficiency of discharge and COP of the system. 262

Figure 7.14: Schematic of SHSC (discharging process) 264

Figure 7.15: Schematic of SHSC (charging process)....264

Figure 7.16: The construction small scale of SHSC....265

Figure 7.17: Halogen lights....266

Figure 7.18: Solar coating on the heat pipe 266

Figure 7.19: Removable perforated pipe for the adsorbent material installed inside the collector (right: plan view, left: top view) 267

Figure 7.20: The heat pipe inserted through the fins....267

Figure 7.21: Kipp & Zonen pyranometer....269

Figure 7.22: Installation of flowmeter....270

Figure 7.23: Temperature variations of inlet and outlet of domestic water and material in the perforated pipe for Adsorption Test 1 272

Figure 7.24: Temperature variations of inlet and outlet of domestic water, material in the perforated pipe & solar intensities for Desorption Test 1....273

Figure 7.25: Temperature variations of inlet and outlet of domestic water, material in the perforated pipe for Adsorption Test 2 275

Figure 7.26: Temperature variations of inlet and outlet of domestic water, material in the perforated pipe & solar intensities for Desorption Test 2....276

Figure 7.27: Cumulative energy for Test 1&Test 2....277

Figure 7.28: Comparison of COP Test 1 and Test 2 278

Figure 8.1: Initial Arrangement of the Heat Pipe Assembly for Testing 284

Figure 8.2: THSS Design....286

Figure 8.3: Constructed THSS System....287

Figure 8.4: Heat pipe section of constructed THSS 287

Figure 8.5: Adsorption section....288

Figure 8.6: Adsorbent cartridge for the adsorption section....289

Figure 8.7: Water cartridge for the evaporator section 289

Figure 8.8: Cotton wool installed in water cartridge in evaporator section 289

Figure 8.9: Water cartridge installed inside the evaporator section 290

Figure 8.10: Side View of Adsorbent section (Fully insulated) 290

Figure 8.11: Ball valve connecting both sections 291

Figure 8.12: Cross section of Thermocouples position 291

Figure 8.13: 3kW Kensa Heat Pump 292

Figure 8.14: Revised Heat Pipe Arrangement 294

Figure 8.15: Final Schematic Arrangement for the THSS & Thermocouples position 295

Figure 8.16: Energy Price with inflation rate of 7% 298

Figure 8.17: THSS spend, saved and payback period 300

Figure 8.18: Cumulative GHG emission for THSS and Boiler in 20 years of lifespan 302

Figure 9.1: Proposed Modification to Heat Pipe, Circulate Water Vapour through Evaporator during desorption.....310

Figure 9.2: Option 2 piping arrangement 311

LIST OF TABLES

Table 2.1 Comparison between physisorption and chemisorption 23
Table 2.2: TES energy storage density.....27
Table 2.3: Properties of silica gel.....29
Table 2.4: Chemical composition of zeolite.....30
Table 2.5: Properties of zeolite.....30
Table 2.6: Properties of vermiculite 32
Table 2.7: Particle size and loose bulk density of vermiculite 33
Table 2.8: Lists of some common refrigerants with high latent heat.....34
Table 2.9: Characteristics of TCMs investigated by different authors.....38
Table 2.10: Summary of adsorption heating/cooling systems 49
Table 2.11: Summary of mathematical models used by different authors. 59
Table 2.12: Summary of heat and mass transfer enhancement techniques.....76
Table 3.1: Brief methodology of THSS research.....84
Table 4.1: The detail construction of the glass and metal wick 94
Table 4.2: Summary of results from horizontal rig.....110
Table 4.3: Summary of temperature variations of tested adsorbent materials.....120
Table 4.4: Amount of materials for experimental testing 122
Table 4.5: Comparison of results with previous research.....123
Table 4.6: Typical chemical analysis of properties of vermiculite 137
Table 4.7: Summary of specimen characteristics from MIP. 153
Table 4.8: Summary of specimen density. 154
Table 4.9: Summary of operating condition for the specific heat testing. 161
Table 5.1: Descriptions of THSS-R134a/1234yf 172
Table 5.2: Value of Parameter used for the adsorption isotherm 177
Table 5.3: Simulation physical Data for selected composite material.....182
Table 5.4: Assumptions for solar heat regeneration.....192
Table 5.5: Summary results of adsorbent heat (Q_{ads}) from the numerical analysis.....205
Table 5.6: Summary results of all COP from the numerical analysis.....206
Table 6.1: Sensor uncertainties.....211

Table 6.2: Specification of main components in the THSS-R134a system.....214
Table 6.3: Equations used in the analysis 217
Table 6.4: Summary of Temperature Variations of Vermiculite-$CaCl_2$.....226
Table 6.5: Result of mass change for the adsorbent and water 227
Table 6.6: Temperature variations and compressor performance during desorption process. 236
Table 6.7: Performance comparison of all test.....237
Table 7.1: Assumptions use in modelling.....244
Table 7.2: Heat loss coefficients and surface areas of building components 249
Table 7.3: Thermocouple position 268
Table 7.4: Specifications for CMP 11.....269
Table 7.5: Comparison between numerical and experimental results 279
Table 8.1: Thermocouple position and descriptions.....295
Table 8.2: Steady-State Temperatures Monitored in the Pipe System during desorption296
Table 8.3: Overall performance of Domestic-Scale THSS 296
Table 8.4: Capital Cost for THSS systems.....299
Table 8.5: List of input parameters for THSS.....299
Table 8.6: Discount rate of THSS 301

NOMENCLATURES

A	Heat transfer area, [m^2]
$Astp$	Heat transfer area between adsorbent material and adsorbent pipe, [m^2]
C	Specific heat, [$kJ / kg \cdot K$]
COP	Coefficient of performance [-]
D_s	Effective surface diffusion [m^2 / s]
D_{s0}	Pre-exponential term [m^2 / s]
E_a	Activation energy of surface diffusion, [J / mol]
E_d	Energy storage density per unit mass [Wh/g]
$E_{d,dr}$	Energy storage density per unit volume [kWh/m^3]
Fr	Collector heat exchanger efficiency [-]
h	Heat transfer coefficient, [$W / m^2 \cdot K$]
h_{stp}	Heat transfer coefficient from adsorbent material to adsorbent pipe [$W / m^2 \cdot K$]
h_1	enthalpy of the refrigerant at the inlet of the compressor [kJ/kg]
h_2	Enthalpy of the refrigerant at the outlet of compressor [kJ/kg]
h_3	Enthalpy of refrigerant from the outlet of the condenser coils of the system [kJ/kg]
ΔH_r	Reaction enthalpy [kJ/mol]
ΔH_w	Reaction enthalpy per kg of water vapour [kJ/kg]
ID	Pipe Internal Diameter, [m]
I	total solar radiation [kW/m^2]
K	calorimetric constant [-]
$k_s \cdot a_p$	Effective coefficient of mass transfer, [s^{-1}]
L	Evaporation latent heat of refrigerant, [kJ / kg]
$\dot{m}_a$	air mass flowrate from dehumidifier [kg/s]
$\dot{m}_w$	air mass flowrate from collector to fan-coil [kg/s]
$\dot{m}_{ad}$	air mass flowrate during discharge/desorption [kg/s]
M	Mass, [kg]
n	Constant related with the property of adsorbent
η_{col}	collector efficiency [-]
η_c	charging efficiency [-]
$\boldsymbol{\eta_v}$	volumetric efficiency [-]
$\boldsymbol{\eta_{comp}}$	compressor efficiency [-]
$\boldsymbol{N}$	rotational speed [rpm]
OD	Pipe Outside Diameter, [m]
P	Vapour pressure [kPa]
P_s	Saturated vapour pressure corresponding to adsorbent temperature [kPa]
ΔQ	Heat Flow [mW]

Q_{us}	Solar heat gain [kW]
Q_{loss}	Heat loss [kW]
Q_{tr}	Heat transfer from solar collector to the adsorbent [kW]
Q_{char}	Heat from charging/desorption process [kW]
Q_{wa}	Water flowrate [kg/s]
q	Adsorption amount per kilogramme of dry adsorption, [kg/kg]
dq/dt	Adsorption rate, [$kg/kg \cdot s$]
q^*	Equilibrium adsorption content at T_s and P
Qst	Isosteric Heat of Adsorption, [kJ/kg]
R_p	Particle radius, [m]
S_c	Length of the compressor [mm]
U	heat loss coefficient [-]
ρ	Density [kg/m^3]
T	Temperature, [K]
$\Delta \mathbf{T}$	Temperature Lift (°C)
t	time [s]
$\tau\alpha$	Absorption/transmission coefficient [-]
td	Desorption time [hr]
V_0	Maximum porosity in per kilogramme of adsorbent [m^3/kg]
v_1	specific volume at the suction side [m^3]
v_d	displacement volume [m^3]
W_f	Fan energy [kW]
W_{oi}	total ideal input electric power to the compressor [kW]
X_c	Reaction advancement during charging /desorption [-]
X_d	Reaction advancement during discharge/adsorption [-]

SUBSCRIPT

a	atmosphere/ambient/air
ads	adsorption
Al	Aluminium
ew	Evaporator wall
eva	Evaporator
dis	discharge
d	indoor
f	final
s	adsorbent material
sp	sample
co	Copper Pipe with fins
col	collector
p	Adsorbent pipe
p,s	VCC
in	Inlet
out	outlet
w	Water
w_a	wall
b	block
f	floor
r	roof
v	ventilation

ABBREVIATION

COP: Coefficient of performance

DSC: Differential scanning calorimetry

EES: Engineering equation solver

ESEM: Environmental scanning electron microscopy

GWP: Global warming potential

HAM: Heat and mass transfer

HP: Heat pump

IRR: Internal rate of return

ODP: Ozone depletion potential

SCP: Specific cooling power

SEM: Scanning electron microscopy

SGCC: Silica gel+$CaCl_2$

SPPWF: Single payment present worth factor

TCM: Thermochemical material

TES: Thermochemical energy storage

THSS: Thermochemical heat storage system

VCC: Vermiculite +$CaCl_2$

1. INTRODUCTION

1.1 Background

Climate change, global warming, heat islands and high-energy consumption are interrelated and are becoming issues in current industrialisation and globalisation agendas. As predicted by EIA (2013), from 2013 to 2040 the world energy consumption will be increased from 600 quadrillion Btu to approximately 800 quadrillion Btu (see Figure 1.1). This scenario will have an adverse effect on global carbon dioxide emissions (see Figure 1.2) with an approximate predicted marginal increase from 12 to 30 billion metric tonnes between 1990 and 2040. With the depletion of fossil fuels for energy generation, researchers all over the world are investigating the most sustainable alternative energy sources for all inhabitants. As fossil fuel resources such as oil, natural gas, and coal are becoming scarcer and more expensive, many energy conservation strategies are more feasible to employ. Furthermore, it is necessary to find more sustainable, efficient and economical ways to utilise energy not only in the field of energy production, transmission, distribution and consumption, but also in the area of energy storage (ES) (Lee, 2013).

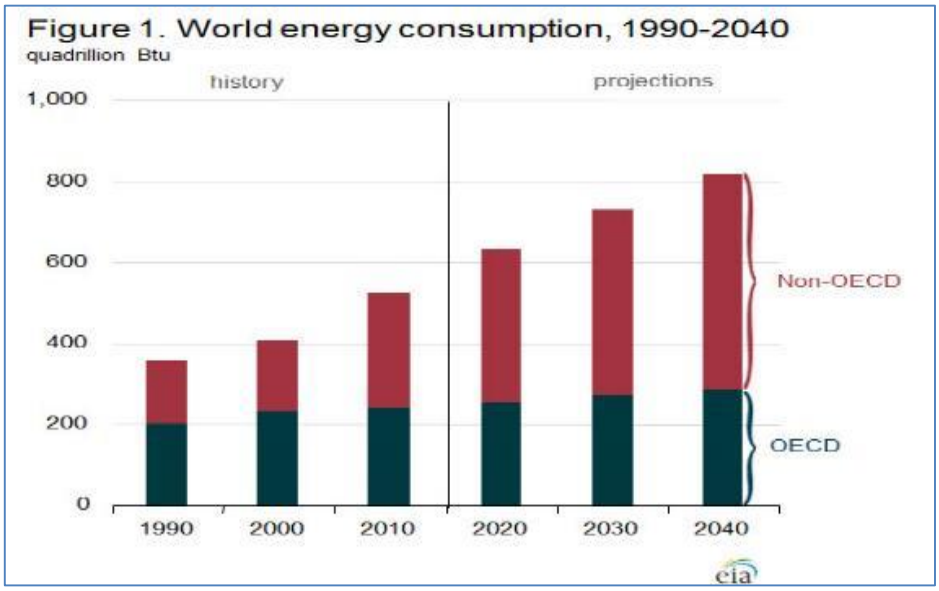


Figure 1.1: World energy consumption, (EIA, 2013)

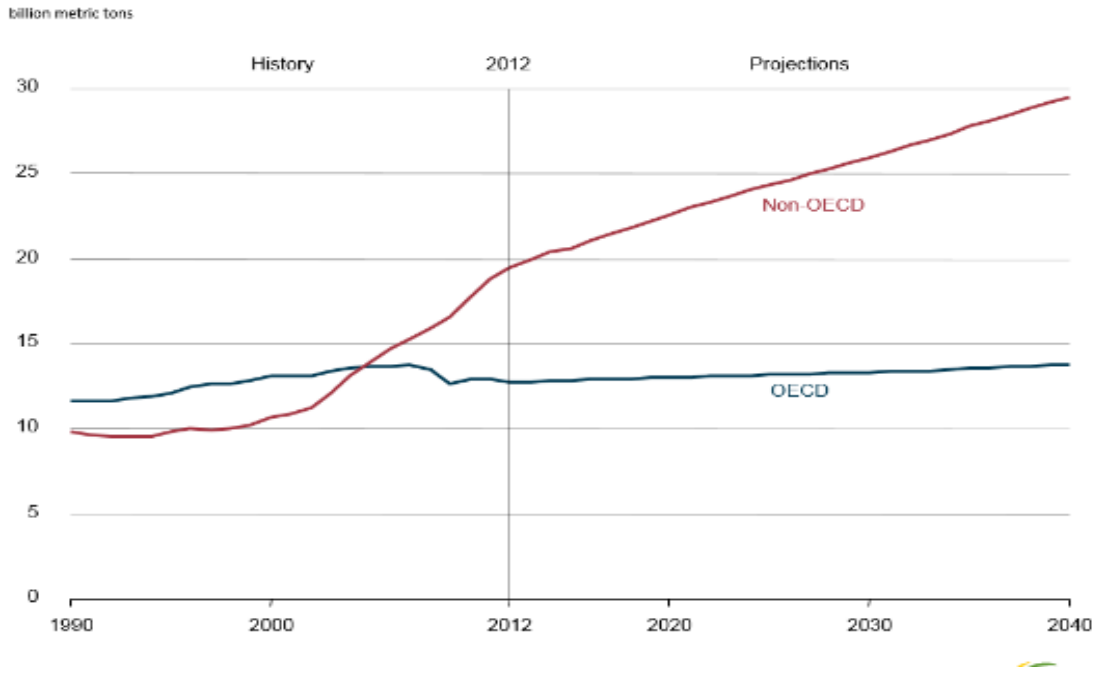


Figure 1.2: Carbon dioxide emission, (EIA, 2013)

Residential and commercial building energy consumption makes up 20% to 40% (Lombard et al. 2008) of world primary energy consumption. In the UK, energy use in the domestic sector accounts for around 30% of total energy consumption and has risen by 23% over the last 35 years (Utley & Shorrock, 2008). Furthermore, space

heating still accounts for over half of energy use in the housing stock (DECC, 2013). Therefore, the need to supply an alternative energy source for building applications is a significant challenge for all countries in order to mitigate the use of primary energy from fossil fuel.

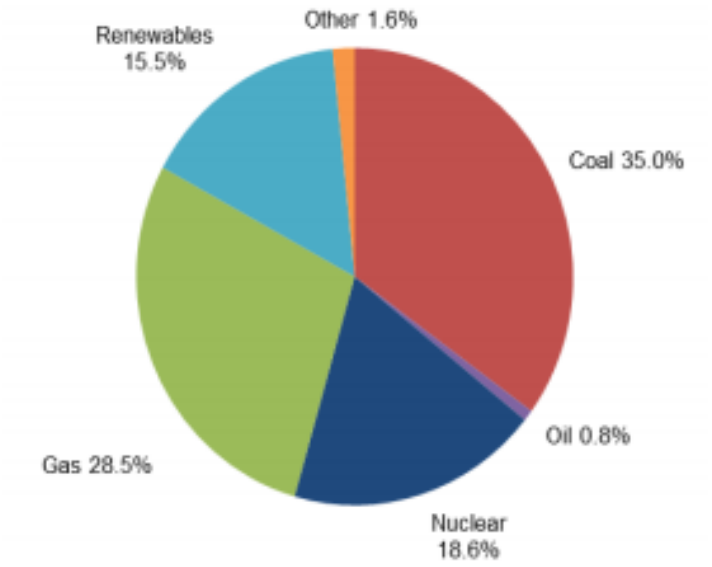


Figure 1.3: U.K. energy mix (DECC, 2011)

The typical alternative energies that have penetrated the market, and which are generated as part of the energy mix for the national grid, are renewable energies such as solar, biomass, geothermal and hydropower. For instance, renewable energy in the United Kingdom forms nearly 15.5% of the total energy mix (see Figure 1.3). However, using such energy involves some drawbacks and limitations such as inconsistency in supply and demand. Drawbacks such as this require alternative or new technologies for storing the energy for end-use. Means of retaining the stored energy is another challenging issue that needs to be investigated. Therefore, this research aims to develop a novel Thermochemical Heat Storage system using off-peak power and low energy sources to minimise energy demands from fossil fuels.

1.2 Statement of Problems

One problem is that the storage of energy plays a vital part wherever the supply cannot be controlled to meet the demand. Solar power has great daily and seasonal fluctuations in supply, and its demand varies, and therefore, some energy storage is necessary for the most of its applications. Because solar radiation cannot be stored as such, it needs to be converted into electrical, mechanical or thermal energy, and for that the appropriate storage device is required (Ouden, 1982).

In previous energy systems, energy demand has been relatively stable, and the supply chain has only needed to produce energy to meet demand directly and on time. However, instability of daily and seasonal energy demand has become more visible recently due to generated energy and the supply cannot be delivered to meet the demand directly (Paksoy, 2007). Furthermore, energy production from renewables and decentralisation of power plants induces instability of energy demand (Paksoy, 2007). Figure 1.4 illustrates the phenomenon of the volatility of renewable energy supply and demand. The additional technology of energy storage solutions is needed to bridge the gap caused by the daily and seasonal changes of renewable energies.

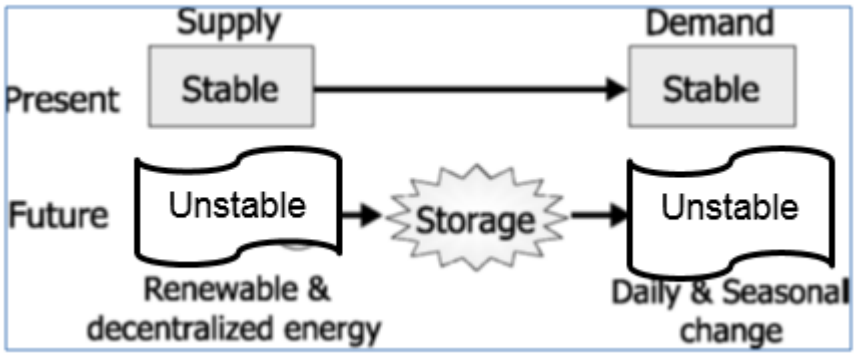


Figure 1.4: Trend shift of energy relationship between energy supply and demand (Paksoy, 2007)

Renewable energies such as solar power have some limitations such as low solar intensity during the winter in countries with cold climates or during rainy season for hot and humid countries. These constraints will require development of new technologies for energy storage in order to meet the needs of the supply and demand for building applications, such as heating and cooling. Many researchers have investigated energy storage solutions including thermal energy storage. For example, application Phase Change Material (PCM) has been investigated as a possible solution by Regin et al., 2008; Zhang et al., 2008; Tay et al., 2012; Mosaffa et al., 2013). However, low thermal conductivity was reported by previous researchers (Castell et al., 2008; Medrano et al., 2009; Tay et al., 2013) which would lead to low heat transfers and therefore difficulty in meeting the supply and demand for building applications. Furthermore, an organic material such as paraffin is expensive (Sharma et al., 2009) and would be uneconomical and unsuitable for long term use as energy storage for building applications in the future (Delgado et al., 2012; Cabeza & Mehling, 2003). Other methods of energy storage such as sensible energy storage which involve using water, including ice thermal storage or solar ponds, have been investigated by Ezan et al. (2011), Abdullah et al. (2013), Sanaye & Shirazi (2013). However, the storage density of water can only reach 0.2 GJ/m^3 (for a typical storage tank) whereas the storage density of a thermochemical energy storage system could reach up to 0.5-3 GJ/m^3 (Abedin & Rosen, 2012). Furthermore, the temperature range for a thermochemical energy store could reach up to 200°C compared to the 110°C reached by water. Hence this shows that thermochemical energy stores can store approximately 90% more energy than water for high-temperature applications. Another problem associated with sensible heat storage is heat loss and the high volume of space required for storing. This would involve inefficient systems and a large footprint of space for energy storing in building plans.

Thermochemical materials (TCM) have higher energy densities compared to latent PCMs or sensible (water) storage media due to their high heat rate of adsorption ranging from 1000 to 6000 kJ/kg (Sur and Das, 2010). Because of a higher energy storage density, thermochemical energy storage systems can provide more compact energy stores compared to latent and sensible energy stores. This attribute is particularly beneficial where space for the energy is limited or valuable (Abedin & Rosen, 2011).

Thermochemical energy storage (TES) effectiveness and compactness relies heavily on the design of the adsorbent material/bed of the system. Substantial research on adsorbent materials such as composite materials and liquid media have been carried out (Zhu et al., 2006; San & Hsu, 2009; Huang et al., 2010; Hongois et al., 2011; Tanashev et al., 2013). These studies have analysed the possible composite materials with the highest potential energy storage density for the energy storage applications. Thermochemical energy storage systems are relatively compacted, which is achieved by using new nanocomposite materials. Based on this literature, the aims of this study is to develop the high performance of energy storage systems using a Thermochemical Heat Storage System (THSS) that uses an adsorbent heat pipe with high thermal conductivity and high heat storage density, which would be economically attractive in the long term for use in building applications.

1.3 Objective and Scope of the Project

To achieve the above aims the following objectives were independently investigated. The overall goals of this research were:

a) To develop a unique adsorbent heat pipe with a high thermal performance that is economically feasible for long term usage.
b) To develop a highly efficient reactor (adsorbent bed) and evaporator.

c) To analyse various nanocomposite adsorbent materials within the parameters of high energy storage densities, low desorption temperatures, compactness, and affordability.

d) To reduce the energy usage of a heat pump via an off-peak energy source or renewable energy source such as solar or ground heat with high Coefficients of Performance (COP).

e) To develop a solar heat storage collector and to analyse the efficiency of using renewable energy that is integrated with a solar collector.

f) To develop a domestic-scale prototype of thermochemical heat storage systems based on diurnal space heating and domestic hot water systems.

1.4 Scope of the Project

To successfully meet the above targets, the scopes of the project are divided into six separate areas:

a) To review the background and literature reviews of past work on heat pipe and thermochemical energy storage, solid reactant materials and working fluids for building applications.

b) To develop a mathematical model and thermodynamics analysis on adsorbent heat pipes and the efficiency of an adsorbent bed with regard to charging, storing and discharging. Analysis of the COP of a heat pump generated with low-grade energy/an underground heat source.

c) To build-up and test a small-scale THSS and validate the concept of an adsorbent heat pipe reversible process using a selected adsorbent material.

d) To develop a model and a small-scale solar heat storage collector (SHSC) for space heating application in the building.

e) To carry out experiments on a domestic-scale of Thermochemical Heat Storage Systems (THSS) with an actual domestic hot water/heating usage pattern in the UK.

f) To discuss the technical, economic and environmental benefits of the proposed systems.

1.5 Novelty and Timeliness

The aim of this research is to develop a novel THSS system using off-peak power and renewable sources to reduce energy demands from fossil fuels. The novel THSS system will include:

a) A novel adsorption heat pipe which incorporates a reactor section (adsorbent section) and an evaporator section within the design. A unique configuration will enhance the heat transfer and improve the overall performance of the energy storage system.

b) Unique adsorbent materials including silica/zeolites/molecular sieves and nanocomposite adsorbent materials (vermiculite) that have been scientifically synthesised.

c) Experimental evaluation on a laboratory scale of THSS using a selected nanocomposite material of Vermiculite+$CaCl_2$ incorporated via a unique design of a heat-pump circuit.

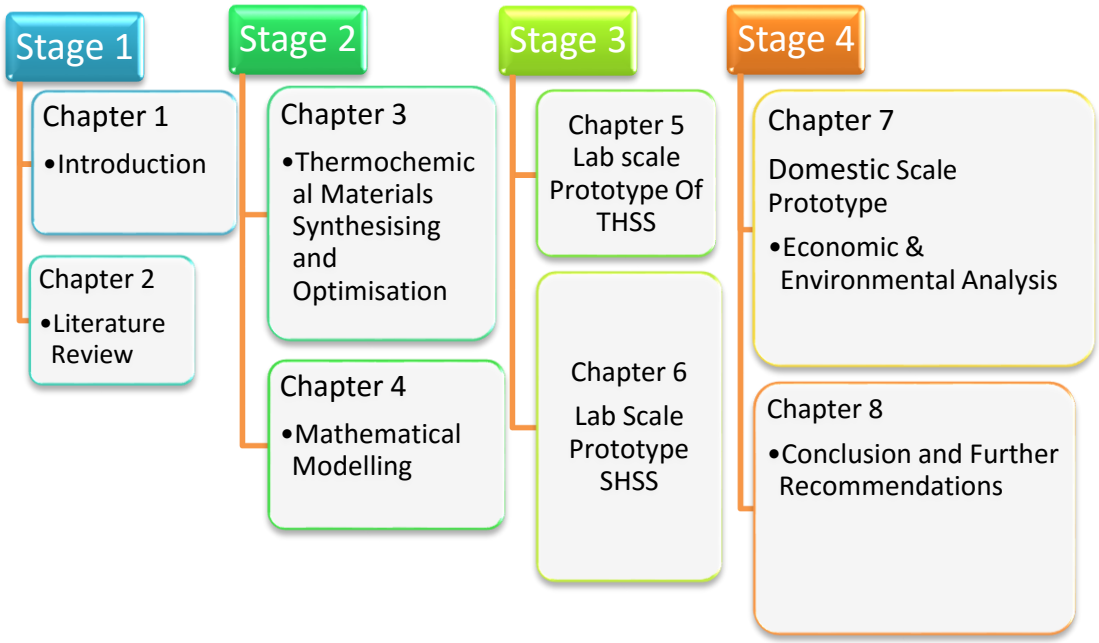
d) Experimental evaluation on a domestic scale of THSS using a selected nanocomposite material of Vermiculite+$CaCl_2$ incorporated via a heat-pump circuit and a simulated low-grade heat source using a water tank.

This research will lead to a novel THSS integrated with a heat pump, which can reduce annual heating demands and increased heat pump efficiency, compared to

the conventional heat–pump systems. The advanced material development underpinning this study will accelerate the viability of thermal storage technology by delivering affordable, compact thermal stores. It is, therefore, timely concerning its considerable capability of saving energy and reducing the amount of CO_2 emissions into the environment.

1.6 Methodological Approach

The project work involved the following stages:



Stage 1: Background and Literature Review

Task: A literature review will be carried out to collect relevant information on the theory of adsorption heating and cooling applications, energy storage theory, background, thermochemical energy storage and implementation, the theory of adsorption, adsorbent materials and nanocomposite adsorbent materials. The literature review will

support the research by developing an understanding of the issues related to thermochemical energy storage and its performance. It will act as a baseline for development of high performance systems with improved compactness which will lead towards more efficient energy storage systems for building applications.

Stage 2:

Task 1: Material Screening & Synthesising

Task 1 involves doing a material screening on the potential adsorbent materials such as silica gel/$CaCl_2$, Vermiculite/$CaCl_2$, Zeolite/$CaCl_2$ and others composites materials. The synthesis involves testing the temperature lift using the horizontal and vertical rigs, specific heat using DSC and physicochemical examination on pore distribution using MIP (Mercury Intrusion Porosimetry), ESEM (Environmental Scanning Electron Microscope) & SEM (Scanning Electron Microscope).

Task 2: Mathematical Modelling

The mathematical modelling will be carried out in order to determine the temperature of the adsorbent section. COP is established using a different type of refrigerant gas (R134a or R1234yf) or solar energy.

Stage 3:

Task 1: Testing of THSS Using Small-Scale Rig in the Laboratory

Designed and constructed small-scale version of THSS to test the performance of the novel systems.

Task 2: Modelling and Testing of Solar Heat Storage Collector Using Small-Scale Rig in the Laboratory

Modelling and experimental testing of a small-scale solar heat storage collector to verify the performance of the novel systems.

Stage 4:

Task 1: Experimental Investigation of Domestic-Scale Prototype of Thermochemical Heat Storage Systems (THSS)

A domestic-scale prototype of THSS theoretically modelled, designed and constructed to test the performance of the novel systems.

Task 2: Economic and Environmental Analysis

Firstly, economic and environmental analysis conducted and discussed for household application. Payback period and gas (CO_2) emissions are estimated and evaluated. Lastly, conclusions will be drawn and future work recommended.

1.7 Thesis Structure

The thesis is divided into nine chapters, including this introductory chapter. The study will be presented in the following sections:

Chapter 1: Introduction

Chapter 1 covers the introductory section and the driving forces of this work. The objectives, scopes, and novelty aspects of the project are detailed. In addition, the methodological approach to fulfilling the objectives is provided in this chapter.

Chapter 2: Background and Overview of Thermochemical Heat Storage and Materials

Chapter 2 introduces the background theory of thermochemical heat storage, thermochemical materials and working pairs, and the theory of adsorption systems.

Reviews of mathematical modelling methods commonly used by the current and previous researchers and heat and mass transfers of thermochemical storage systems are introduced here.

Chapter 3: Thermochemical Material (TCM) Screening, Synthesising and Optimisation

Continuing from the review chapter, the selected TCMs will be subject to experimentation. Therefore, Chapter 3 covers the material screening, synthesising and optimisation of thermochemical materials that have the advantage of high heat storage capacity, high porosity and that are environmentally friendly. The synthesising involves temperature lifting through horizontal and vertical adsorption heat pipes, thermal analysis using a differential scanning calorimetric (DSC) for the heat storage density investigation and mercury intrusion porosimetry (MIP) for pore size distribution investigation. This chapter also provides the evidence highlighting the thermochemical material with the most potential, as selected based on the advantageous characteristics mentioned previously.

Chapter 4: Performance Investigation of THSS

Chapter 4 describes the mathematical modelling of THSS using an Engineering Equation Solver (EES) for the adsorption and desorption process. The type of thermochemical materials was simulated, namely the Vermiculite + $CaCl_2$ (VCC). In the desorption process, three types of heat source were analysed consisting of: i) electrical element, ii) heat pump circuit, iii) solar thermal. In the heat pump circuits, two types of refrigerant gases were analysed; R134a and R1234yf. The parameters used to analyse the effect on system performance (COP & heat generated) were the type of adsorbent

materials, the mass of the adsorbent material, the heating temperature, and adsorption and desorption times.

Chapter 5: Experimental Investigation on a Small-Scale Prototype of THSS with Heat Pump Circuits

The aim of this chapter is to carry out an investigation of small-scale Thermochemical Heat Storage Systems (THSS-R134a) using a heat-pump circuit for the regeneration of the heat source. The working pair for this prototype is the composite of vermiculite impregnated with calcium chloride and water as the refrigerant in the evaporator pipe. The integration with a heat-pump circuit is to analyse the performance of a THSS-R134a using an off-peak power source in the desorption/charging cycle and utilising renewable energy sources to minimise energy demands from fossil fuels.

Chapter 6: Modelling and Experimental Investigation on Solar Heat Storage Systems

Chapter 6 introduces a build-up performance of a novel solar heat storage system that involves the integration of a solar collector with the composite material of Vermiculite + $CaCl_2$ to generate heat storage. A laboratory scale solar heat storage system has been tested for its performance with dependent variables changes such as average solar light intensities with an average of 850W/m^2 & 950W/m^2 to achieve the maximum temperature of 60°C for desorption process. This section also provides a mathematical model of solar heat storage systems using EES.

Chapter 7: Experimental Investigation of a Domestic-Scale Prototype of THSS Integrated with a Heat Pump.

This chapter provides an experimental investigation into a domestic-scale prototype that could deliver an estimated 24kW of energy of basis diurnals. This section also provides the design options for improving the heat and mass transfer of reactor/adsorption pipes, evaporator pipes, plus the whole system configuration. Also included in this chapter is the general discussion on the environmental, social and economic benefits of THSS.

Chapter 8: Conclusion and Further Recommendations

Chapter 8 provides conclusions to each theoretical and experimental question in every chapter, and gives further recommendations to those researchers endeavouring to continue study in this area.

2. LITERATURE REVIEW

2.1 Introduction

The solid/gas sorption or thermochemical sorption technologies have excellent prospects. In addition to efficiently utilising solar energy or waste heat as primary energy, they can use the non-polluting refrigerants with no moving parts, which makes the system less noisy and it would require less maintenance. Therefore, heating or cooling using adsorption cycles can be a real alternative to conventional vapour compression machines. Additionally, these systems appear to have low ODP (ozone depletion potential) and low GWP (global warming potential) (Wang et al., 2005) and therefore protect the atmosphere. Sorption technologies are alternative systems that are suitable for cooling and heating in buildings. Sorption technologies were introduced in the Faraday era of the 1800s (Critoph, 2012) when ammonia was used for cooling. Then from the 1920s, silica gel was selected as the adsorbent material. After the energy price crisis in the 1970s zeolite became another option for sorption cooling, and was considered as competitive to its counterparts (vapour compression systems). Since then, according to Critoph (2012), adsorption refrigeration and heat pumping technologies have not been developed further, either for technical or economic reasons.

2.2 History of Thermochemical Energy Storage

Thermochemical Energy Storage started with the energy crisis in the 1970s when research increased into better alternative energy and energy storage. In Sweden and Switzerland, researchers pioneered the technology of a chemical heat pump using

ammonia systems with NH4/Cl, LiCl, $MgCl_2$, $CaCl_2$, and $FeCl_2$/ammonia as the chemical substance working pairs (Paksoy, 2007). According to Paksoy (2007) a long distance thermal energy store was introduced in Germany in 1970 and the application of this technology continued into the 1980s.

In Japan from 1984 to 1992 the Agency of Industrial Science & Technology started using ammonia with $FeCl_2$, $NiCl_2$, NaI and $NaScN/NH_3$ and halogenated inorganic reactant/water of $MgCl_2$, $CaCl_2$, $CaBr_2$ and $MnCl_2/H_2O$ as working pairs for chemical heat pumps. Then the development of this research was examined by using CaO/H_2O working pairs for the chemical heat pump application (Ogura et al., 1991). Extending this study, Kato et al. (1998) conducted a survey of the durability of the repetitive cyclic operation of MgO/H_2O and found that a magnesium hydroxide material showed high durability during a repetitive magnesium oxide/water reversible reaction and higher heat output performance than common magnesium hydroxide or magnesium ethoxide. The solid reactor is the most critical piece of equipment in chemical heat pump design. Therefore, to achieve better performance in these systems, enhancement of solid reactor beds for the chemical heat pump has been carried out in Japan and the UK respectively.

Darkwa & O'Callaghan (1997) investigated the thermochemical technology of inorganic oxides for minimising energy consumption and pollution from automobile engines and found that inorganic oxides such as calcium oxides can be stored for a very long period, even at ambient conditions, without losing their potential for energy production. This study was the first step in achieving viable thermal storage systems.

2.3 Investigation of the Thermochemical Energy Storage (TES)

Technically, TES would also be in the mixed boundary condition of chemical storage and sorption storage, as illustrated in Figure 2.1 (N'Tsoukpoe et al., 2009; Ding & Riffat 2012). Sorption can be termed as a phenomenon of fixation or capture of gas or vapour (sorbate) by a substance in its condensed phase (solid or liquid), called sorbent (Hauer, 2007).

Sorption phenomena can involve both thermo-physical and thermo-chemical aspects (Inglezakis et al., 2006). The heat of adsorption is usually less in physisorption processes and large in chemisorption. The term ''sorption'' is a general definition which includes both absorption and adsorption (Hadorn, 2005). The general term "sorption" is used when both adsorption and absorption occur simultaneously.

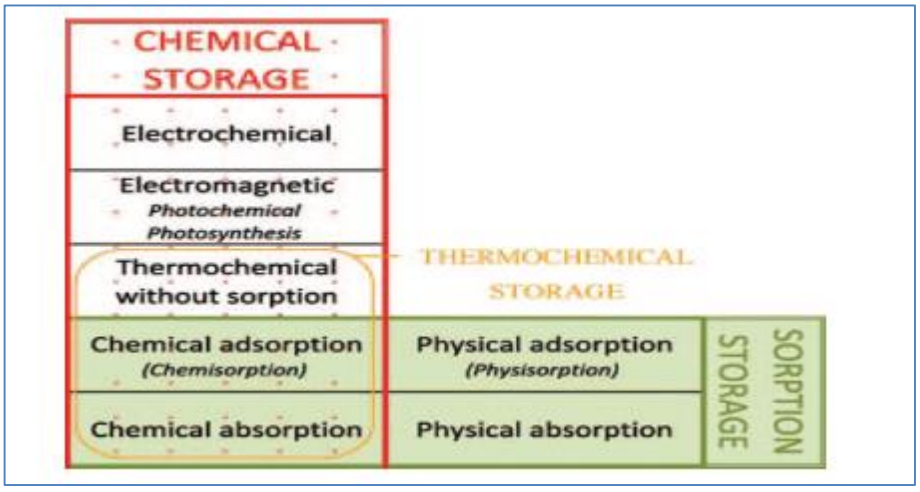


Figure 2.1: Chemical storage and sorption classification (N'Tsoukpoe et al., 2009)

TES is based on reversible chemical reactions (Shkatulov et al., 2012). The principle of sorption in TES is based on performing a reversible chemical reaction (desorption) which allows adsorption of heat in the course of the decomposition (desorption) process that is endothermic. A reverse synthesis reaction is exothermic and results in giving the stored heat back (Kawasaki et al., 1999; Hauer, 2008). The reversible physicochemical reaction, C, is the thermochemical material (TCM). With the heat supply on C, C can be disassociated into components A and B, which can be at any phase and stored separately. Both A and B are termed as reactant/working pairs or a sorption couple, and C will be formed with a heat release when to A and B are put together (Yukitaka, 2007; Ding & Riffat, 2012).

$$C + Heat \Leftrightarrow A + B \qquad 2.1$$

TES can be further defined by its processes. TES processes are divided into three phases:

i) Charging, also known as an endothermic reaction. A heat source is required for the dissociation process of C.

ii) Storing. This stage occurs after the charging process and A and B will be formed and stored.

iii) Discharging is where A and B are associated with an exothermic reaction and material C is regenerated and the recovered energy released (see Figure 2.2).

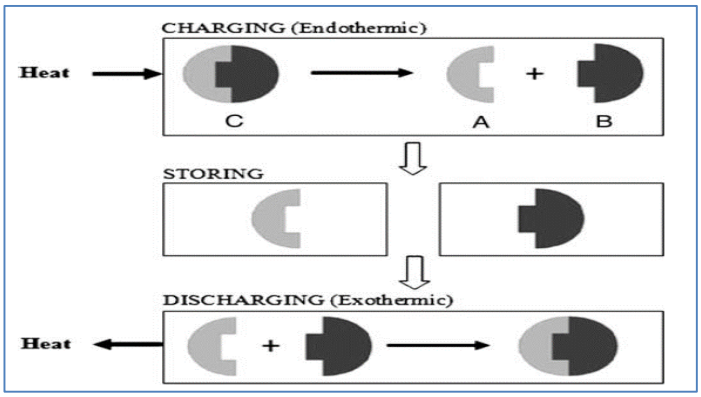


Figure 2.2 Process involved in a thermochemical energy storage cycle (Abedin & Rosen, 2011; Ding & Riffat, 2012)

TES is in the subcategories of chemical and thermal energy storage systems. It can be divided into an open or closed system. In open systems, the gaseous working fluid is released into the environment and the entropy released (Bales, 2007). However, in closed systems, the working fluid and entropy are discharged into the environment via a heat exchanger, and a closed system normally works with a closed working fluid that is inaccessible from the atmosphere. As illustrated in Figure 2.3, the closed systems can be divided into two (2) working principles; adsorption and absorption. For the adsorption process, gas is bonded on the surface of a solid, while in the absorption process, a new compound of the adsorbent and working fluid is formed.

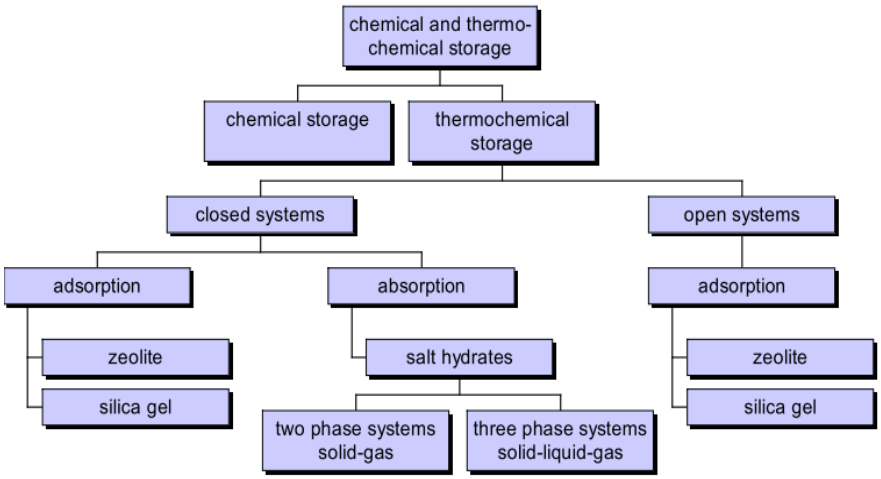


Figure 2.3: Classification of chemical and thermochemical storage

Chemical reactions offer larger energy storage densities compared to the sensible heat and phase change materials due to the high energy processes involved in the reversible destruction and reformation of chemical bonds. In thermochemical reactions, the products of the endothermic reaction contain the energy as chemical bond energy, which is retrieved by the exothermic reverse reaction. Consequently, the products are stable at low temperatures and can be transported over long distances. Thermal dissociation reactions are also attractive in this respect if the products of the endothermic dissociation exist as two phases and are easily separable.

Some of the advantages of TES (Garh et al., 1985; Bales, 2005; Hadorn, 2006) include:

(i) Long term storage - reactants and products can be stored at ambient temperatures with consequent low energy losses.

(ii) Compactness - energy is stored by breaking chemical bonds, with the resultant high energy storage density approximately two times greater than sensible and latent heat systems.

(iii) High efficiency - the storage subsystem can be integrated into a complete system, thereby minimising waste heat losses (efficiency of thermochemical energy storage ranges from 50-69% (Abedin and Rosen, 2012a).

(iv) Low cost - the basic chemicals are inexpensive and readily available, and ambient temperature storage allows for less expensive containment material and eliminates the need for insulation.

(v) Transportability - many of the possible chemical systems are composed of gaseous and liquid species that are transported easily at ambient temperature and thus the endothermic and exothermic reactors can be physically separated by long distances.

(vi) Recombination of the endothermic reaction products in a fuel cell.

(vii) The use of the reaction products as the working fluid in a thermodynamic cycle.

2.3.1 Absorption Process

Absorption is technically termed as a liquid-gas system and a promising storage option because they can be pumped and used as the heat transfer fluid in solar collectors and heat exchangers. It also can be defined as a process in which the sorbate diffuses into the liquid or solid sorbent accompanying a phase change and/or a chemical reaction. Materials recently investigated comprised of aqueous solutions of Calcium Chloride ($CaCl_2$), Lithium Chloride (LiCl), Lithium Bromide (LiBr), Sodium Hydroxide (NaOH), Potassium Hydroxide (KOH) and Ammonia (Lele, 2015). Absorption systems require

energy for the regeneration process, typically known as the driven energy. An example of driven energy in absorption systems is industrial waste heat, automobile exhaust, and solar energy. Previous researchers have used absorption systems driven by industrial waste energy (Ma et al., 2003; Romero & Rodriguez-Martinez, 2008; Quoilin et al., 2011), automobile exhaust (Javani et al., 2012) and solar energy (Li & Sumathy, 2000; Katejanekarn et al., 2009; Crofoot & Harrison, 2012). Some of the researchers had also placed emphasis on cascading absorption systems with a vapour compression system to improve their performance (Wu & Eames, 2000; Eames & Wu, 2000). However, improvements on low COP are required in the reactor design, with low manufacturing costs to be adopted in the long term.

2.3.2 Adsorption Process

Solids and the fluid adsorbed on the solid surface are referred as adsorbent and adsorbate respectively. Adsorption may be due to a physical process referred as physical adsorption, or physisorption, caused by Van der Waals forces or a chemical process referred as chemical adsorption or chemisorption, involving valency forces (Srivastava & Eames, 1998). The physical adsorption/physisorption involves only a relative weak intermolecular force, whereas chemisorption includes the formation of a chemical bond between the sorbate molecule and the surface of the adsorbent (Ruthhaven, 1984). The general features, which distinguish physisorption and chemisorption are illustrated in Table 2.1.

Table 2.1 Comparison between physisorption and chemisorption (Ruthhaven, 1984)

Physisorption	**Chemisorption**
Low heat of adsorption (< 2 or 3 times latent heat evaporation)	High heat of adsorption (> 2 or 3 times latent heat of evaporation)
Non-specific	Highly specific
Monolayer or multilayer	Monolayer only
No dissociation of adsorbed species	May involve dissociation
Only significant at relatively low temperature	Possibly over a wide range of temperature
Rapid, non-activated, reversible	Activated, may be slow and irreversible
No electron transfer although polarisation of sorbate may occur	Electron transfer leading to bond formation between sorbate and surface

An adsorption process means the gaseous or liquid phase of a component is on the inner surface of a porous material. During the desorption step, heat is put into the sample. The adsorbed component, water molecules as illustrated in Figure 2.4, are removed from the inner surface. As soon as the reaction is reversed, the adsorption is started by combining water molecules with the sample. The molecules adsorbed and the heat brought into the system during desorption will be released. The adsorption step represents the discharging process (Hauer, 2007).

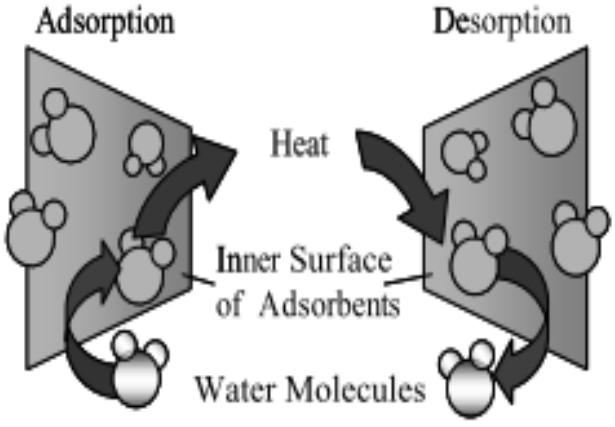


Figure 2.4: Adsorption process of water vapour on solids (Paksoy, 2007)

2.3.3 Open TES

In an open sorption TES, the air is transporting water vapour and heat in and out of the packed bed of solid adsorbents/reactor, where the air is in contact with a liquid desiccant. Meanwhile, the desorption mode or hot air stream enters the adsorbent bed/reactor and desorbs the water from the adsorbent and exits the bed cooler and is saturated (see Figure 2.5) (Hauer, 2007). The main chemical reaction of an open TES is similar to equation 2.1. In an open TES, the heat transport fluid is not separate from materials A, B and C. Open TES systems operate in an open loop coupled with the ambient conditions, and an air stream transports water vapour and heat in and out of the adsorbent bed/reactor of thermochemical materials (Hauer, 2007). TES in open sorption systems was investigated by Hauer & Fischer (2011), Zondag et al. (2013) & Bertsch et al. (2014). These authors had put emphasis on the high storage capacities of these systems compared to sensible heat storages and the possibility to support drying processes by the application of this technology.

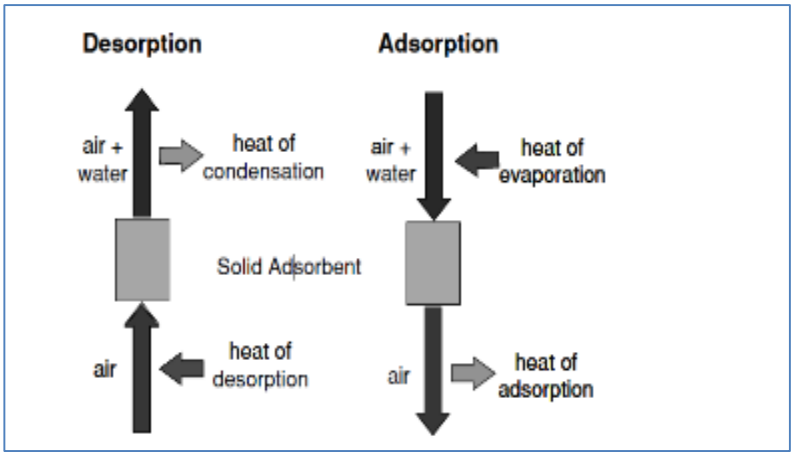


Figure 2.5: Open sorption storage system using a packed bed of solid adsorbent (N'Tsoukpoe et al., 2009; Hauer, 2007)

Wu et al. (2009) did a numerical analysis on an open TES of composite adsorbent materials, and the experimental analysis was designed to validate the theoretical analysis. These authors found that the composite adsorbent material has the potential of validating use of thermal storage materials for low-grade thermal energy storage owing to its high specific storage capacity and low regenerating temperature as the specific heat TES increased noticeably while the COP of the TES system decreased. The energy and exergy comparison of open and closed TES has been investigated by Abedin & Rosen, (2012) who found that for open storage of Zeolite, 13X as a thermal material could achieve the energy and exergy of 69% and 23% respectively. In Japan, Liu et al. (2013) did an experiment involving honeycomb filters made of a mesoporous composite material for an open sorption thermal energy storage system. These authors found that the composite mesoporous material supported with $CaCl_2$ showed potential for storing low-temperature industrial waste heat with a high volumetric heat storage density and concluded that the composite mesoporous material has the advantage of a long duration for supplying stable heat with a low heat loss.

2.3.4 Closed Thermochemical ES

A closed TES is based on the same physical effect as the open storage. However, the engineering is quite different from open sorption systems. The closed system could precisely be described as evacuated or air-free systems. In closed systems components, which do not exist in the atmosphere, can be used because there is no connection to the ambience (Hauer, 2007).

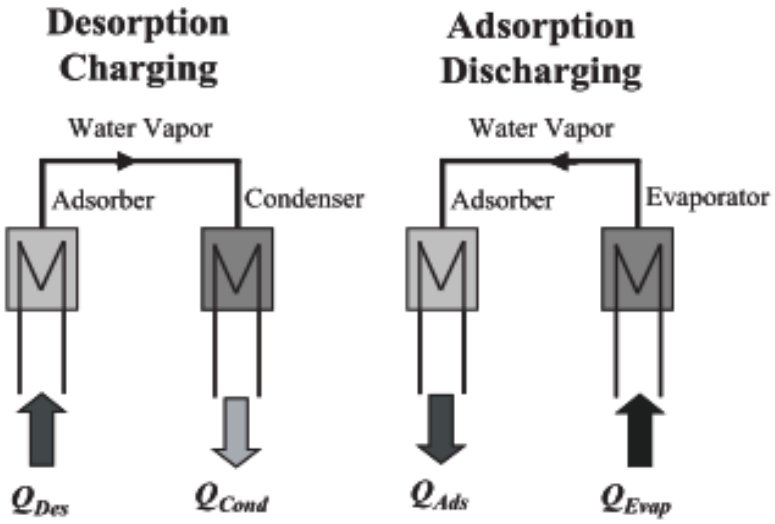


Figure 2.6: Operation principle of a closed thermochemical system (Hauer, 2007; N'Tsoukpoe et al., 2009)

The typical example is the working principle of a closed TES, as illustrated in Figure 2.6, where water vapour is used as the adsorbate material. The heat is transferred from the adsorbent using a heat exchanger and is stored in the condenser. In the desorption stage, heat is transported to the absorber, and water vapour is condensed in the condenser. During the adsorption, the heat is being delivered to the evaporator that is taken from the absorber. Lu et al. (2003) investigated a closed adsorption cold storage system with a zeolite/water working pair used for locomotive air conditioning. These authors conclude from their experimental and thermodynamic analysis that this working pair have large cold storage capacities of 600 kJ per 1 kg of zeolite. Furthermore, they claimed that adsorption cold storage could make use of low-grade thermal energy with no pollution and no energy losses. Bales (2007) constructed laboratory prototypes of thermochemical storage units of a closed adsorption system with silica gel and zeolite as a solid sorbent material and concluded that heat exchangers are the key components of a thermochemical energy storage system.

Other than that, they found that because of the low heat conductivity of zeolite and silica gel, the distance of the adsorbing material from the thermal conduction surfaces should be optimised.

Abedin & Rosen (2012) studied the energy and exergy of open and closed TES and found that differences between energy and exergy efficiencies. These authors also suggested that the selection of a TES for a particular application requires other factors beyond the thermodynamic including environmental effects, economics, thermochemical material degradation and cycling behaviour over time, reliability and maintenance requirements. Some of the closed TES prototypes and experimental studies are listed in Table 2.2. This material could be a potential to be adopted for the THSS in the future.

Table 2.2: TES energy storage density

Working pair	**Thermal energy storage density**	**References**
Silica gel/water	50 (kWh/m^3)	Bales et al. (2008)
Zeolite /water	180 (kWh/m^3)	Bales et al. (2008)
Zeolite+$MgSO_4$/water	166 (kWh/m^3)	Hongois et al. (2011)
Silica gel+$LiCl_2$/water	163.6 (kWh/m^3)	Yu et al. (2014)
Silica gel+$CaCl_2$/Water	1000 kJ/kg	Zhu et al. (2006)
$BaCl_2$+vermiculite/ammonia	680 W/kg	Veselovskaya et al. (2010)
$MgCl_2/NH_3$	2000 kJ/kg	Li et al. (2014)
Activated carbon + silica gel +$CaCl_2$	378 W/kg	Tso & Chao (2012)
$Mg(OH)_2$ + vermiculite	540 kJ/kg	Shkatulov et al. (2012)

2.4 Adsorbent Materials

The general term `sorption' is used when both adsorption and absorption occur simultaneously (Inglezakis & Poulopoulos, 2006). Adsorbents having a special affinity for polar substances like water are termed `hydrophilic'. These include silica gel, zeolites, and porous or active alumina. Non-polar adsorbents, termed `hydrophobic', have more affinity for oils and gases than for water. These substances include activated carbons, polymer adsorbents, and silicates (Srivastava & Eames, 1998). The types of adsorbent materials are described in the following sections.

2.4.1 Silica Gels

Silica gels ($SiO_2.xH_2O$) are solid amorphous structures formed by condensing soluble silicates from solutions of water (about 5%) or other solvents. Advantages include relatively low cost and relative simplicity of structural customisation. They are available as large as spherical beads about 5 mm in diameter or as small as grains of a fine powder. The temperature for use is at 200°C due to adsorption capacity loss when overheated and the loss of water. The silica pore size ranges from 2 to 3nm (Type A) to about 0.7nm (Type B) both of which are commercially available for all applications (Srivastava & Eames, 1998). Silica gel has a large capacity for absorbing water, especially in a high relative vapour pressure (0.5 P/P_s at 50% of relative humidity) (Airxchange, 2007). Therefore, it is broadly used as a desiccant for humidification purposes (Owen and Kennedy, 2009). The properties of silica gel are simplified as seen in Table 2.3. Silica gel is utilised in applications such as drying gases, refrigerants, organic solvents, transformer oils, desiccant packing and double glazing and the dew point control of natural gas (Crittenden, 1998). Thus, from this review, we can see that there is a potential for silica gel materials to be used for the heating of a building.

However, the performances of this material need to be investigated experimentally to come to a final conclusion on the appropriate desiccant material to be chosen for this research.

Table 2.3: Properties of silica gel (Hauer, 2008)

Property	Wide	Narrow
Inner surface (m^2/g)	300-500	600-800
Pore diameter (Å)	25-50	10-15
Specific heat (kJ/kgK)	0.92-1.0	0.92-1.0
Heat conductivity(W/mK)	0.14-0.2	0.14-0.2
Packed bed density(kg/m^3)	450	700

2.4.2 Zeolites

Zeolites are alumina silicate minerals. They are mined rather than synthesised. Zeolites have a very open crystalline lattice that allows molecules like water vapour to be held like an object in a cage. They have a high heat of adsorption and the ability to hydrate and dehydrate while maintaining the structural stability that is useful for various thermal storage and solar refrigeration systems. It is this hygroscopic property combined with the rapid exothermic reaction that occurs when zeolites are taken from a dehydrated to a hydrated form that make natural zeolites an efficient storage material for solar and waste heat energy (Dincer & Rosen, 2011). The properties and chemical composition of zeolite are simplified by Hauer (2008) as can be viewed in Table 2.4 and Table 2.5.

Table 2.4: Chemical composition of zeolite

Zeolite	Composition	Pore Diameter	SiO_2/Al_2O_3
Type A	$Na_{12}[(AlO_2)_{12}(SiO_2)_{12}].27H_2O$	4.1nm	2.0-2.5
Type B	$Na_{86}[(AlO_2)_{86}(SiO_2)_{106}].264.H2O$	7.4nm	2.0-3.0

Table 2.5: Properties of zeolite

	Type A	Type X
Inner surface (m^2/g)	800-1000	800-1000
Specific heat (kJ/kgK)	0.8-0.9	0.8-0.9
Heat conductivity(W/mK)	0.58	0.58
Packed bed density(kg/m^3)	750	700

Typical applications for zeolite are used for separation of oxygen from air, drying of gases, drying of refrigerants and organic liquids and separation of solvent systems (Crittenden, 1998). Previous investigations of storing zeolite as an adsorbent material and water as the adsorbate material for TES were carried out by Tatlier et al. (1999) & Lu et al. (2003). A few researchers, such as Restuccia et al. (2005), Atakan et al. (2013) & Dawoud (2013) have moved forward to using a zeolite coating on the heat exchanger to improve heat and mass transfer. These authors placed emphasis on investigating the adsorbent kinetic behaviour during the adsorption process and claimed that this method had increased COP of the systems.

2.4.3 Activated Carbons

Like other adsorbents, carbons have a large internal surface and especially large capillaries. This capillary volume gives them a high capacity to adsorb water vapour at a relative humidity of 45 to 100%. Activated carbons are made by pyrolysing and carbonising source materials, such as coal, lignite, wood, nut shells and synthetic

polymers, at high temperatures (700 to 800°C). Activated carbons are available in many forms including powders, micro-porous, granulated, molecular sieves and carbon fibres. The activated carbon in the powdered form (15 to 25 mm particles) is used for adsorption of liquids and in granulated (sieved granules of 4 to 20 mesh or about 3 mm to 0.8 mm diameter) or pellet (extruded pellets of 4 to 6 mm length) forms for air purification and gas separation. Activated carbon in microporous form has a molecular sieving ability and is widely used for separation of nitrogen and oxygen in the air. Activated carbon fibre (diameter of 7 to 15 mm) is made by carbonising synthetic fibres and is available in forms of mats, cloth, and fibre chips and is used for air and water purification (Ruthhaven, 1984; Suzuki et al., 1991).

2.4.4 Metal Oxides

Metal oxides including titanium oxide, zirconium oxide, and magnesium oxide have been used as adsorbents for special applications involving chemisorption. For example, cerium oxide is used for adsorption of fluoride in waste water (Suzuki et al., 1991). Previous investigations involving use of metal oxide for TES were conducted by Kato et al. (2009), Shkatulov et al. (2012) & Miguel et al. (2014). These authors reported that metal oxides have high-temperature lift during the exothermic process. However, these TCMs required high regeneration temperatures of 200-300°C. Therefore, this temperature will only be captured from the industrial waste heat or high solar intensities.

2.4.5 Vermiculite

Nowadays researchers have put effort into using more environmentally friendly and cheap materials such as vermiculite. Expanded vermiculite (a common agricultural

product) is chosen as the porous matrix for the composite sorbent due to its macroporous structure that is expected would prevent agglomeration of the salt and improve mass transfer. Veselovskaya et al. (2010) have investigated novel ammonia sorbents with a ‘‘porous matrix modified by active salt” for adsorptive heat transformation by using a $BaCl_2$/vermiculite composite for a lab-scale adsorption chiller. From their investigation, they concluded that this material can provide efficient operation of the chiller using a low potential heat source (80–90°C) giving COP of 0.54 ± 0.01 and SCP ranging from 300 to 680 W/kg. However, in another investigation of similar materials done by these authors it was highlighted that the disadvantage of barium chloride ($BaCl_2$) (in comparison with calcium chloride) is that it has a molar mass almost twice as high (208 and 111 g/mol respectively). This leads to a lowered ammonia uptake related to a unit mass of sorbent. Therefore, to improve the performance of using vermiculite as the host matrix, due to its larger pore size and surface area compared to another common adsorbents (silica gel, zeolite, molecular sieve), is one of the objectives that thrives in these research investigations.

Preliminary physical properties and densities of vermiculite are shown in Table 2.6 & Table 2.7. From this review, vermiculite might be considered as the adsorbent material with most potential to be adopted in a THSS prototype due to the fact that this material is the cheapest and most commercially available in the market.

Table 2.6: Properties of vermiculite (Dupre Chemical, 2011)

Typical Properties	
Sintering Temp	1260°C
Melting Point	1330°C
Thermal Conductivity	0.063 W/m^{2}K
Specific Heat	1.8 kJ/kgK

Table 2.7: Particle size and loose bulk density of vermiculite (Dupre Chemical, 2011)

	Nominal Particle Size (mm)	Loose Bulk Density (kg/m^3)
Large Grade (Micafil)	3-15	70
Medium Grade	2-8	85
Fine Grade	0.5-3	100
Superfine Grade	0.5 – 1.7	105
Micron Grade	0.1 – 1.0	120

2.5 Refrigerant for THSS

2.5.1 Water

Most of the research has been keen to choose water as the refrigerant in THSS because water is natural and environmentally friendly with zero ODP (ozone depletion potential) and GWP (Global Warming Potential), as well as being inexpensive. Furthermore, water is an excellent refrigerant with good thermodynamic properties since it is neither toxic nor flammable. According to a study conducted by Zhong (2006), as summarised in Table 2.8, water has the highest latent heat of 2258 kJ/kg (at 100°C) which gives an advantage of being able to extract the heat during the evaporation process. Furthermore, it would be able to attain high energy storage density of 2163kJ/m^3. Few examples of previous research on using water as the refrigerant pair with zeolite (Lu et al., 2003; Hu et al., 2009; Schnabel et al., 2010), silica gel (Restuccia et al., 2005; Bales, 2007) and a composite (Pons et al., 1996; Chan et al., 2012). These investigations involve a laboratory-scale adsorption cooling system. There are few or insignificant studies done on extracting the heat for heating systems using methods such as underfloor heating or hot water storage via an adsorption heat pump.

Table 2.8: Lists of some common refrigerants with high latent heat.

Refrigerant	Boiling Point (°C) @ 1 bar	Latent Heat (kJ/kg)	Latent Heat per Unit Volume (kJ/m^3)	ODP	GWP
Ammonia	-34	1368	932	0	0
Formaldehyde	-19	768	626	0.02	620
R32	-52	382	463	0	675
Chlorine	-34	288	450	1	4000
R22	-41	235	331	0.05	1700
Water	100	2258	2163	0	0
Sulphur Trioxide	45	508	905	n/a	n/a
Methanol	65	1102	872	1	2.8

2.5.2 Ammonia

The next possible option for a refrigerant for the adsorption heat pump is ammonia. This refrigerant has the second highest latent heat of 1368 kJ/kg (at-34°C) with zero ODP (ozone depletion potential) and low GWP (Global Warming Potential). An experimental investigation using ammonia as working pairs for an adsorption heat pump has been carried out by Critoph (1998) & Veselovskaya et al. (2010). Ammonia is widely used as a refrigerant in adsorption systems due to its advantages such as high enthalpy of evaporation, stability, wide temperature range and low freezing temperature (Anyanwu & Ogueke, 2005). However, poor heat and mass transfer performance caused by the phenomena of agglomeration and swelling during the reaction with ammonia, make the choice of proper composite adsorbents important (Yang et al., 2009). However, most of these investigations involved only cooling applications; fewer concentrated studies on the heating application in the building. Therefore, this study could bridge the gap between research applications on employing adsorption heat pumps for heating purposes in the building. This system will become

an alternative to a conventional heating system such as electrical heating or a boiler that require high energy and consequently produce high levels of CO_2 emissions.

2.6 TES Working Pairs Materials

There are several possible adsorbent/adsorbate working pairs that can be used in TES. The choice should be made carefully since the performance of the system differs according to the chosen working pair. The proper selection is largely based on the temperature of the heat source, the desired characteristics of the TES, the properties of the working pair constituents and the affinity between them (which depends on the chemical, physical and thermodynamic properties of the substances), and even on their cost, availability and environmental impact. Choice of adsorbate will also affect the performance of TES. The adsorbate, or refrigerant, must fulfil the following requirements (Sur & Das, 2010):

- Evaporation temperature below 0°C (for refrigeration purposes; it can be higher in the case of air-conditioning applications).
- Small molecular size so as to facilitate the adsorption effect.
- High latent heat of vaporisation and low specific volume when in the liquid state.
- High thermal conductivity,
- Low viscosity.
- Thermally stable with the adsorbent in the operating temperature range.
- Chemically stable in the operating temperature range.
- Non-toxic, non-corrosive and non-flammable.
- Low saturation pressures (slightly above atmospheric pressure) at normal operating temperature.

- The absence of ecological issues, unlike common refrigerants.

Such factors listed above need to be considered when selecting the working pair for a Thermochemical Heat Storage System (THSS). An extremely porous desiccant will increase the exposed surface area, and so higher rates of absorption ensue. In addition, the appropriate concentration of the vapour local to the desiccant and the diffusion through the desiccant are essential to ensure the absorption below the desiccant beds surface (i.e. the subsequent layers). Raising the thermal conductivity of the desiccant will enhance the rate of heat transfer, resulting in a greater driving potential (e.g. pressure and temperature differences) between the adsorbate and the desiccant (Tahat et al., 1995). The characteristics of thermochemical material (TCM) has been reviewed by N'Tsoukpoe et al. (2009), Ding & Riffat (2012), Yu et al. (2013). Most of these reviews summarise the current TCM, which is used for various applications such as heating and cooling applications. The performance variables such as energy storage density and temperature reaction can be seen in Figure 2.7. As can be seen, thermochemical materials (TCM) have the highest energy storage density when compared to latent and sensible energy storage materials. Heat from the chemical reaction of $CaCO_3$ has the highest energy storage density of approximately 7000 MJ/m^3 compared to silica gel at 1000 MJ/m^3. PCM materials have the third highest energy storage density of approximately 700MJ/m^3 when compared to water at 200MJ/m^3. The temperature lift for chemical reactions is in the range of 400°C to 1000°C, which is considered as an appropriate temperature for industrial applications. Besides this, the TCMs have excellent repetitive storage properties, and there is no heat loss to the environment during storage. Furthermore, with their high energy

storage density, TCMs can provide more compact energy storage compared to latent and sensible TES systems.

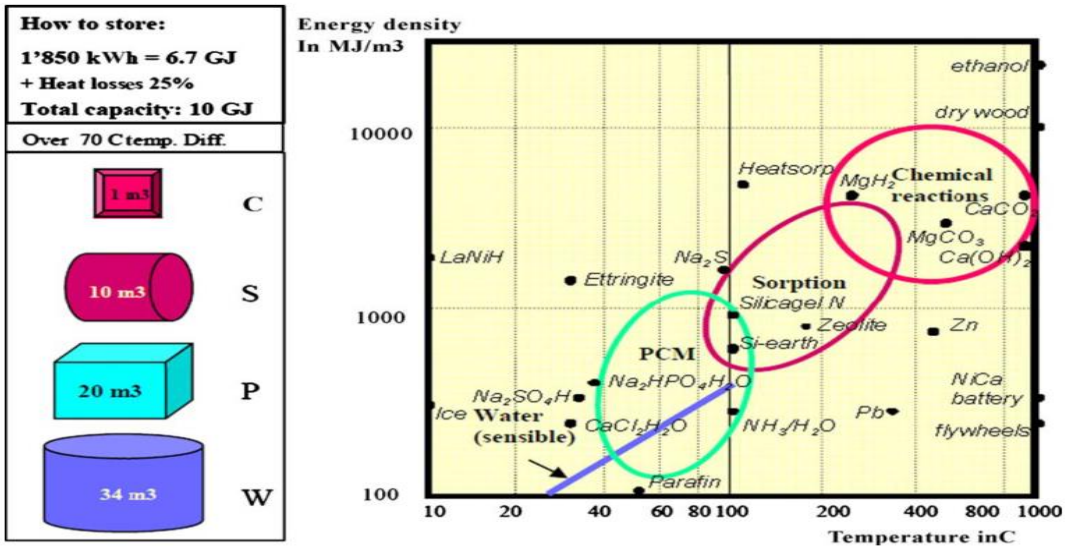


Figure 2.7: Different energy storage materials (Hadorn, 2005; N'Tsoukpoe et al., 2009)

Some of the TCM research on using metal oxides is shown in Table 2.9. The magnesium sulphate heptahydrate or $MgSO_4.7H_2O$ is investigated by Visscher & Veldhuis (2005) and presented theoretically, an excellent potential solution regarding solar energy storage with a high density of almost 780 kWh/m^3 at a temperature level of 122°C. Van Essen et al. (2008) have observed the same phenomenon in a study of characterisation of this material and concluded that the application of magnesium sulphate as a thermochemical storage material is quite problematic. Furthermore, Balasubramanian et al. (2010) had developed a mathematical model on the TES of salt hydrates using magnesium sulphate heptahydrate as a study case. These authors found that $MgSO_4 \cdot 7H_2O$ could not store heat due to energy lost by the salt to the released vapour during the thermochemical reaction and suggested ways to improve process performance, for example, by properly selecting materials for thermochemical

energy storage. The process performance is enhanced by introducing a smaller heat flux and considering materials that have larger thermal conductivities, higher specific heat capacities, and lower thermochemical desorption rates.

Table 2.9: Characteristics of TCMs investigated by different authors.

Compound	Dissociation Reaction			ES density of C, GJ/m^3	Turnover Temperature, °C	Realisation Potential %	References
	C	A	B				
Magnesium sulphate	$MgSO_4.7H_2O$	$MgSO_4$	H_2O	2.8	122	9.5	Visscher & Veldhuis (2005); N'Tsoukpoe et al. (2009); G. Balasubramanian et al. (2010); Abedin & Rosen (2011)
Silicon oxide	SiO_2	Si	O_2	37.9	4065	9.0	Visscher & Veldhuis (2005); Voort (2007)
Iron carbonate	$FeCO_3$	FeO	CO_2	2.6	180	6.3	Visscher & Veldhuis (2005); Voort (2007)
Iron hydroxide	$Fe(OH)_2$	FeO	H_2O	2.2	150	4.8	Visscher & Veldhuis (2005)
Calcium sulphate	$CaSO_4.2H_2O$	$CaSO_4$	H_2O	1.4	89	4.3	Visscher & Veldhuis (2005)
Sodium sulphate	NaS_5H_2O	NaS	H_2O	2.8	110	-	Iammak et al. (2004); Boer et al.(2004)
Strontium bromide	$SrBr_2.6H_2O$	$SrBr_2$	H_2O	0.22	43	-	Lahmidi et al. (2006); Mauran et al. (2008); Abedin & M. Rosen (2012)
Calcium hydroxide	$Ca(OH)_2$	CaO	H_2O	2.2	25	-	Darkwa (1998); Fujimoto et al. (2002);Ogura (2003); Darkwa et al. (2006)

A: Working Pair, B: Adsorbent, C: Adsorbate

Iammak et al. (2004) investigated sodium sulphate ($NaS{\cdot}5H_2O$) in a modular chemical energy storage system and found that sodium sulphate has a high thermal power combined with a high energy storage density. However, in the same year Boer et al. (2004) developed a prototype of sodium sulphate–water ($NaS{\cdot}H_2O$) as the working fluid for the applications of solid sorption cooling systems and found that this material is corrosive and suggested avoiding any direct contact of NaS with metal in the

systems. Lahmidi et al. (2006) investigated a strontium bromide ($SrBr_2.6H_2O$) base on solar thermal processes of a heating/cooling application. They validated the simulation through experimental studies suggesting that strontium bromide is a promising material for TES for building applications. Another example investigation on strontium bromide was conducted by Abedin & M. Rosen (2012) which used the reactant and water as the working fluid in closed sorption storage systems. These authors highlighted that properties of TCM such as durability and cyclic behaviour were the important factors that affect the performance of TES.

2.7 Development of Composite Thermochemical Materials (TCMs)

In sorption technologies, composite working pair TCM with high energy generation and enhancement of heat transfer has been reviewed (Ziegler & Grossman, 1996; Srivastava & Eames, 1998; Cot-Gores et al., 2012). The composite adsorbents (or complex compounds) made from porous media and chemical sorbents are commonly a combination of metal chlorides and expanded graphite, activated carbon, active carbon fibre, zeolite or silica gel. The objectives of using composite adsorbents are to improve heat and mass transfer of chemical adsorbents and to increase the adsorption quantity of physical adsorbents (Wang et al., 2006a). The addition of chemical sorbents to the physical adsorbents could result in higher adsorption quantities than that of physical adsorbents alone (Wang & Vineyard, 2011).

Cot-Gores et al. (2012) reported and listed the working pairs of sorption processes and chemical reactions (see Figure 2.8). These authors claimed that use of composite materials will improve heat and mass transfer performance in the reactive bed. A family of new working materials for solid sorption has been reviewed by (Aristov et al., 2002) and are known as “salt water sorbents”. These authors experimented on the composite

material or *"hygroscopic salt inside a porous matrix with open pores"* of $CaCl_2$ and LiBr as impregnated salts with different micro-macroporous silica gel as host matrices to absorb 0.75g H_2O of the dry sorbent for air-conditioning systems. They found that the sorbed water could be removed with a low temperature of 70 to 120°C, and therefore suggested that these new composite materials are suitable candidates for various thermal applications which require low-temperature heat sources.

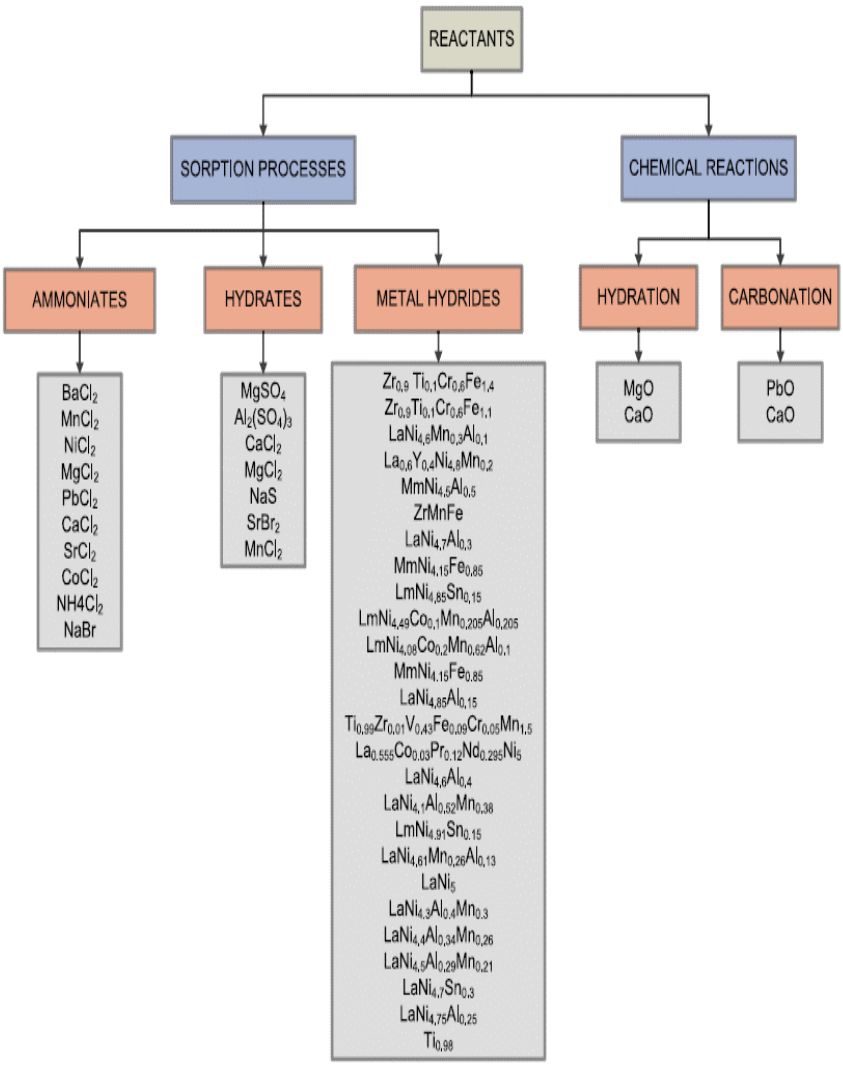


Figure 2.8: Overview of working pairs tested in prototypes under experimental conditions (Cot-Gores et al., 2012)

Daou et al. (2006) studied the same hygroscopic salt of $CaCl_2$ and a hosting matrix adsorbent of silica gel for refrigeration and air-conditioning applications. From this investigation, they found that the SCP (specific cooling power) is increasing, and the rate of desorption of the composite samples is higher than that of the pure silica gel, which is found to be a function of the calcium chloride content.

Similar experiments of impregnation of $CaCl_2$ with silica gel, (Zhu et al. 2006; Ponomarenko et al., 2010; Glaznev et al., 2011; & Tso & Chao, 2012) adopted this TCM for the open sorption application. These authors found that the composite sorbent provides great potential to obtain the small-size TES system with high energy storage density that can be employ for low-grade heat storage (Zhu et al., 2006). Another example study of open sorption systems was executed by Wu et al. (2007) who found that the concentration of the $CaCl_2$ solution is a significant factor affecting the storage properties. Moreover, they claim that the $CaCl_2$ solution of 30% showed the highest and most stable storage capacity of 1020J/g at a low charging temperature of about 90°C.

Ponomarenko et al. (2010) synthesised the composite of $CaCl_2$@SBA-15 with the mass ratio Ca/Si = 0.58 via impregnation of nanostructured mesoporous silica SBA-15 with a saturated aqueous solution of calcium chloride. In their experiments, these authors found that the dispersed salt forms dehydrated at a relative vapour pressure 2.5–4 times lower than the bulk one. This indicates the dramatic change of the salt sorption properties due to the pore size effect which leads to the increase in the surface energy of the confined salt and its hydrates. They suggested that nanostructured mesoporous silica is a promising matrix for tailoring the particular sorbents of a ‘‘guest-host” type.

Tanashev et al. (2013) investigated the thermal conductivity of composite sorbents, “salt in porous matrix”, for heat storage and transformation of $CaCl_2$, $MgCl_2$, and LiBr, (salts) with matrices (mesoporous) silica gel and alumina. They found that the salt solution leaks out of the silica mesopores and forms a liquid film on the external surface of primary silica particles that strongly facilitates the heat transfer between adjacent particles and enhances the bed heat conductivity. However, no such threshold behaviour was found for $CaCl_2$/alumina composites probably because the structure of the alumina pore leads to the formation of a confined salt solution that wets the alumina surface and simultaneously occupies both meso/macropores of the matrix.

Yu et al. (2013) listed a new classes of materials, including aluminophosphates (AlPOs), silico-aluminophosphates (SAPOs) and metal-organic frameworks (MOFs). These new materials have recently emerged as promising porous materials for heat storage, as shown in Figure 2.9. Apart from high energy storage density, there is some limitation involved in using inorganic salt with the host matrix, such as corrosion. Due to this, heat and mass transfer enhancement metal needs to be considered as an addition in order to avoid corrosion inside the reactor for an extended period.

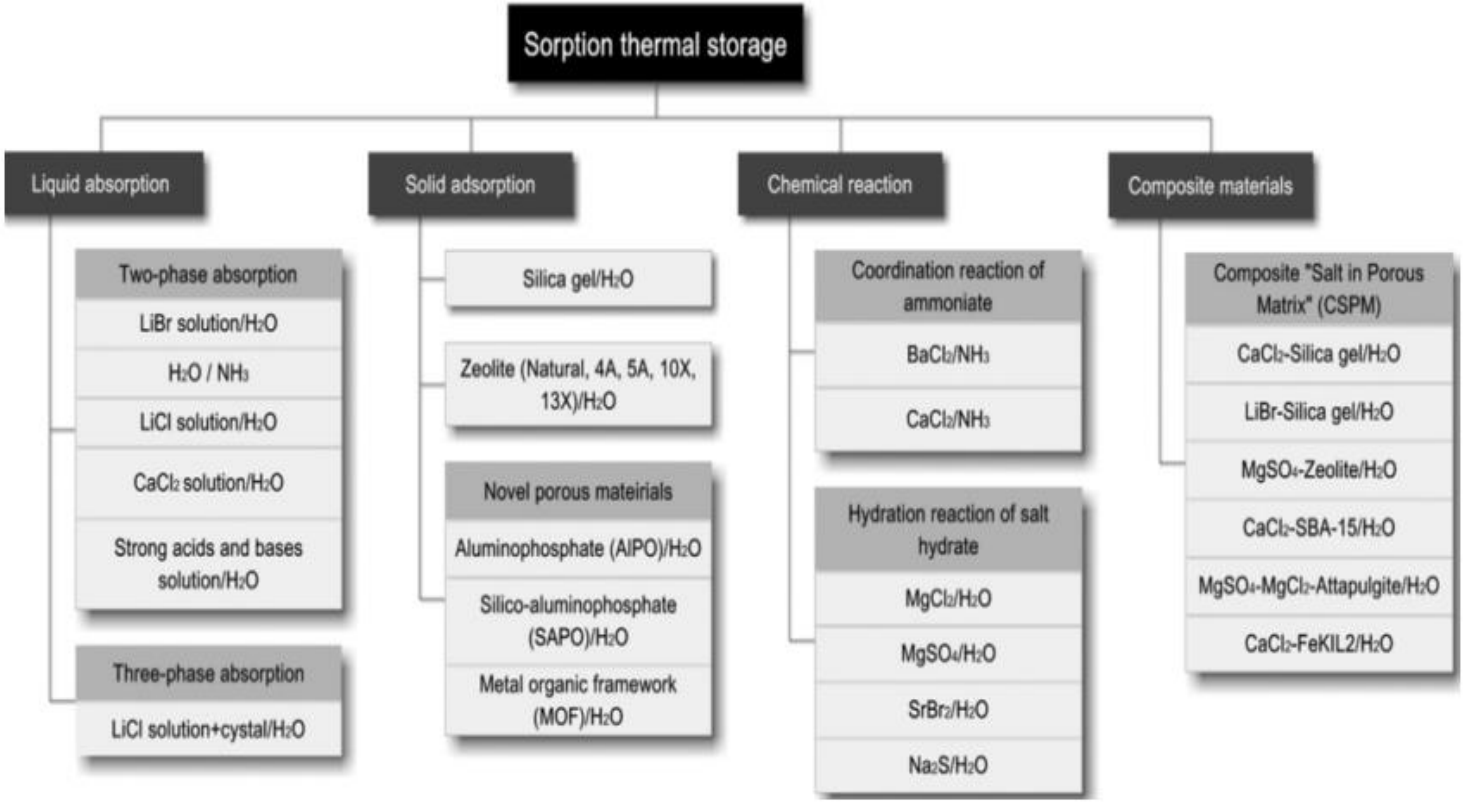


Figure 2.9: New classification of TCM materials (Yu et al., 2013)

2.8 Selected Studies on Current Thermochemical Heating/Cooling Systems

Adsorption heating/cooling systems are being widely investigated due to their advantages such as high energy storage density, low toxicity, low regeneration temperature and low cost. Veselovskaya et al. (2010) synthesised and tested a laboratory-scale adsorption chiller using a composite adsorbent composed of $BaCl_2$ impregnated into expanded vermiculite. They reported that vermiculite was chosen as the porous matrix for the composite sorbent due to its microporous structure that is expected to prevent agglomeration of the salt and improve mass transfer. Furthermore, the authors used a flat plate heat exchanger as the generator to enhance the heat and mass transfer. From this investigation, they found that the theoretical estimation of adsorbent kinetics fitted well with the experimental results giving a COP of 0.54 and a SCP ranging from 300 to 680 W/kg. Thus, they suggested that the proposed methods and composite materials could effectively be applied to low energy heat regeneration (80°C-90°C) cooling systems. The motivation behind using a plate heat exchanger is to increase the area of heat transfer in the adsorbent generator. Furthermore, using a metal plate may increase the thermal conductivity, and hence enhance the performance of the adsorption chiller. This investigation has provided evidence that using natural resources such as vermiculite will improve the heat and mass transfer in sorption cooling technology. However, this investigation is based on lab-scale prototype systems meaning further study is needed to apply the results as a final cooling/heating system application in buildings.

Stitou et al. (2012) carried out an experimental investigation of a solar assisted THS system used for air conditioning in a pilot plant for housing (see Figure 2.10). The plant,

which has a daily cooling capacity of 20 kWh, consists of a solid–gas thermochemical sorption processer that is assisted at 60–70°C by 20m^2 of flat plate solar collectors. The solid reactive $BaCl_2$ and a phase change refrigerant, NH_3, were used as the sorption couple. From their studies, they found that the average efficiency of the solar collectors needed to be at least 40–50% while the process COP needed to have about 30–40% efficiency. This investigation has shown that the solid-gas thermochemical can be adopted for cooling systems to scale for the cooling demand of a building. However, the integration of phase change material and TCM is technically a complicated system to manufacture and commercialise. Therefore, simpler and cheaper cooling/heating systems need to be investigated in order to alleviate high manufacturing costs and to promote economical systems to be employed in the future.

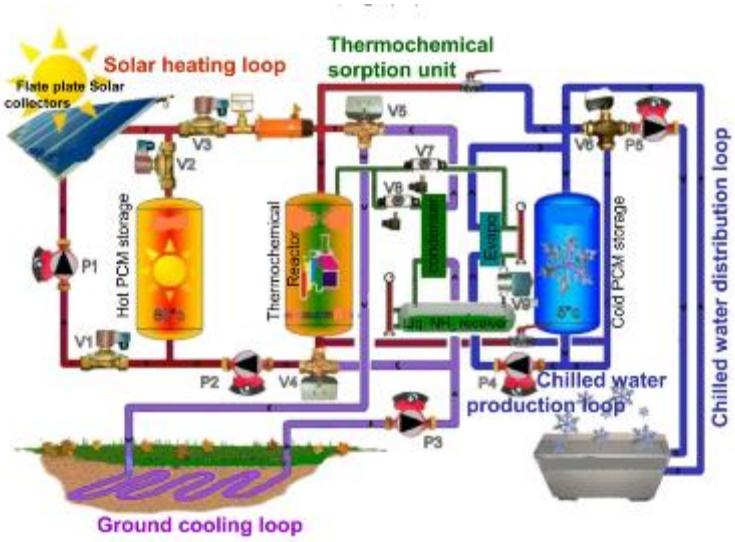


Figure 2.10: View of the solar sorption pilot plant for air-conditioning, flat plate solar collectors, and the thermochemical reactor design.

Another experimental study involving TES was carried out by Hamdan et al. (2013). This study used a working pair of sodium chloride as a sorbent and water as a sorbate. A few parameters that have been identified as influential to the performance in their

experiments were the amount of vaporised water from the evaporator, the initial system temperature and the effect of the type of salt on the increase in temperature of the salt. The results showed that lithium chloride salt has more of an effect on the performance of the heat pump than sodium chloride. Furthermore, the pump performance improved with the increased amount of water vaporised. This experimental study shows that to improve the performance of thermochemical energy storage, the water that is vaporised is vital. Further investigation is required to follow up this conclusion, mainly involving the kinesis of vapour transport and factors influencing the amount of water that vaporises.

An integrated concept using solar thermal energy with sorption storage systems was investigated by Hassan & Mohamad (2013). Using the available solar energy in a hot and humid country, these authors developed a solar adsorption cooling system as shown in Figure 2.11. As can be seen, the construction involved the use of a rotation flat plate solar collector to attain maximum solar intensities for the desorption. From this experiment, these authors found that the chiller produced a daily mass of 2.63kg of 0°C cold water with the respective COP of 0.66. This investigation indicates that hot-humid or hot–arid countries could utilise the surplus of solar energy by integrating with a TES system. Furthermore, by using this concept, the COP of systems increased and the energy required to desorb/dehydrate the material could be alleviated with free energy sources such as solar energy.

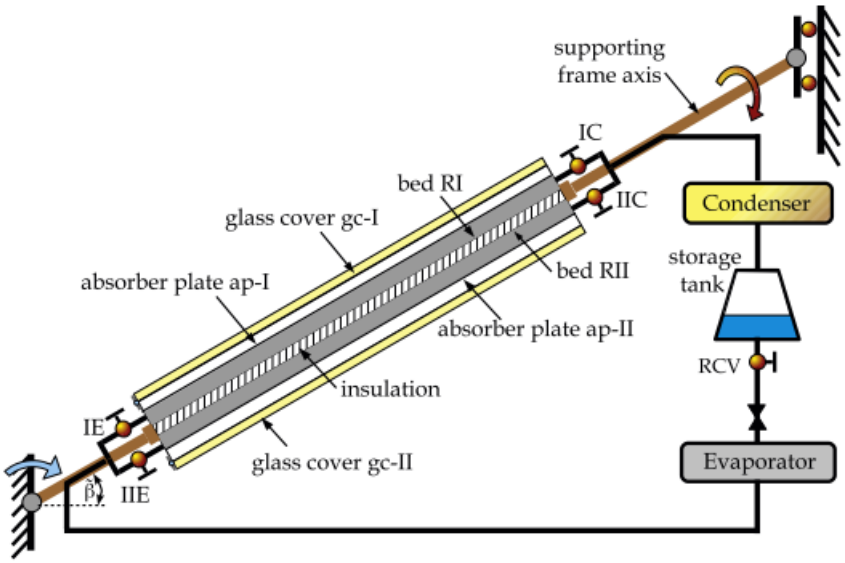


Figure 2.11: Schematic representation of the proposed CO-SAR system.

Finck et al. (2014) experimentally investigated a 3kWh of heat storage module for a space heating application. Figure 2.12 shows the construction of the heat storage module involving a zeolite coating on the fin-type heat exchanger adsorber. These authors using the regeneration with solar collectors in a temperature range of 80 to 120 °C and a condensation temperature of 20 to 30°C. By using 41kg of zeolite, this system could generate a heating power range of 730 to 1600W and a maximum energy content of 14.3MJ (4kWh). However, further investigation is needed as the decreasing temperature between desorption and condensation will lower the energy content. This experiment showed that a larger scale 3kWh of heating storage could increase the actual performance of a space heating system. The operating condition in this study will become a reference for researchers investigating alternative methods to improve the performance of TES systems.

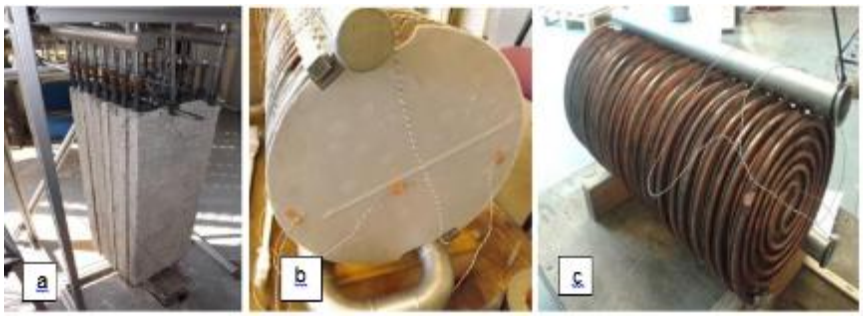


Figure 2.12: (a) adsorber/desorber unit (b) evaporator/condenser unit front view (c) evaporator/condenser unit back view (Finck et al., 2014)

There are several other studies into both open and closed adsorption systems used for various purposes as shown in Table 2.10. The materials used, storage type, method, analysis and results are shown. It is clear from the broad spectrum of usage that adsorption heat storage can be used in wide range of applications, including heat storage, air conditioning, and ice making systems. However, research and development on the use of THSS for hot water and heating applications for the building is in crucial need of being investigated due to the limited amount of previous literature on the subject.

Table 2.10: Summary of adsorption heating/cooling systems

References	Nature of research	Materials used	Concept	Application	COP	Heating/cooling storage/Energy storage density
van Essen et al. (2009)	Experimental	$MgSO_4$ Hydrate	Close sorption	Heat Storage	-	2.2 GJ/m^3
Zajaczkowski et al. (2010)	Experimental	Expanded graphite (EXG) and carbon fibres (CF)	Close sorption	Refrigeration	0.48~0.96	-
Hauer & Fischer (2011)	Experimental	Zeolite/water	Open sorption	Dishwasher	-	1.05kWh to 0.80kWh per washing cycle
Maggio et al. (2009)	Numerical	Lithium chloride –Silica gel	Close sorption	Ice-maker	0.33	daily ice production (DIP) of 20 kgm^2
Veselovskaya et al. (2010)	Experimental	$BaCl_2$ /Vermiculite	Close sorption	Air-conditioning	0.54 ± 0.01	300 to 680 W/kg Cooling
Stitou et al. (2012)	Experimental	$BaCl_2/NH_3$	Phase change & close sorption	Air-conditioning	1.5~2.3	0.8~1.2 kWh cooling
Gong et al. (2012)	Experimental	Lithium chloride –Silica gel	Close sorption	Air-conditioning	0.41	4.99 kW cooling
Ahmed (2012)	Numerical &Experimental	Silica gel/Water	Close sorption	Refrigeration	0.66	
Zondag et al. (2013)	Experimental	$MgCl_2{\cdot}6H_2O$	Open sorption	Heat Storage	12	50W heating
Li et al. (2013)	Numerical & experimental	$CaCl_2/NH_3$	Solid –gas sorption	Seasonal Storage	0.60-heat recovery 0.34 - winter	1043 kJ/kgsalt 579 kJ/kgsalt,

Alam et al. (2013)	Numerical	Silica gel/water	Close sorption	Solar adsorption cooling	0.3	10kW cooling
Hamdan et al. (2013)	Experimental	Lithium chloride & Sodium chloride	Close sorption	Chemical Heat pump	-	-
Yu et al. (2014)	Experimental	Lithium chloride/Silica gel	Close sorption	Thermal energy storage	-	108 kWh/m^3 cooling 163.6 kWh/m^3 heating
Hassan & Mohamad (2013)	Numerical	Activated carbon-methanol	Solar adsorption	Refrigeration	0.66	2.63 kg cold water at 0°C
Sadeghlu et al. (2014)	Numerical	Zeolite 13X/$CaCl_2$	Close sorption	Refrigeration	0.5	517 W/kg cooling
He et al. (2014)	Experimental	Zeolite /activated carbon	Close sorption	Refrigeration	0.25~0.35	0.2kW/L (Volumetric cooling power)
Pan et al. (2014)	Experimental	Activated carbon – $CaCl_2$/NH3	Close sorption	Refrigeration	0.197	205.2 W/kg specific cooling power/1.64 kW cooling capacity
Finck et al. (2014)	Experimental	Zeolite/water	Close sorption	Heat Storage	-	730 – 1600 W heating
Zettl et al. (2015)	Experimental	Zeolite-LiCl/$MgSO_4$ & $MgCl_2$/$MgSO_4$	Open sorption	Heat storage	-	5kWh –heating (70kg composite material)
Lele (2015)	Numerical & experimental	SrBr2·6H_2O	Close sorption	Heat storage	0.78	140 kWh/m^3

2.9 Mathematical Modelling Simplification on Thermochemical Heating/Cooling systems

The performance parameters of the adsorption heat pump that are commonly used are Coefficient of Performance (COP) and Specific Cooling Power (SCP). All the models are based on adsorption phenomena, no matter if the model is simple or complex. One of the radical equations describing adsorption phenomena is the adsorption equilibrium (Yong & Sumathy, 2002). The mathematical modelling has been reviewed (Yong & Sumathy, 2002) and in summary, most of the mathematical modelling of closed adsorption systems is commonly broken down into three models of varying complexities: i) the thermodynamic model, ii) the lumped parameters model, iii) the heat and mass transfer model. Many researchers use the thermodynamic model to investigate the overall performance of the adsorption refrigerant cycles, but in this particular research the focal point will be on the adsorption heating in the condenser section that is transferred via a heat exchanger or a heat pipe to the building. Therefore, the selection of mathematical models shall be discussed regarding the heat transfer through the condenser and evaporator sections of the system.

2.9.1 Thermodynamic Model

In most of the modelling applied to the thermochemical adsorption cycles, the thermodynamic model is the simplest, in which details of heat transfer are not considered. In this model, only first and second law analyses are performed, and this kind of model is used to reveal the high-performance limits. The first law analysis gives real clarification as to the expected performance of a cycle, and it is essential to carry out the second law analysis in order to study the quality of the process that gives the reason for the performance degradation. Most of the thermodynamic models use the

Clausius–Clapeyron equation which assists to establish a relationship between the saturated refrigerant vapour pressure and its temperature in the adsorption process.

Cacciola & Restuccia (1995) developed a thermodynamic model on a reversible adsorption heat pump. These authors started the thermodynamic model from a single bed model which was then developed into a two beds model, as illustrated in Figure 2.13. The model used two of the adsorption systems either in a heat pump or cooling operation and good heat/cold was produced during a complete cycle per kilogramme of adsorbent. The calculated COP for cooling and heating were in the range of 0.75 to 0.85. Therefore, it can be concluded that this model applies appropriately to the two adsorbent beds, especially in the reversible mode of the adsorption heat pump.

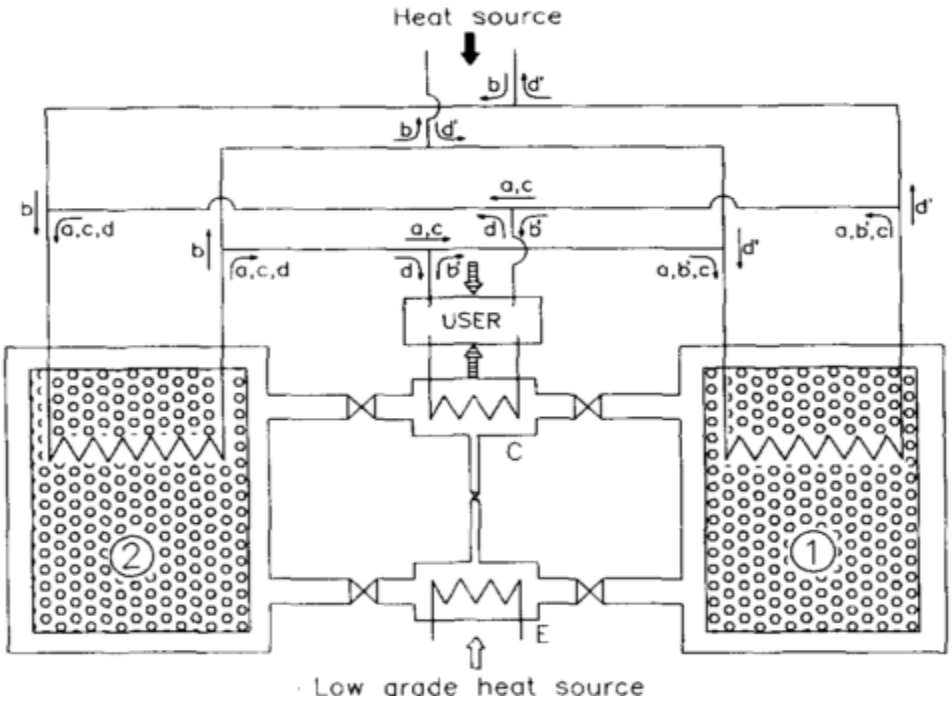


Figure 2.13. Scheme of a double-adsorber heat pump. Phases: a) regeneration b) desorption in bed 2 b') adsorption in bed 1 c) regeneration d) adsorption in bed 2 d') desorption in bed 1. Components: 1& 2) adsorbent beds C) condenser E) evaporator

Later, Restuccia et al. (2004) moved forward on improving the investigation and modelling of the selective water sorbent for solid sorption chiller. These authors modelled a prototype of adsorption refrigeration with 1 kg of dry adsorbent SWS-1L (silica gel and $CaCl_2$) granules (0.8–1.6 mm in size). A simplified model was used for a single bed including the thermal capacities of the various components and consideration of the adsorbent as a ‘‘black box’’, as illustrated in Figure 2.14. They concluded that the mathematical model of the prototype solid sorption chiller on this composite material allowed the SCP (specific cooling power) to reach up to 0.6 at a low desorption temperature of 90–95°C. However, there were some limitations which affected the COP in this model namely heat losses, the heat capacity of the inert masses and the lack of optimisation of the heat exchangers’ efficiency.

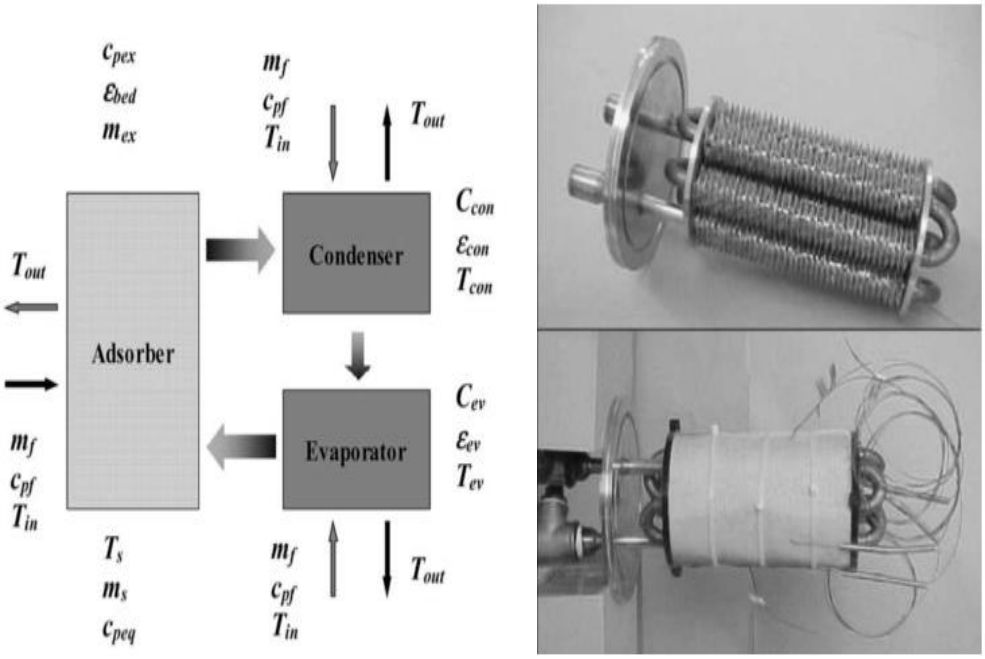


Figure 2.14: Schematisation of the studied system and the parameters considered for each component and the adsorber as developed by Restuccia et al. (2004)

Daou et al. (2008) investigated the theoretical comparison of the refrigerating performances of a $CaCl_2$ impregnated composite adsorbent with the host silica gel. The validating data is measured on a purposely-constructed single-bed basic cycle lab-scale adsorption chiller as illustrated in Figure: 2.15. The main features of these models are the SCP which is defined as cooling power yielded by the evaporator per unit mass of adsorbent and over the half cycle time of adsorption operation and the mass ratio of normal silica gel. By using this model, these authors found that the maximum COP value was 0.62 and that there was a good agreement between experimental and theoretical results. However, low COP obtained from this investigation due to the system is not designed to enhance heat and mass transfer, and it was a conventional lab-scale adsorption chiller. Therefore, improvement in the modelling and design of the system needs to follow to achieve higher COP and to improve the design of the heat and mass transfer in the systems for real applications.

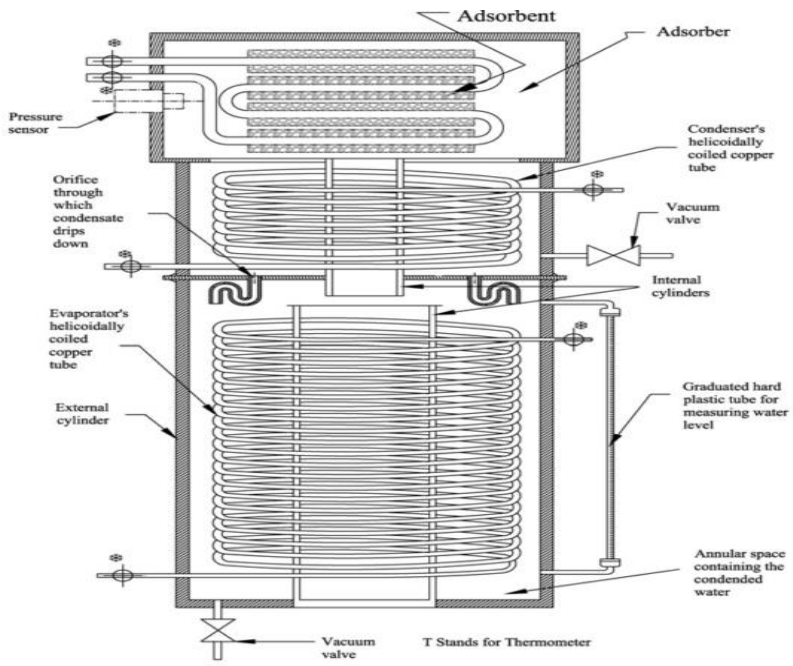


Figure: 2.15: Experimental rig with the different instruments used for measurement.

2.9.2 Lumped Parameter Model

The lumped parameter model is a predictive model for two adsorbers/reactors/adsorbent beds. These models assume that each component of the systems, such as the adsorber, evaporator, and condenser are homogeneous. However, this model is limited appropriately to a water falling films evaporator and water condenser heat exchangers. In Douss & Meunier's (1988) study, numerical instabilities occurred especially in small time steps. Cho and Kim (1992) executed theoretical and experimental studies on the recovery of a low-grade waste heat using a silica gel/water adsorption cooling system. From their simulation, these authors estimated the overall heat transfer coefficient for the three components (adsorber, condenser, and evaporator) from the measured flow rate and temperature. They found that the thermal performance of the system predicted by this numerical model had shown good agreement with experimental data.

Sami & Tribes (1996) conducted a study on improving the lumped parameter model to predict the dynamic performance of adsorption cycles with heat recovery. These authors aimed to predict the performance of air-cooled evaporators and condenser-type heat exchangers and have added new submodels. From their experimental data it can be said that their model predicts the dynamic performance of adsorption systems well, and there appears to be good agreement with the experimental data.

Cacciola et al. (1999) reported a simplified dynamic model in integral form, to evaluate the performance of an adsorption heat pump when heat transfer in the adsorbent reactors is the only cycle time limiting factor. The main aim for this study is to investigate the effect of an increasing amount of metal in the adsorbent bed and the

COP of the specific power. These authors reported that an improvement in heat transfer is achieved by increasing the metal content of the adsorber bed, but may result in a reduction in the COP and can eventually increase the investment cost per watt obtained. Therefore, it is crucial these important factors are considered when the effort is made to increase the heat transfer in the reactor beds. It is a useful method for comparison of different strategies, for improvement of the performance and improvement of economic feasibility of heat pump systems.

Wang & Chua (2007) investigated and improved a lump-parameter design model to study the water circulation heat recovery scheme as applied to two-bed silica gel water adsorption chillers (see Figure 2.16). The improvements to this model were the emblematic temperature trends typically found in the switching phase the chiller operation, a loophole which the previous model overlooked. They claimed that the previous model overestimate the system response time and the temporal hot water outlet temperatures which would be over predicted the chiller COP. They concluded that the lump-parameter model could clearly explain the water circulation heat recovery scheme just like the distributed-parameter model.

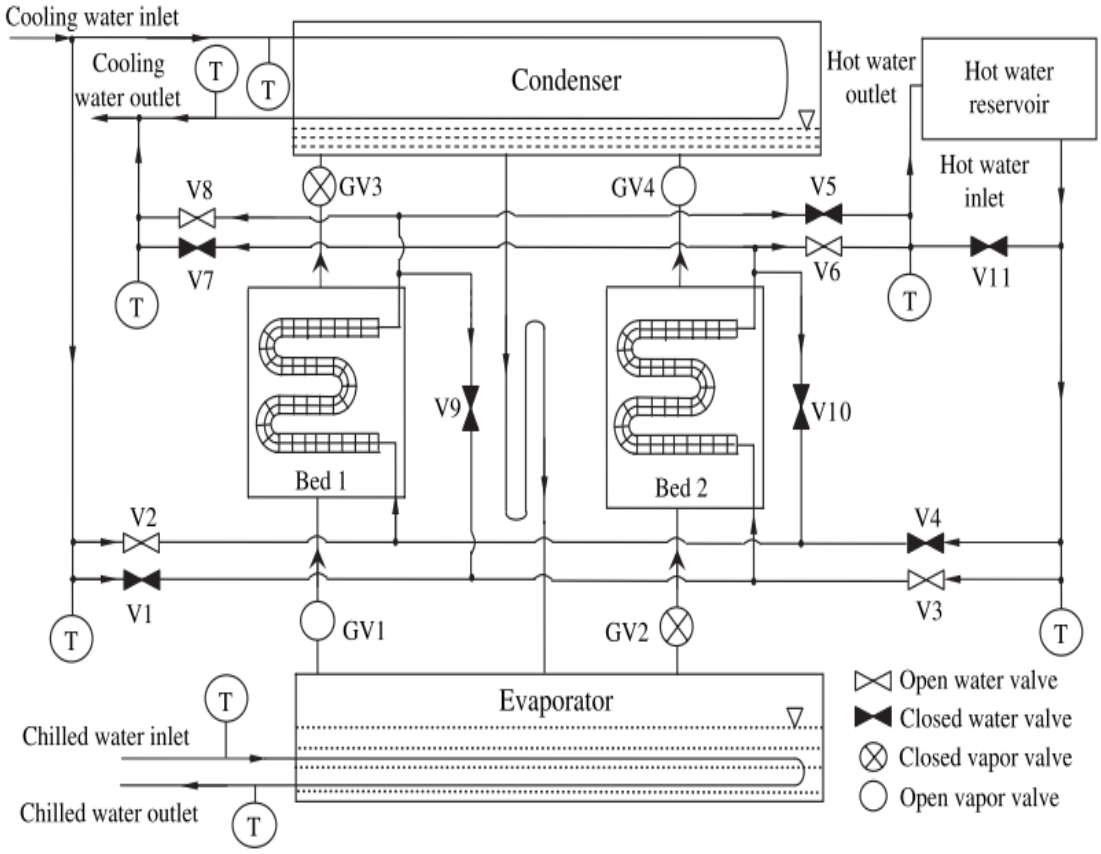


Figure 2.16: A schematic of a two-bed silica gel/water adsorption chiller manufacture by Nishiyodo Kuchouki Co

Zhang et al. (2011) developed a simulation of the operating characteristics of the silica gel–water adsorption chiller powered by solar energy. A lumped-parameter model was introduced for the operating characteristics investigation by using programming tools Matlab/Simulink. From their simulation results, they found that when the chiller was by solar energy, the open flow of the hot water with a short cycle time and the closed flow of hot water with a longer sequence time were better. Based upon this review, most of the researchers used a lumped-parameter model due to its simplicity and its easy integration with any numerical software system.

2.9.3 Heat and Mass Transfer Model

Heat and mass transfer models are models in which the temperature or mass content of the adsorbate varies not only with time but also with space, and the governing equations are always partial differential equations. As such, it is necessary for optimum design of adsorption machines. Based on the geometry of the adsorber, the models can be grouped into one-dimensional, two-dimensional, and three-dimensional models. The complexity and linearity of heat and mass transfer models excludes the possibility of having an analytical solution. Hence, an alternative numerical method is needed to meet the requirements for simulation of adsorbent bed dynamics (Yong & Sumathy, 2002). The simplified mathematical models are summarised in Table 2.11.

Table 2.11: Summary of mathematical models used by different authors.

Ref	Open/ Close	TCM working pairs	Equation			Results/Comments
			Heat/Mass balance equation	Energy balance equation	Adsorbent equilibrium relationship	
Thermodynamic Models						
Cacciola & Restuccia (1995)	Close	Zeolite (13X and 4A type)/water	-	Energy supplied to evaporator $Q_e = m_{z=(w_{\max} - w_{\min})}\left[L(T_e) - \int_{Te}^{Tc} Cp1\,(T)dT\right]$	$\ln(p) = a(w) + b(w)/T$	Evaporation temperature Te=5°C, adsorption and condensation temperature Ta = Tc = 40 °C. Zeolite/water is the most suitable pair to be used in domestic applications in southern European countries.
Restuccia et al. (2004)	Close	Composite of zeolite + $CaCl_2$ + water (SWS)	-	$\left[\dot{m}_f C_{pf}\left(T_{f-\frac{con}{ev}} - T\right)\right]_{con/ev} = \left[\dot{m}_f C_{pf}(T_{in} - T_{out})\right]_{con/ev}$	$\ln(p) = a(w) + b(w)/T$	The cooling COP is 0.6 at low desorption temperature (90-95°C). Low specific power of the tested device is due to the unoptimised design of the adsorber heat exchanger and grain shape of the adsorbent.
Daou et al. (2008)	Close	Silica gel/Calcium chloride (composite adsorbent)	-	Adsorption heating: Clausius – Clayperon relationship	Dubinin-Astakhov model	The half cycle time reduced to the optimal value of 50 minutes. A maximum COP value of 0.62 is predicted if the composite adsorbent used in a single bed system.
Lump Parameter Model						
Cacciola et al. (1999)	Close	Zeolite/water	-	$Q_{co} = m_a[(w_b - w_e)L(T_{co})] + \int_{T_b}^{T_e} \frac{dw}{dt} C_{pav}(Tz - T_{co})dT_Z$	$\ln(p) = (A_0 + A_1 w + A_2 w^2 + A_3 w^3) + \frac{(B_0 + B_1 w + Bw^2 +}{T}$	Improvement in heat transfer by increasing the metal content of the adsorber bed may result in a reduction in the COP and can eventually increase the investment cost per watt obtained.

Wang & Chua (2007)	Close	Silica gel/water	-	$\rho_f c_{vf} \frac{V_{con}}{N_2} \frac{dT_K}{dt} = \frac{dMcooling}{dt} [h_f(T_{K-1}) - h_f(T_K)] + u_{cooling} \frac{A_{bed}}{N} (T_{bed,i} - T_K)$	Linear driving force $\frac{dq}{dt} = 15 \frac{D_{so} e^{\frac{-Ea}{(RT)}} (q^* - q)}{R_{p^2}}$	Favourable agreement with the experimental data at assorted operating conditions. Lump-parameter model can clearly explain the water circulation heat recovery scheme just like the distributed-parameter model.
Zhang et al. (2011)	Close	Silica gel/water	-	$\frac{T_{ad,out} - T_b}{T_{(ad,in)}} = exp\left(\frac{-KA_{ad}}{\dot{m} \cdot c_{p,w}}\right)$	Non-equilibrium adsorption rate equation $\frac{d_x}{d_\tau} = \frac{15 D_{so} exp[-E_a/(RT_b)}{R_P^2} - x)$	The heat source and the initial temperature will influence the performance of the systems.
Heat And Mass Transfer Model						
Tatlıer et al. (1999)	Close	Zeolite/water	$-k_z A_r {}^{\partial T_z}/_{\partial_r} = h_{ou} A_r (T_z - T_{at}) + F c_{pz} (T_z - T_{at})$	$({}^1/_r)\left({}^{\partial T}/_{\partial r^2}\right) + {}^{\partial^2}/_{\partial r^2} = ({}^1/_\infty)\left({}^{\partial T}/_{\partial t}\right)$	$D_{ae} = 1.31x10^{-9} e^{-\frac{680.7}{T}} (\frac{m^2}{s})$	The zeolite is synthese as a continuous layer on heat exchanger tubes.
Dawoud et al. (2007)	Close	Zeolite/water	$\frac{\partial \rho}{\partial t} = -\frac{\partial \dot{m}_{v''}}{\partial z}$	$\frac{\partial}{\partial t}\left(\rho zeo(x) \cdot \mu(x,T) = \frac{\partial}{\partial_z}\left(\lambda \cdot \frac{\partial T}{\partial z}\right)\right) - \frac{\partial}{\partial_z}(\dot{m}_v \cdot h_v)$	$D_0 = D_\infty \cdot \exp\left(-E_a/(R_m \cdot T)\right)$	Heat transfer is by conduction. A constant micropore diffusion coefficient is only capable of describing the diffusion in the low concentration region (below 5 g/100 g).
Hu et al. (2009)	Close	Zeolite/H_20		(Wang Q, 2001)		With the increase of cycle time, the capacities of adsorption and

				$(\rho_s c_{p,s} + \varepsilon\rho_A C_{pA} + \rho_s x c_p)\frac{\partial T}{\partial t} = \lambda_a\left(\frac{\partial T}{r\partial r} + \frac{\partial^2 T}{\partial}\right) + \rho_S \Delta H \frac{\partial x}{\partial t}$	$x^* = x_0 \exp\left[-k\left[\frac{T}{T_S} - 1\right]^\gamma\right]$	desorption tend to reach equilibrium gradually.
Wu et al. (2009)	Open	Silica gel/$CaCl_2$/water	$h_m = \frac{15D_s}{R_{P^2}}$	Heat and mass balance = $m_a\, c_{p,a}\, \frac{\partial T_a}{\partial t} = -m_a\, c_{p,a}\, \frac{\partial\, T_a}{\partial\, x} + k_a\, A_a \left(\frac{\partial^2 T_a}{\partial x^2} + \frac{\partial^2 T_a}{\partial y^2} + \frac{\partial^2 T_a}{\partial z^2}\right)$	$D_s = \frac{1}{\xi}\, D_{s,0}\, \exp\left(-\frac{Q_s}{RT}\right)$	TES capacity and the COP of the system depends on the ratio between the total heat input to the total heat released from the adsorber.
Niazmand & Dabzadeh (2012)	Close	Silica gel water	Mass balance model $\epsilon_t\, \frac{\partial \rho_g}{\partial t} + \vec{\nabla}.(\rho_a) + (1-\epsilon_t)\rho_s \frac{\partial \overline{w}}{\partial t} = 0$	Fins energy balance= $\rho_{fin}\, cp_{fin}\, \frac{\partial T_{fin}}{\partial t} = \frac{1}{r}\frac{\partial}{\partial r}\left(r\lambda_{fin}\frac{\partial T_{fin}}{\partial r}\right) + \frac{q"_1}{\delta} + \frac{q"_r}{\delta}$	Linear driving force $\frac{\partial \overline{w}}{\partial t} = \frac{15D_s}{(d_p/2)^2}\,(w_{eq} - \overline{w})$	By increasing the fins' number, decreasing the height and reducing the cycle time, the total cooling power will increase.

2.10 Heat and Mass Transfer Enhancement of an Adsorption Bed/Reactor

Among the three components (adsorber, evaporator, condenser) used in adsorption refrigeration or heating systems, only the adsorber/adsorbent bed is of particular interest, while the others are similar to conventional adsorption systems. The recognised drawback of a solid/vapour adsorbent bed is the poor heat transfer. The heat and mass transfers have critical roles in improving the cycle performance, and their optimisation is one of the technical challenges to face in progressing adsorption refrigeration systems. To optimise an adsorber, it is essential to control these limiting factors (Wang et al., 2005). Some of the enhancement methods that have been studied in previous investigations are a fin type adsorbent tube, an embedded adsorbent bed with a metal foam, a consolidated adsorbent, an adsorbent coating, and a multi-tube adsorbent coating.

2.10.1 Fin Type Adsorbent Tube Module/Heat Exchanger

A fin type heat exchanger is applied for heat transfer for cooling and heating systems, such as in the radiator of an automobile cooling system or an evaporator coil for the air-conditioning. The idea of using a heat exchanger as the adsorber tube is to increase the heat transfer surface areas so the heat adsorption from the adsorbent material will easily transport to the fins of the heat exchanger. However, this method involves parameters that need to be optimised, such as the fin pitch and fin length which may affect heat and transfer in the adsorbent bed. Kubota et al. (2008) investigated the cooling output performance of a prototype adsorption heat pump with fin-type silica gel tube module (FST) (Figure 2.17) to enhance the heat and mass transfer rate in the absorber bed. The advantage of using this method is not only improving high heat transfer rate but also high water vapour permeability of the packed bed through the stainless steel mesh. They developed a prototype adsorption heat pump, equipped with the optimised fin-type silica

gel tube (FST) module. The systems are manufactured and operated under various regeneration temperatures, adsorption/desorption times and pre-heating or pre-cooling time conditions. These authors did a numerical and experimental analysis of this system and found that the maximum cooling output was 3.12 kW. From this investigation, the authors concluded that this prototype AHP (adsorption heat pump) system could operate by using thermal energy of 333–353K as a regenerative heat source of silica gel, and this system could continuously generate chilled water at 283K or lower for air conditioning. This investigation put emphasis on using a variable number of fins, fin pitches, and fin lengths to create a surface area ideal for enhancing the heat and mass transfers. However, there were some limitations to the process at the desorption stage, where the adsorber pressure became higher than the average pressure in the condenser, caused by the restriction of the condenser's cooling capacity. Therefore, more improvements need to be made to resolve the problems associated with high pressure build up in the adsorber, hence thus improving the cooling capacity of the systems.

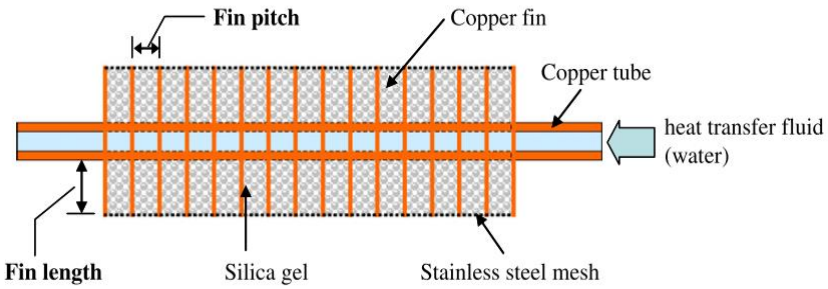


Figure 2.17: Fin type adsorber heat exchanger

Veselovskaya & Tokarev (2011) studied novel ammonia sorbents with a ‘‘porous matrix modified by active salt” for adsorptive heat transformation, with the testing on the “$BaCl_2$/vermiculite” composite in a lab-scale adsorption chiller. The idea of using vermiculite was to increase the mass transfer, a possibility due to its microporous

structure and to prevent the agglomeration of the salt. The adsorbent was placed in the plate heat exchanger as the adsorbent generator (see Figure 2.18). From this investigation, they found that the theoretical estimation of adsorbent kinetics fitted well with the experimental results giving a COP of 0.54 and a SCP ranging from 300 to 680 W/kg. Thus they suggested that the proposed methods and composite material could effectively apply to low energy heat regeneration (80°C-90°C) cooling systems. The reasoning for using a plate heat exchanger is to increase the area of heat transfer in the adsorbent generator. Furthermore, use of a metal plate may increase the thermal conductivity, and hence enhance the performance of the adsorption chiller.

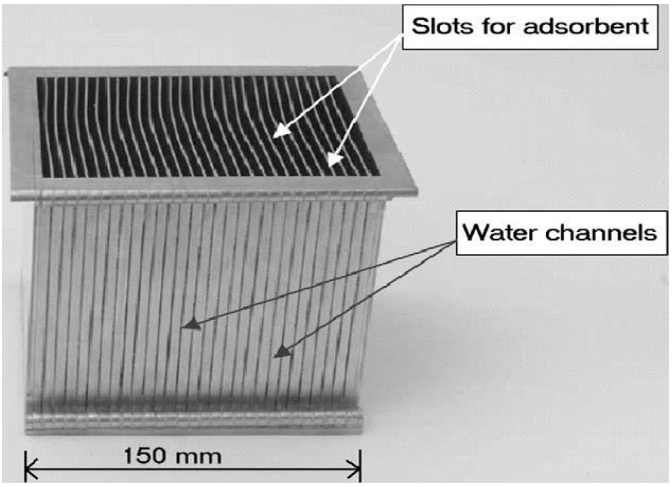


Figure 2.18: Plate heat exchanger generator design

Another similar approach is to use the heat exchanger as a medium for enhancing the heat and mass transfer in the adsorbent bed, as done by Aristov et al. (2012). This investigation primarily placed emphasis on the reallocation of adsorption and desorption times for optimisation of cooling cycles. These authors used a new composite, $LiNO_3$/silica KSK (SWS-9L)/water sorbent, and specifically synthesised it for adsorptive chilling units driven by low-temperature heat (65-75°C). Composite SWS-9 was

synthesised by impregnation of a dry commercial silica KSK into a saturated aqueous solution of $LiNO_3$. 350g of sorbent grains 0.25-0.50 mm in size were embedded inside a compact heat exchanger of a finned flat-tube type (aluminium) (Figure 2.19). From the prototype investigation of the systems, the study found that with the adsorption phase extended in duration by half, the desorption phase will be shortened. Practical recommendations were also suggested to reallocate the length of adsorption and desorption phases rationally.



Figure 2.19: Overall (right side) and detailed (left side) view of the A-HEX tested by Aristov et al. (2012)

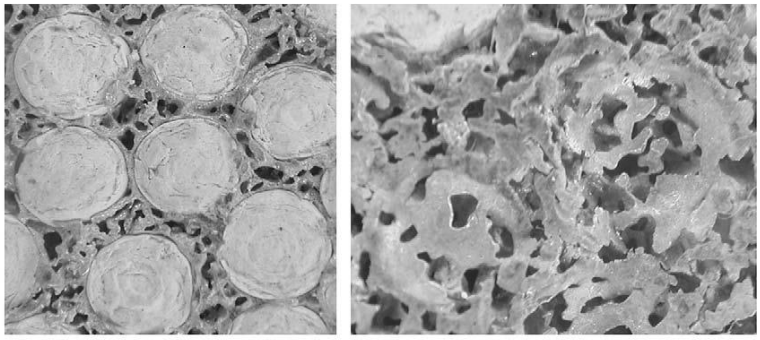
Apart from using the heat exchanger to increase the heat and mass transfer, these authors had also extended the study to investigate optimisation of the grain layers of the composite materials (Aristov et al., 2012). They have recommended that the adsorbent grains have to be small enough to reach “grain size insensitive” mode, but still need to be sufficiently large to avoid the pressure gradient along the layer. The advantage of this method is that the heat transfer area could be increased with the use of conventional heat exchanger fins. Furthermore, the adsorbent material will be easier to be fill up between the fins or by coating the fins within the adsorbent. However, a limitation of this method

could be that the amount of mass of the adsorbent would be limited to the size of the heat exchanger. Therefore, the scale of the heat exchanger would affect the performance of the adsorbent systems. Another limitation could be the granule size of the adsorbent material used to fill up the fins; the granule size needs to be small enough to fit into the spaces between the fins. Conversely, the granule size would also have to be the optimum size to be at its most efficient for the heat and mass transfer in the adsorbent bed/adsorber. Thus, extensive experimental studies and models need to be developed to validate the design and additional research data needs to be collected for adsorption refrigeration and heating systems

2.10.2 Embedded Adsorbent Bed with Metal Foam

Another method of enhancing the heat and mass transfer in the adsorbent bed or adsorber is by using an embedded adsorbent material with metal foam. The main idea of this approach is to increase the thermal conductivity by using a metal that is higher than the adsorbent material itself. Many researchers have chosen aluminium foam as the metal embedded in the adsorbent material. This is because aluminium is less corrosive than other metals when embedded with the adsorbent materials. Hu et al. (2009) embedded a composite of zeolite and salt (NaCl) (Figure 2.20) with aluminium foam to improve heat and mass transfer of automobile air-conditioning. This study used the hot-wired method to measure the effective thermal conductivity of the composite material, giving a reading of 2.89 W/mK. With the increase in cycle time, the capacities of adsorption and desorption tend to reach equilibrium gradually, with the COP of thicker adsorbents getting higher because of the effect of the heat capacity of the tube. The study concluded that the composite zeolite/foam aluminium can improve the values of the COP (0.1 to 0.6) and SCP (50 to 650 W/kg) greatly at short cycle time compared with

zeolite/water systems. However, the application of this investigation is targeted to automobile air-conditioning, and as in this case the regeneration of the adsorbent bed mainly derived from the waste heat of the engine, it would be difficult to predict the results within the actual system performance of an adsorption air-conditioning/heating system for buildings.



(a) Surface of composite zeolite/foam aluminum (with zeolite particles)

(b) Surface of composite zeolite/foam aluminum (without zeolite particles)

Figure 2.20: Composite material of zeolite/foam investigated by Hu et al. (2009).

Another similar investigation which involves aluminium foam embedding with zeolite was carried out by Bonaccorsi et al (2013). This study puts emphasis on the method of using hydrothermal and microwave synthesisers and found that the microwave synthesising was much faster than the conventional synthesising, though this does not detrimentally affect the small pore molecular sieve zeolite (SAPO 34& SAPO 44) coating. On the other hand, Bonaccorsi et al. (2013) had also conducted a study on using graphite foam as an alternative to metal foam with zeolite SAPO 34 as the adsorber heat exchanger. The experimental procedure is carried out by changing the porosity percentage of graphite foam, the specific area, and the density. They found with a percentage porosity of 85% the thermal conductivity could be improved by 24 W/m^2K which is much higher than that of aluminium foam. The advantage of using this method is that the thermal conductivity

increased and thus increases the heat and mass transfer in the adsorbent bed. However, this approach could have its limitations due to porosity size of the embedded adsorbent bed. This phenomenon might be due to the adsorbent materials fill in the void area of the foam. As a result, the porosity size might become smaller and affect heat and mass transfer in the adsorbent bed. The tailoring of the embedding metal foam needs to be evaluated in order to have the maximum size of porosity to enable more efficient heat and mass transfer in the system.

2.10.3 Consolidated Adsorbent

A consolidated adsorbent is the compression of the prepared composite material to become a compact composite block. Wang et al. (2005) have reviewed this technology over the course of the last two decades since it was originally introduced in the application of adsorption systems. From their review, they claim that the thermal conductivity and wall heat transfer coefficient has been largely enhanced through the consolidated adsorbent. Li et al. (2009) studied the heat transfer and sorption characteristics of a consolidated composite sorbent for solar-powered thermochemical cooling systems. The working pair for this investigation was a consolidated composite sorbent made from barium chloride ($BaCl_2$) and expandable graphite type mesh 80 (see Figure 2.21). The experiments put emphasis on the effectiveness of heat and mass transfer in the systems alongside the working temperature and working pressure that showed that the rate of total conversion was very sensitive to the working temperatures and pressures. The experimental result indicates that the composite sorbent can utilise solar energy or a low-grade waste heat source with a temperature ranging from 75 to 90°C effectively, and that the consolidated composite block with an apparent density of 250 kg/m^3 could incorporate 0.61 kg of ammonia per kg of the reactive salt. Furthermore, they assessed the COP

obtained with the consolidated composite sorbent and found that it varied between 0.50 and 0.53 when the evaporation temperature ranged from 0° to 15°C, with a regeneration temperature of 80°C, which is suitable for the solar-powered thermochemical ice-making application.

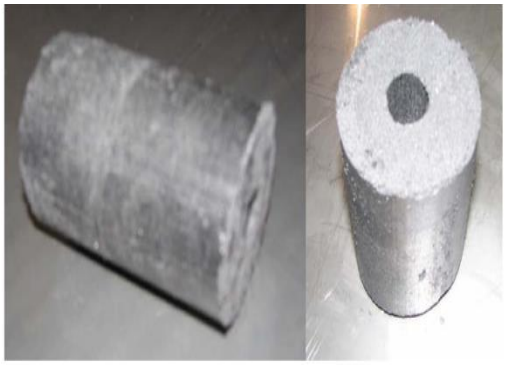


Figure 2.21: Consolidated composite block

Li et al. (2009) had previously conducted a similar investigation using manganese chloride $MnCl_2$ as a chemical to consolidate with the composite block. They found that the average SCP varied between 200W/kg and 700W/kg when the evaporation temperature ranged from -35°C to 0°C, and that the COP was 0.34 at the generation temperature of 180°C. Both experiments have a similar methodology, but the heat source for the $MnCl_2$ is much higher than that needed for $BaCl_2$ (180°C and 80°C respectively.) This result indicates that the heat source for the $MnCl_2$ should regenerate with the main heat source, and therefore a low-grade heat such as an underground heat source may not be suitable. A limitation of this technology is that a compressed composite is subjected to excessive mass transfer resistance corresponding to lower evaporating pressure. In the case of low operating pressure fluids like water or methanol, mass transfer limitations appear to be critical and need huge numbers of pores to be introduced within the adsorbent or in an adsorber, which may make the adsorbent materials more

expensive (Wang et al., 2005). From this review, it can be concluded that further investigation is required to develop a more efficient and inexpensive method to adopt in the long-term.

2.10.4 Adsorbent Coating

Many researchers have studied the use of an adsorbent coating on heat exchanger metal fins, pipes or in metal foam. This type of adsorbent bed or adsorber could generate a high speed of heat and mass transfer rate. Furthermore, diffusion in the adsorbent is accepted as the primary mechanism of mass transfer since there is no void in coated adsorbents. Liu et al. (2009) investigated the impact of adsorbent finishing and absorbent filming on exchange energy efficiency of an air-to-air cellulose fibre heat and mass exchanger of an open sorption cooling systems. The solid desiccant of a $CaCl_2$ coating on the cellulose fibre membrane was compared with a film of the liquid adsorbent of LiCl. A clear membrane is also considered in the heat and mass transfer investigations in their study (see Figure 2.22). Experimentally, this investigation indicated that both methods have potential for improving energy (enthalpy) exchange efficiency, particularly the moisture transfer efficiency of the exchanger. However, they claimed that a major difficulty is the complexity of the liquid desiccant that may be carried away by the passing airstreams, which may have adverse impacts on occupant health and air quality. Thus they suggested that adsorbent finishing is a more suitable option for improving the energy exchange of the exchanger, although its efficiency was lower than that of the absorbent filming. This research will contribute to the knowledge of coating the cellulose fibre membrane as a means of improving the performance of heat and mass transfer for open sorption systems. Detailed explanations and improvement of theoretical modelling will

entail having more reliable and validated research data alongside the experimental results.

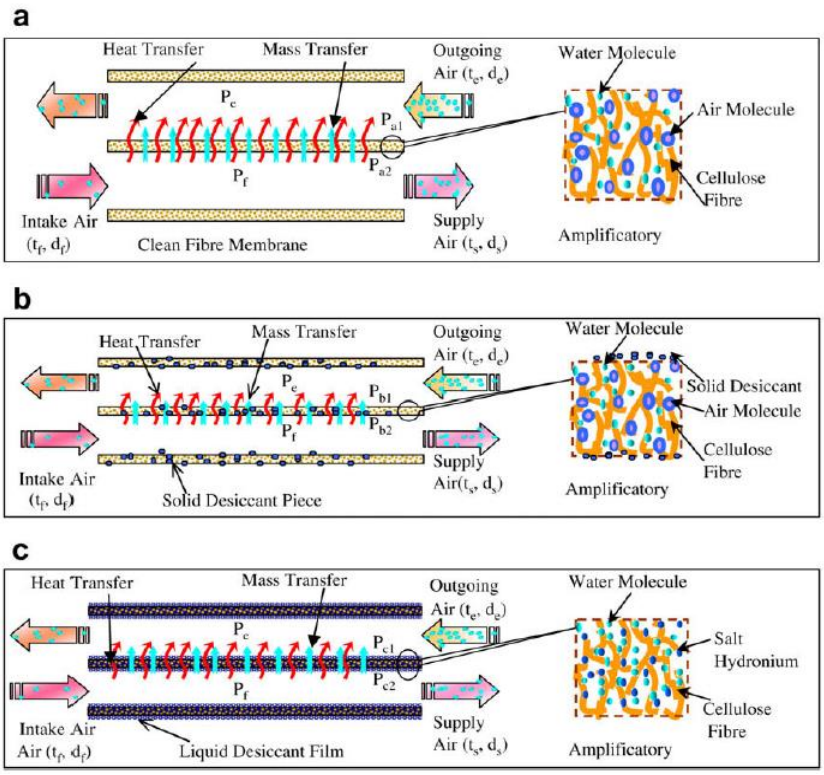


Figure 2.22: Schematic diagram of three types of cellulose fibre membranes (a) Clean fibre membrane (b) Solid desiccant-coated fibre membrane (c) Liquid desiccant-soaking fibre membrane (Liu et al., 2009).

Another method of adsorbent coating application is closed adsorbent coating, as done by Schnabel et al. (2010). The authors investigated different phenomena, namely the adsorption kinetics of zeolite coatings directly crystallised onto metal supports for heat pump applications (Figure 2.23). From these studies they found that the heat transfer resistance of the crystal and the metal layer of the zeolite A and X coatings seemed to be lower than that of the reference sample, whereas the open pore structure of the zeolite X sample reduced the effective conductivity of the layer. Later, Bonaccorsi et al. (2013) investigated and synthesised a zeolite coating on stainless steel copper and aluminium

heat exchanger fins using a method of in situ continuous growth (see Figure 2.24). From this investigation, they found that there were a few possible factors which would affect the performance of adsorption heat pumps such as the coating thickness, adhesion, and protective action. A similar study into the adsorbent kinetic investigation was carried out by Dawoud (2013) who found that the COP of the heat pump module increases almost linearly with increasing zeolite layer thickness or the coated zeolite mass, but with slower adsorption kinetics.

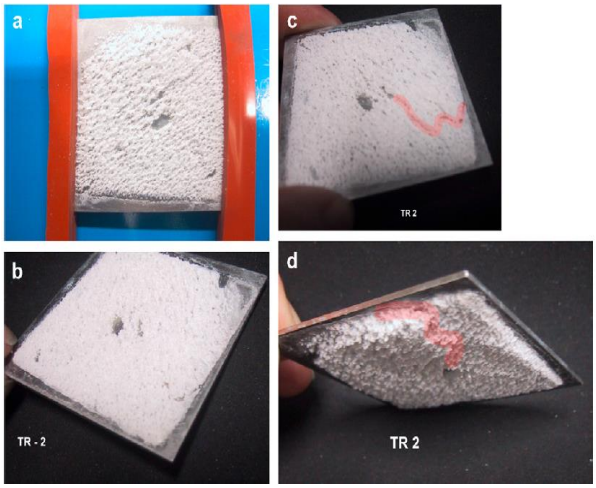


Figure 2.23: Pictures of the zeolite X coating (a) before and (bed) after the kinetic measurement, as investigated by Schnabel et al. (2010)

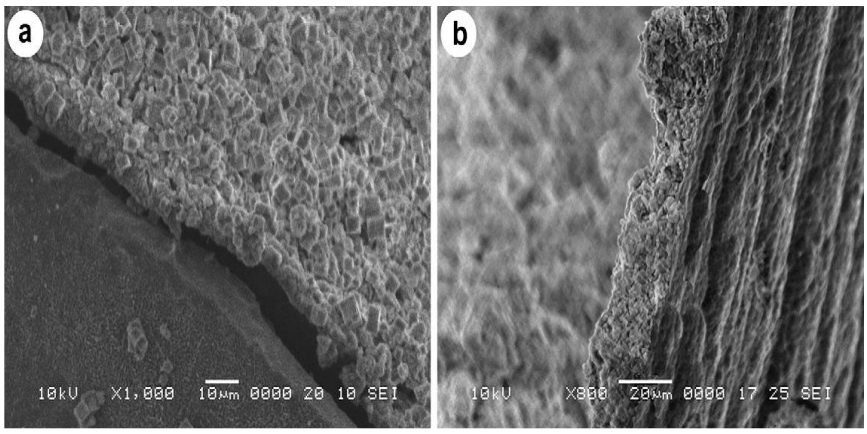


Figure 2.24: Zeolite SAPO on stainless steel (a) and aluminium (b) (Bonaccorsi et al., 2013).

Another similar approach on using a coating of zeolite was studied by Atakan et al. (2013), with their study investigating adsorption kinetics and isotherms of zeolite coatings directly crystallised onto fibrous plates for heat pump applications. They found that high contact areas provided by the zeolite and metal and the use of copper might be useful for improving heat transfer while the thickness of the zeolite coating should be at the optimum thickness to make sure that the stability of the coating is not compromised. From these results they concluded that the direct crystallisation of zeolite on porous metal fibrous plates might favour the stabilities of zeolite coatings, besides their heat transfer properties.

2.10.5 Adsorbent with Multi Cooling Tubes

Another method used for enhancing the heat and mass transfer is by using multiple cooling tubes filled with the adsorbent materials. Technically, this method is similar to the adsorbent in the heat exchanger fins. Conversely, this technology is using multi-cooling tubes instead of fins. Wang & Zhang (2009) investigated the design and created a performance prediction of an adsorption heat pump with multi-cooling tubes. The method used was to fill the multiple adsorber cooling tube with silica gel, as shown in Figure 2.25. The mass of the adsorbent filled each adsorber of the AHP (adsorption heat pump). The cooling capacity of the AHP is 2.5 kW with the driving heat source temperature of 85°C. It was found in the results that the COP and the SCP of the designed AHP are 0.5 and 85W/kg respectively. However, they found that by increasing the hot water temperature, the systems became less effective. Furthermore, they suggested that if adsorption technology is brought forward into practical applications, the easier manufacturing process needs to be considered. They had also pointed out that the wall thickness of the metal sheet of the cooling tube is vital to the heat capacity of the metal. Consequently,

they have suggested that a thin metal sheet is necessary in the manufacture of the cooling tubes.

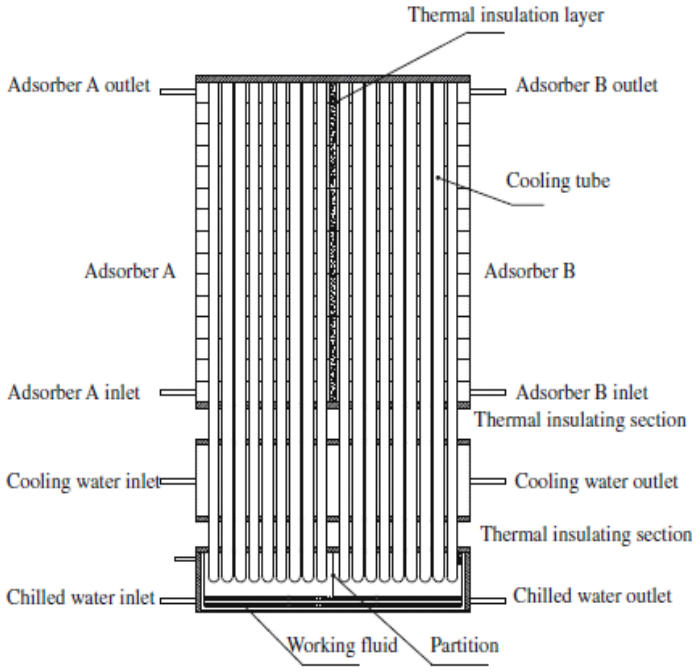


Figure 2.25: Adsorption heat pump with multiple cooling tubes by (Wang and Zhang, 2009).

A novel solar adsorption cooling tube has been developing by Khattab et al. (2012) for the application of ice-making as illustrated in Figure 2.26. The authors used carbon and methanol as the working pairs for the refrigeration. Their experimental results show that the tube performance on sunny days in winter is as efficient as performance on summer days (7kg /m^2 ice is produced), and on cloudy winter days about 4 kg/m^2 of ice is produced. They also claimed that cooling of more than 7 kg/m^2 of water would cool the

water to 10°C, which may indicate that this technology is suitable for the air-conditioning system.

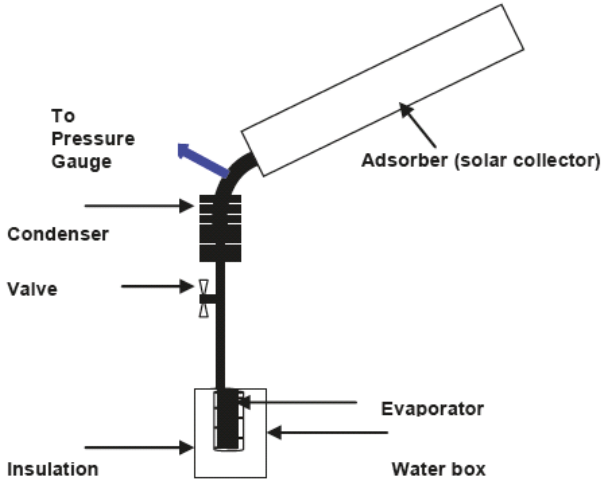


Figure 2.26: Adsorption solar tube (Khattab et al., 2012)

2.10.6 Summary Heat and mass transfer enhancement techniques

It is crucial that heat and mass transfer enhancement techniques are investigated in a Close Thermochemical Heat Storage System.

Table 2.12 summarises different techniques that have been used by previous researchers to achieve the high energy storage density, the SCP and the COP of the systems.

Table 2.12: Summary of heat and mass transfer enhancement techniques

Ref	Open/Close Sorption	TCM working pairs	Nature	Regeneration temperature (°C)	Techniques	Application/ Results/Comments
Fin type adsorbent tube Module/heat exchanger						
Kubota et al. (2008)	Close	Silica gel/water	Experimental & theoretical	(59.85-79.85)	Fin type silica gels tube module	Cooling output per unit absorber doubled. Maximum cooling output 3.12 kW achieved under the operation conditions.
Dawoud et al. (2007)	Close	Zeolite/water	Experimental & theoretical	100	Consolidate zeolite layer with heat exchanger	Cell wall heat transfer coefficient ($\propto_w$) of 230 W m^{-2} K^{-1}, a micropore diffusion coefficient at infinite temperature (D∞) of 1.58 X 10^{-4} m^2 s^{-1} and an activation energy (E_a) of 32.41 kJ mol-1
Veselovskaya et al. (2010)	Close	Composite $BaCl_2$/vermiculite /NH_3	Experimental	90	Composite adsorbent material slotted in the heat exchanger fin/plate	Low potential heat source (80–90 °C) giving a COP of 0.54 and a SCP ranging from 300 to 680 W/kg.
Riffel et al. (2010)	Close	Silica gel/water& zeolite/water	Experimental & theoretical	Silica gel (65-90) Zeolite (70-90)	Fin type heat exchanger embedded with silica gel/zeolite	The conductivity (λ) of zeolite is higher than silica gel at 0.4 & 0.3 W/m.K respectively. Heat transfer coefficient of silica gel is higher that zeolite *(h)* (330 & 269.3 W/m^2 K)

Aristov et al. (2012)		Silica gel/water	Experimental	80°C	Layers of loose grains (with *n* layer) (*n*=1, 2, 4, and 8) located on a heat transfer metal support.	Cycle powers of prototypes are 2-6 times lower than those measured in LTJ (Large Temperature Jump) test.
Jiang et al. (2014)	Open	Silica gel/water	Experimental & theoretical	cooling	Composite silica gel coated heat exchanger (CCHE).	CCHE has better dehumidification performance compared with SGCHE (silica gel coated heat exchanger.
Consolidated Adsorbent						
Li et al. (2009)	Close	$BaCl_2$ /NH_3	Experimental	75 to 90	Expanded graphite composite consolidated with $BaCl_2$.	The COP obtained with the consolidated composite sorbent varied between 0.50 and 0.53 when the evaporation temperature ranged from 0 to 15°C and at a generation temperature of 80°C the density of 250 kg m^{-3} (composite block) could incorporate 0.61 kg of ammonia per kg of the reactive salt.
Li et al. (2009)	Close	MnCl/NH_3	Experimental	180	Expanded graphite composite consolidated with $MnCl_2$.	SCP varied between 200Wkg^{-1} and 700Wkg^{-1} when the evaporation temperature ranged from -35°C to 0°C, COP of 0.34

						at the generation temperature of 180 °C, the heat sink temperature of 25°C and the evaporation temperature of 30° C.
Adsorbent material embedded in metal foams						
Hu et al. (2009)	Close	Zeolite/H_20/NaCl	Experimental & theoretical	-	Zeolite embedded with aluminium foams with NaCl distributed in between the zeolite.	Zeolite/foam, aluminium thickness 5 mm and cycle time 8 min, the SCP reaches the maximum value 641 W/kg with the COP 0.24. Automobile air-conditioning application.
Bonaccorsi et al. (2013)	Close	Zeolite/water	Experimental	-	Zeolite embedded with aluminium foams	Synthesis using microwaves was much faster compare to the hydrothermal method.
Bonaccorsi et al. (2013)	Close	Zeolite/water	Experimental	-	Zeolite embedded with graphite foams	The thermal conductivity of a graphite foam of 85% porosity was 24 W/m K.
Adsorbent Coating						
Liu et al. (2009)	Open	$CaCl_2$/water	Experimental & theoretical	-	$CaCl_2$ coated the fibre membrane and $LiCl_2$ filming the fibre membrane.	Improvement on energy (enthalpy) exchange efficiency, particularly moisture transfer efficiency of the exchanger.
Schnabel et al. (2010)	Close	Zeolite A& X/water	Experimental & theoretical	95	Zeolite coatings directly crystallised on metal supports.	Directly crystallised sample exhibited a better performance of at least up to 85% of final loading and heat rejection,

						compared to the reference sample consisting of a polymer-zeolite structure glued on the metal support.
Ge et al. (2010)	Open	Silica gel /polymer	Experimental & theoretical	60	The fin-tube heat exchanging devices coated with silica gel and polymer materials.	Moisture removal of both methods (silica gel/polymer) increases significantly with the increase of regeneration temperature, and silica coating obtains the COP of 0.6 when regeneration temperature equal to 70°C.
Bonaccorsi et al. (2013)	Close	Zeolite/water	Experimental	-	In situ direct growth coating of zeolite on heat exchanger fins.	Surface coverage, adhesion and mechanical properties should be considered for a valuable coating.
Dawoud (2013)	Open	Zeolite/water	Experimental	90	Adsorber heat exchanger coating with zeolite.	500μm gives the effect of 7% enhancement in the adsorption speed on the small scale and the COP of the adsorption heat pump module has increased almost linearly with increase of the zeolite layer thickness for the full-scale experiment. The COP of adsorption heat pump ranges from 1.16 to 1.25.
Atakan et al. (2013)	Close	Zeolite/water	Experimental	-	Adsorber heat exchanger coating with zeolite directly crystallised on fibrous plates	Directly crystallised zeolite coating on fibrous plates will stabilise the coating and heat transfer properties.

Vasta et al. (2014)	Close	Zeolite/water	Experimental	-	Zeolite coated graphite heat exchanger plate.	The direct-grown coatings showed a mechanical resistance of 0.78 Mpa while the dip coated plates showed resistance of0.82 Mpa.
Adsorbent with multi cooling tubes						
(Wang & Zhang (2009)	Close	Silica gel/water	Experimental & theoretical	85	Silica gel filled multiple cooling tubes.	The COP and the SCP of the designed AHP adsorbent are 0.5 and 85 W/kg respectively, temperature (hot water; 85°C, cooling water; 30°C, the chilled water; 15°C) and the heating/cooling time are about 630s.
Khattab et al. (2012)	Close	Carbon/methanol	Experimental	≤110° C	Solar tube filled with carbon.	Summer days, (7kg /m^2 ice is formed), cloudy winter days about 4 kg/m^2 of ice is formed.

2.11 Conclusions of the Chapter

The theoretical investigation of the adsorption cooling/heating will clarify the fundamentals of investigating the performance of the system. The theoretical modelling will also act as a validation tool for many researchers in order to improve the heat and mass transfer in the adsorbent bed, the coefficient of performance and specific cooling or heating power of adsorption technologies. Most of the researchers are keen to apply a lumped parameter method due to its simplicity and the fact that it can be solved numerically using any modelling programme. However, a few of the researchers who seek to conduct thorough investigation tend to adopt the heat and mass transfer model, which is much more complicated and is solved analytically. Nevertheless, the lumped parameter is the purest mathematical method due to its simplicity and because it is more familiar for researchers in this field.

Adsorption cooling or heating is the most promising technology to alleviate high dependency of energy use by adopting the conventional vapour compression systems. However, the uptake of adsorption systems is still at the laboratory scale due to a few drawbacks of low heat transfer in the adsorbent bed. The most common enhancement method that this review revealed is embedding the adsorbent material in the heat exchanger fins. Technically, most of the researchers have chosen insertion of metal inside the adsorbent bed or adsorber. This method will increase the thermal conductivity of the adsorbent bed which is relatively lower than metal.

The relevant parameters of investigating the heat and mass transfer enhancement of the adsorption cooling system are the COP (coefficient of performance), SCP (specific cooling power), adsorption/desorption time and maximum power (W) per mass (kg) of

adsorbent material. The most desirable result from the adsorption systems is to attain 1 kW per kg of adsorbent mass. Other than that, apart from enhancing the heat and mass transfer in the adsorbent bed, the working pairs are also becoming an important factor to be considered. Furthermore, the regeneration temperature for the desorption process should not be higher than the heat extracted through the adsorption process. From this review, five working pairs have been noted for their high energy densities and low regeneration temperature. These working pairs consist of silica gel+$CaCl_2$/water, vermiculite +$CaCl_2$/water, silica gel +$MgSO_4$/water and vermiculite+$MgSO_4$/water.

These working pairs suggest that the regeneration temperature would be in the temperature range that could utilise waste heat such as various heat engines, fuel cells and motor vehicles. This alternative would be a more economical and sustainable technology to adopt in the long run. In this review, most of the research investigated the cooling/refrigeration applications and it was found that the literature related to heat storage was minimal. Thus, more investigation needs to be conducted into the heating applications in order to alleviate high dependency on fossil fuels as a primary energy source and to promote more sustainable technology in the future.

Continuing from this review, brief methodology of this research and the thermochemical materials screening, synthesis & optimisation will be discussed in chapter 3 and chapter 4 respectively.

3. METHODOLOGY

This chapter introduces experimental and numerical methodologies that were selected based on the literature review and objectives of research, as introduced in Chapter 1. As outlined in section 1.6 this research consisted of four different stages, directed by the process flow as seen in Figure 3.1, and a brief methodology outline in every chapter, as summarised in Table 3.1.

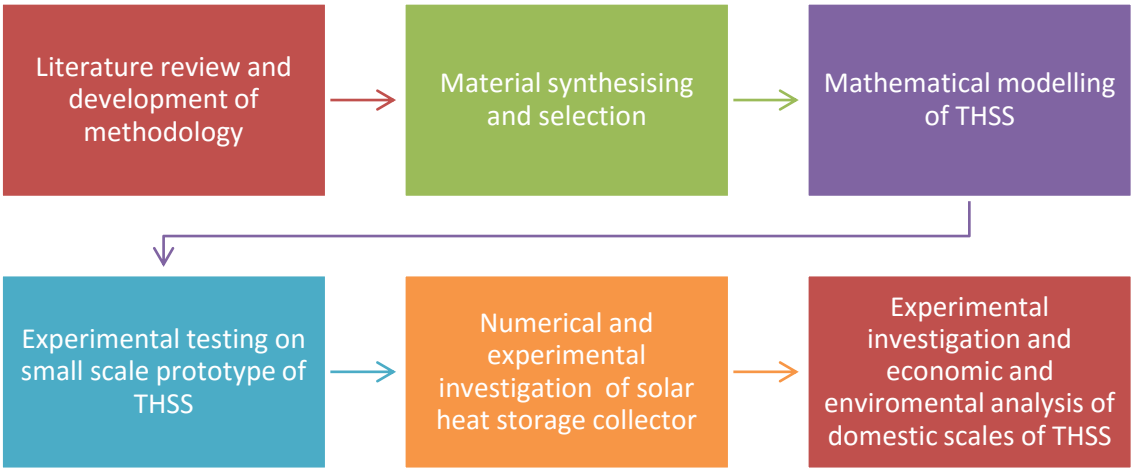


Figure 3.1: Process flow of THSS research

Table 3.1: Brief methodology of THSS research

Stage	*Description*	*Task*	*Method*
1st **Literature Review and Development of Methodology (Chapter 1&2)**	Literature review was carried out to collect relevant information on theory of adsorption heating and cooling applications, energy storage theory, background, thermochemical energy storage and application, theory of adsorption, adsorbent material, and nanocomposite adsorbent material, mathematical modelling of THSS.	i. Review of energy storage and thermochemical energy storage (TES). ii. Review of heat and mass transfer for THSS. ii. Review of mathematical modelling for THSS.	Analysed and reviewed literature on similar topics and summarised the mathematical modelling method, heat and mass transfer enhancement, and the composite material with the most potential to be tested.

2nd Material Screening and Synthesising (Chapter 4)	Executing material screening and synthesis to evaluate adsorbent pair materials such as silica gel+$CaCl_2$, vermiculite+$CaCl_2$, and other composites materials with high adsorption temperature lift, high heat storage capacity, high sorption uptake, high porosity and physical scanning on structure.	i. To investigate temperature lift from selected composite material. ii. To investigate temperature lift and water uptake. iii. To investigate the pore existence and chemical scanning on the composite materials. iii. To investigate the heat storage density of the selected composite materials.	i. Using a horizontal rig for adsorption temperature lift. ii. Using vertical rig for adsorption and desorption test. iii. Using Environmental Scanning Electron Microscopic for hydrated sample and Scanning Electron Microscopic for dehydrated sample. iii. Using differential scanning calorimetry to determine the specific heat of material and calculate the heat storage capacity.
Mathematical Modelling (Chapter 5)	The mathematical modelling was carried out to: i. Investigate the performance of a composite material of	i. To find out mathematical modelling methods, independent parameters and	i. Using lumped parameter method to derive the formulae based from the literature review in Chapter 2

	silica gel +$CaCl_2$ and vermiculite +$CaCl_2$. ii. Investigate the performance of those two composite materials using different types of heat source for desorption (heating clamp, heat-pump circuit and solar thermal).	appropriate assumptions for the chosen composite materials. ii. Determine an adsorption equilibrium equation, the heat balance equation and performance parameter equation such as adsorption, heat and COP.	and formulae related to performance investigation. ii. Calculate and analyse the performance of the systems based on the independent variables' set up, such as the heating temperature, mass of adsorbent material and the time.
3rd Experimental Testing On Small - Scale Prototype of THSS (Chapter 6)	Design and build a small scale prototype and investigate the performance parameters, such as temperature lift from exothermic reaction and heat storage density.	i. Finalise design from the modelling result. ii. Prepare the selected composite material to be tested. iii. Test the complete systems for the adsorption process and desorption process. iv. Analyse the performance of the system based on changing rate of the weight ratio between the adsorbent material and water.	i. To check the finalised design. ii. Use similar method for preparing the composite material in Chapter 4. iii. Measure and monitor the temperature lift in the adsorption section and evaporator section. iv. Calculate/measure the water uptake (g/g), heat storage density (kWh/kg, kWh/m^3), and coefficient of performance. (COP).

Numerical, Build -up and Experimental Investigation of Solar Heat Storage Collector	To develop a numerical analysis, build-up and execute experimental testing on a small -scale solar heat storage collector using the concept of an open sorption system.	i. To design a small scale solar heat storage collector. ii. To determine the independent variables and dependent variables to investigate the performance of the SHSS. iii. Investigate the performance of SHSC using different concepts of heat transfer consisting of air to air heat exchange and air to water heat exchange. iv. To build a small-scale SHSC and test its performance using different solar light power.	i. Develop a design based on a similar concept found in current literature. ii. Use current literature to determine the formulae to calculate the performance based on the set-up independent variables such as mass flow rate $(\dot{m})[\frac{kg}{s}]$, solar collector area $(A)[m^2]$ and time $(t)[s]$. iii. Determine the energy balance equation and calculate the performance of SHSC based on the three independent variables listed in (ii). iv. - Prepare the composite material using a similar procedure as found in Chapter 4. - Put the dried composite material inside the aluminium cartridge of SHSC. - Test the SHSC for the adsorption and desorption test and monitor the temperature rise during both processes. - Weight the composite material before and after the test.

			- Calculate thermal energy and the COP from the experimental testing data.
4th Build-up and Experimental Investigation, Economic and Environmental Evaluation on a Domestic Scale of THSS	To build, test the performance of and carry out the economic and environmental evaluation on a domestic scale of THSS.	i. To design the domestic scale of THSS. ii. To install the complete domestic scale THSS for testing. iii. To prepare composite materials and test for adsorption and desorption process. iv. To execute economic and environmental analysis based on domestic heating systems.	i. Develop a design base from a similar concept found in current literature. ii. Finalise the design and install all main components and subsystems. iii. - Prepare the composite materials similar to the procedure in Chapter 4 with the estimated amount of weight to meet the demand of domestic heat storage. - Load the material in the adsorption section before the test. - Conduct a leakage test to make sure that the systems are in perfect vacuum. - Conduct the adsorption and desorption test and monitor the temperature rise and drop during both tests. iv. Estimate heating demand for small households and energy prices for gas and electric.

			- Estimate the price impact due to inflation rate. - Calculate the internal rate of return (IRR) of the proposed systems using a single payment present worth factor (SPPWF). - Calculate the CO_2 emissions based on the UK Guidelines - Outline further recommendations on this research.

4. THERMOCHEMICAL MATERIALS SCREENING, SYNTHESISING AND OPTIMISATION

4.1 Introduction

A thermochemical adsorption heat pump is considered more environmentally friendly as it has the ability to use water as the refrigerant for heating and cooling purposes. However, some limitations can be found involving the development of these systems, namely the low thermal conductivity and poor heat and mass transfer performance of the packed bed reactor. This is mainly related to the low thermal conductivity of the metal salts - for example 0.1–0.5Wm^{-1} K^{-1} for metal chlorides (Hauer, 2008; Mauran et al., 1993; Wang et al., 2006b) and about 1$Wm^{-1}K^{-1}$ for metal hydrides (Muthukumar & Groll, 2010) - the low heat transfer between the solid bed and the reactor (heat exchanger) wall (Meunier, 1998) and the swelling and agglomeration phenomena occurring during the sorption process with ammonia or water (Abhat & Huy, 1983).

One way to solve the problems related to heat and mass transfer is by using a composite material in the adsorbent bed. Therefore, thermochemical heat storage systems (THSS) can be based on the application of a unique adsorption heat pipe, which uses a range of adsorbent materials including nanocomposite adsorbent materials (for example, $CaCl_2$/silica or $CaCl_2$/vermiculite and water) as a working media. Furthermore, composite adsorbents made from metallic foams, zeolites, and natural graphite have good prospects for improving the heat transfer rates in the adsorbent beds, consequently increasing the refrigeration or heat pump system performance (Pons et al., 1996). The

principal mechanisms of water sorption that take place on a composite sorbent - salt inside a porous host matrix - are (a) solid absorption (or a chemical reaction) which is responsible for about 10-15% of the total sorption, and (b) liquid absorption (about 80%). In addition, heterogeneous adsorption on the matrix surface which is responsible for 3-4% can be neglected.

Objective

The primary objective of this chapter is to investigate material screening on the various adsorbent materials impregnated with the hygroscopic salt solution. Emphasis will be placed on the temperature uplift, water uptake (g adsorbate/g of adsorbent), high heat storage capacity, strong physical structure and large pore size distribution, as can be employed in THSS for building applications.

4.2 Synthesis of Composite Adsorbent Materials

A new working pairs family known as ‘salt water sorbent’ (SWS) is being investigated by Aristov et al. (2002), Daou et al. (2006) and Glaznev et al. (2011). Composite adsorbents incorporating inorganic hygroscopic salt in the porous matrix have been recognised as promising materials for energy storage systems due to their enhanced sorption capacity in comparison to common working fluids such as water, ammonia and methanol (Gordeeva & Aristov, 2012). The salt water sorbent is composite adsorbents consisting of two component systems, a host matrix component and another which is an inorganic hygroscopic salt placed inside the pores of the host matrix. The concept of these materials is basic; the organic salt known as *S* will react with a sorbate vapour *V* (commonly water) which gives the results in the formation of a complex *S.NV* hydrate of

the salt and sorbate molecules according to the reaction; *S+ NV= S.NV* (see Figure 4.1). This principle is to allow the dispersion from the porous matrix where it affects the phase composition and the sorption properties of the salt and provides heat and mass transfer to salt particles located in the matrix grains. The structural differences of the composite adsorbent compared to conventional adsorbent materials (silica gel, zeolite, or molecular sieves) will improve its water adsorption capacity. This notion is widely investigated by many researchers for multiple applications such as heating and cooling, drying, ice making and others.

In order to develop composite adsorbents with the most potential for THSS the concept of impregnation methods needs to be adopted, where the host matrix is impregnated with an aqueous salt solution. The synthesis procedure involves initially drying the matrix adsorbent (silica gel, molecular sieve, and vermiculite), filtration, drying the composite at a high temperature and then finally weighing the adsorbent material.

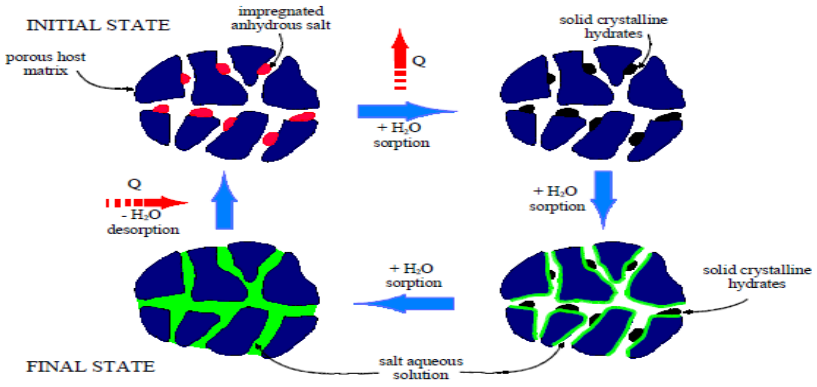


Figure 4.1: Mechanism of adsorption on composite adsorbent (Aristov, 2003)

4.3 Experimental Investigation of Temperature Lift – Using Horizontal Glass and Metal Heat Pipe

This experiment investigated the thermochemical performance of temperature lift in the adsorbent pipe and conversely the temperature drops in the evaporator pipe. Two glass vessels make up the main apparatus of this experiment. The first glass vessels were used to hold the adsorbent material (adsorbent vessel) and the other held water (evaporator vessel). Based on the principle of the mechanics of an adsorption pumping pipe, a scaled heating system was applied as shown in Figure 4.2. It consists of two vacuumed glass vessels separated with a valve through a steel pipe; one contains water/wick, and the other one is filled with a dry adsorbent. The reaction will occur when the valve is opened. The adsorbent will adsorb water vapour, and then water in wick will begin to evaporate, and consequently the water vessel section is cooled while the temperature in the adsorbent vessel is increased. The detailed construction of the horizontal glass and metal wick is shown in Table 4.1.

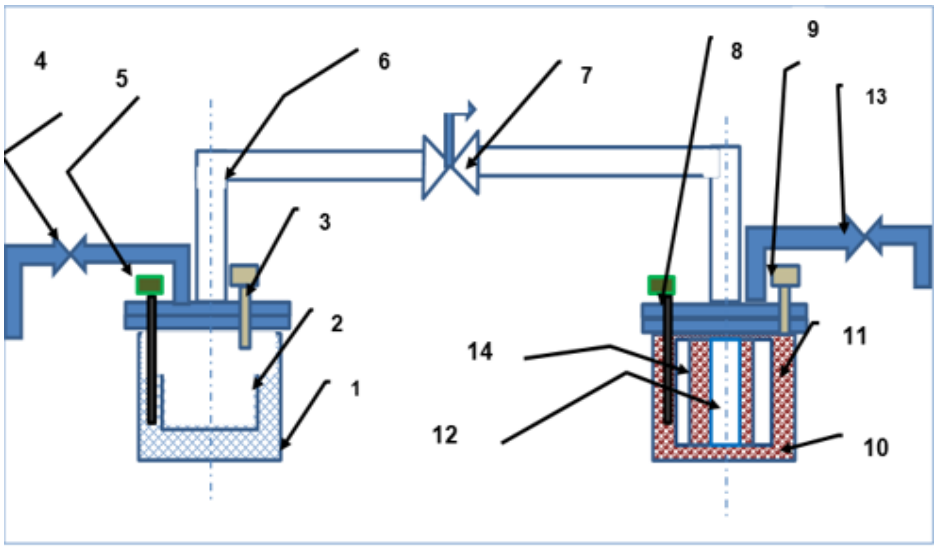


Figure 4.2: Schematic of horizontal glass and metal

Table 4.1: The detail construction of the glass and metal wick

Item	*Description*
1	Water vessel (evaporation section)
2	Water c/w wick
3	Pressure transducer
4	Ball valve connected to vacuum pump
5	Thermocouple for evaporator section
6	50 mm diameter stainless steel pipe
7	Ball valve
8	Thermocouple for adsorption section
9	Pressure transducer
10	Adsorbent vessel
11	Adsorbent material
12	Aluminium wick
13	Ball valve connect to vacuum pump
14	Aluminium wick

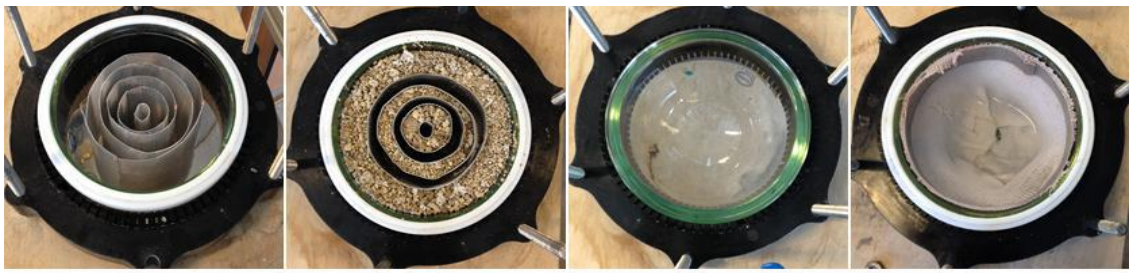


Figure 4.3: Adsorption glass vessel showing aluminium mesh: (a) without adsorbent (b) with adsorbent. Evaporation glass vessel: (c) without wick material (d) with wick material.

To enhance the heat and mass transfer of water vapour in the adsorbent vessel, the aluminium wick is used as a casing for the adsorbent material (see Figure 4.3 a&b). Furthermore, round constructed aluminium meshes are used in the adsorbent pipe to allow mass water evaporation when the vessel is evacuated (see Figure 4.3 c&d).

4.3.1 Data Acquisition

The horizontal glass and metal rig is also equipped with the data acquisition apparatus such as a data logger, a desktop computer complete with Data Taker software, thermocouples, and digital pressure gauges. Figure 4.4 illustrates the multichannel data taker DT 500 for the data acquisition of the glass and metal rig. The data will be monitored by the desktop computer with the Data Logger software. The data were set to be at one-second intervals to develop a more accurate and reliable output from the experiments.



Figure 4.4: Data Taker DT 500

4.3.2 Measuring Equipment

The major measuring equipment consists of the thermocouples and pressure sensors. Thermocouples are used to gauge the temperature in the evaporation vessel and the adsorption vessel. The pressure sensor is used to gauge the pressure in both vessels to ensure vacuum conditions. The thermocouple used in these experiments is a K type, with a temperature range of -50°C to 2000°C and the accuracy of ± 1.5° C, as shown in Figure 4.5. A digital pressure sensor, UNIK 5000, is used to monitor the vacuum pressure in the glass and metal rig. The accuracy of this pressure sensor is ± 0.04% with

the operating temperature range 55~125°C (-67~257°F) and pressure range -1 ~ 1.6 bar_g. All sensors were calibrated before the experiments were conducted.

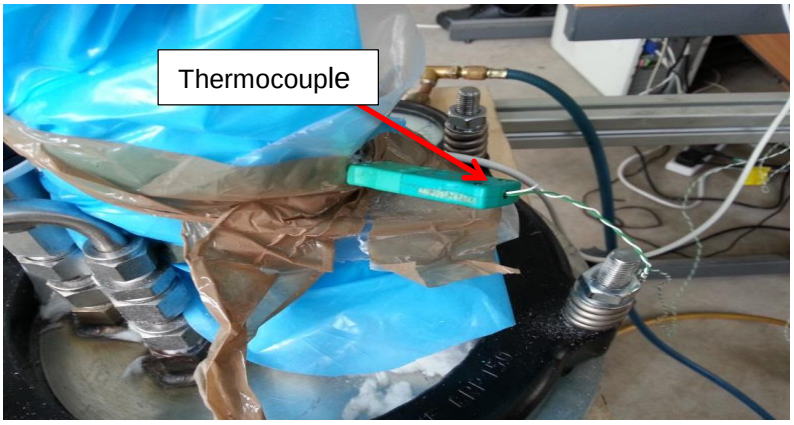


Figure 4.5: A photo showing a thermocouple attached to one of the vessels.

4.3.3 **Experimental Procedure for the Horizontal Rig and Vertical Rig.**

Adsorption Test

i. Prepare the composite material: spray with $CaCl_2$ liquid concentration and dry the material in the oven at 150°C for about 24 hours.
ii. Installation of the adsorbent pipe and the evaporation pipe.
iii. Insulate the adsorbent pipe for the adsorption test.
iv. Leakage test is conducted before the material is loaded inside the rig to make sure that the adsorbent pipe is under vacuum conditions.
v. Weigh the dry material and calculate the mass of water to use in the evaporator section.
vi. Put the dry material in the multi-chamber perforated cartridge and then into the adsorbent bed (adsorption section for vertical rig).

vii. Vacuum the system using the vacuum pump until the system is perfect vacuumed and turn off to start the test.

viii. Monitor the temperature rise through data taker software. When there is no more temperature rise and the adsorbent material is considered to be in the equilibrium stage, stop the test by closing the separator valve.

ix. Dismantle both pipes and weigh the hydrated adsorbent material and water quickly and reinstall the rig.

Desorption Test

i. Insulate the evaporator pipe using ice jacket for the desorption test.

ii. Repeat the leakage test again to confirm that the system is in a perfect vacuum.

iii. Turn on the heating controller (with temperature set to 60°C) and keep the desorption test running for up to 5 hours.

iv. Open the separator valve between the adsorbent pipe and the evaporator pipe and monitor the temperature using Data Taker software.

v. Dismantle the rig and quickly weigh the mass of water and the adsorbent material using a digital weigh machine.

4.3.4 Materials Preparation

From the literature review in Chapter 2, the five composite adsorbent materials with most potential have been selected to be included in the material screening. These materials are silica gel, vermiculite, and molecular sieve 10A (see Figure 4.7~Figure 4.11). These materials were sprayed with a fully concentrated $CaCl_2$ or $MgSO_4$ in a tray (Figure 4.12) and dried in the oven for approximately 24 hours to ensure that the material was

completely dried, and there was no mass of water on the surface of composite materials. This process ensures that the adsorption process is efficient, and the desired temperature will be attained. The whole procedure of synthesising is illustrated in Figure 4.6. The host matrix of the molecular sieve was not impregnated with $MgSO_4$ due to thermal instability, and because agglomeration occurs during oxidisation with magnesium (Akolekar and Kaliaguine, 1994; Fernandez et al., 2002). The composite adsorbents synthesised and tested with the test rig included:

i. Silica gel with calcium chloride ($CaCl_2$).
ii. Vermiculite with calcium chloride ($CaCl_2$).
iii. Molecular sieve 10A with calcium chloride ($CaCl_2$).
iv. Silica gel with magnesium sulphite ($MgSO_4$).
v. Vermiculite with magnesium sulphite ($MgSO_4$).

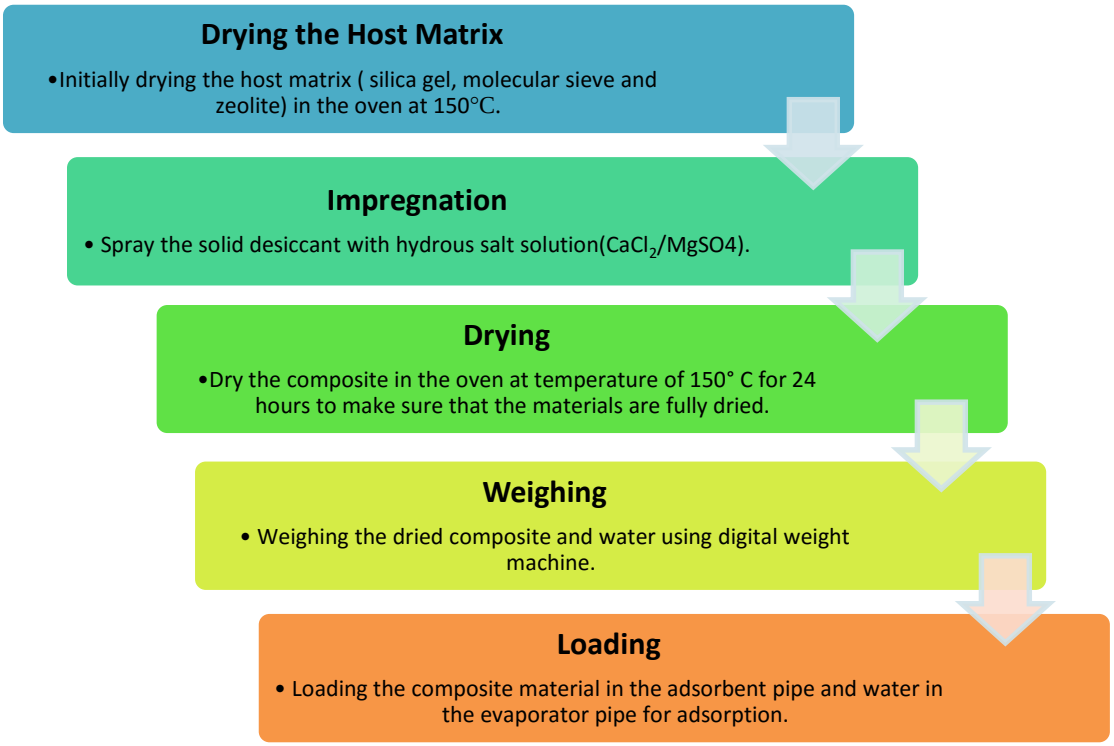


Figure 4.6: Procedure on synthesising of composite adsorbent.



Figure 4.7: A photo showing silica gel considered for test.



Figure 4.8: A photo showing raw vermiculite considered for test.



Figure 4.9: A photo showing molecular sieve 10A considered for test.



Figure 4.10: A photo showing dry calcium chloride considered as salt solution for impregnation.



Figure 4.11: A photo showing of dry magnesium sulphate considered as salt solution for impregnation.

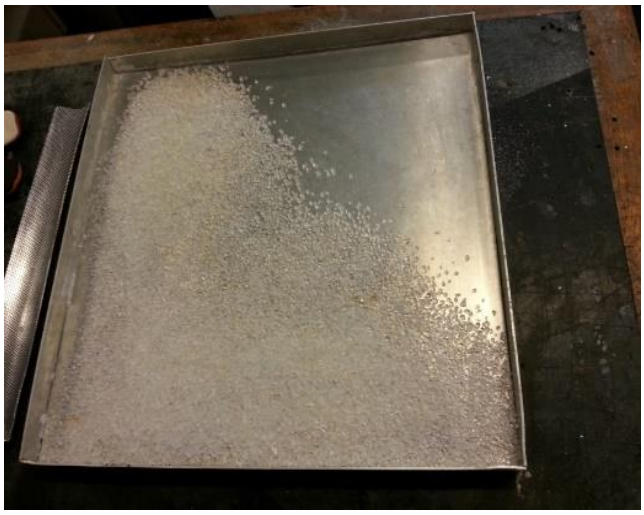


Figure 4.12: Photo is showing the tray of impregnated adsorbent material to be dried in the oven.

4.3.5 Results and Discussion from Temperature Lift Experiments Using Horizontal Glass and Metal Rig

The main objective of this experiment is to investigate the temperature lift in the adsorption vessel during the adsorption process. A total of five tests were conducted and Figure 4.13 to Figure 4.17 illustrate results from the tests conducted, each with a different composite material as the independent variable.

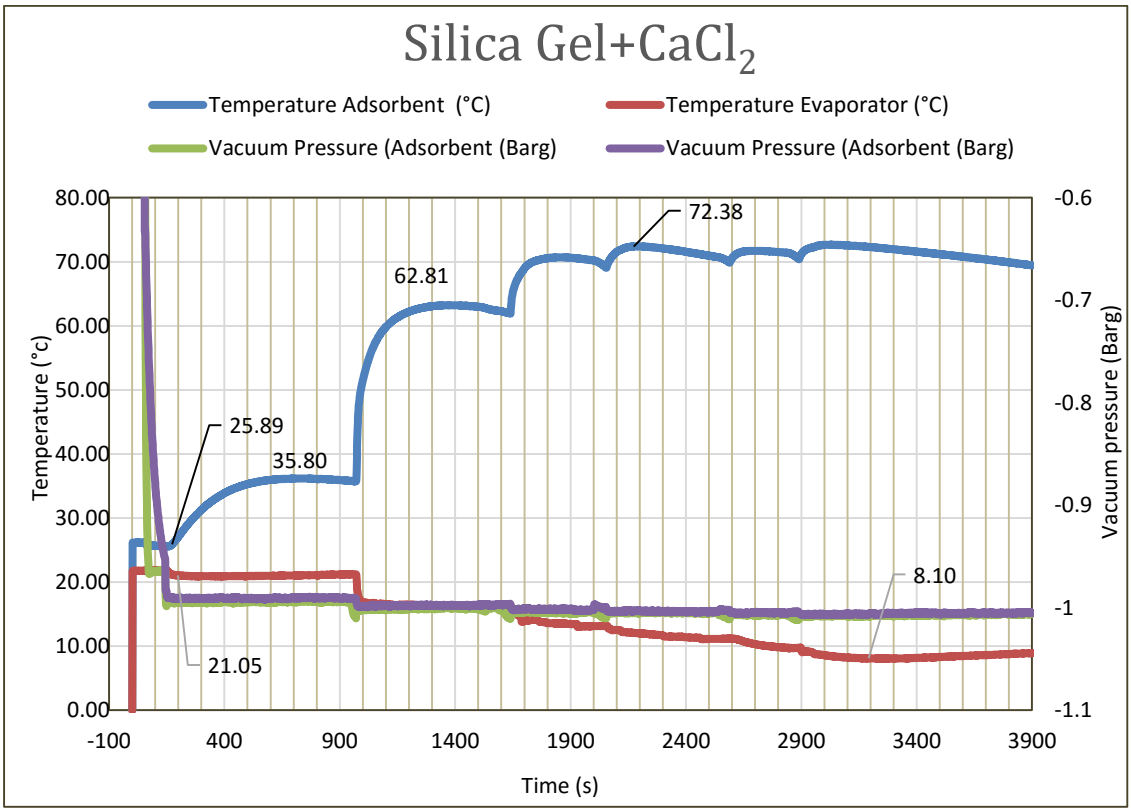


Figure 4.13: The temperature variants of adsorbent and evaporator for silica gel+$CaCl_2$/Water – Test1

Figure 4.13 shows the temperature variations from the adsorption test of silica gel+$CaCl_2$/water. The results show that the maximum temperature rise in the adsorption vessel is 72.40°C from its initial temperature of 25.90°C. Besides this, the evaporator vessel showed a temperature drop of 8.10°C from its initial temperature of 21.05°C. The temperature difference (ΔT) achieved from this test is 46.50°C for the adsorbent vessel and 13.0°C for evaporator vessel.

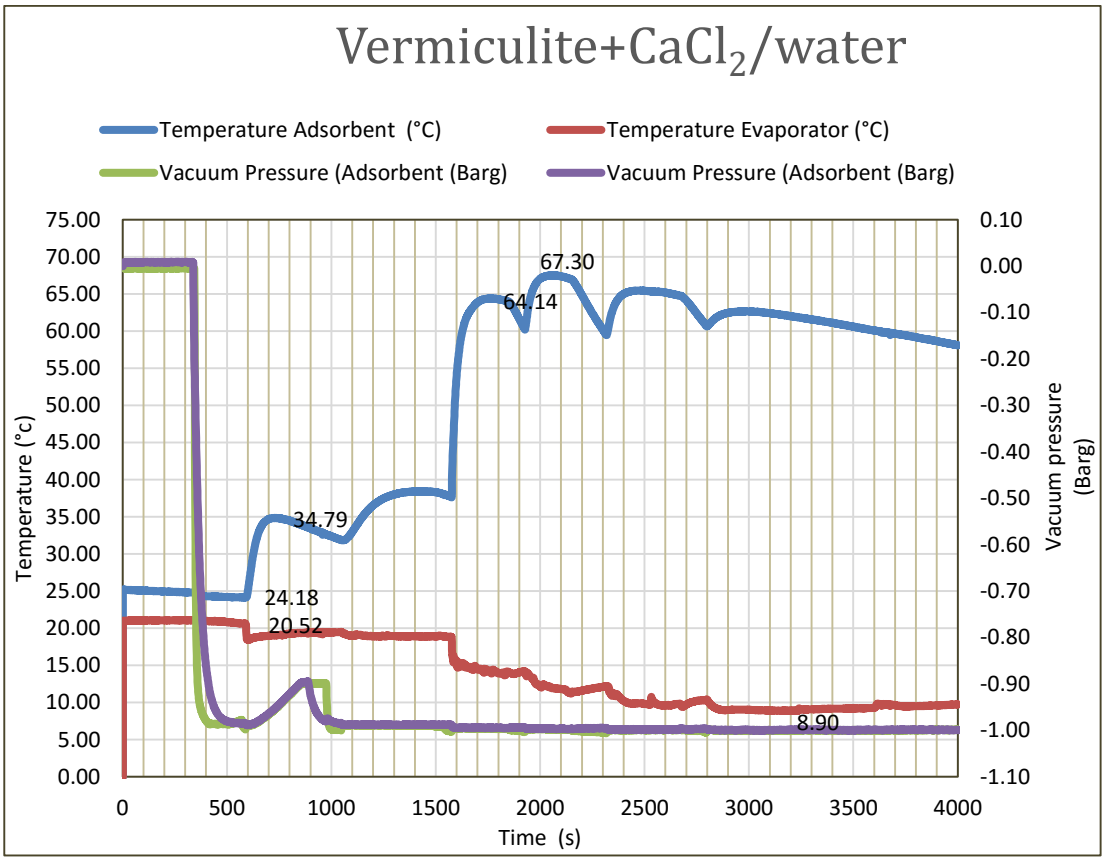


Figure 4.14: The temperature variants of adsorbent pipe and evaporator pipe for vermiculite+$CaCl_2$/water - Test 2

The next possible material available for THSS is the vermiculite + $CaCl_2$ (see Figure 4.14). This TCM gives a temperature lift of 67.30°C in the adsorbent pipe. This TCM reached a maximum temperature at 2000s from the start of the test, a result that is relatively similar to Test 1. The evaporator temperature showed a temperature drop down to 8.90°C from its initial temperature at 20.50°C.

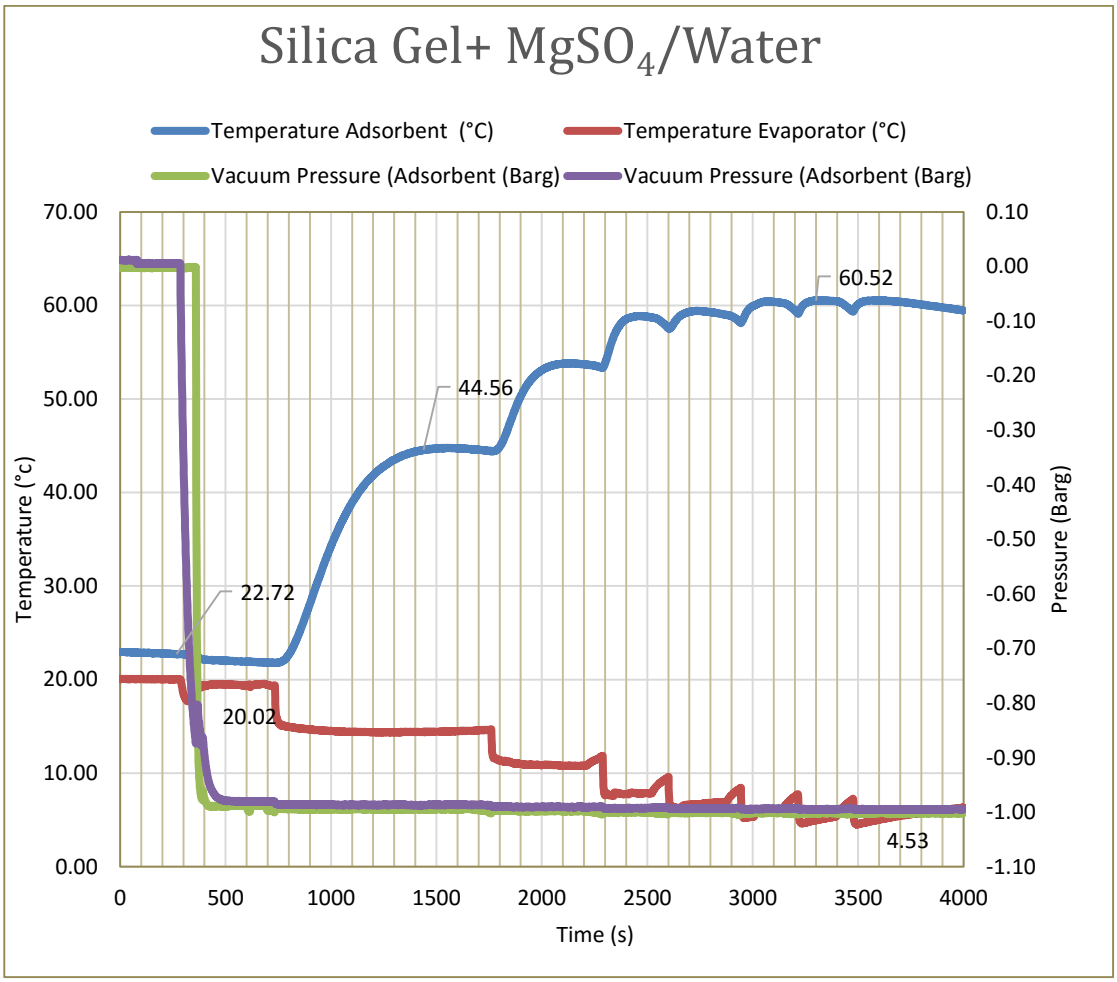


Figure 4.15: The temperature variants of the adsorbent pipe and evaporator pipe for silica gel +$MgSO_4$/water - Test 3

Test 3 was conducted to investigate the TCM of silica gel+$MgSO_4$/water. Figure 4.15 shows the temperature variations from the adsorption process. The maximum temperature lift achieved by this composite material was 60.50°C. Therefore, it can be concluded that using an aqueous salt of $MgSO_4$ is not effective for inducing a temperature lift during the adsorption process. This TCM could not achieve a higher temperature than Test 1 & Test 2 by 4000s in the adsorption process. Consequently, this TCM has the lowest temperature drop at 4.50°C in the evaporator section. From these results we could

suggest that this TCM is more suitable for cooling applications due to the low evaporation temperature.

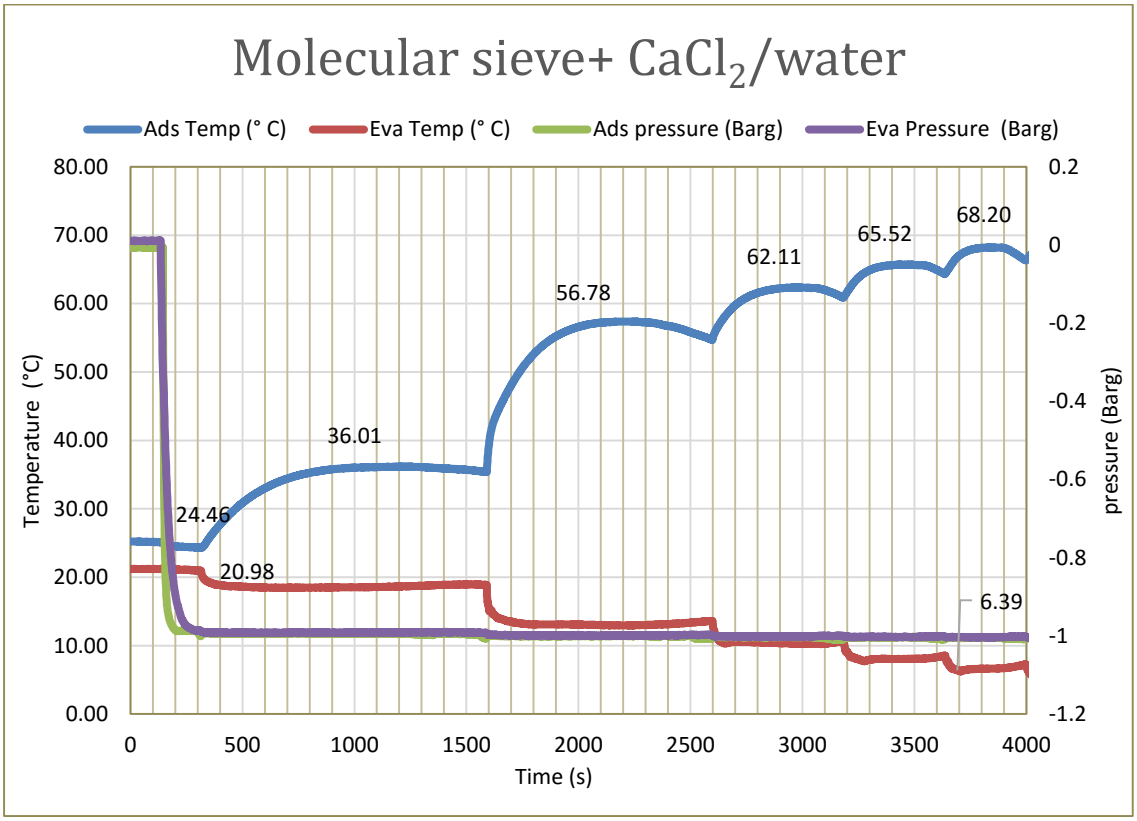


Figure 4.16: The temperature variants of adsorbent and evaporator for molecular sieve +CaCl2/water - Test 4

Figure 4.16 shows the temperature variation of the TCM consisting of a molecular sieve+$CaCl_2$/water from the adsorption test. From the graph we can see that this composite material achieved a maximum temperature of 68.20°C during the adsorption process. The evaporator pipe showed a temperature drop at 6.40°C, a temperature which is considered a suitable temperature for cooling in buildings. Furthermore, with a maximum temperature of 68.20°C during adsorption process, this TCM would also be suitable for use as a heating application in buildings.

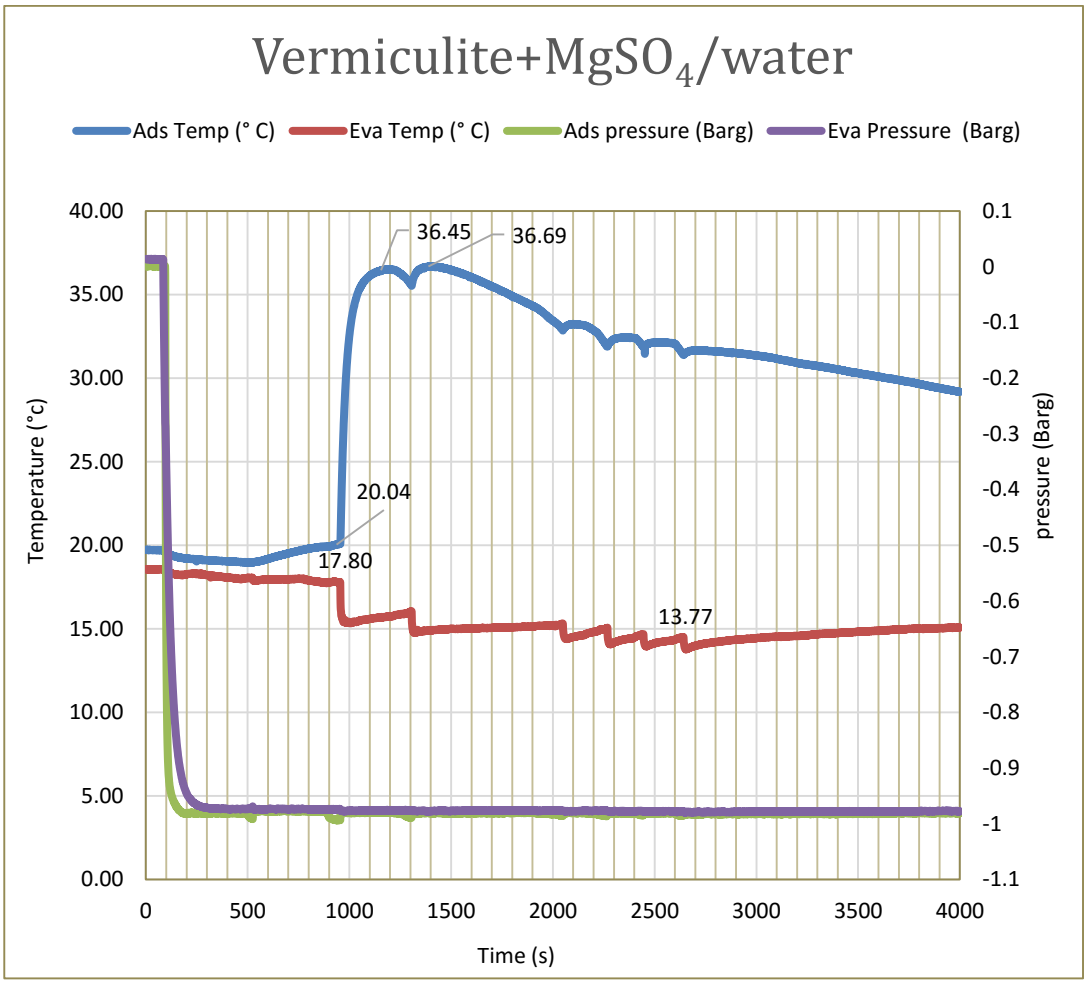


Figure 4.17: The temperature variants of adsorbent pipe and evaporator pipe for vermiculite +$MgSO_4$/water – Test 5

Figure 4.17 shows the temperature variations during the adsorption process of the TCM of vermiculite+$MgSO_4$/water. From the results it can be seen that this TCM has the lowest temperature lift of 36.70°C, which is deemed insufficient for heating applications in buildings. However, this temperature may be suitable for different applications such as evaporative heating or cooling in buildings. The evaporator pipe showed a high of 13.77°C, a temperature that is not suitable for cooling. Therefore, it can be suggested that this TCM is not appropriate to employ for use in the heat storage system.

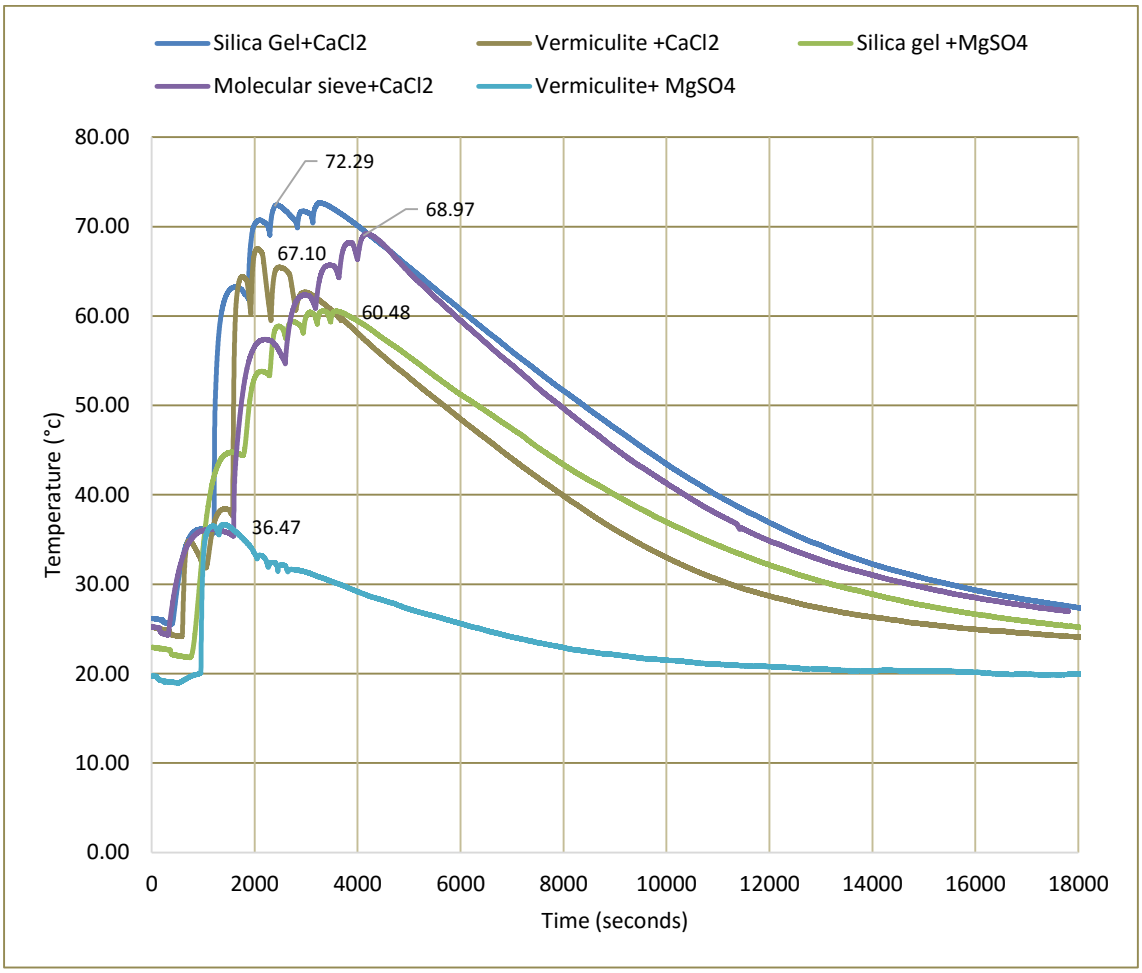


Figure 4.18: Adsorption temperature for tested TCMs from horizontal metal and glass rig.

Figure 4.18 showed the comparison of adsorption temperatures of five TCMs tested in the experiment using the horizontal glass and metal rig. The results indicate that these TCMs reached the maximum temperature between 1000s and 4000s in the adsorption process. The host matrix of silica gel, vermiculite, and the molecular sieve impregnated with the aqueous salt of $CaCl_2$ achieved higher temperature lift ranges, ranging from 68°C to 72°C. The host matrix impregnated with the aqueous salt of $MgSO_4$ had the lowest temperature lift from 36°C to 60°C. The aqueous solution of $CaCl_2$ has a higher

temperature lift than $MgSO_4$. Within five hours of the adsorption process, all tested TCMs return to their initial temperature.

4.3.6 Summary of Results from Horizontal Glass and Metal Rig

The experimental testing of the horizontal glass and metal rig is to investigate which composite material will lift the temperature in the adsorbent pipe to the appropriate temperature for heating applications in buildings. As can be seen from Table 4.2, silica gel impregnated with $CaCl_2$ gave the highest temperature lift of 72.70°C meaning that it is a potential candidate for use as the adsorbent material for this research. However, the total duration of the adsorption process of this material is the second longest (55mins) compared to all other materials tested. The molecular sieve + $CaCl_2$ displayed the second highest temperature lift in the adsorbent pipe when compared to silica gel + $CaCl_2$. Unfortunately, this material took the longest amount of time to complete the adsorbent process out of all the materials tested. This may be a limiting factor of this material in heating applications due to the longer time required to transfer the heat from the adsorbent pipe to another media such as a heat exchanger or heat pipe. Therefore, we can conclude that a molecular sieve + $CaCl_2$ is not a suitable candidate for use in this research. By looking at the adsorption process achieved in these experiments, the fastest completion time was 23 minutes as achieved by use of vermiculite+$MgSO_4$. However, the temperature lift in the adsorbent pipe using this TCM was the lowest of all materials tested (36.70°C). From these experiments, we can conclude that the most suitable candidate is the vermiculite +$CaCl_2$ due to the high temperature lift of 67.30°C. Furthermore, this material is considered the cheapest in comparison to other adsorbent materials - £15.37 per 100 litres compared to silica gel at £66.20 per 0.5litres (Ding, 2013).

Table 4.2: Summary of results from horizontal rig

	Test 1	Test 2	Test 3	Test 4	Test 5
Description	Silica gel+$CaCl_2$	Vermiculite +$CaCl_2$	Silica gel+ $MgSO_4$	Molecular sieve (10A) + $CaCl_2$	Vermiculite + $MgSO_4$
Weight of Adsorbent (grammes)	550	240	240	575	155
Weight of Water (grammes)	100	100	100	100	100
Vacuum Pressure in Pipe (bar)	-0.98	-0.98	-0.98	-0.98	-0.98
Adsorption Process Completed (mins)	50	33	55	74	23
Max. Adsorbent Temperature Achieved (adsorption section) (°C)	72.70	67.30	60.50	68.20	36.70
Min. Adsorbate Temperature Achieved (evaporation section) (°C)	8.10	8.90	4.70	6.2	13.80

4.4 Adsorption and Desorption Test with Vertical Glass and Metal Rig

Experimental testing using a horizontal rig has a limitation on installing a heat source for the desorption process. This can be solved by using a vertical rig design which includes the installation of an electrical heating clamp as the heat source. Aside from this advantage, the design can help to solve the problems associated with water vapour transport which occurred in the horizontal rig. The rig used in this experiment, illustrated in Figure 4.19, consists of two (2) QVF DN50 glass pipes (300x300mm), which are connected together vertically by a steel pipe assembly via DN50 stainless steel flanges. The detailed construction of this rig is similar to the horizontal glass and metal rig used

in the previous experiment but differs in that, this rig is installed with a heating plate connected to an electric heater for the desorption test. For a good heat transfer between water vapour and the sorption material a large contact area is required. This can be achieved through the perforated multi-chambered adsorbent cartridge, which is made of aluminium and copper and used as the adsorbent bed (see Figure 4.20). The details of a schematic drawing of the vertical pipe are shown in Figure 4.21. The rig was fully insulated during the adsorption process to prevent heat loss from the adsorbent pipe and during desorption (Figure 4.22a), and the evaporator pipe was insulated using an ice jacket to create a temperature difference in order to ease the evaporation of water vapour (Figure 4.22b). The ice jacket will also simulate the low-grade heat source available in a real scale system. The evaporator pipe was also inserted with the aluminium and a cotton wick (Figure 4.23 (c) & (d)). The idea of constructing this wick is to provide a large surface area to enhance the heat and mass transfer of the adsorbate (water) in the adsorbent pipe and the evaporator pipe. The temperature and pressure were measured using K-type thermocouples and digital pressure sensor respectively. The rig was also equipped with a data monitoring system to capture temperature and pressure behaviour in the adsorbent pipe and the evaporator pipe. All the measuring equipment was calibrated before the experiments were executed.

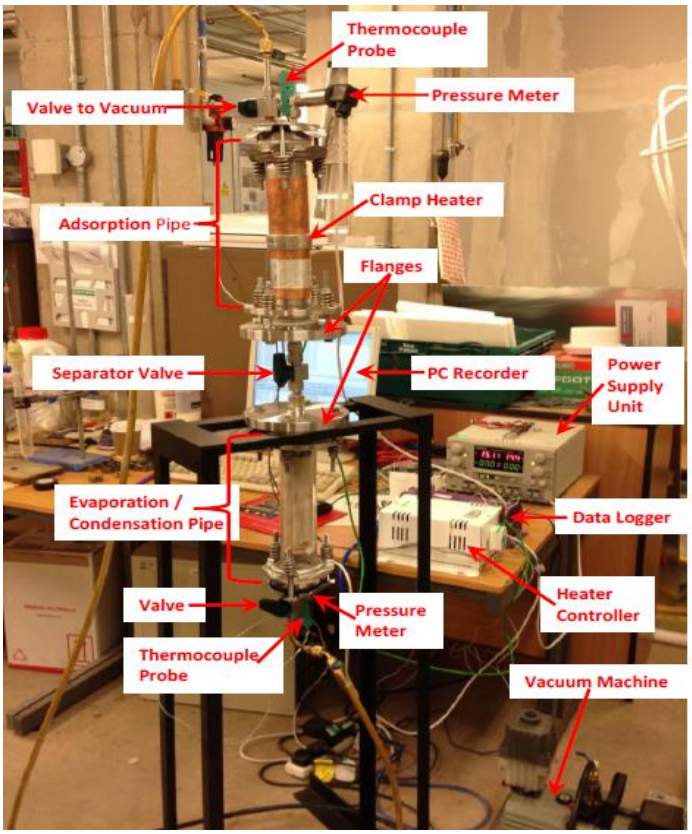


Figure 4.19: A photo showing the vertical heat pipe for the adsorption and desorption test.

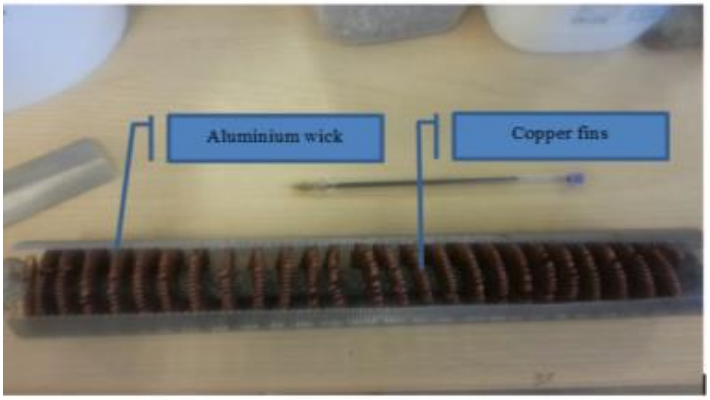


Figure 4.20: The multi-chamber perforated cartridge used in the adsorption pipe.

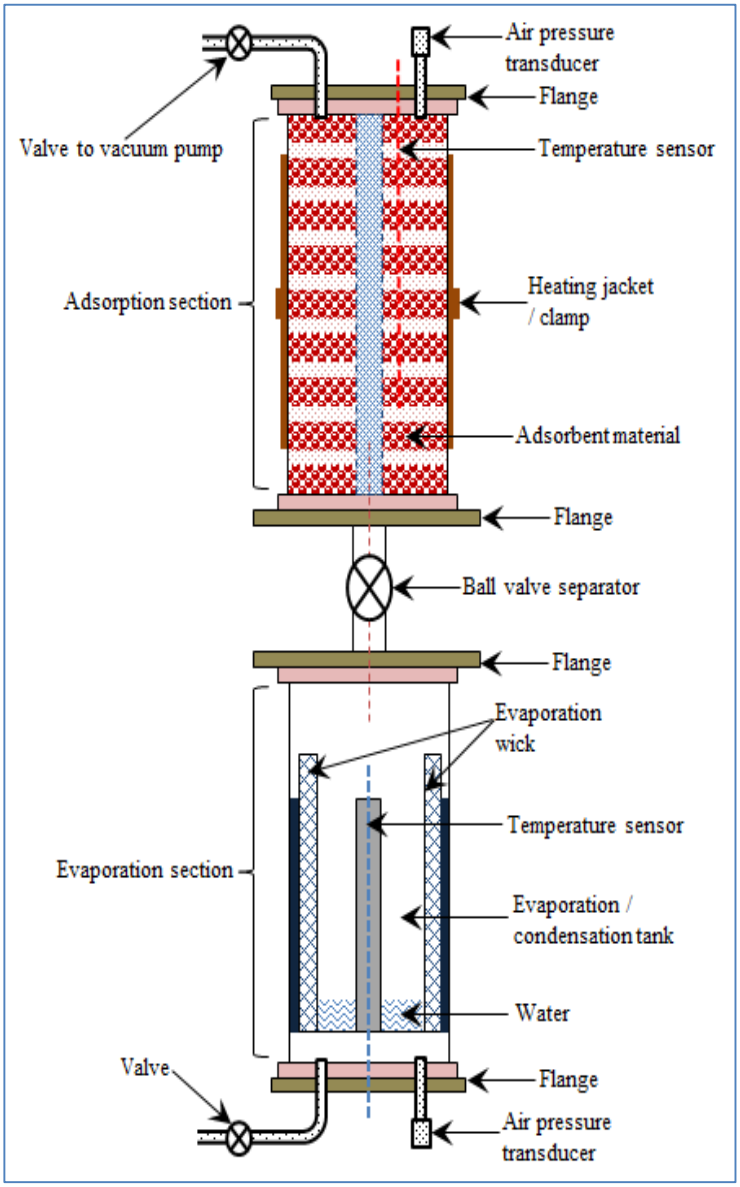


Figure 4.21: The schematic of the vertical adsorption heat pipe for the adsorption and desorption test.

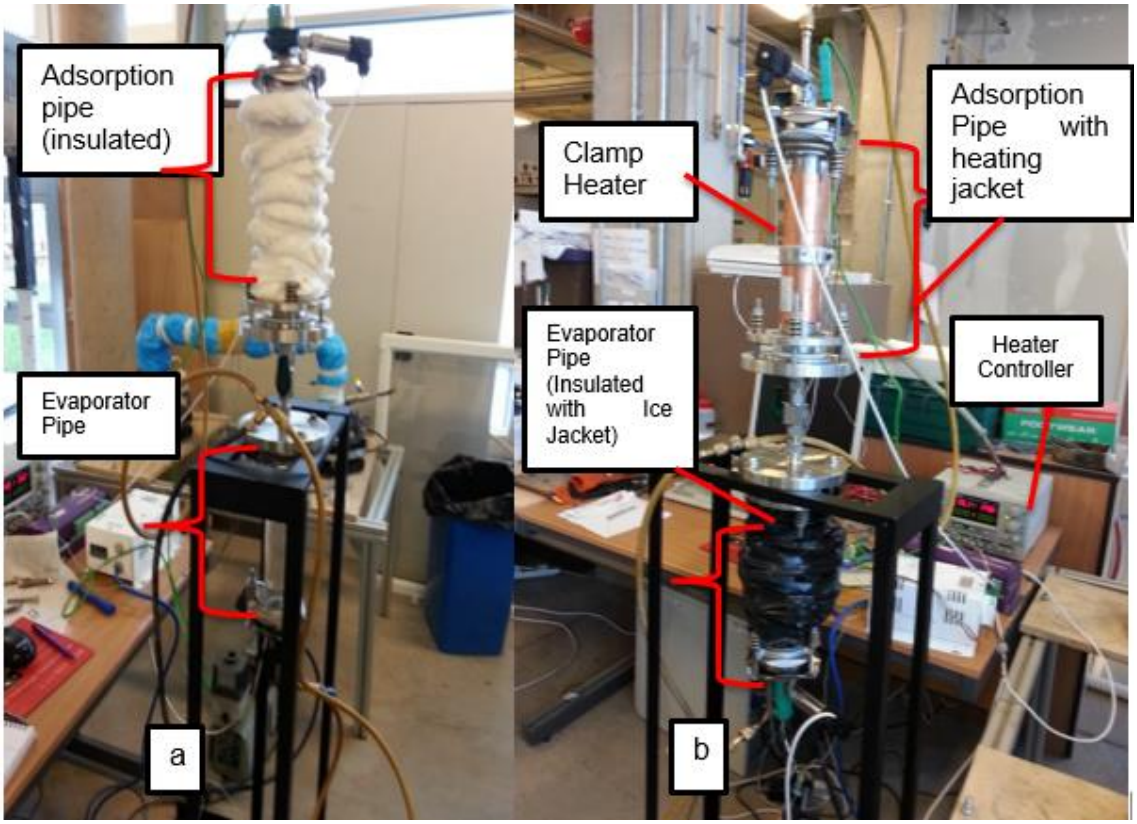


Figure 4.22: Vertical glass pipe rig. (a) Insulated adsorption pipe for the adsorption test, (b) insulated with ice jacket for desorption test.

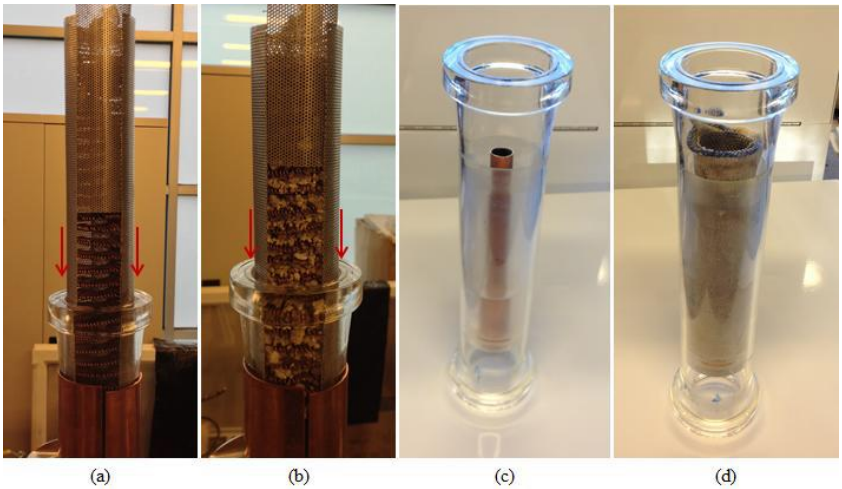


Figure 4.23: Adsorbent pipe showing cartridge (a) without adsorbent (b) with adsorbent. Evaporation pipe showing water container (c) without wick material (d) with wick mat.

4.4.1 Results and Discussion for Vertical Rig Test

The investigation into adsorption and desorption tests is designed to study the physical performance of the selected composite thermochemical materials when adsorbing and desorbing a mass of water from the evaporator pipe with a low regeneration temperature. Based on the results of the temperature lift in the adsorption process from the horizontal rig, two working pairs have been selected for this test: vermiculite+$CaCl_2$/water and silica gel+$CaCl_2$/water.

Figure 4.24 to Figure 4.29 illustrated the temperature variations for the adsorption and desorption process.

Adsorption Test Results

The main objective of this adsorption test was to investigate the temperature rise of chosen composite materials within the vertical glass and metal rig construction. It is important to note that during the adsorption test this rig was fully insulated to prevent heat loss throughout the experiments.

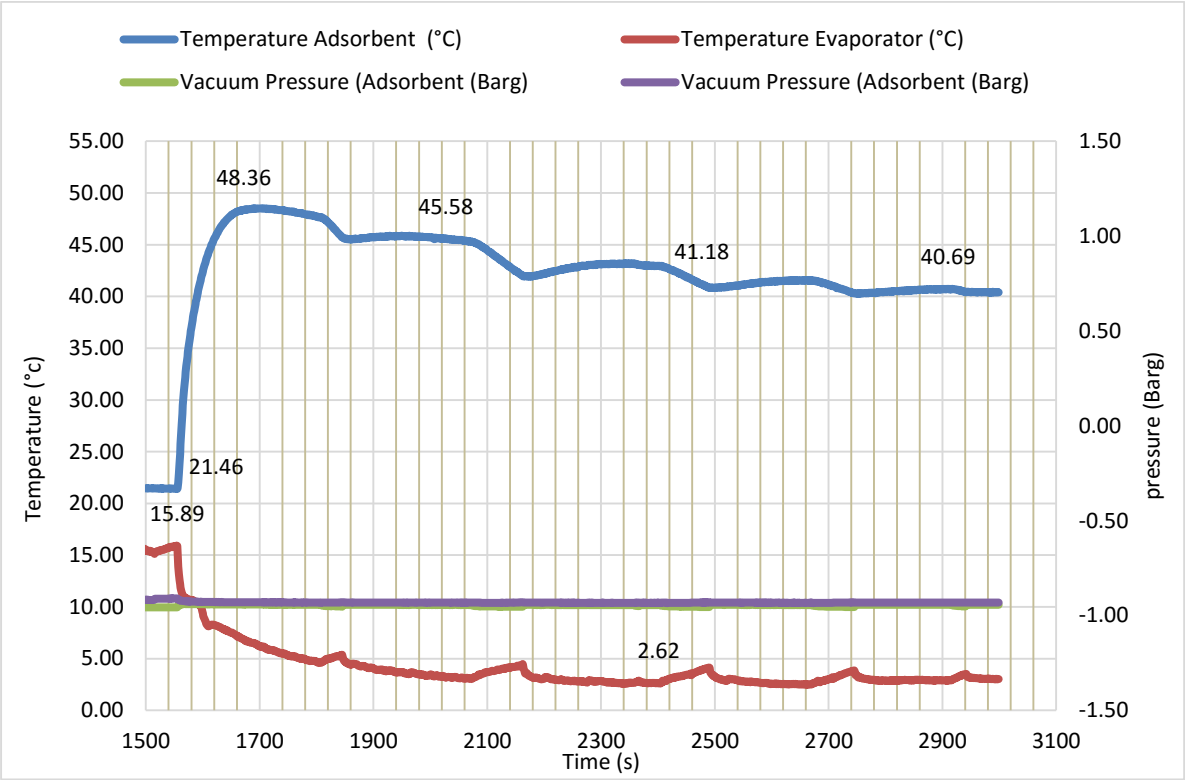


Figure 4.24: Illustration of temperature variation for adsorption test on vermiculite

Figure 4.24 shows the temperature variation for vermiculite+$CaCl_2$/water during the adsorption process. It can be seen that the temperature of the adsorbent pipe increased from an initial temperature of 21.50°C to 48.40 °C without of the system needing to be re-vacuumed. This shows that the vertical rig works well with the vacuumed operations. Consequently, the evaporator pipe has shown a low-temperature drop of 2.60°C, which was not achievable using the horizontal rig. Hence using a vertical rig is far more efficient compared to horizontal lift in terms of adsorption temperature increase and achievement of a lower temperature in the evaporator section.

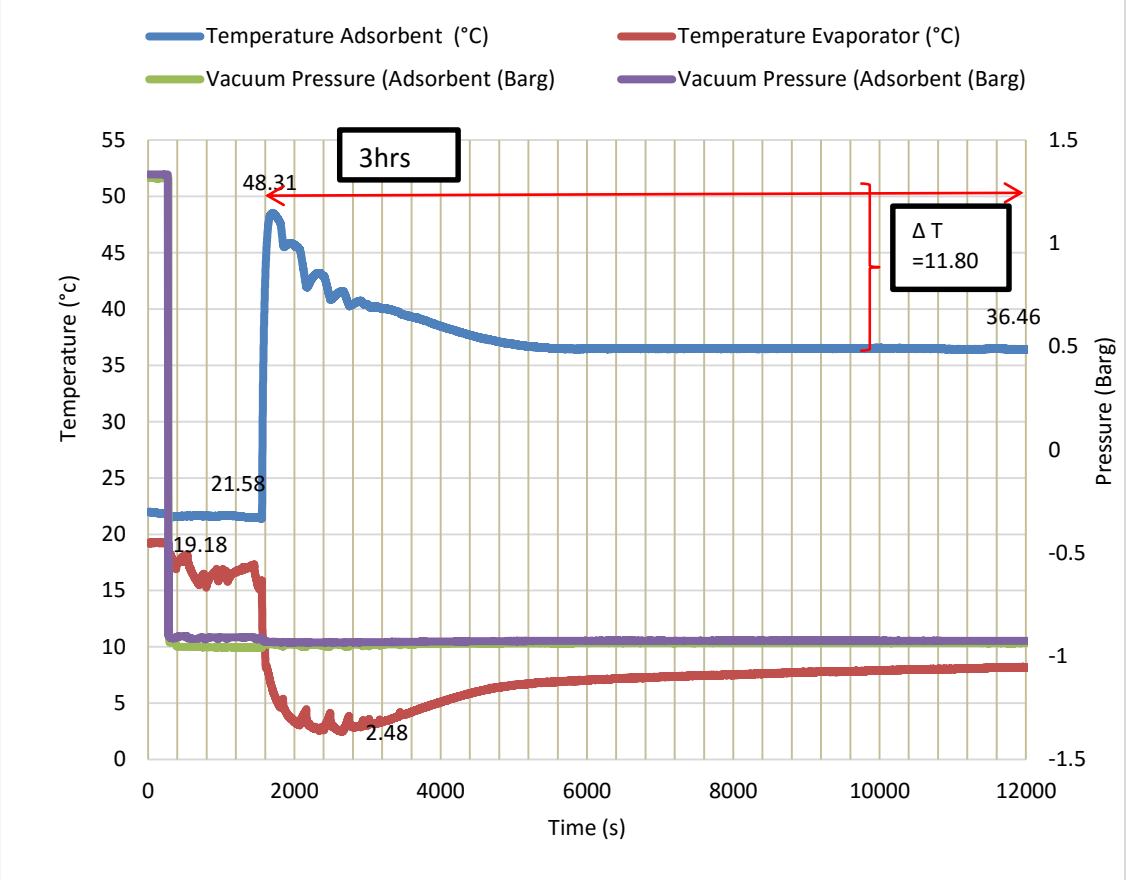


Figure 4.25: Illustration of temperature variations of vermiculite+$CaCl_2$/water in a six-hour time frame of the adsorption process.

Additionally, it was found that when the rig was idle for an extended period, the temperature of vermiculite+$CaCl_2$ could be maintained at a high temperature between 48.40°C and 36.50°C (ΔT = 11.90°C) (see Figure 4.25). This would indicate that this composite material could maintain the appropriate temperature to be transferred to other media such as a heat pipe or heat exchanger for the heating application, with a low-temperature drop.

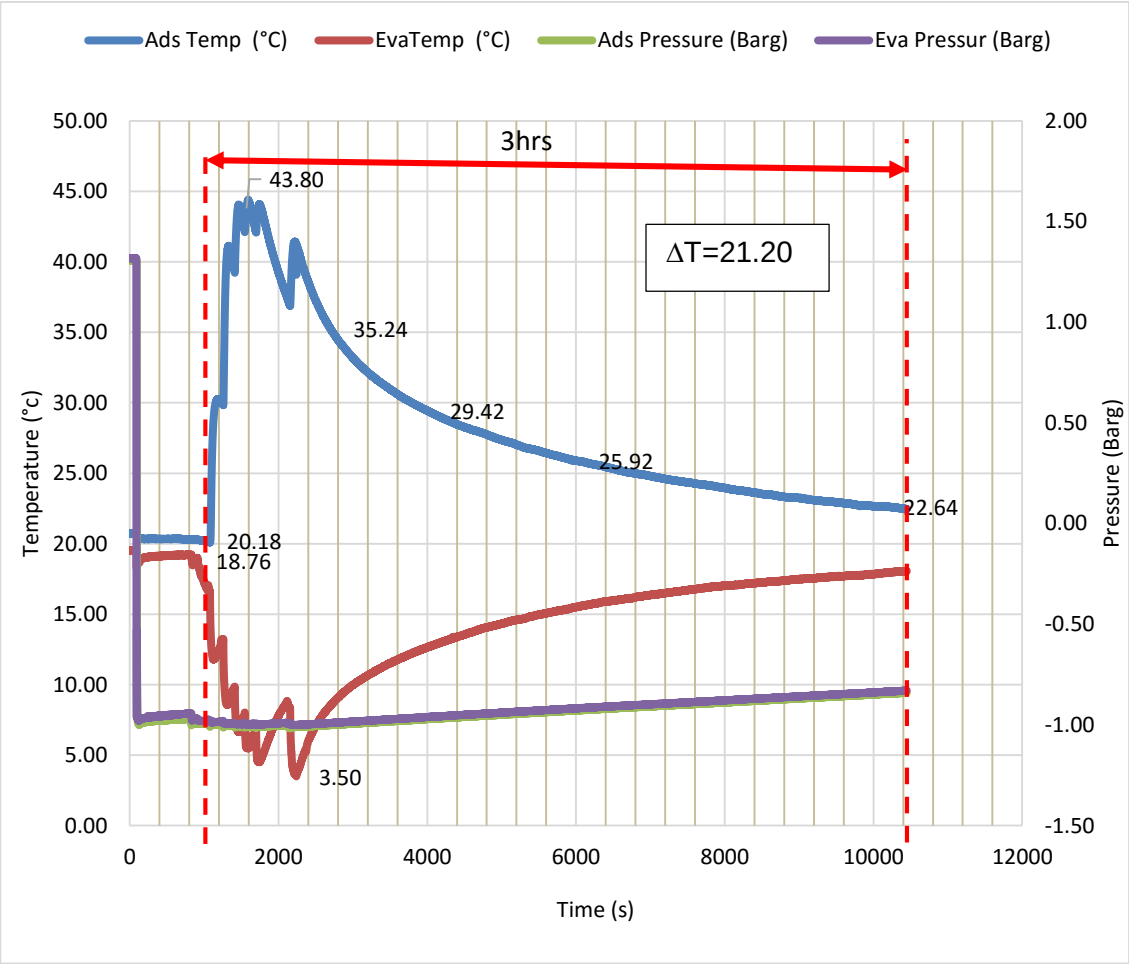


Figure 4.26: Illustration of temperature variation during the adsorption test for silica gel+$CaCl_2$/water - Test 2

A second adsorption test involving working pairs of silica gel+$CaCl_2$/water was conducted and the temperature variation results are shown in Figure 4.26. From these results, it can be seen that the adsorption pipe increased to 43.80°C from an initial temperature of 20.20°C. However, the temperature drop occurred quicker than that of working pair vermiculite+$CaCl_2$. Three hours into the adsorption process the adsorption pipe temperature differed (ΔT) at 21.20°C. This is nearly double the temperature drop compared to Test 1. The evaporator pipe showed a slightly higher temperature than Test 1 at 3.5°C.

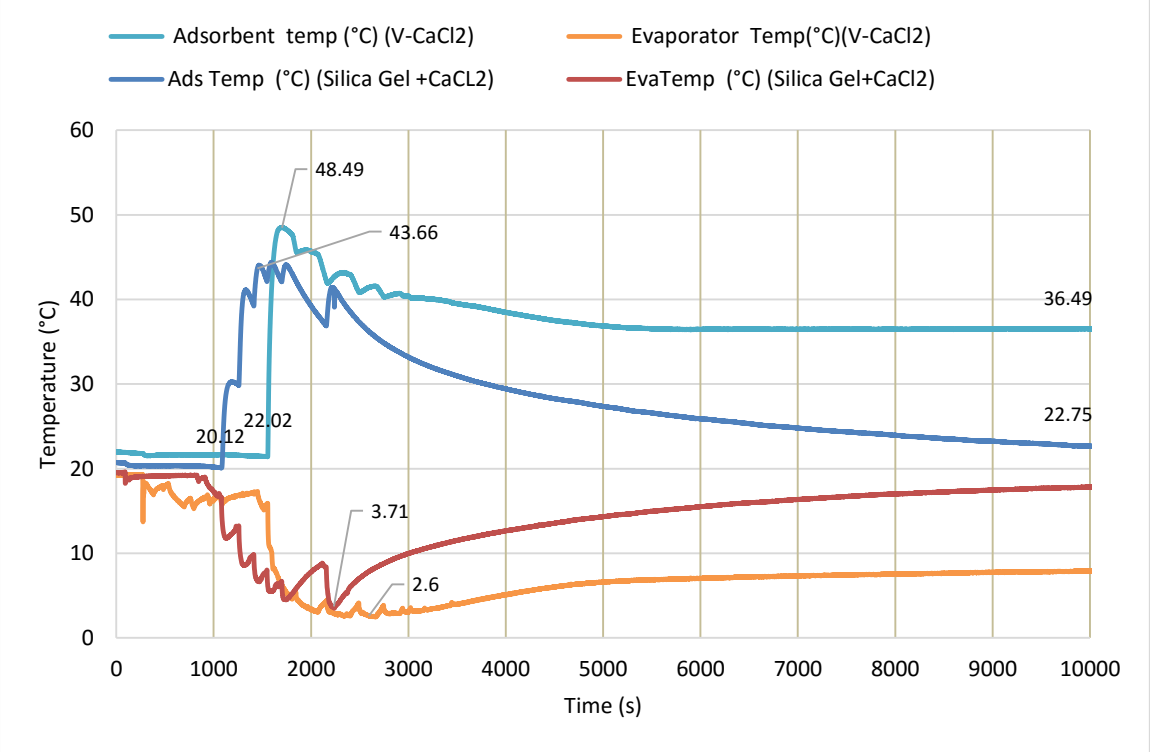


Figure 4.27: Illustration showing a comparison of temperature variations of two tested working pairs.

From Figure 4.27 it can be seen that the working pair of vermiculite+$CaCl_2$ increased the adsorption temperature immediately from the first vacuum. In comparison, silica gel+$CaCl_2$ required re-vacuuming in order to achieve a higher temperature output in the adsorption pipe. Within three hours of the adsorption process vermiculite+$CaCl_2$ showed a lower temperature drop in the adsorption pipe compared to silica gel+$CaCl_2$ (see Table 4.3). This result indicates that vermiculite+$CaCl_2$ is better at maintaining the adsorption temperature for a longer period than silica gel+$CaCl_2$.

Table 4.3: Summary of temperature variations of tested adsorbent materials

Materials	T_{in} Ads (° C)	T_{in} Eva (° C)	T_F Ads (°C)	T_F Eva (°C)	Temperature Drop	Δ T Ads (°C) @ duration
Vermiculite+ $CaCl_2$ /water	21.5	17.2	48.4	2.60	3°C @ 5mins	11.90°C @ 3 hr
Silica gel +$CaCl_2$/water	21.5	18.76	43.8	3.50	3°C @ 6.5mins	22.20°C @ 3hr

Desorption Test

Another objective of this test is to investigate the effectiveness of the adsorbent material to desorb a mass of water from the adsorbent pipe to the evaporator pipe with a low regeneration temperature that can be drawn from waste heat or a low-grade heat source. The desorption test was conducted using a clamp heater with a constant temperature of 60°C.

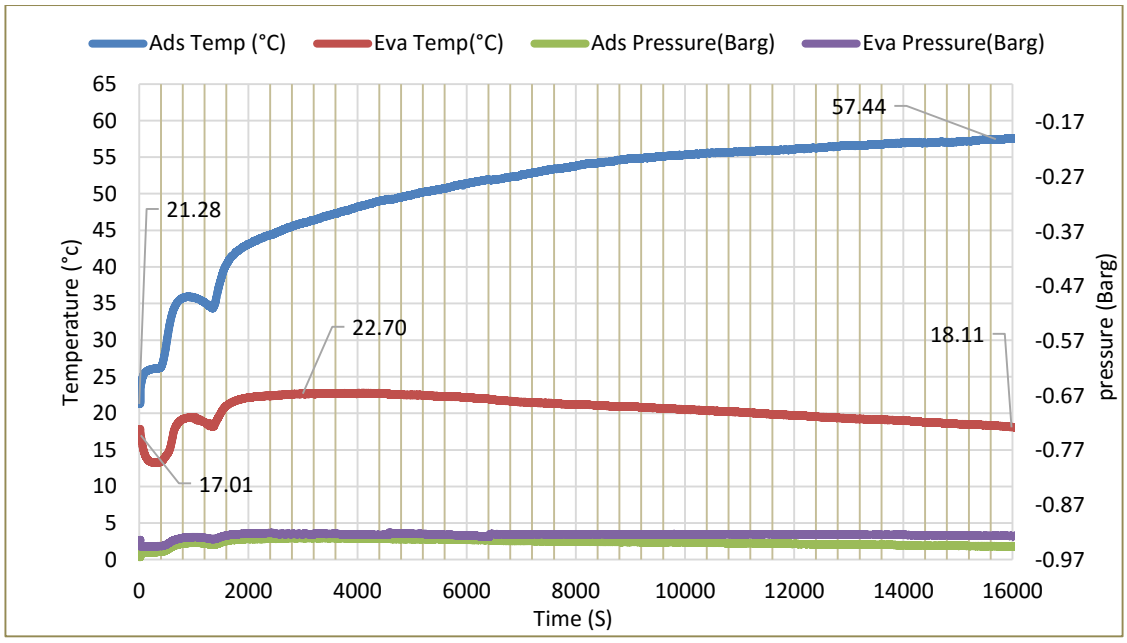


Figure 4.28: Illustration of the desorption test on vermiculite +$CaCl_2$ /water

Figure 4.28 shows the result from the desorption test of vemiculite+$CaCl_2$. As the graph shows, the temperature rise in the adsorbent pipe was 57.44°C, meaning we can conclude that the temperature from the heating clamp transferred effectively to the adsorption pipe. Furthermore, vermiculite+$CaCl_2$ could desorb back 23g of water from 40g of adsorbed water, giving a total water uptake of 0.56g/g. This would indicate that an impregnated composite material could attain a higher energy storage density through the thermochemical reaction and the ability to absorb more water compared to conventional adsorbent materials.

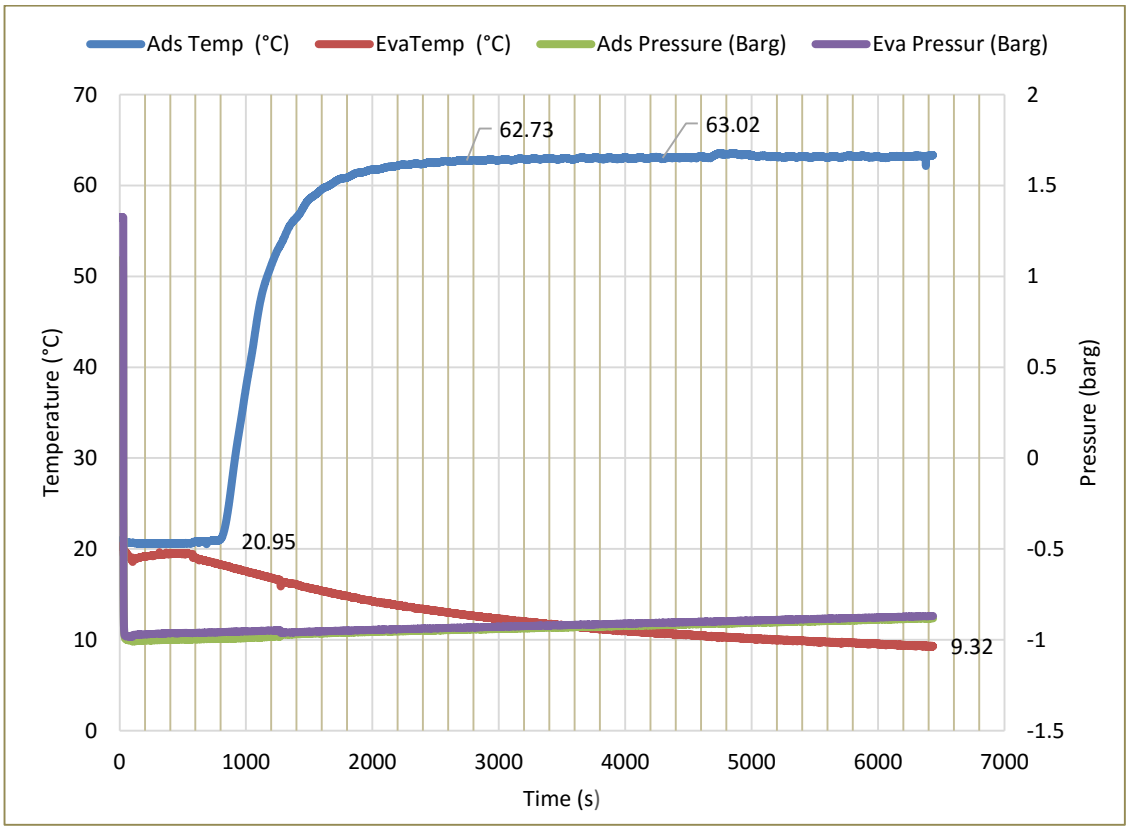


Figure 4.29: Illustration of temperature variations during desorption test for silica gel+$CaCl_2$

Figure 4.29 shows the results from the desorption test for the working pair of silica gel+$CaCl_2$. As the results show, the temperature in the adsorbent pipe increased more

quickly than that of vermiculite+$CaCl_2$. The adsorption pipe temperature increased from 20.95°C to 63.02°C and the evaporator temperature exhibited a temperature drop to 9.32°C. Furthermore, from the analysis of the water uptake via the adsorption process as seen in Table 4.4, the initial weight of dry vermiculite+$CaCl_2$ was hydrated from 49g to 89g (40g of water being adsorbed by this adsorbent), giving a water uptake of 0.55g H_2O/g of adsorbent. Silica gel+$CaCl_2$ would absorb a small amount of water (approximately 5g) which gives a water uptake result during the adsorption of 0.025g H_2O/g of adsorbent. Silica gel+$CaCl_2$ incurs a lower water uptake due to the fracturing that occurs during the drying of the materials which can lead to agglomeration and hence weaken the heat and mass transfer during adsorption.

Table 4.4: Amount of materials for experimental testing (grammes)

Materials		**M** (Before Adsorption)	**M** (After Adsorption)	**∆ M** (Adsorption)	**M** (After Desorption)	**water uptake** (g_{H20}/g_{ads})
TCM1	Vermiculite + $CaCl_2$	49	89	40	66	0.55
	Water (H_2O)	60	37	23	59	
TCM 2	Silica gel +$CaCl_2$	198	203	5	195	0.025
	Water	60	55	5	198	

Table 4.5: Comparison of results with previous research

Salt	Host Matrix	Water Sorption (g/g)	Remarks	Ref
$CaCl_2$	Silica gel KSK	0.70	SWS-1L	(Aristov et al., 1996; Aristov et al., 2002)
	Silica gel KSM	0.25	SWS-1S	(Aristov et al., 1996)
	Vermiculite	1.13	SWS 1V	(Aristov et al., 2000)
	Vermiculite	**0.55**	**VCC**	**Current study**
$MgSO_4$	Silica gel KSK	0.65	SWS 3L	(Aristov, 2003)

The comparative analysis on water sorption from previous research for similar composite materials summarised in Table 4.5 also indicates that impregnated vermiculite has a higher water sorption compared to other impregnated adsorbent materials such as silica gel. It can be inferred from these experimental results and literature that vermiculite+$CaCl_2$ has high water sorption compared to silica gel+$CaCl_2$.

4.4.2 Conclusions from the Temperature Lift and Adsorption/Desorption Investigations Using Horizontal and Vertical Glass and Metal Rigs.

From this survey, the most promising material to be adopted for the THSS is vermiculite+$CaCl_2$ due to the capability of uplift of temperature to 67.50°C in the adsorbent bed with a horizontal glass and metal rig. Furthermore, as concluded from the adsorption/desorption test with a vertical adsorption heat pipe, this composite material would be able to maintain a higher temperature in the adsorbent pipe for up to six hours with a lower temperature drop (3hours at ΔT=11.90°C) compared to silica gel+$CaCl_2$ (3hours @ ΔT=22.20°C). From the adsorption test results it was confirmed that vermiculite+$CaCl_2$ is able to absorb a significant amount of water under the vacuum condition. It was found that vermiculite+$CaCl_2$ had a water uptake of 0.55g/g compared

to silica gel+$CaCl_2$ which only had 0.025g/g. Additionally, during the desorption period, with the desorption temperature at approximately 60°C, the hydrated vermiculite+$CaCl_2$ was able to desorb the mass of water at 23g which gives the desorption water of 0.55g/g. This shows that vermiculite+$CaCl_2$ would be able to desorb a mass of water with a low regeneration temperature. Furthermore, the range of the regeneration temperature is within that of available waste heat, such as the exhaust outlet from an air-conditioning system or a boiler. From these results, the conclusion can be drawn that vermiculite impregnated with $CaCl_2$ is the most promising adsorbent material to be adopted for the THSS system as it has a high water uptake and high temperature lift. Additionally, on looking at the environmental perspective, this material is considered a non-hazardous and environmentally friendly material which will be more sustainable for future generations as a whole.

4.5 Investigation of Microscopic and Physicochemical Properties of Thermochemical Materials (TCM).

Further tests were conducted to find a suitable TCM for this study using a microscopic experiment. To develop a highly efficient adsorbent pipe, the composite material should have the capacity for adsorbing and desorbing the adsorbate (water or ammonia) through its high porosity. However, published data on the composite adsorbent materials' properties are very limited. This experiment is designed to examine the relationship between pores and salt impregnation on the prepared composite TCM.

4.5.1 Microscope Scanning

A preliminary microscope scan of the prepared impregnated silica gel particle shows that the pure dry silica gel surface and inner structure are stronger compared to a particle of

a composite of silica+ $CaCl_2$ (see Figure 4.30). The particle of silica gel impregnated with $CaCl_2$ displays signs of having ruptured into small pieces, as clearly shown in Figure 4.31. Similarly, structures of a particle of silica gel + $LiNO_3$ show fracture lines using the same scanning method (see Figure 4.32). There is currently a lack of literature related to adsorption systems pertaining to cases of ruptures as investigated in this study. However, it is assumed here that during the preparation of the composite material, the composite material might have been exposed to a high temperature or chemical reaction during drying which could lead to this rupturing.

The fracture of a composite material might also result in the agglomeration and swell of and therefore low heat and mass transfer would occur. In the available literature, some of the researchers emphasised the study of different working pairs to improve this phenomenon. Tokarev et al. (2010) have explored a new novel adsorption material that involved the composite of $BaCl_2$/vermiculite, $BaCl_2$/γ-Al_2O_3 and $BaCl_2$/ (carbon subunit) with ammonia as the adsorbate. Through material synthesis, they found that the phenomena of agglomeration and swelling did not occur during their sorption experiments. Furthermore, they also found that this novel composite material has improved the ammonia uptake with a corresponding increase in the COP of 0.3 to 0.6. In this study we recognise this as a potential research opportunity to study vermiculite as a host matrix due to its advantages as inducing a high adsorbate uptake. The literature emphasising sorption studies of vermiculite impregnated with aqueous salts is rarely published so this would be a new field of study. This material synthesis would bridge the gap between employing composite TCMs within sorption technology.

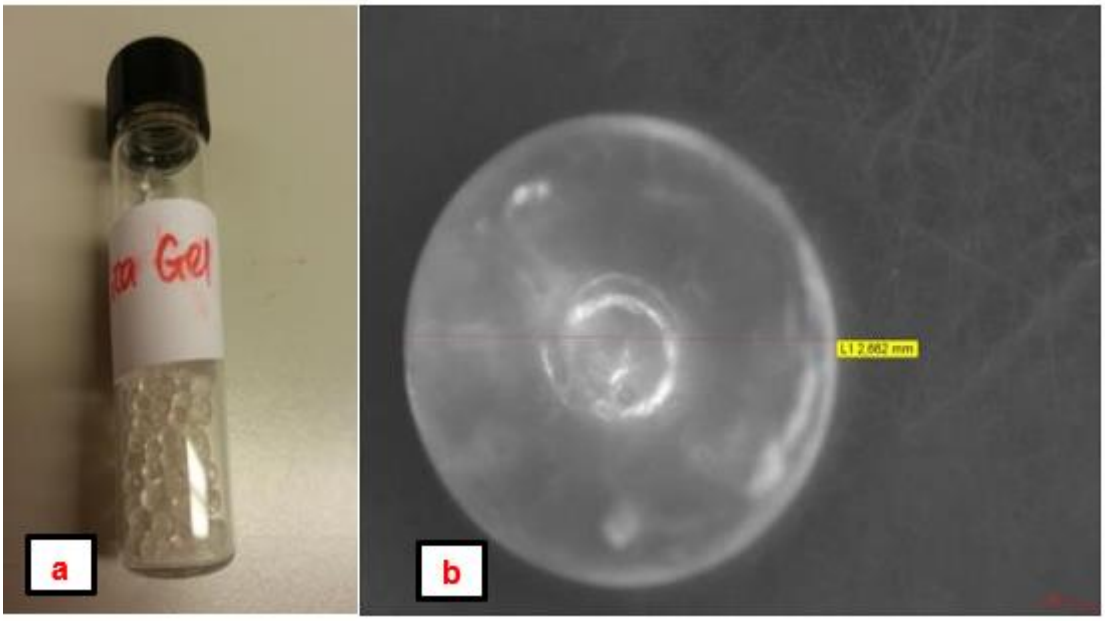


Figure 4.30: a) prepared saturated pure silica gel in an airtight casing and (b) a single granule through a microscope (500µm scale.)

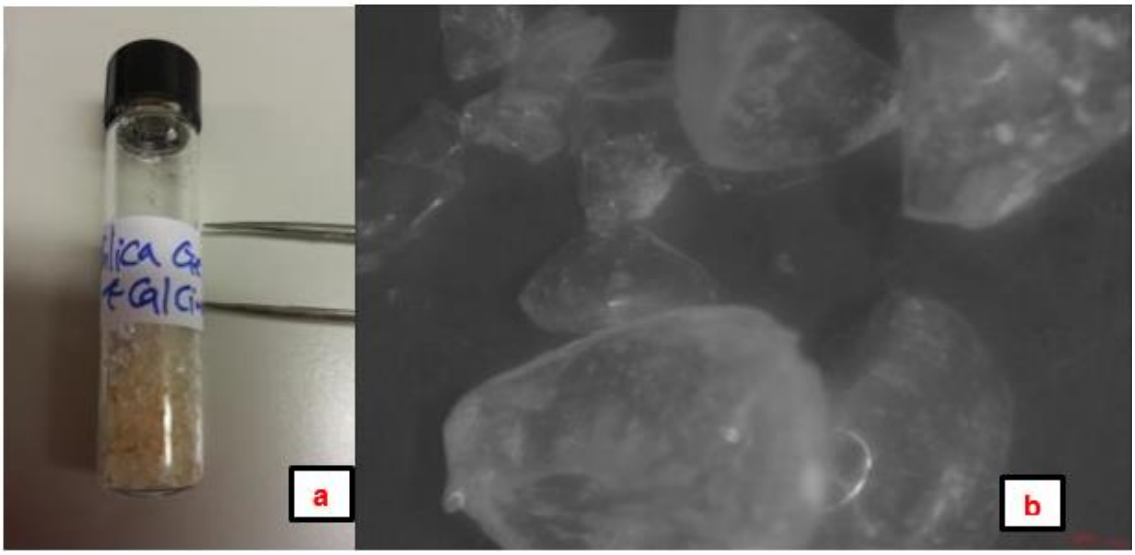


Figure 4.31: (a) prepared saturated silica gel+ $CaCl_2$ in an airtight casing and (b) a broken granule through a microscope (500µm scale.)

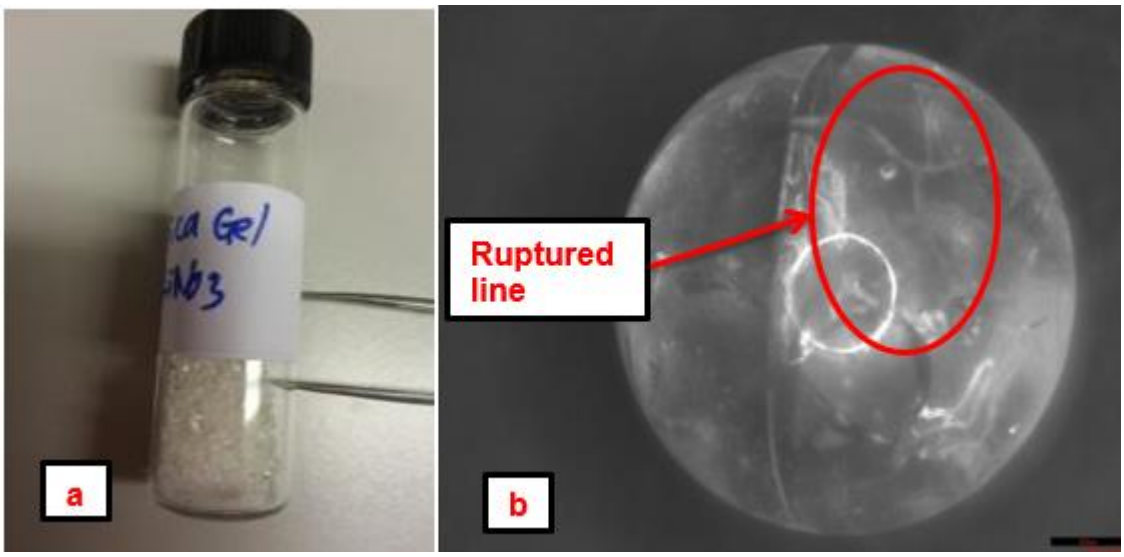


Figure 4.32: (a) prepared saturated silica gel+ $LiNO_3$ and (b) a single granule through a microscope (500µm scale.)

4.5.2 **Electron Beam Microscopic Scanning**

To have a visualisation of the effectiveness of impregnation of composite materials, the existence of pores in each particle will be examined through the use of electron beam microscopic scanning. The two most common methods currently used for existing investigations are the ESEM (Environmental Scanning Electron Microscope) and SEM (Scanning Electron Microscope).

Environmental Scanning Electron Microscopy (Hydrated Materials)

The prepared composite material, which needs to be analysed through DSC, is saturated approximately forty-eight hours before testing. This ensures that the specimen is fully saturated with water. An ESEM is capable of capturing images of the specimen in the wet mode and thus it was used for this study. The ESEM was developed in the mid-

eighties and its primary advantages lie in permitting the user to vary the sample environment through a range of pressures, temperatures, and gas compositions. The ESEM retains all of the performance advantages of a conventional SEM but removes the high vacuum constraint on the sample environment. Wet, oily, dirty, non-conductive samples may be examined in their natural state without modification or preparation. The ESEM offers high resolution secondary electron imaging in a gaseous environment of practically any composition, at pressures as high as 50 Torr, and temperatures as high as 1500°C (Kimseng and Meissel, 2001). The ability of this electron microscope to scan a wet specimen is necessary for scanning the composite specimens prepared for this experiment. Due to these properties this equipment was chosen to investigate the existence of water particles inside the porous matrix and salt solution on the surface of impregnated composite materials.

The ESEM works, as shown in Figure 4.33, by acceleration of the electron column which focuses a beam of electrons onto the sample surface. Interactions between the sample and the beam of electrons cause a variety of signal emissions. The signals are detected and reconstructed into a virtual image displayed on a computer display monitor (Kimseng & Meissel, 2001)

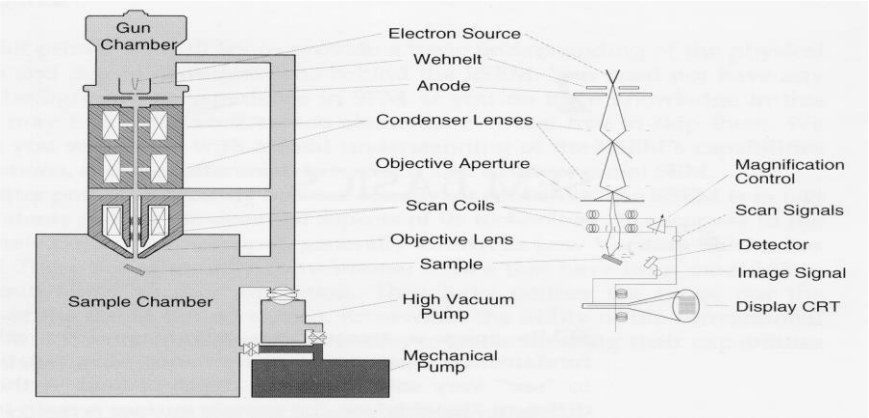


Figure 4.33: A schematic representation of an ESEM (Kimseng and Meissel, 2001).

ESEM on Silica Gel+$CaCl_2$

The impregnated silica gel+$CaCl_2$ scanned through the ESEM featured some of the obvious signs suggesting existence of water particles, as shown in Figure 4.34 (a~b). As the ESEM is able to scan when the subject material is wet, the silica gel + $CaCl_2$ particle was fully saturated with the aqueous salt solution. As shown in Figure 4.35 (a~b), the water particle is covering the surface of the silica gel particle and the crystallised salt when the specimen was still in a saturated condition. This indicates that the impregnation of the composite silica gel with the salt solution was successfully prepared as the existence of crystallizing salt and water particle from ESEM scanning. However, the pores of this composite material were hard to visualise. This might be due to the particle of water covering the surface of this material therefore preventing the ESEM from capturing the inner particles. On the other hand, when the specimens are dry, the crystalline salt of $CaCl_2$ is clearly seen on the surface of the particle, which was shown in Figure 4.36 (a~b).

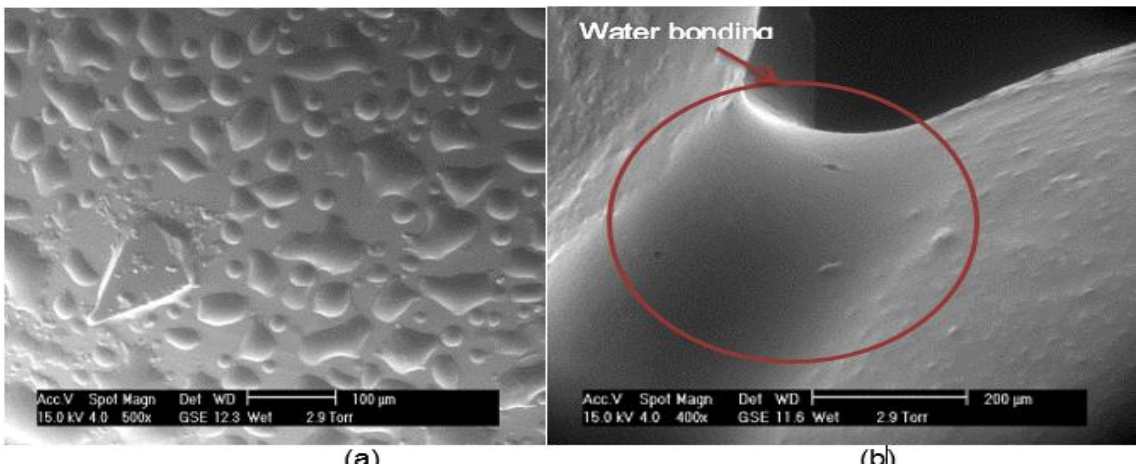


Figure 4.34: ESEM images of a water particle on the surface of a silica gel granule and a water particle bonding on two granules

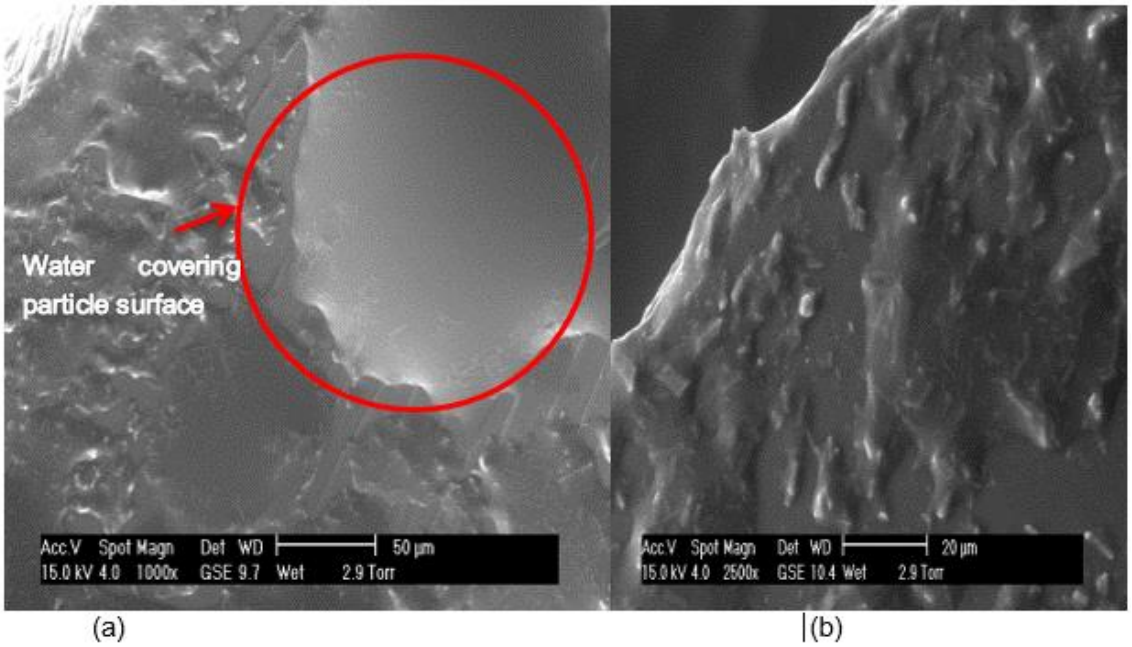


Figure 4.35: ESEM images of saturated silica gel+$CaCl_2$ .with (a) a water particle covering the surface of the particle and (b) the crystallised salt covered by a water particle.

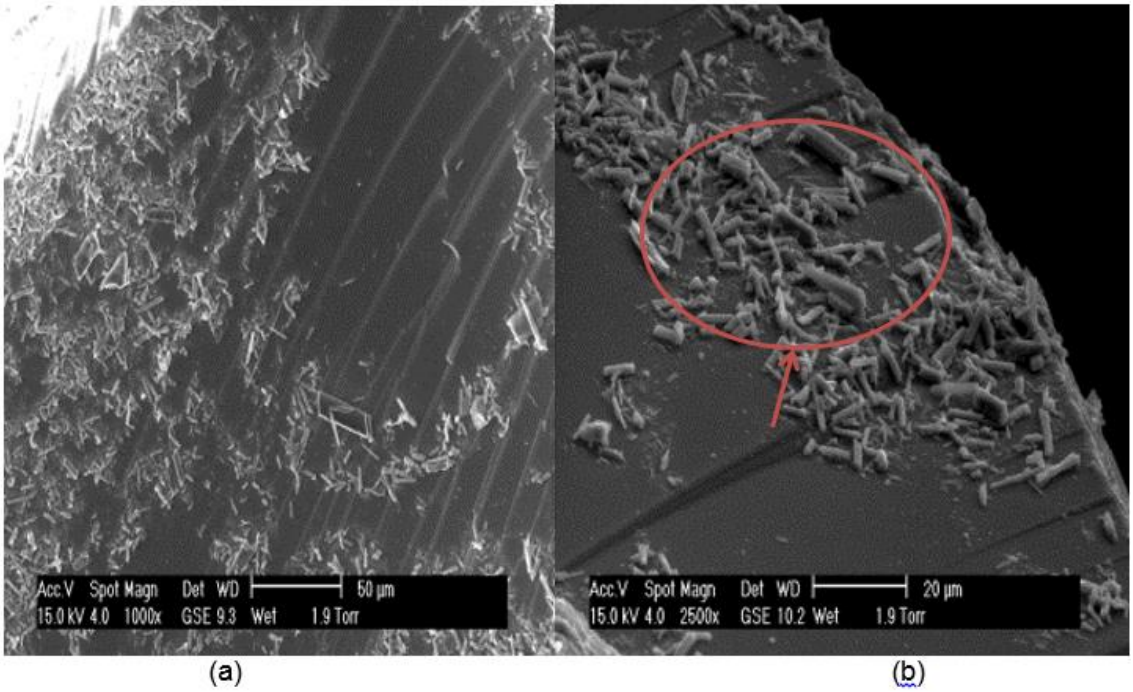
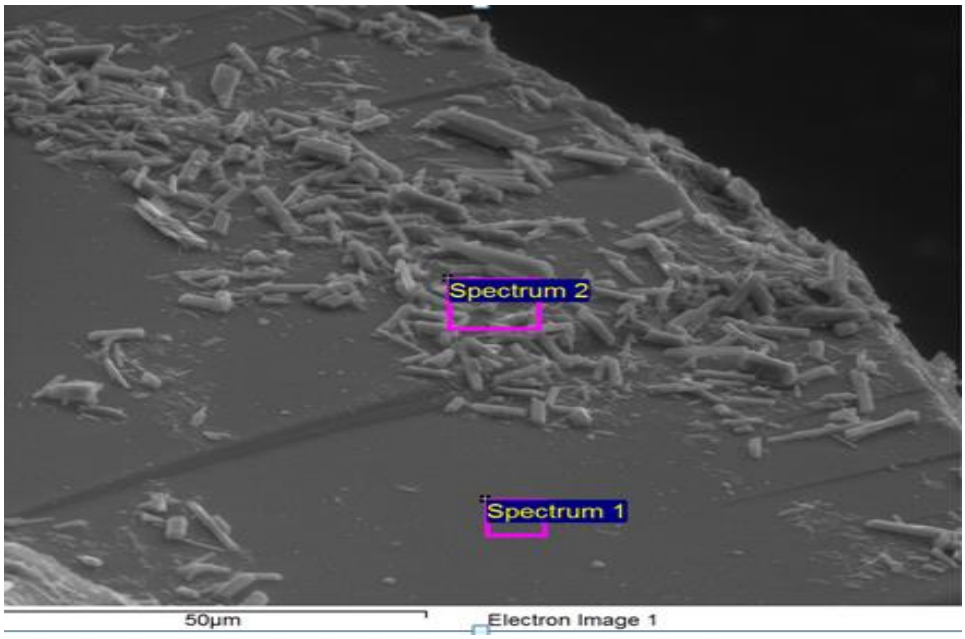
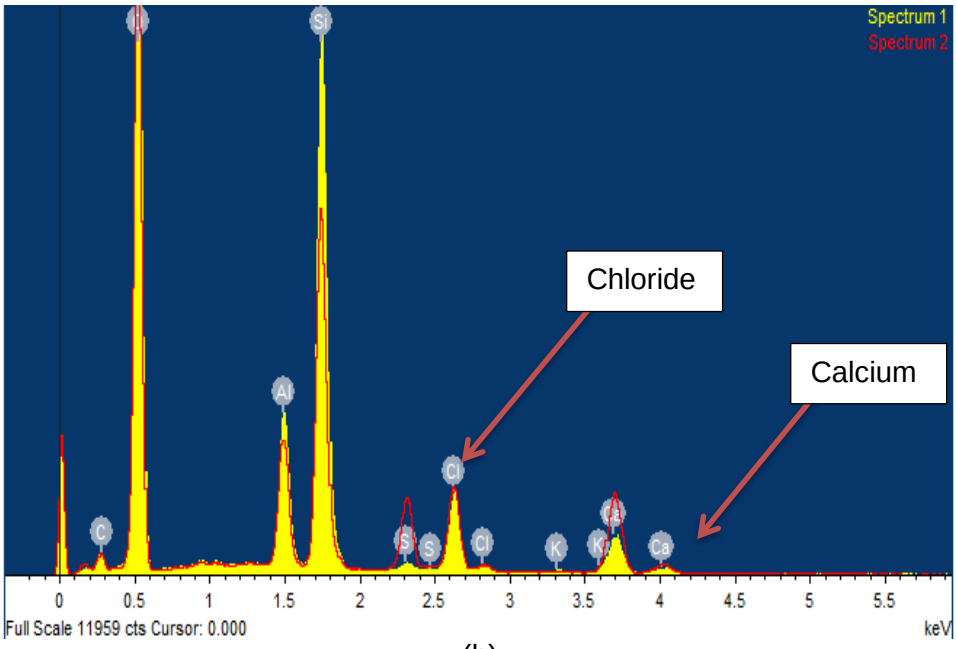


Figure 4.36: ESEM images of a composite of silica gel+$CaCl_2$ showing $CaCl_2$ crystallisation after the material dried



(a)



(b)

Figure 4.37: ESEM images & morphology of dry silica gel +$CaCl_2$.

Another analysis carried out was to determine the existence of a chemical element in the composite material. The morphology of dry silica gel +$CaCl_2$ is shown in Figure 4.37 (a~b). From Figure 4.37b, the chemical elements of calcium (Ca) and chlorine (Cl) can be seen in the x-ray, which indicates that the structure of $CaCl_2$ was formed in a

crystalline phase and was not detrimentally affected by the adsorption or desorption process. The morphology shows a peak of silicon (Si), meaning that the majority of particles in the scan were silica gel. The additional additives such as aluminium (Al) and sulphur (S) were from the aluminium pan and the sulphur from the previous impregnation procedure that may have intruded in the sample.

ESEM on Silica Gel + Lithium Nitrate

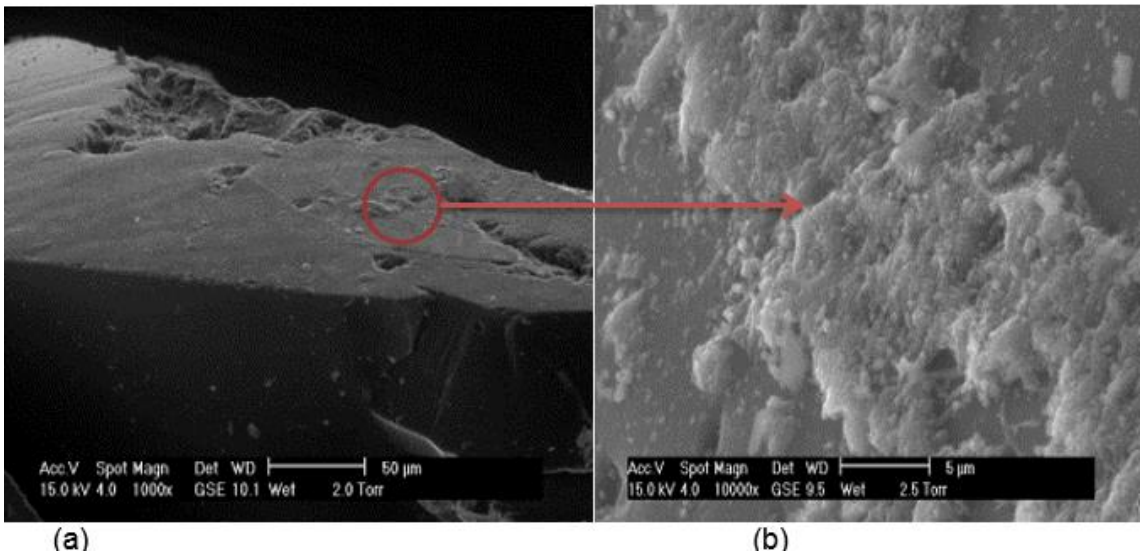


Figure 4.38: (a) ESEM images of a silica gel + lithium nitrate mark and (b) enlarged lithium nitrate on the surface of silica gel.

Figure 4.38 illustrates the magnification of silica gel + lithium nitrate through the ESEM. These ESEM images show the formations of $LiNO_3$ on the surface of the host matrix of silica gel when the material was dehydrated, and the existence of water particles was not captured. This may be due to the lower percentage of water absorption when compared to silica gel+$CaCl_2$. The pore size of these specimens was also difficult to analyse using the ESEM scanner. This may be due to the pore size of silica gel being less than five µm and therefore could not be captured using the ESEM.

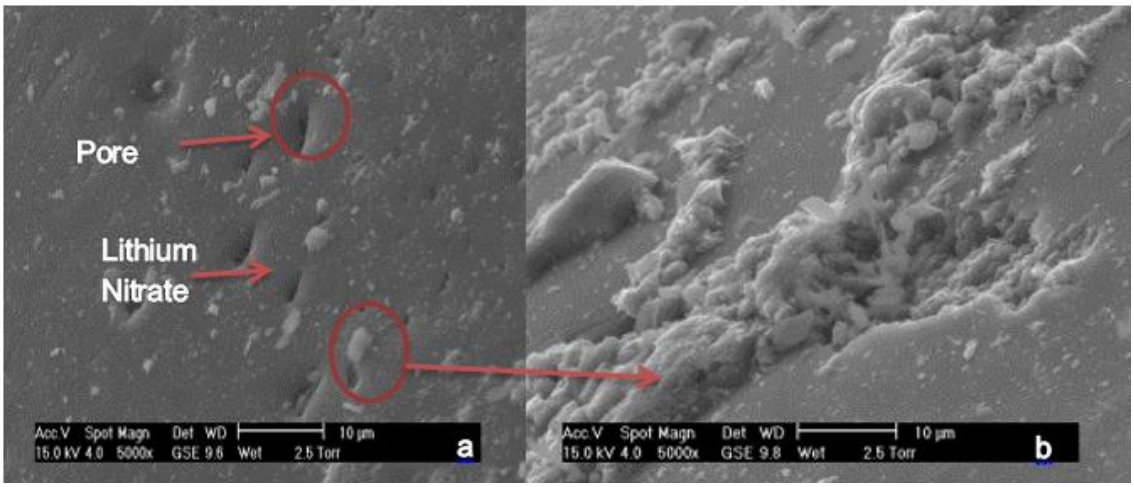


Figure 4.39: (a) ESEM images of pores on the surface of silica gel and (b)lithium nitrate on the surface of silica gel.

Figure 4.39 illustrates different perspectives from Figure 4.38. These images were scanned on a different surface, and some pores were significantly more visible on the surface. However, due to the particles rupturing into small pieces, some of the pores might also be among the layer of ruptured structure of the silica gel. Due to lack of literature reporting similar issues, the assumption of the existence of pores will be removed from this investigation.

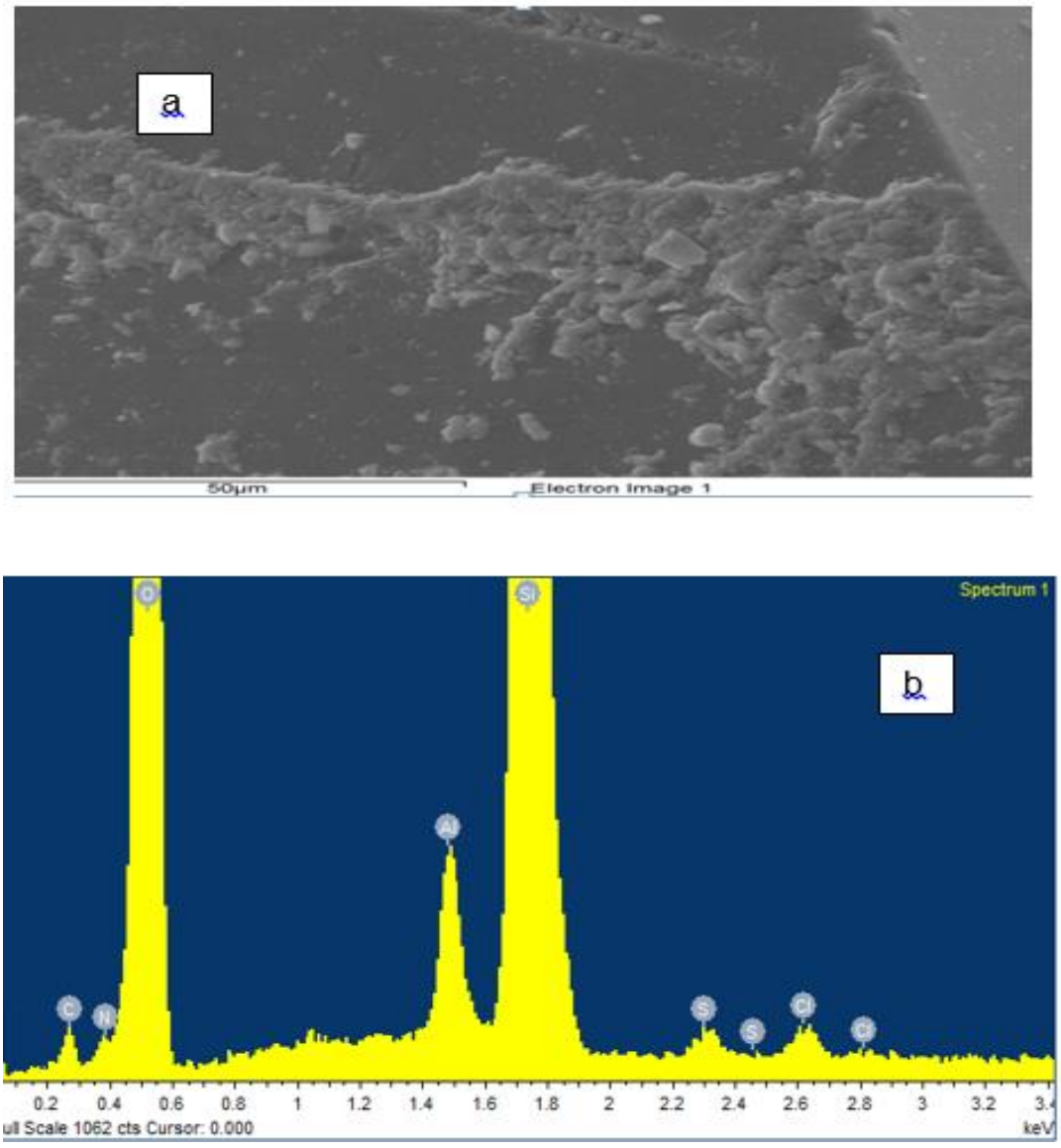


Figure 4.40: (a) ESEM images and morphology of dry silica gel +$LiNO_3$ and (b) X-ray pattern $LiNO_3$.

The morphology of the scan of silica gel+$LiNO_3$ is shown in Figure 4.40. This image shows the major element in the particles is silicon (silica gel). The second peak of the scan illustrates a prevalence of Oxygen (O) from the water particles (H_2O) and $LiNO_3$. Other elements such as Chlorine (Cl) are found in trace amounts due to contamination from the previously prepared materials.

ESEM on Vermiculite +$CaCl_2$

With the use of ESEM scanning, as illustrated in Figure 4.41 (a) and (b), we have exhibited that this hydrated composite material was covered with a layer of water around the outside of the surface structure. This image therefore indicates that the saturation procedure was successful. However, the scan could not quantify the percentage of water absorbed during the saturation process. This problem may be resolved using a different type of experimental procedure or other experiment rigs that could measure the amount of water vapour absorbed by this material. The pore size of the vermiculite can be clearly seen in Figure 4.41 (c) and (d).

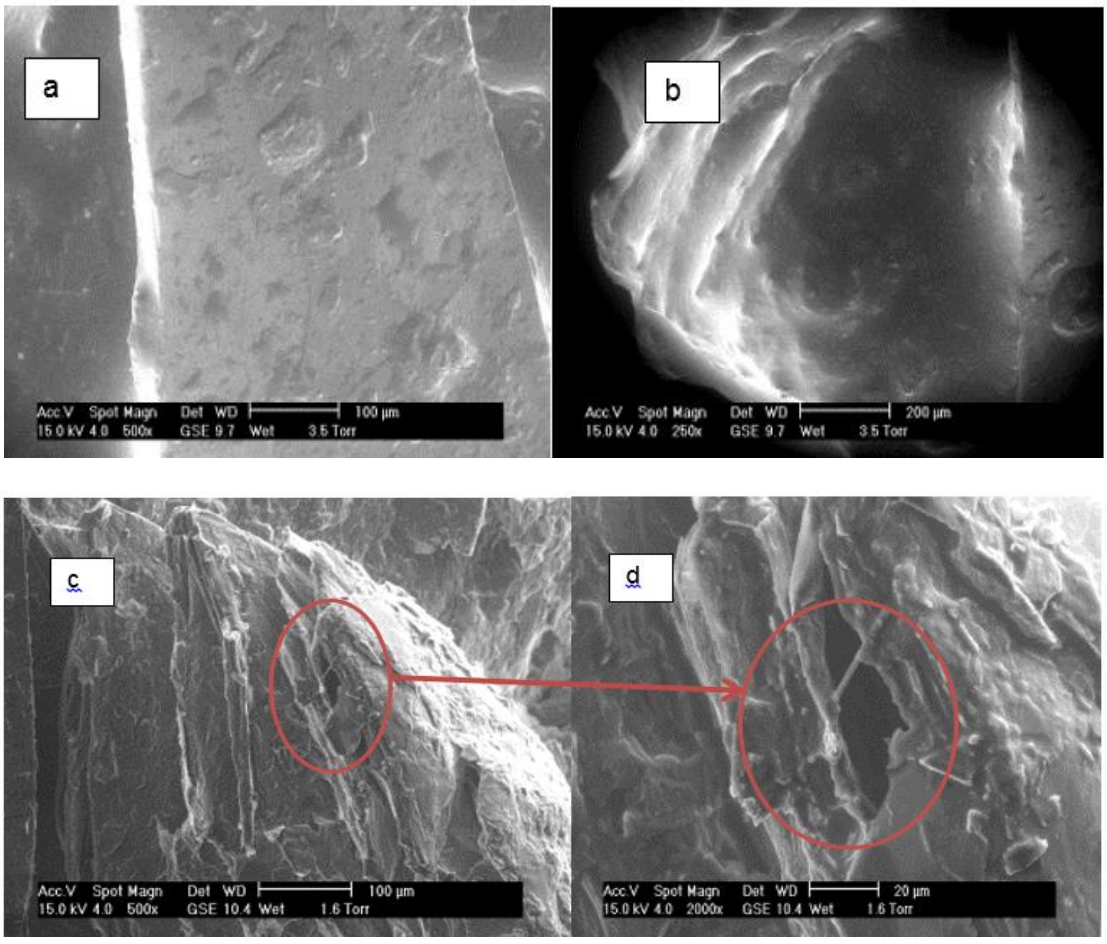


Figure 4.41: ESEM images of vermiculite + $CaCl_2$

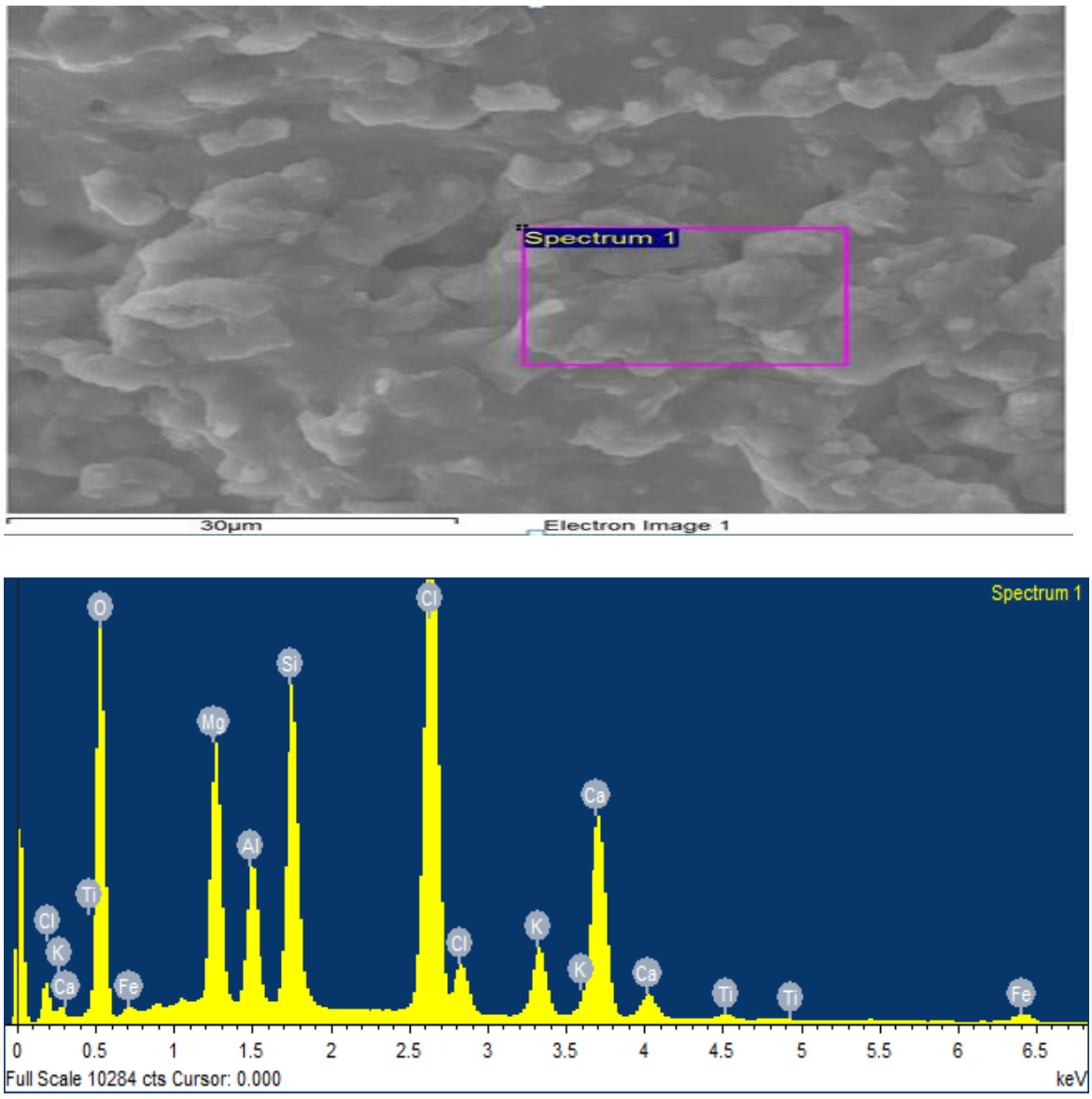


Figure 4.42: Morphology of vermiculite + $CaCl_2$.

From the scan, as shown in Figure 4.42, we can see that the elements chlorine (Cl) and calcium (Ca) were two of the most common within the composite material. Other elements, including aluminium (Al), titanium (Ti) and potassium (K), as well as others, were from the host matrix of vermiculite, as shown in Table 4.6.

Table 4.6: Typical chemical analysis of properties of vermiculite (Dupre Chemical, 2011.)

Material	Percentage	Material	Percentage
Silicon (SiO_2)	39.60%	Iron (Fe_2O_3)	7.93%
Magnesium (MgO)	23.54%	Calcium (CaO)	2.12%
Aluminium (AI_2O_3)	9.22%	Titanium (TiO_2)	1.02%
Potassium (K_2O)	6.11%	Fluorine (F)	0.5%
Water impurities	9.96%		

ESEM on Silica Gel+$MgSO_4$

Figure 4.43 (a-d) show the surface scans of silica gel+ $MgSO_4$, each with a different magnification. In the images it can be seen that the guest salt of $MgSO_4$ clustered in various spots on the silica gel surface. However, the pore size could not be observed in this scan due to the pore size of silica gel in super mesoporous size (2nm>Pores Diameter>1nm) meaning it could not be visualised through the ESEM. Figure 4.43c illustrates a fractured piece from the silica gel granule. This image clearly shows the host matrix of silica gel as fractured after hydration, which will have agglomerated the TCM and thus will be lowering the water sorption ability.

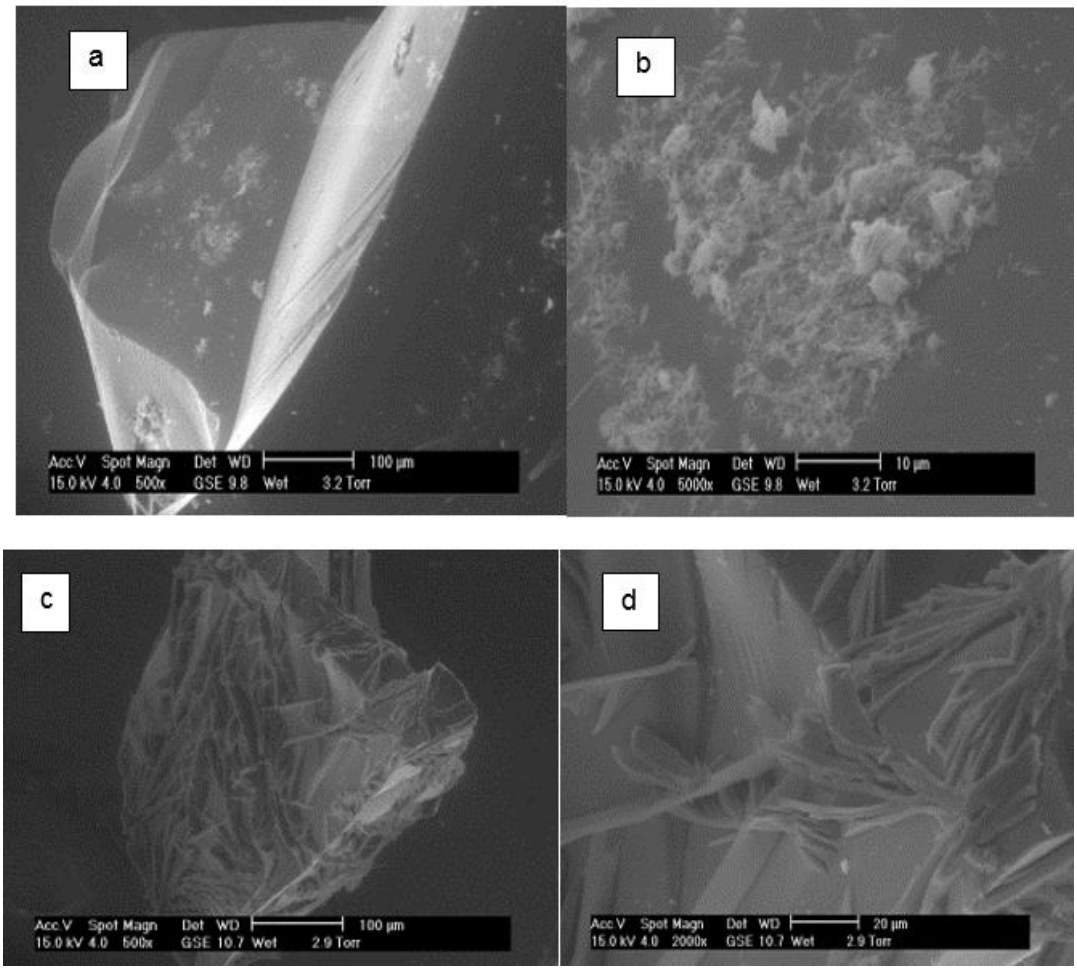


Figure 4.43: ESEM images of silica Gel+$MgSO_4$

Scanning Electron Microscopic (Dehydrated Materials)

A scanning electron microscopic (SEM) was chosen for use on dehydrated materials in order to investigate the existence of salt impregnation within the host matrix (vermiculite, silica gel). This method has been used by many researchers for investigating the pore size distribution of adsorbent materials adopted for Thermochemical Energy Storage (Bales et al., 2008; Ristić et al., 2012; Myat et al., 2013; Zheng et al., 2014; Grekova et al., 2014). In this particular experiment, the material needs to be dry before scanning

can take place. The prepared, impregnated materials were kept in a vacuum container in the lead up to the experiments in preparation.

SEM on Vermiculite + $CaCl_2$

Figure 4.44 (a~d), show the surface structure of vermiculite+$CaCl_2$ at different magnifications. These images show that the structure of vermiculite pores is in-between the surface layer and some are in the spot forms (see Figure 4.44 a&b). This may indicate that the vermiculite matrix has a higher porosity percentage than silica gel. This could be an advantage for absorbing more water vapour during the adsorption process. Furthermore, with a high level of porosity, the guest salt would be able to entrap not only on the surface of the host matrix, but inside of the whole matrix form (see Figure 4.45). Figure 4.46 has shown that the pore size of this material is possible to capture using the SEM. This may be due to the size vermiculite pores falling into the category of a microspores (Pores Diameter<2nm) structure.

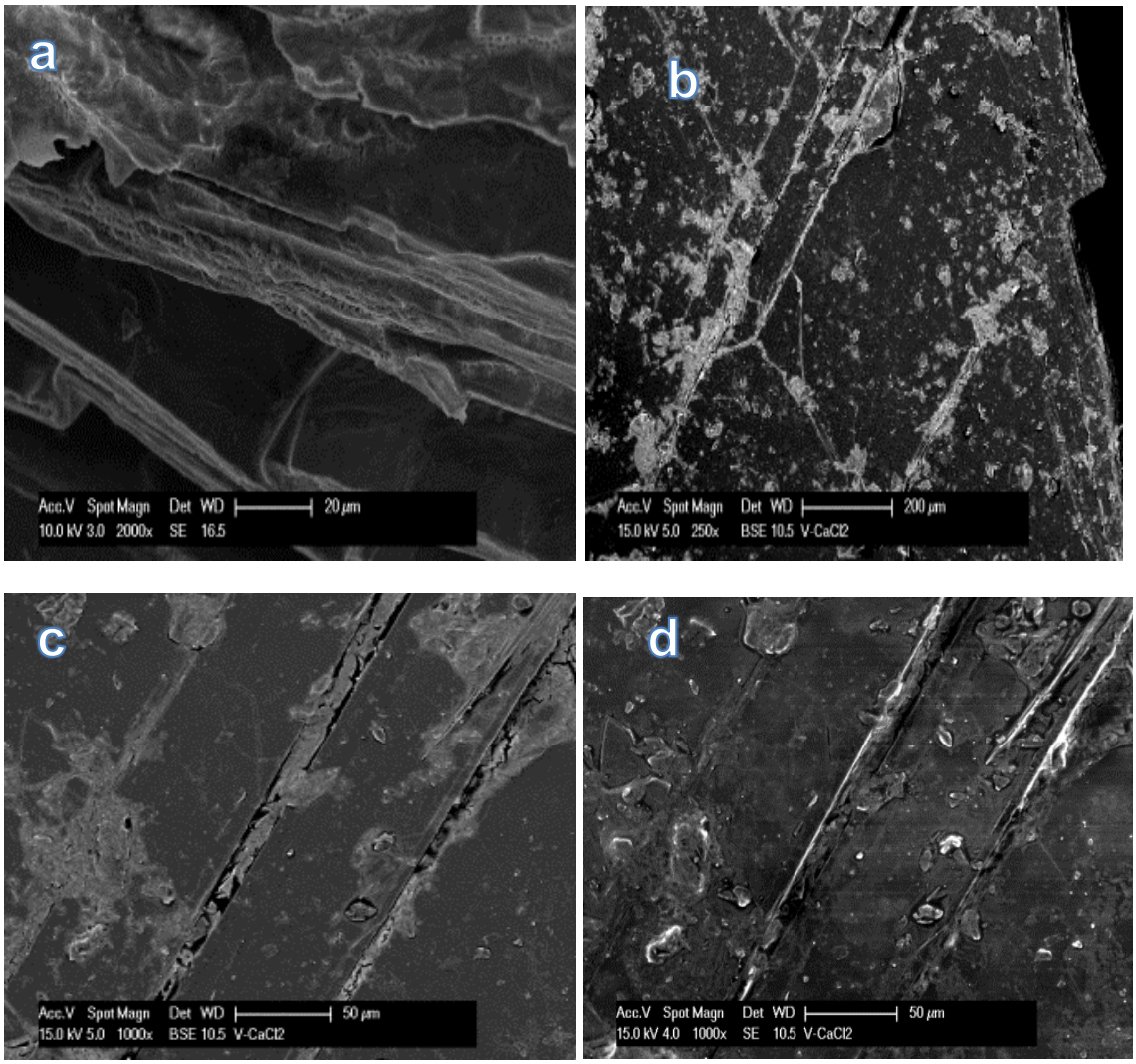


Figure 4.44: SEM images of vermiculite +$CaCl_2$ (a) magnified at 2000x, (b) magnified at 250x, (c) (d) magnified at 1000x.

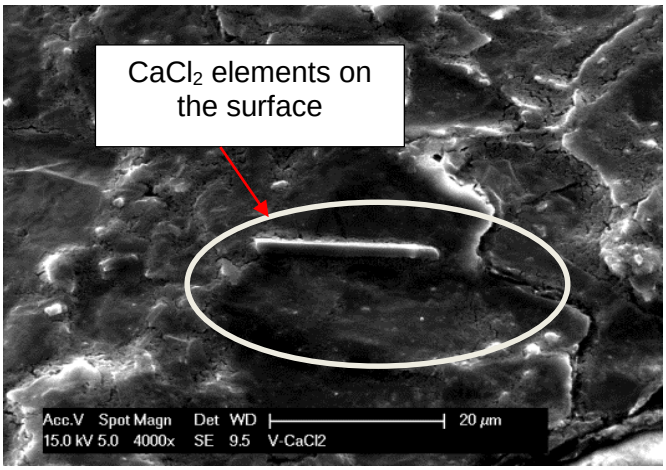


Figure 4.45: SEM image showing appearance of $CaCl_2$ in crystallised form on the surface of vermiculite+$CaCl_2$.

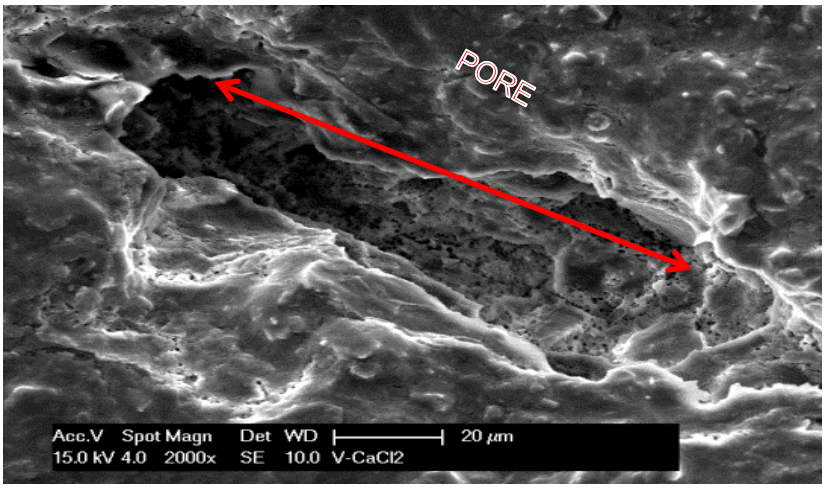


Figure 4.46: SEM image showing appearance of pore on random section of surface of vermiculite+$CaCl_2$

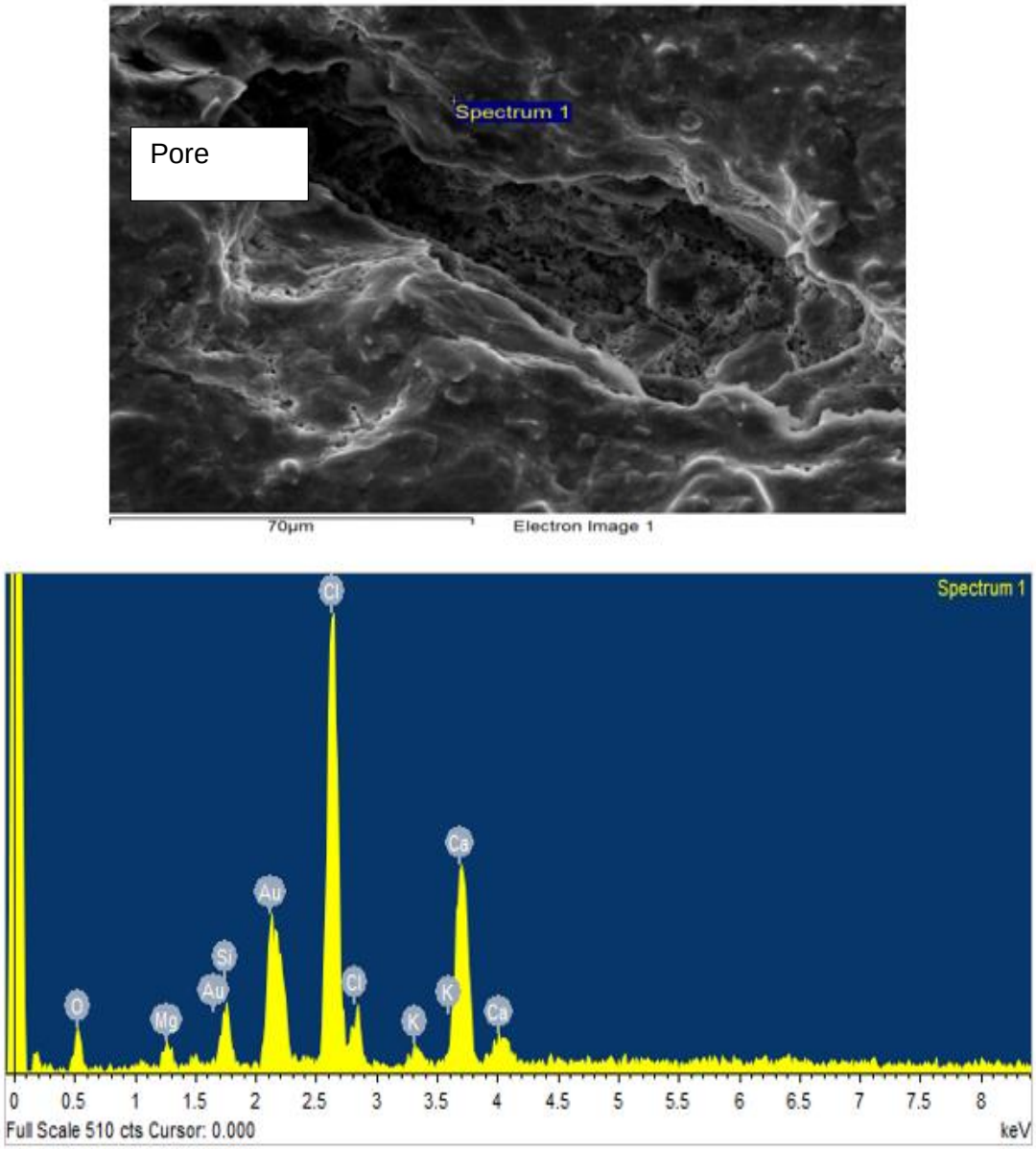


Figure 4.47: Chemical element morphology of vermiculite +$CaCl_2$.

The material morphology in Figure 4.47 indicates that the aqueous salt compound entrapped inside the vermiculite matrix consists of calcium (Ca) and chlorine (Cl). Other chemical elements such as Au, K, O, and Si are some of the elements that make up vermiculite. The peaks of Cl and Ca on the morphology diagram are showing that the salt solution successfully impregnated the host matrix of vermiculite. This morphology

noticeably differs from Figure 4.42 due to the scan being carried out on random sections of the surface.

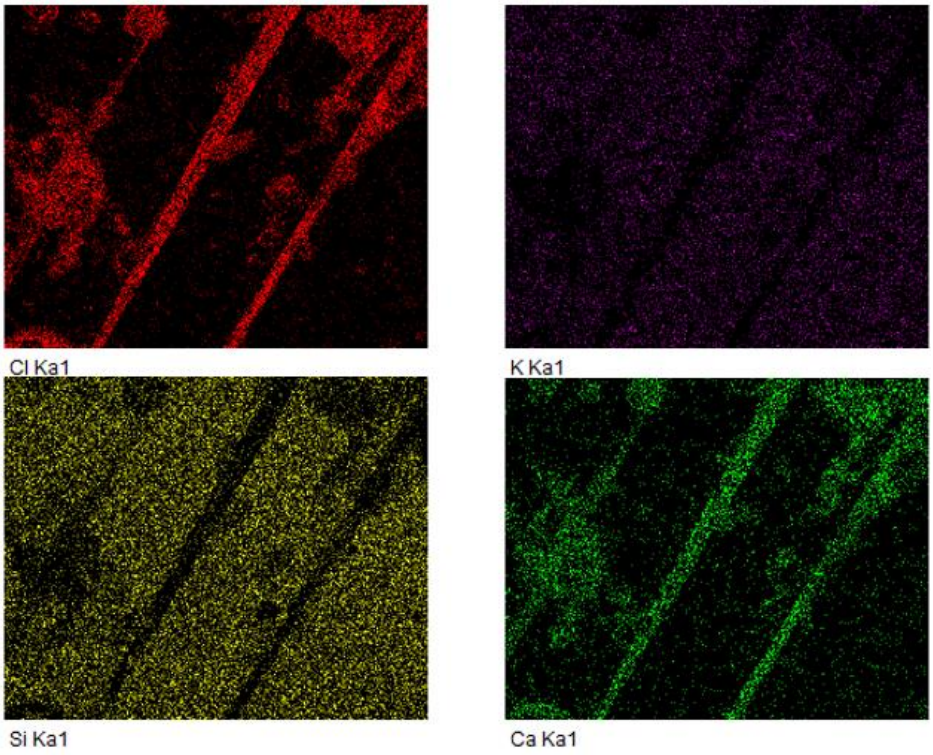


Figure 4.48: Chemical element colour coding scan of vermiculite+$CaCl_2$.

Another chemical element scan was carried out through colour coding scanning as shown in Figure 4.48. As can be seen from this scan, the chemical elements Cl (red), K (purple), Si (yellow), and Ca (green), were observed. These elements are derived from the properties of vermiculite and aqueous salt of $CaCl_2$. However, the properties are not limited to these chemicals. These chemicals were captured above others due to the higher number of particles that existed in the scanned sample.

SEM of Vermiculite + $MgSO_4$

Another SEM of vermiculite with the different guest salt of magnesium sulphate ($MgSO_4$) is shown in Figure 4.49 a~d. This scan shows that vermiculite is not detrimentally affected by the desorption process. There is no evidence of the structure of the host matrix of vermiculite expanding. Figure 4.49b shows the enlarged surface from SEM Figure 4.49a and this SEM illustrates that this layer of vermiculite could be considered to be the pore structure. Figure 4.49d shows the presence of aqueous salt on the surface and the layers of vermiculite.

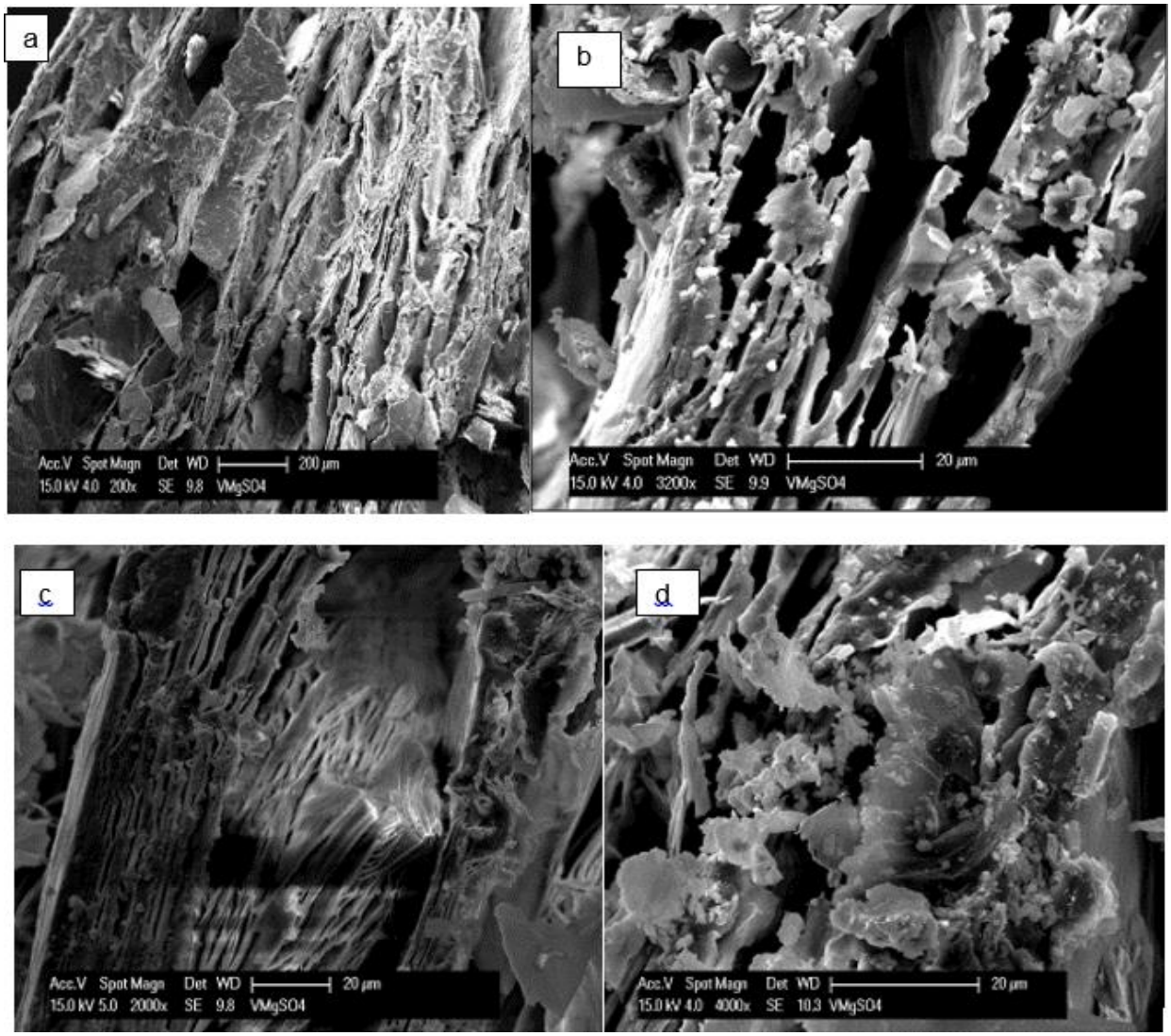
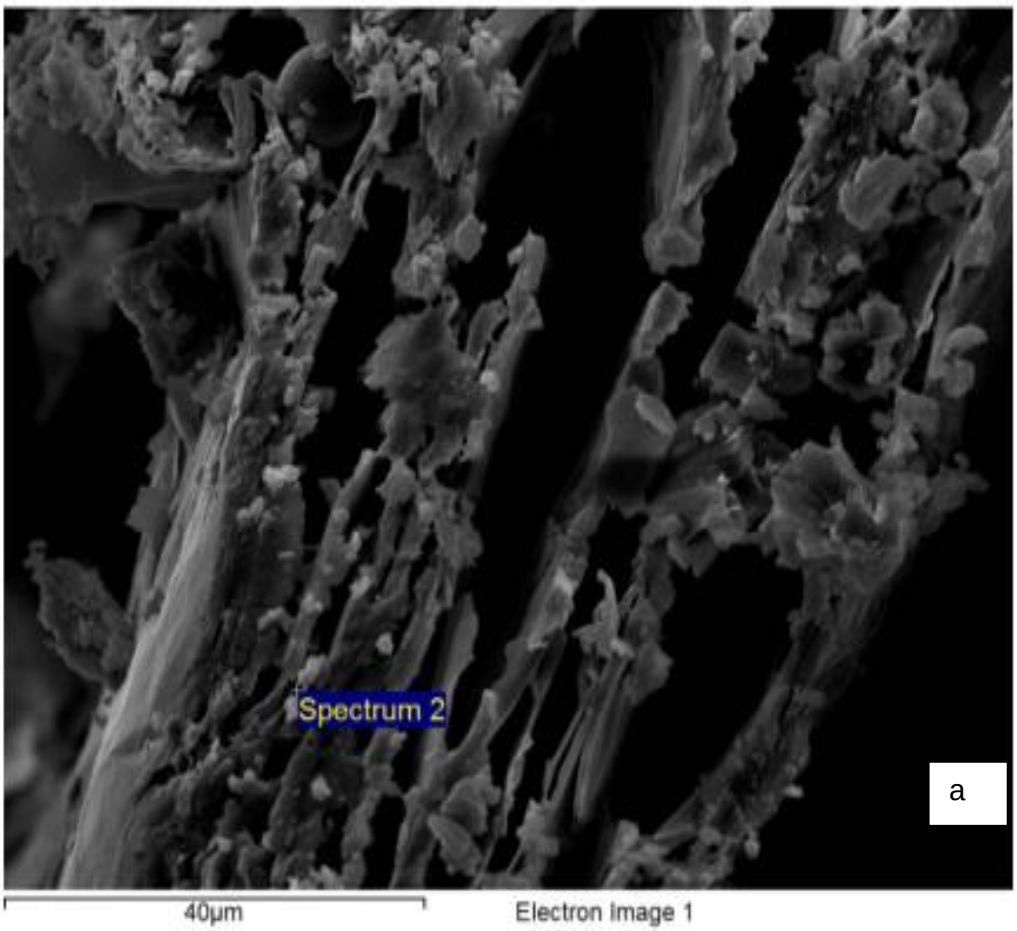


Figure 4.49: SEM images at magnification (a) 200x, (b) 3200x, (c) 2000x and 4000x of vermiculite+$MgSO_4$.



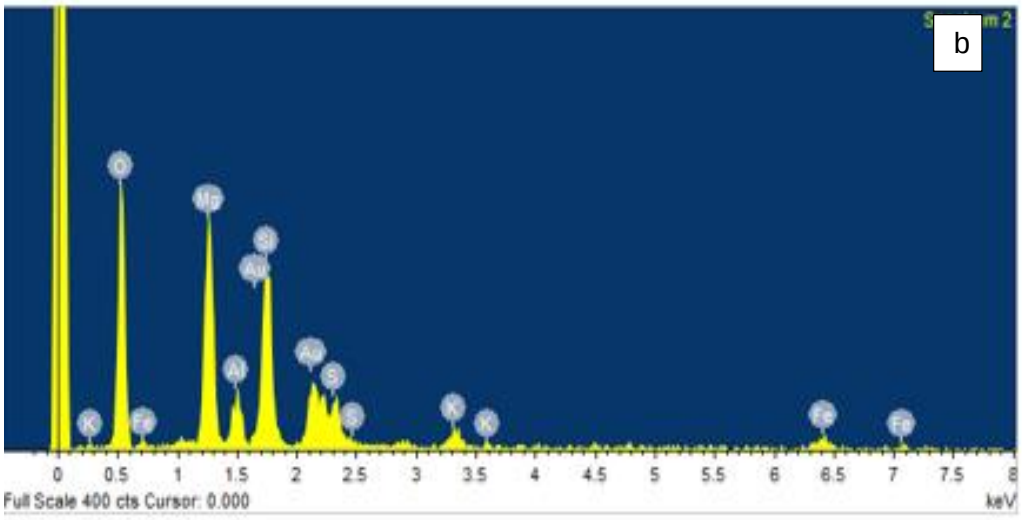


Figure 4.50: Morphology of random surface section of vermiculite +$MgSO_4$.

A further chemical element scan conducted on Vermiculite+$MgSO_4$ is shown in Figure 4.50 a~b. The elements observed from Spectrum Two demonstrate that O, Mg, and Si make up the majority of elements at the surface and others such as K, Au, Al, and Fe are minimal. Hence, this shows that the maximum amount of salt impregnated the whole surface of vermiculite and that the minimal amounts of metal are from the small sample of vermiculite.

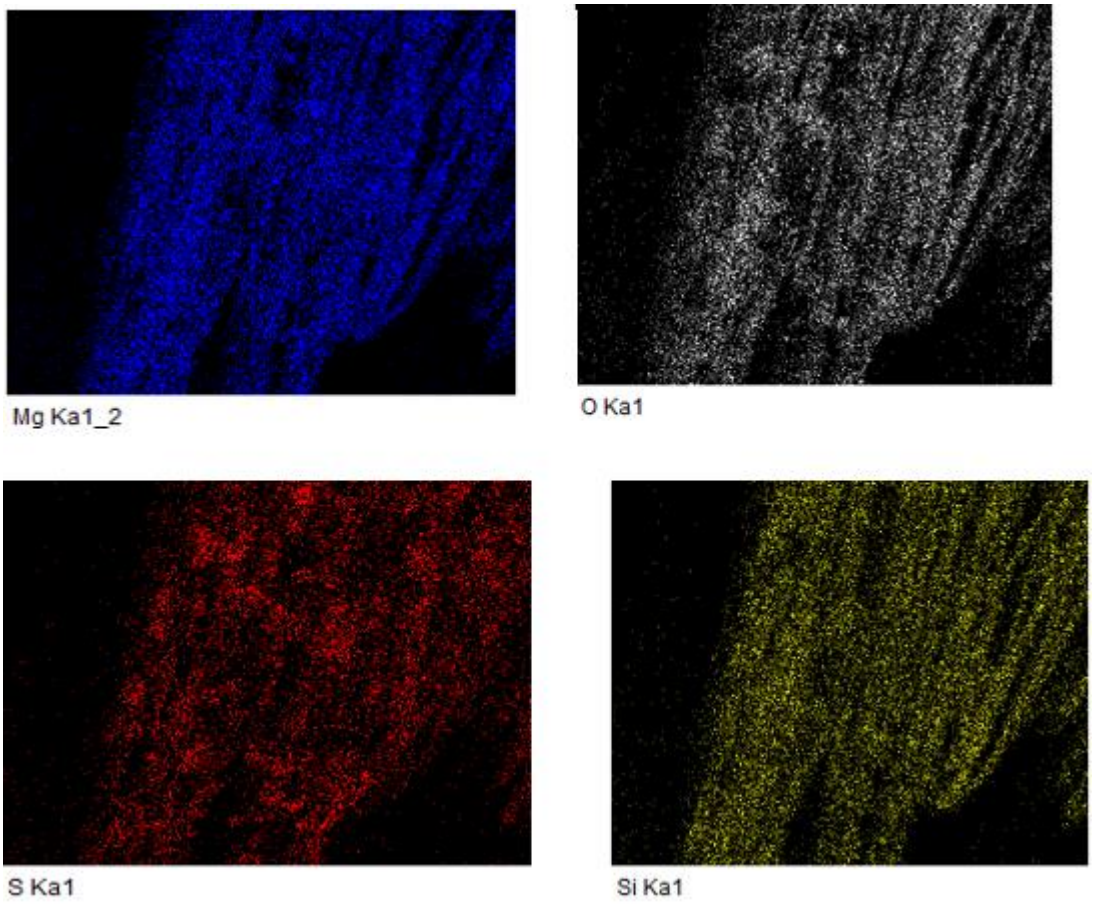


Figure 4.51: Chemical element colour coding scan of vermiculite+$MgSO_4$.

The colour coding scan clearly depicts the presence of $MgSO_4$ in the Spectrum Two surfaces of vermiculite. It can be seen that Mg (blue), O (grey) and S(red) are from the

aqueous salt solution of $MgSO_4$. The Si (yellow) has derived from the host matrix of vermiculite.

Summary of Microscopic Scanning

The microscopic scans using an ESEM and a SEM were carried out to analyse the surface structure of an impregnated composite material of a host matrix of silica gel and vermiculite. The ESEM analysis suggested that the host matrix of vermiculite can adsorb water vapour through larger pores, and the aqueous salt becomes entrapped in its layers. The visual analysis of porosity of the host matrix using the SEM suggested that vermiculite+$CaCl_2$ and vermiculite+$MgSO_4$ have a similar surface structure and that the impregnation of salt was successful, as shown by the morphology of these two composite materials. However, the host matrix of silica gel pores could not be visualised through these means of scanning. Therefore, we conclude that the host matrix of vermiculite could be a potential candidate for adoption in a Thermochemical Heat Storage System.

4.6 Investigation of Pore Size Distribution and Pore Volume of Thermochemical Materials.

The main consideration in tailoring and optimising the composite material is to have the optimum size of pore and volume distribution in order to achieve water vapour sorption to maximum effect and thus attain high energy storage. In this study, the analysis of pore size was conducted through the ESEM/SEM investigation. However, the morphology scans were only carried out on a small particle and the pore size distribution could not be analysed using the ESEM/SEM alone. A more detailed investigation is required to analyse the pore volume and pore size distribution in the samples. The properties

investigated in these experiments included specific surface area, pore volume *(Vp)* and pore size distribution *(Øp)* of selected potential candidates for the adsorbent material of choice. These were executed using the Brunauer-Emmet-Teller (Brunauer et al., 1936) and Barret-Joyner–Halenda (BJH)(Barrett et al., 1951) methods through Mercury Intrusion Porosimetry (MIP) respectively. Therefore, another experimental study has been carried out on the prepared material to determine the pore size and volume distribution. Most of the researchers in this field using the technique of Mercury Intrusion Porosimetry to determine pore size and pore volume in the adsorption research are academics such as Kuravi et al. (2013), Casey et al. (2014) and Casey et al. (2015).

The term "porosimetry" is used as a blanket term to describe the measurements of pore size, volume, distribution, density, and other porosity-related characteristics of materials. All instruments assume a cylindrical pore geometry using the Young-Laplace equation, (otherwise known as the Washburn equation):

$$\Delta P = \gamma\left(\frac{1}{r_1}+\frac{1}{r_2}\right) = \frac{2\gamma cos\theta}{r_{pore}} \quad (4.1)$$

It relates the pressure difference across the curved mercury interface (r_1 & r_2 describe the curvature of that interface) to the corresponding pore size (r_{pore}) using the surface tension of mercury (γ) and the contact angle (θ) between the solid and the mercury (Giesche, 2006). Therefore, referring to equation 4.1, we need to know the surface tension (γ) and the contact angle (θ) of the specimens of the composite materials. By measuring the volume of mercury that intrudes into the sample material with each pressure change, the volume of pores in the corresponding size class can be calculated. The volume of mercury that enters the pores is measured through a mercury penetrometer. These devices are very sensitive and can detect a change in mercury

volume of under 0.1µL (Micrometrics Instruments Corporation, 2014). In this study, the surface tension of 485 dyne/cm and the contact angle of 140° were used to determine the pore diameter. The change of mercury for this study was according to the manufacturing data, which is 22.065µL/pF. The penetrometer was constructed of glass (an insulator) and filled with mercury (a conductor). The stem of the penetrometer is a capillary that acts as a reservoir for the analytical volume of mercury. (Micrometrics Instruments Corporation, 2014). The illustration of the penetrometer is shown in Figure 4.52.

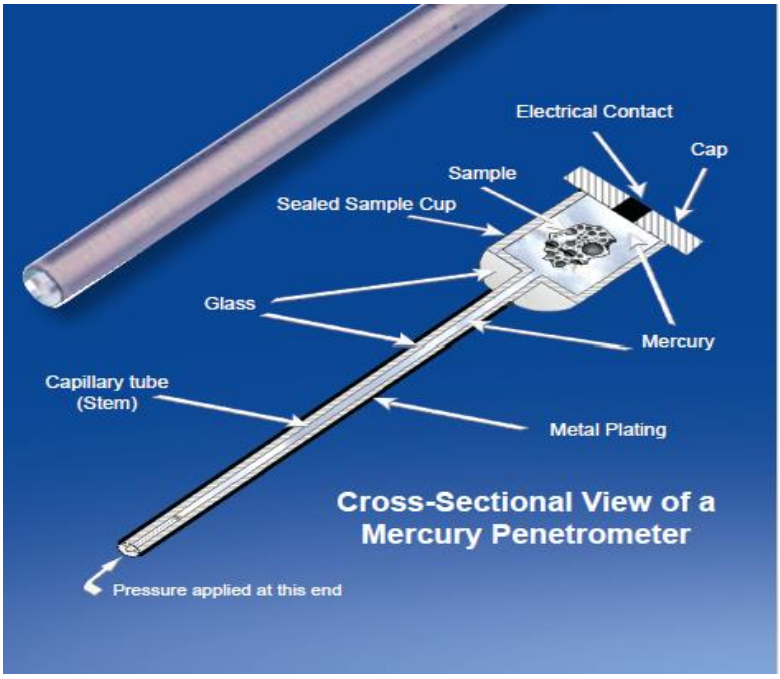


Figure 4.52: Cross-sectional view of penetrometer diagram (Micrometrics Instruments Corporation, 2014).

4.6.1 Experimental Setup and Procedure

The matrix texture was analysed using the Micromeritics Instrument Corporation Auto Pore IV 9500 VI.09 which was chosen because it could determine a broad pore size distribution (0.003 to 360 micrometres). The blank penetrometer was weighed before the low-pressure test commenced and the data inserted into the programme. The systems

consist of two types of pressure port, namely the low-pressure port and high-pressure port which were shown in Figure 4.53. The low-pressure port was used to evacuate the specimen, removing air and residual moisture from the pore systems. This procedure is crucial in order to avoid possible air pockets and contamination issues. The specimen particle is filled with mercury while the entire systems are still under reduced pressure. The slow increase of pressure in the systems would allow the mercury to penetrate the largest pores in the specimen or any voids between the specimen particles. In this study, the low-pressure evacuation was set to 70μm Hg and mercury-filling pressure was 0.51psia. The mercury-filled penetrometer was then weighed again before being transferred to the high-pressure port. In the high-pressure systems, the specimen was surrounded by hydraulic liquid, and pressure up to 60,000 psi was applied in an isostatic method. These testing procedures were repeated on different composite materials. During the low-pressure and high-pressure systems tests, the pressure flow was monitored by means demonstrated by the schematic drawing as shown in Figure 4.54. This schematic will highlight the pressure flow in the systems and errors or ambiguous process flows would be detected by the pressure readings.

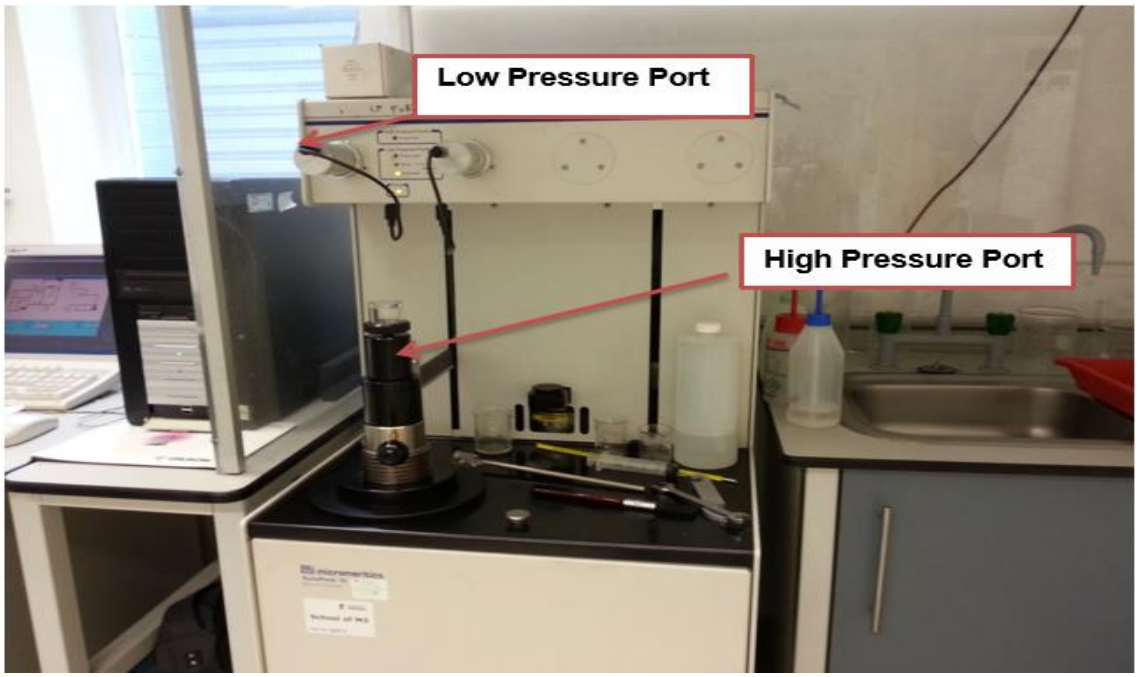


Figure 4.53: Micrometrics Auto Pore IV 9500 photo (Micrometrics Instruments Corporation, 2014).

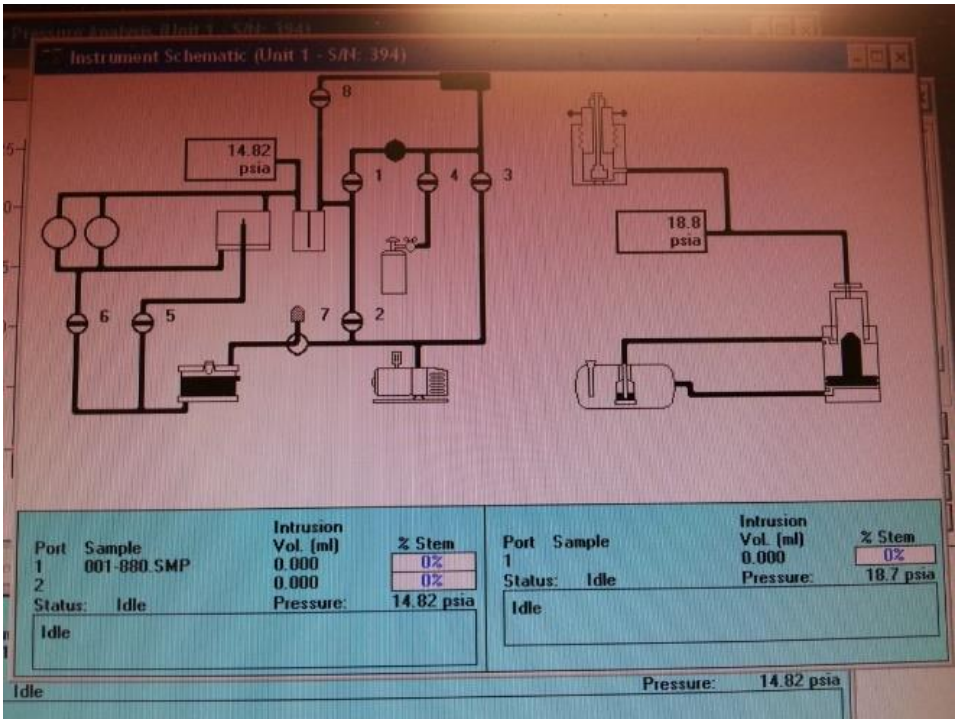


Figure 4.54: A schematic of pressure flow inside the systems.

4.6.2 **Result and Discussion of MIP**

The main objective of this experiment is to study the pore volume and pore size and distribution of the composite materials that have been tailored to this study's needs using the host matrix of vermiculite impregnated with a saturated aqueous salt solution of $CaCl_2$, $LiNO_3$, and $MgSO_4$. Table 4.7 summarises the results of these studies. From these results we understand that the raw vermiculite has the highest pore intrusion volume of 4.12 mL/g compared to other impregnated composite materials. This suggests that vermiculite may possess the potential for higher water adsorption and hence could attain higher heat adsorption levels for cooling and heating applications. However, the composite materials have lower intrusion volumes. Out of the three composite materials, the composite material of vermiculite+$LiNO_3$ has the highest intrusion volume of 2.476 mL/g. The second lowest is the vermiculite+$MgSO_4$, and the lowest is vermiculite+$LiNO_3$ with the value of 1.7737 mL/g & 1.6021 mL/g respectively. From this result we can predict that the pores of the composite materials are filled with a layer of crystallised salt of $CaCl_2$, $LiNO_3$, and $MgSO_4$ that may be affected by smaller pore volume. This also leads to the assumption that the composite materials could attain higher temperature lifts during the adsorption as achieved from the effectiveness of the impregnation procedure.

It is also possible for the density of the specimen to be determined by this experiment. Table 4.8 summarises the calculated density of the TCMs tested. The table shows that vermiculite+$CaCl_2$ has a high density of 0.49g/cc compared to that of vermiculite+$LiNO_3$ and vermiculite+$MgSO_4$ (0.3204 g/cc & 0.4328g/cc respectively). The calculated values are in agreement with the results from the MIP apparatus. This shows that the impregnation of $CaCl_2$ garners more success than other salts because of its high density.

Table 4.7: Summary of specimen characteristics from MIP.

Characteristic	**Units**	**Specimens tested**			
		Raw vermiculite	Vermiculite + $CaCl_2$	Vermiculite + $LiNO_3$	Vermiculite + $MgSO_4$
Total intrusion volume	mL/g	4.1185	1.6021	2.4762	1.7737
Total pore area	m^2/g	15.001	28.963	35.757	34.369
Median pore diameter (volume)	µm	3.1996	2.1921	5.5133	4.6221
Median pore diameter (area)	µm	0.3126	0.0077	0.0073	0.0069
Average pore diameter (4v/a)	µm	1.0982	0.2213	0.277	0.2064
Bulk density at 0.51 psi_a	g/mL	0.2158	0.4891	0.3202	0.4325
Apparent (skeletal) density	g/mL	1.9368	2.2605	1.5464	1.8572
Porosity	%	88.8599	78.363	79.2925	76.7129
Stem volume used	%	53	54	54	46

Table 4.8: Summary of specimen density.

Specimen	Specimen (g)	Penetrometer (g)	Penetrometer +specimen (g)	Penetrometer + specimen +Hg	Density of Hg (g/cc)(@25°C)	Mass of Hg (g)	Volume of Hg	Specimen mass after test	Volume of Hg+ specimen (ml)	Bulk specimen volume	Bulk specimen density (g/cc)
Blank	0	60.4633	60.4633	150.1388	13.534	89.6755	6.6259	-	-	-	-
Vermiculite +$CaCl_2$	0.3832	60.4733	60.8605	139.9389	13.534	79.0784	6.6259	79.0784	5.8429	0.7830	0.4894
Vermiculite +$LiNO_3$	0.2439	60.4636	60.7075	140.0807	13.534	79.3732	6.6259	79.3732	5.8647	0.7612	0.3204
Vermiculite +$MgSO_4$	0.2934	60.5041	60.7975	141.2978	13.534	80.5003	6.6259	80.5003	5.9480	0.6779	0.4328

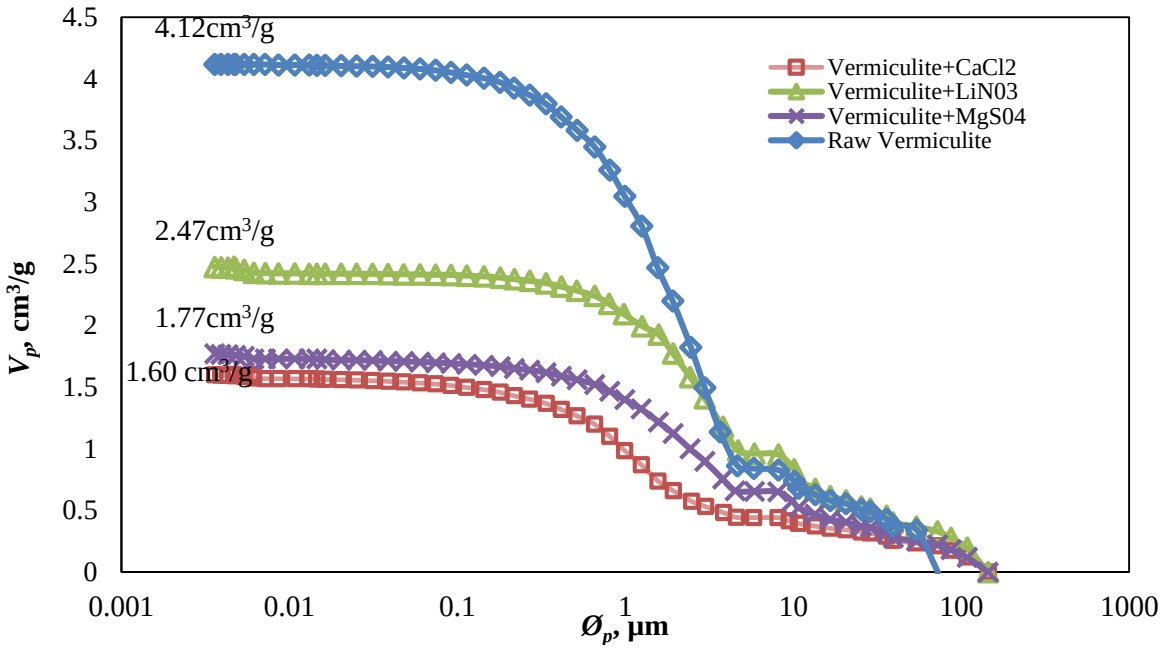


Figure 4.55: Pore volume of raw vermiculite and other composite vermiculite adsorbents.

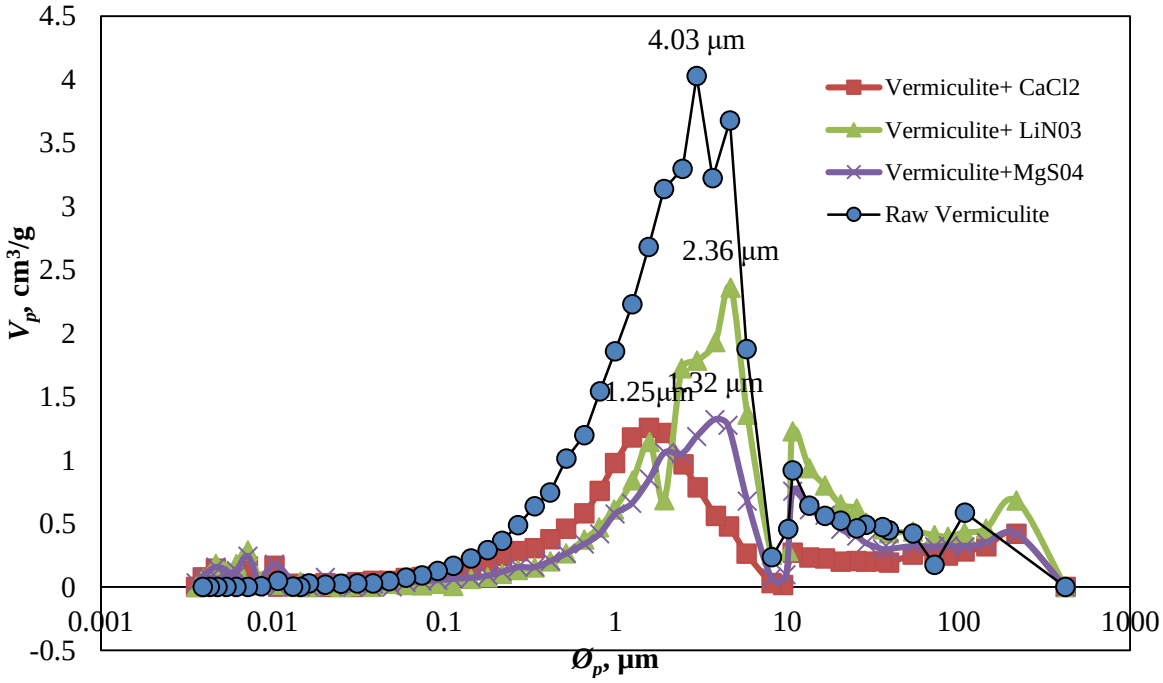


Figure 4.56: Pore size distribution of raw vermiculite and other composite vermiculite adsorbents.

Apart from the pore volume comparison, another important factor that may affect the performance of the thermochemical heating pipe system is the pore diameter. From the results of the experiment, we see that the composite materials of vermiculite+$LiNO_3$ have the higher pore diameter compared to that of vermiculite+$CaCl_2$ and vermiculite+$MgSO_4$. However, it was reported that $LiNO_3$ had a lower energy storage density compared to $CaCl_2$ (Jabbari-Hichri et al., 2015). The pore volume and pore size distributions of raw vermiculite and other vermiculite based composite adsorbents are shown respectively in

Figure 4.55 and Figure 4.56. The pore volume of raw Vermiculite was observed to be around 4.12 cm^3/g, which is much larger than that of other vermiculite-based composite adsorbents, which pore volumes range between 1 cm^3/g and 2 cm^3/g. Therefore, impregnation of $CaCl_2$ can be chosen as the potential candidate to be employed for the THSS. The pores of the composite adsorbents have been filled with hygroscopic salts after impregnation, significantly reducing the pore volume of the composites but overall improving their adsorption and energy storage density properties. This would indicate that vermiculite has a high capacity for adsorbing water vapour compared to other impregnated hydrophilic materials such as silica gel. Consequently, this would also suggest that impregnated vermiculite would attain a high heat storage density and consequently a high level of efficiency for the THSS.

4.7 Thermal Analysis Investigation

The thermal analysis is based on the detection of temperature changes in the heat content (enthalpy) or the specific heat of a sample. When thermal energy is supplied to the sample, its enthalpy and temperature rise by a determined amount for a given energy input and specific heat of the sample. The specific heat of the material changes gradually in temperature when in a particular physical state, but changes discontinuously during a change of state. As the sample temperature increases, the supply of thermal energy may initiate a physical or chemical change in the sample, such as melting or decomposition, and also bring about a change in enthalpy, the latent heat of fusion and the reaction heat. Such enthalpy changes are detected by thermal analysis and then viewed comparatively with the processes occurring in the sample.

Thermal analysis involves a wide variety of techniques (Friedli, 2015):

a) dynamic adiabatic calorimetry,
b) differential thermal analysis, DTA
c) differential scanning calorimetry, DSC
d) thermogravimetric, TG
e) thermal mechanical analysis, TMA
f) dynamic mechanical thermal analysis, DMTA

In this study, the DSC was used to analyse the specific heat of prepared composite material because this method was often used for optimising formulations, material selection and analysis of finished products. Furthermore, the measurement of heat flow through the samples provides quantitative and qualitative analysis about physical and chemical changes that comprise endothermic and exothermic reactions or changes in heat capacity (Dyball, 2013).

4.7.1 **Introduction**

The DSC technique is part of the thermal analysis group. The DSC machine can be used to determine specific heat, thermal effect, purity, polymorphism, glass transition, oxidative stability, chemical reactions, reaction kinetics, melting behaviour, crystallisation and measurement of endothermic and exothermic processes as a function of temperature or time (temperature range RT-750°C). There are several types of thermal analysis that could be done using the DSC machine. In this case, the method of testing would be determined by the researcher depending upon which type of data analysis is of interest to them. The energy storage density of the composite material is also determined by Differential Scanning Calorimetric (DSC) analysis using DSC Q10 apparatus, in accordance with BS11357-4:2013 . For this means of testing to attain the energy density, the theory of sensible heat storage on materials is used to determine the specific heat of the materials and the working temperature. Some of the experiments use the DSC method to determine the specific heat of silica gel (host matrix) and $CaCl_2$ (guest salt) (Ponomarenko et al., 2010; Aristov & Restuccia, 2000), magnesium hydroxide with vermiculite (Shkatulov et al., 2012) and magnesium sulphite and zeolite (Hongois et al., 2011). However, no study related to the specific heat of vermiculite impregnated with different types of salt hydrates, such as lithium nitrate and magnesium sulphate, have been reported yet. Hence, it is important this experiment be followed by further research.

4.7.2 **Theory**

The energy storage density of the composite material can be determined through analysis using DSC TA Q10 apparatus. Aristov & Restuccia (2000) give a

comprehensive explanation of a similar method for determining the specific heat of various composite impregnated adsorbent materials in their paper, and it is a similar approach which we will adopt in this experiment. Technically, the temperature of the sample and reference can both be maintained at the temperature predetermined by the programme. The amount of energy, which has to be supplied or withdrawn from the specimen and the reference, is the parameter portrayed as the ordinate of thermal analysis curve (see Figure 4.57). The rate of energy absorbed by the specimen is proportional to the specific heat of the specimen since the specific heat at any temperature determines the amount of thermal energy necessary to change the specimen temperature. The DSC operates on the principle that using the same increasing temperature profile, the rate of flow of heat, h_f (i.e. ΔQ/ΔT) into the pan containing the sample will differ from the rate into the reference (empty) pan. The difference in flow can be attributed to the heat capacity of the sample, providing all other conditions are identical. For a continuous scanning test, three runs using the same temperature profile are carried out to determine C_P (Casey, 2013). The C_P of the sample can be calculated using the heat flow rates from the baseline h_f ($h_{f\,\text{base}}$), sample ($h_{f\,\text{sp}}$), and reference ($h_{f\,\text{ref}}$) runs along with the mass of the sample (m_{sp}) and reference (m_{ref}) using Equation 4.2

$$C_{p,sp} = C_{p,ref} \cdot \frac{m_{ref}\,(h_{fsp}-h_{fbase})}{m_{sp}(h_{fref}-h_{fbase})} \qquad 4.2$$

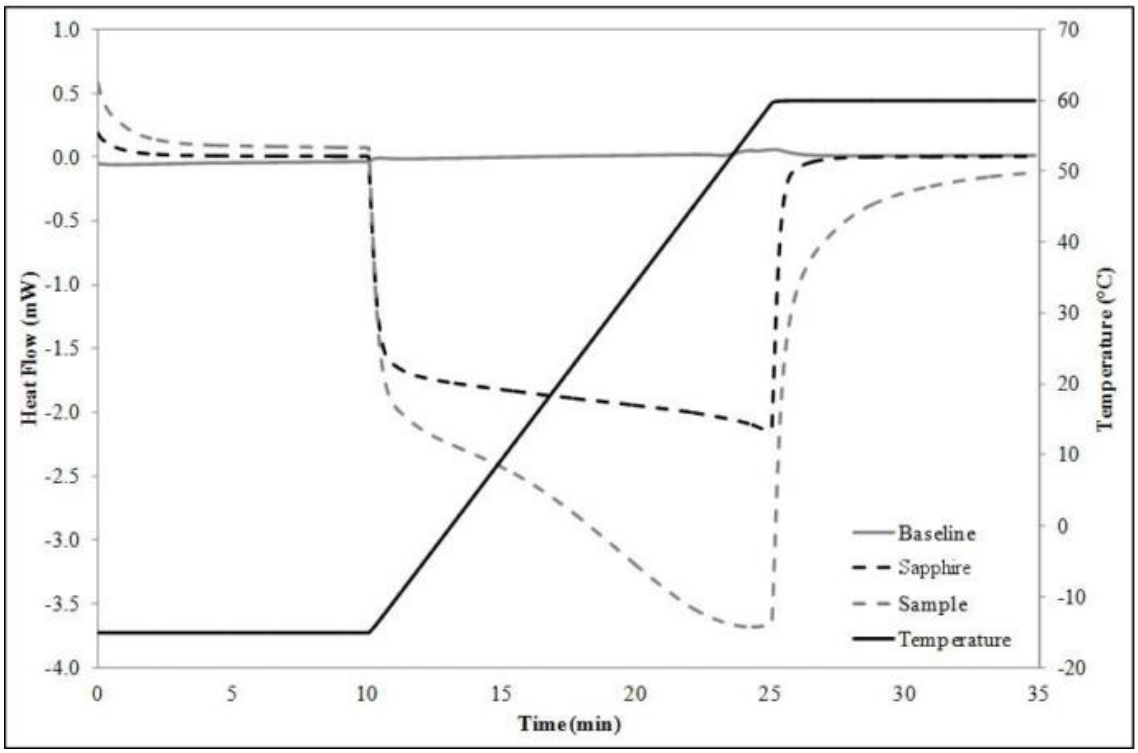


Figure 4.57: Example heat flow curves and temperature profile from a DSC test.

4.7.3 **Experimental Setup and Procedure**

Before the testing began, the composite material was saturated using a potassium nitrate solution for 24 hours. The saturated material was then placed in an airtight bottle to test with the DSC machine. Each granule has been put on the small aluminium pans (see Figure 4.58) and weighed using the digital electronic scale machine (see Figure 4.59a). The weight was recorded in the data acquisition system. The specimen was contained within the aluminium pan using a lid held down with a clamp, as shown in Figure 4.59 (b). The material was placed in the specimen oven as shown Figure 4.60 (a-b). The experimental programme was written into the software, name as “specific heat” in the computer file. The procedure for testing started by equilibrating at 20°C and the specimen was left in an isothermal state for about 5 minutes. Then, the heating process

began with about a 5°C increase per minute to a maximum of 130° C, and finally, the specimen was left in an isothermal state for about 3 minutes before test completion. The test was started by placing the baseline of the specific heat test, that was tested using the empty aluminium pan, in the furnace using the method described above. The time to complete the baseline test took about thirty-seven minutes. When the test was finished, the reference material (sapphire) was placed on one of the empty aluminium pans as shown in Figure 4.58 (a-b) and aluminium caps in (c-d). Then, the method of testing was repeated as according to the baseline procedure and the data saved in the data acquisition software. When the test for reference sample was completed, the reference sample was replaced with the prepared composite material (a single granule of the specimen) in the aluminium pans, and the test was repeated. Each specimen material test was run three times so as to have valid and reliable data for analysis. The summaries of the operating conditions of the test are shown in Table 4.9. From this chart, it can be seen that the initial and final temperatures were determined based on the heat source that could use the least amount of energy from solar thermal sources or heat pump systems.

Table 4.9: Summary of operating condition for the specific heat testing.

Instrument	**Method Description**
Heating rate	5.00° C/min
Initial temperature	20°C
Final temperature	130°C
Sapphire sample mass	14.9 mg
Pan	Aluminium hermetic
Purge gas	Nitrogen 50ml/min
Method 1	Equilibrated at 20° C
Method 2	Isothermal for 5 minutes
Method 3	Ramp 5° C/min to 130° C
Method 4	Isothermal for 3 minutes

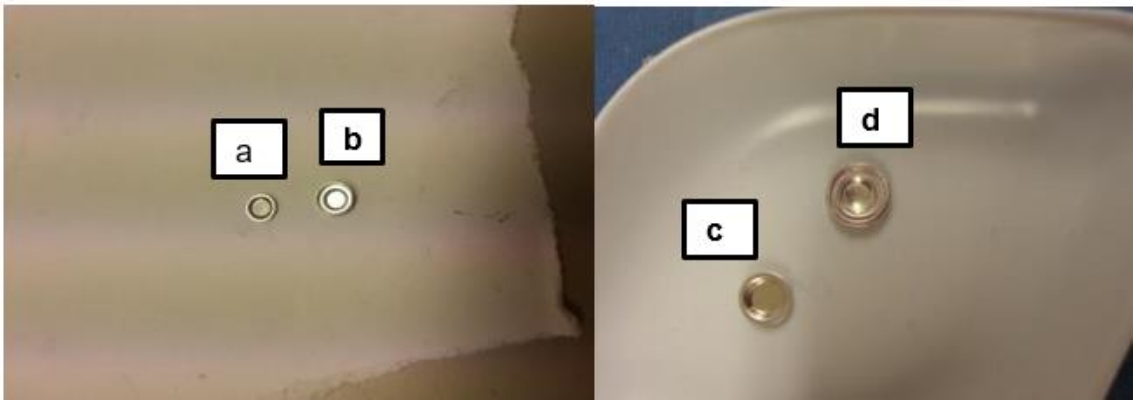


Figure 4.58: Empty specimen pan (a), cap (b&c) and single granule specimen place on the pan (d).

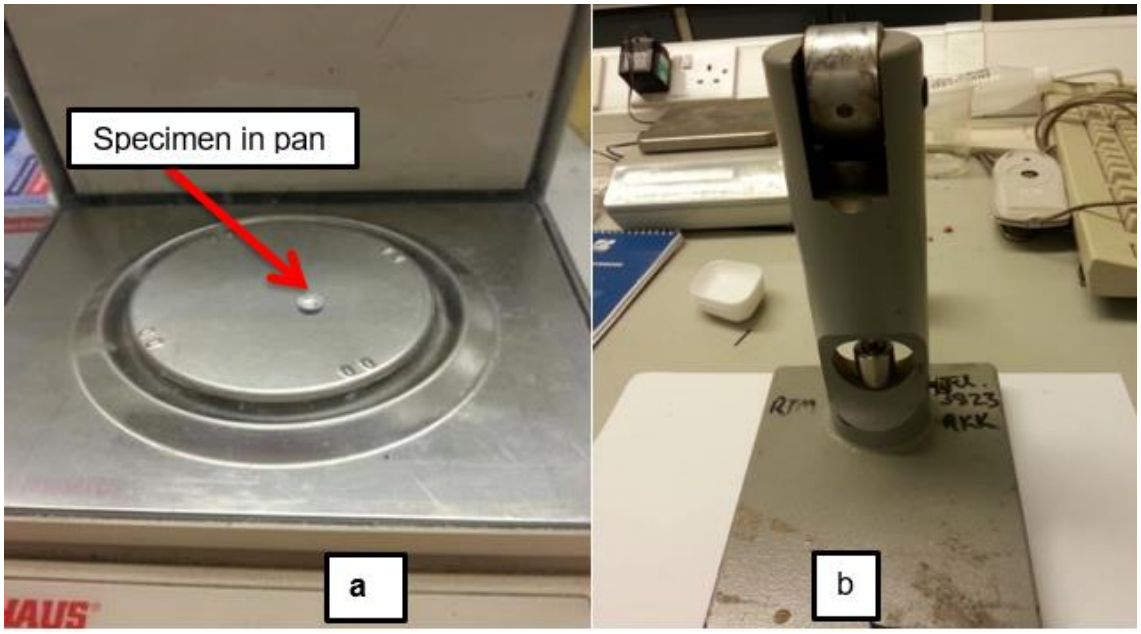


Figure 4.59: Single granule of specimen weight using electronic digital scale (a) and clamps (b).

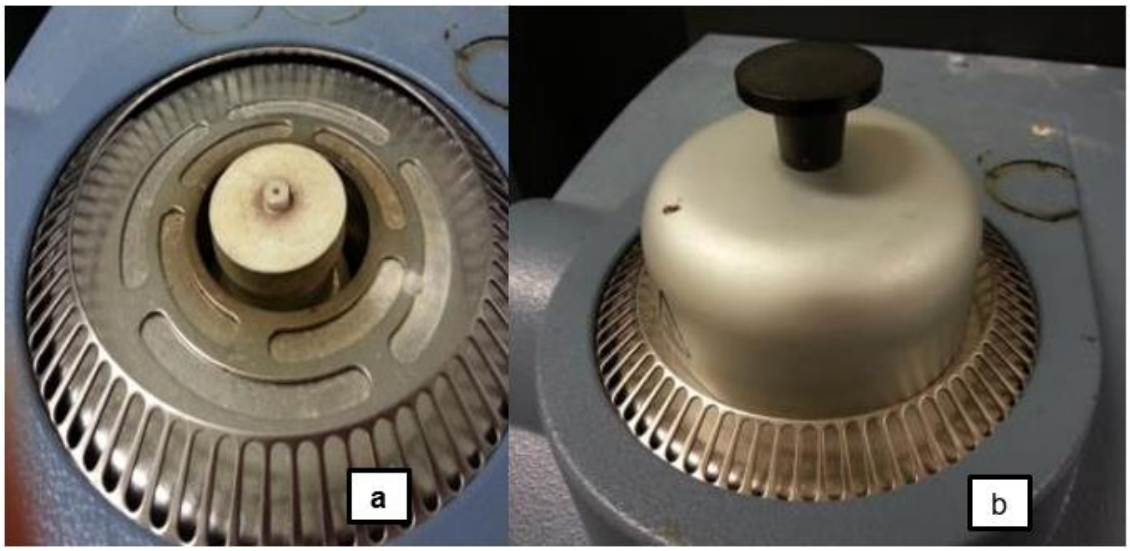


Figure 4.60: Inner part of specimen furnace (a), cover of the specimen furnace (b).

4.7.4 **Procedure on impregnation of composite material**

The composite materials were prepared before the DSC test was conducted. Firstly, the host material (silica gel or vermiculite) was dried in the oven at a temperature of 150°C for 24 hours. Then, the materials were allowed to cool naturally to room temperature before being sprayed with the saturated salt solution of $CaCl_2$, $LiNO_3$, and $MgSO_4$. The impregnated composite material was then dissolved completely over a time of two hours to make sure that the solution would fill the pores of the host matrix. Finally, the impregnated composite material was dried again in the oven at the same temperature of the host matrix; 150°C for 48 hours.

The materials that were tested in these experiments are:

i. Pure silica gel

ii. Silica gel + $CaCl_2$

iii. Silica gel + $LiNO_3$

iv. Vermiculite + $CaCl_2$

v. Vermiculite + $MgSO_4$

4.7.5 Results and Discussion of DSC analysis

Figure 4.61 illustrates the DSC thermograms of tested composite materials. It can be seen that the heat flow peak of these materials varied and this might be due to the inhomogeneous mass used in DSC. Furthermore, the aqueous saturated salt solution may have had the effect of creating the valley in the thermograms. This area under the peak of these thermograms will determine the heat flow, and hence the specific heat is known. The lower valley will give a reading for the high heat storage density of the specimen tested. It can be seen that the TCM of vermiculite +$CaCl_2$/$MgSO_4$ has the lowest valley of 32.79mW/mg to 32.36mW/mg, whereas the lower valley value for pure silica gel and composite silica gel is 25.35 to 31.73mW/g. This result suggests that the TCM with the host matrix of vermiculite has a higher high heat storage capacity compared to silica gel.

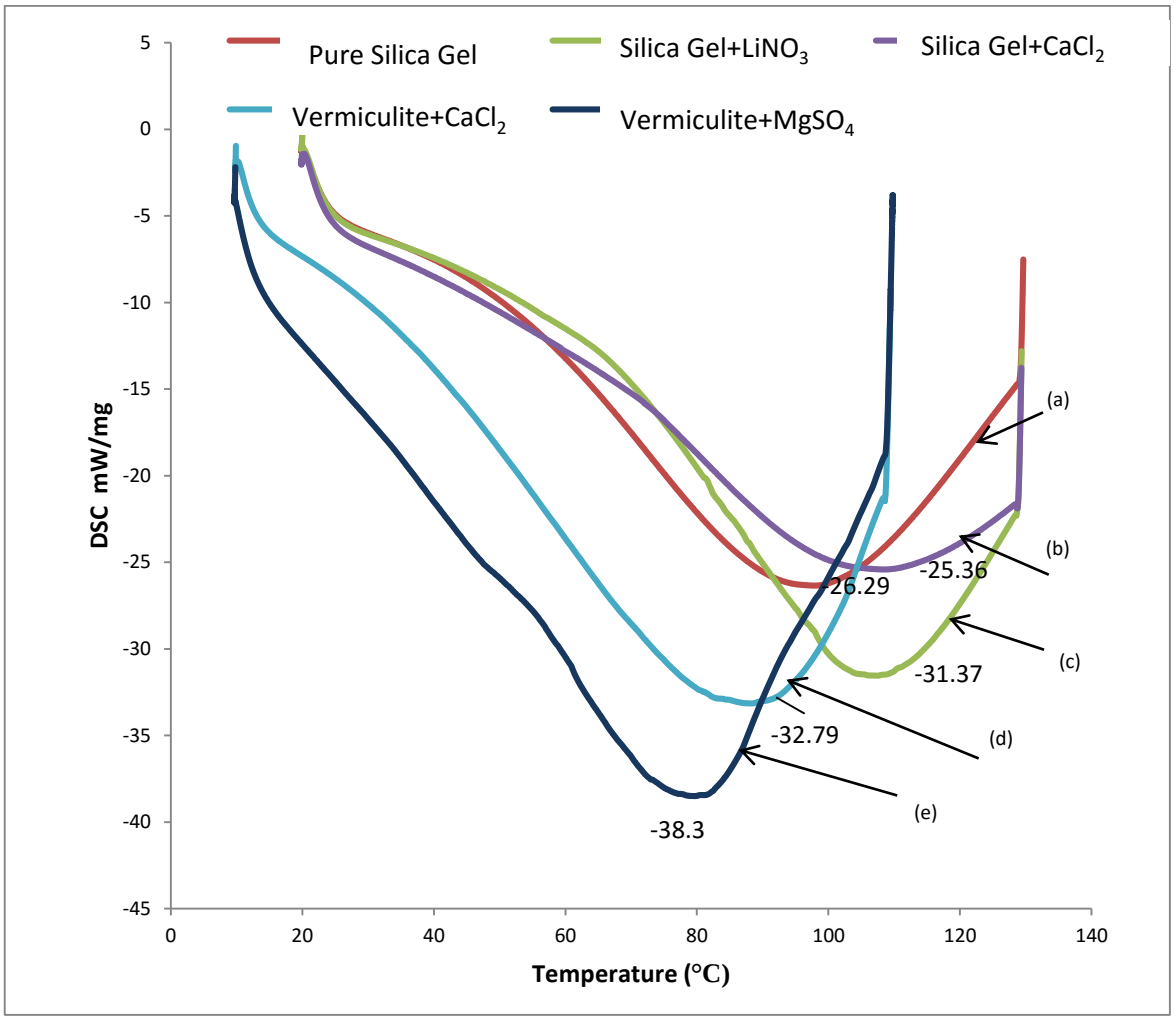


Figure 4.61: DSC thermograms of composite specimens. Pure silica gel (a), silica gel+$CaCl_2$ (b), silica gel+$LiNO_3$(c), vermiculite+$CaCl_2$(d), and vermiculite+$MgSO_4$(e).

The comparison of heat storage capacity analyses is accordance with Figure 4.62. From the DSC analysis tests of pure adsorbents and composite materials, it was found that vermiculite+$MgSO_4$ attained a higher heat storage capacity reading of 407 kJ/kg compared to vermiculite+$CaCl_2$ with a reading of 374 kJ/kg. The host material of silica gel had shown a lower heat storage capacity in the range of 163 kJ/kg to 208 kJ/kg respectively. We can assume from these results that the host matrix of vermiculite could attain a higher heat storage capacity compared to silica gel. Furthermore, from the adsorption and desorption process that was previously conducted using the vertical rig,

vermiculite+$CaCl_2$ achieved a temperature lift of 48°C compared to that of silica gel+$CaCl_2$ at 46°C. Consequently, the regeneration temperature for vermiculite, applied in the desorption test using the vertical rig was 60°C. However, the regeneration temperatures of silica gel were in the range of (60°C-100°C) as reported by Demir et al. (2008). This indicates that the host matrix of vermiculite is a more sustainable material to adopt in the long term due to the low regeneration temperature. Moreover, the low-temperature regeneration can use wasted heat such as that from nuclear plants, various heat engines, fuel cells, and motor vehicles.

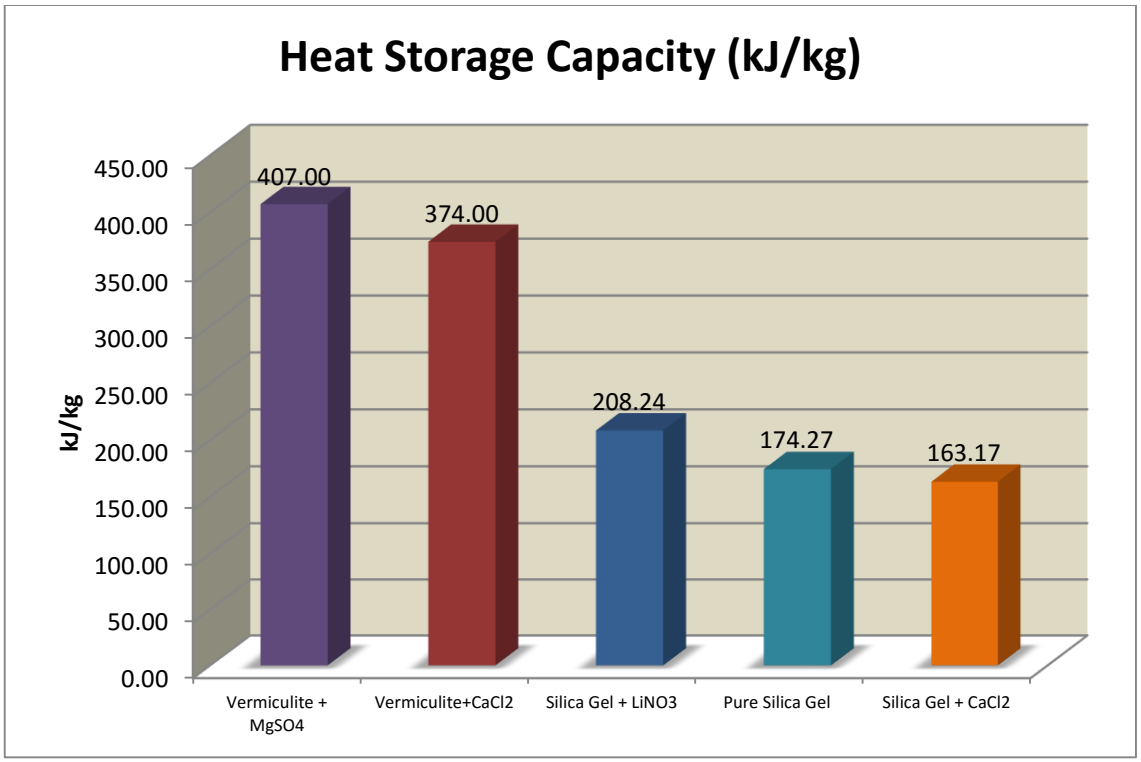


Figure 4.62: Heat Storage capacity comparison

4.8 Conclusions in this Chapter

In this chapter, the work focused on material screening, synthesising, and optimisation in terms of physicochemical analysis. Testing using horizontal and vertical heat pipes has shown that the TCM of vermiculite+$CaCl_2$ has a high-temperature lift of 67.50°C from the adsorption process. From the microscopic scan, we saw that the host matrix of vermiculite has a higher porosity than silica gel. It is important to note also that the hydration process does not detrimentally affect the structure of vermiculite. The MIP analysis suggested that raw vermiculite has the highest pore volumes due to the absence of salt inside the matrix. Furthermore, on comparing composites of vermiculite, vermiculite+$LiNO_3$ showed the maximum pore volume and percentage of porosity. From these results we suggest that this material may be a potential candidate to be adopted for the THSS.

The microscopic scan also suggested that vermiculite would be able to retain its original structure in prolonged cyclic conditions. The most important factor to base the choice of a TCM on is a high heat storage capacity. The DSC testing suggested that vermiculite+$CaCl_2$ has the second highest heat storage capacity of 374KJ/kg. More importantly, this TCM only required a low desorption temperature of 60°C that could be taken from a low-grade energy source. However, in order to conduct a truly thorough investigation on storing the TCM as a THSS, a theoretical analysis is required. This will be the focus of the next chapter of this thesis.

5. PERFORMANCE INVESTIGATION OF THERMOCHEMICAL HEAT STORAGE SYSTEM: MODELLING OF THSS-ELEC, THSS-HP & THSS-SOLAR

5.1 Introduction

The purpose of this exercise is to study the theoretical adsorption and desorption process of a thermochemical heat storage system (THSS) when integrated with an electric heat clamp, a heat-pump circuit, and using solar energy. A numerical model was used to determine the regeneration temperature and THSS performance. The numerical analysis was carried out using two different cycles; an adsorption cycle and a desorption cycle. Three types of desorption methods considered in this models are: i) via electrical heat clamp, ii) via heat pump circuit, iii) via the solar thermal collector. In governing the equations on describing the thermal performance of THSS, the basic refrigerant circuit of a vapour compression system was used for the adsorption heat pump. This is because the regeneration process is similar to the vapour compression systems which use the R134A (THSS-R134a) and R1234yf (THSS-R1234yf) as the refrigerant gas. These refrigerant gases were selected based on previous literature aimed towards investigating adoption of low global-warming potential gases for the proposed systems. Furthermore, it has been reported by Zilio et al. (2011) and Lee & Jung (2012) that R1234yf has four global warming potential (GWP) and zero ozone depletion potential (ODP) compared to the conventional R134a which is 1430 GWP (BOC, 2011). In addition, on utilising the availability of solar energy, regeneration through solar heat has been considered. This

system is known as THSS-SOLAR. In this study, both refrigerants were modelled on the desorption process to investigate their effect on the performance of the THSS. For the adsorption process, the heat of adsorption is calculated using the adsorption equilibrium which is dependent on the pressure and temperature as in accordance with the Linear Driving Force Method (El-Sharkawy et al., 2006; Aristov et al., 2006; Ahmed, 2012). From the material synthesising and selection for this study, the material was chosen for this numerical modelling is vermiculite+$CaCl_2$. These composite material was selected due to the high adsorption temperature. At the end of the modelling process, the performance of THSS was discussed, and the conclusion was drawn by comparing the three adsorption methods.

5.2 **Methodology**

The THSS cycle is similar to the basic heat pump cycle in that it consists of two main operational phases, namely adsorption and desorption. The regeneration phase occurs during night hours, when cheap electricity is available under the 'Economy 7' that is more suitable for households with night storage heaters or that use lots of electricity at night. For the electric heating element this model draws on a concept whereby the household use the electric boiler. For the heat pump circuit, the model suggests using a heat pump as the desorption method for the heat storage system in the home. Using solar energy as the heat source may not influence the tariff change. The physical details of the THSS-R134a/R1234yf system is illustrated in Figure 5.1. Table 5.1 lists the details of THSS-R134a/1234yf.

In the heat pump circuit, adsorption loop is initially combined with the adsorbent in the adsorbent pipe. As the compressor starts to operate, the heat from the refrigerant will desorb the water vapour into the adsorbent pipe and then flow through the evaporator

pipe. The latent heat is reversible, and water vapour is stored as a liquid in the adsorbent pipe. Secondly, the heat pumping phase/adsorption loop will occur during the day. Addressing the model on using solar energy as a heat source, the solar circuit will be activated at the time when the solar intensity is sufficient for the desorption/charging process. In this case, the maximum availability of solar insolation was in the month of June based on Nottingham weather. The useful heat of adsorption in the adsorbent pipe will be used for underfloor heating or domestic hot water during the day.

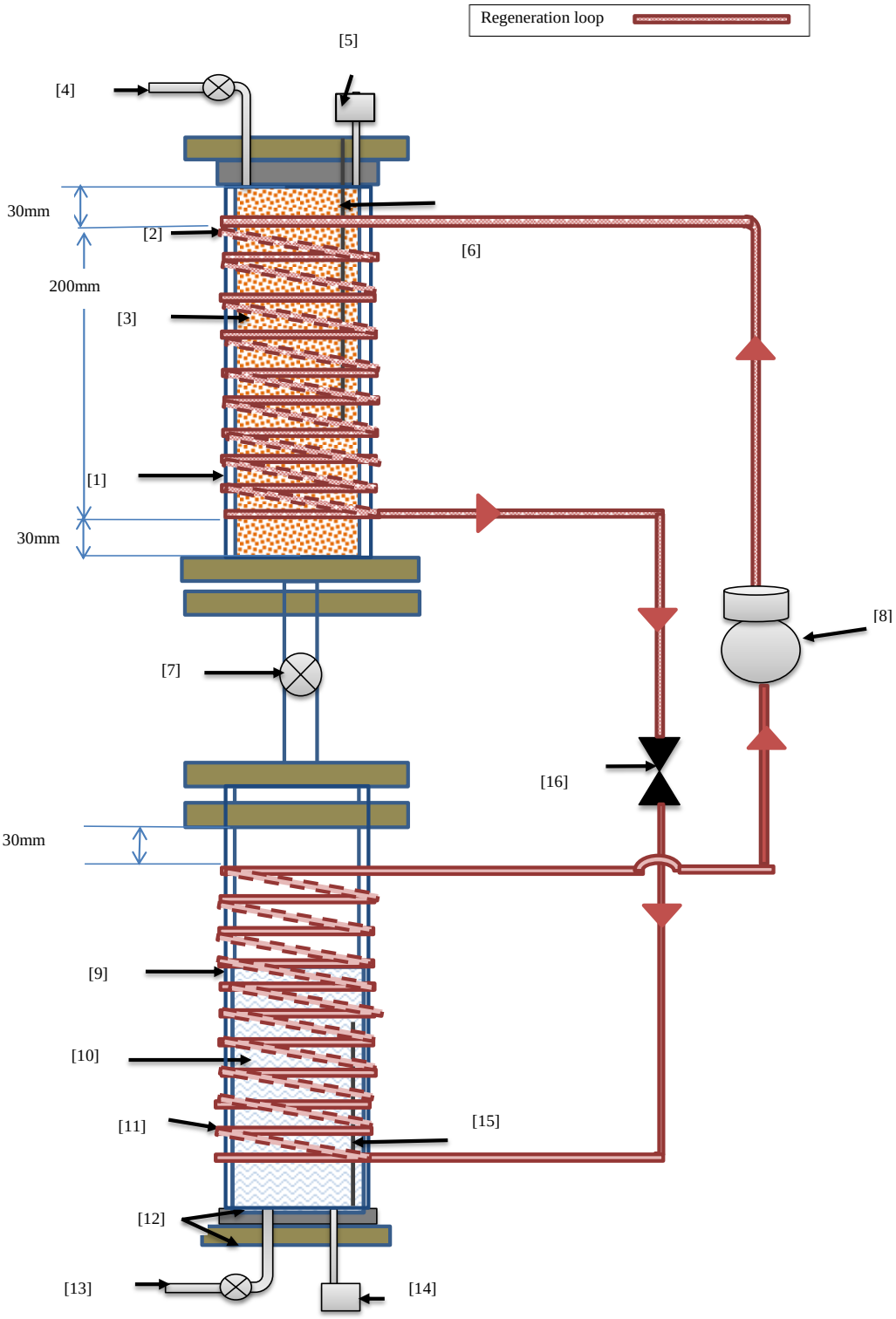


Figure 5.1: Schematic of THSS-R134a & THSS-R1234yf

Table 5.1: Descriptions of THSS-R134a/1234yf

No	Description	Size
Condenser Section		
	Pipe Type	Cylindrical Borosilicate Glass
1	Condenser Pipe	QVF glass, ID 50mm, maximum pressure 4 bar_g, maximum temperature :200°C , heat transfer area: 448 cm^2, thermal conductivity (λ: 1.2 W/m.K), Density (ρ): 2.23 kg/dm^3, specific heat (cp): 0.8 KJ/kg.K
2	Coil pipe	¼" diameter coil
3	Adsorbent material	50gram Vermiculite +$CaCl_2$
4	Valve to vacuum pump	ball valve
5	Pressure sensor	GP pressure transmitter
6	Thermocouple	RTD thermocouple
7	Separation valve	Swagelok ball valve
8	Compressor	miniature DC inverter compressor (ZH2024, Greatcool) displacement of 1.5cm^3/rev, input power of 220W
Evaporator Section		
	Pipe type	Cylindrical borosilicate Glass
9	Evaporator Pipe	QVF glass, ID 50mm, maximum pressure 4 bar_g, maximum temperature :200° C , heat transfer area: 448 cm^2, thermal conductivity (λ: 1.2 W/m.K), Density (ρ): 2.23 kg/dm^3, specific heat (cp): 0.8 KJ/kg.K
10	Water	100 grams
11	Coil	¼" diameter copper tube coil
12	Flanges	Swagelok flange 50 mm diameter
13	Valve to vacuum pump	Ball valve
14	Pressure sensor	GP pressure transmitter
15	Thermocouple	RTD thermocouple
16	Expansion valve	R134a expansion valve

5.3 **EES software**

The Engineering Equation Solver (EES) is used for the modelling of regeneration via heat pumps. The EES, which has built-in functions for the thermodynamic and transport properties of many chemical substances including the refrigerants such as R134a, R1234yf, is normally used for the heat pump. The advantage of this software is that the

programmes allow user-written function, modules, and tabular data that would be useful for reporting the output calculations. There are two major differences between EES and other equation-solving software such as Matlab or Maple. Firstly, the EES allows equations to be entered in any order with unknown variables placed anywhere within the equations and the software will automatically reorder the equations for a more efficient solution. Secondly, EES provides various built– in mathematical and thermo-physical property functions that are useful for solving the engineering calculations. Furthermore, transport properties were provided for all substances, and the library of mathematical and thermo-physical property functions in EES are very extensive. EES also provides a facility for entering and interpolation of tabular data, so that the data can be directly used in the solution of the equation set. In this modelling, the COP of the THSS was determined at different regeneration/desorption temperatures in the condenser (30-60°C) and the output temperature of the condenser with 35-45°C for underfloor heating and 55-60°C for domestic water heating.

5.4 TCM materials and working pairs

From the experimental report that was discussed in Chapter 4, the best possible composite TCM was concluded to be vermiculite+$CaCl_2$. The advantage of using these composite material is that the regeneration temperature is low. It has been reported from various experimental investigations that the required temperature to regenerate these materials is between 60-80°C. These values were based on the previous experimental set-ups by many researchers studying similar composite materials for adsorption cooling or heating systems of vermiculite impregnated with $CaCl_2$, such as the experiment done by Aristov et al. (2002) & Restuccia et al. (2005). Water was chosen as part of the

working pair for this TCM material due to high latent heat, affordability and minimal environmental impact compared to ammonia.

5.5 Working Refrigerant Gas for the regeneration of THSS

The desorption methods were designed with two options; either heat pump working refrigerant R134a or R12345yf. These refrigerants were chosen because they are the most suitable refrigerants for use with a reciprocating compressor.

5.6 Physical Properties of THSS

The physical properties were the most important factor to be considered in the THSS design. The physical properties that were involved in this modelling were discussed as below.

5.6.1 Adsorption Pipe

Figure 5.2 illustrates the adsorption pipe of the THSS systems that is used as a glass vessel for the adsorbent section. The internal parts of the adsorption pipe are inserted with copper wire to increase the heat and mass transfer area and increase the thermal conductivity of the adsorbent bed.

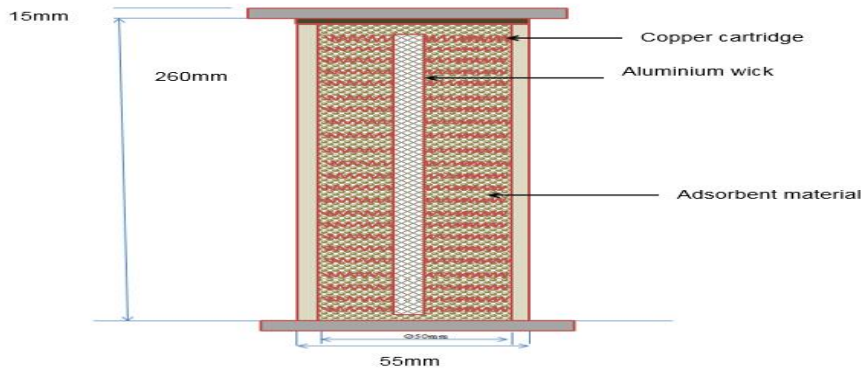


Figure 5.2: Adsorption pipe and dimension

5.6.2 Evaporator Pipe

The evaporator pipe is illustrated in Figure 5.3. This pipe has a similar design to the condenser pipe with the same internal and outer diameters of 50mm and 55mm respectively. However, the evaporator pipe is filled with water to act as the adsorbate. The evaporator pipe was coupled with the adsorption section via a Swagelok pipe and valve as shown in Figure 5.1.

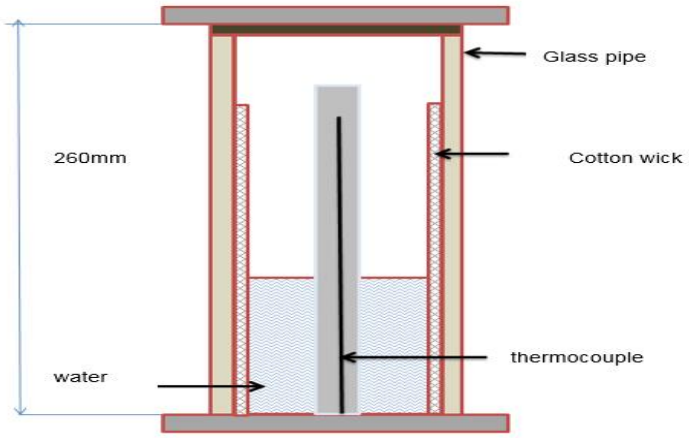


Figure 5.3: Evaporator pipe and Dimension.

5.7 Modelling of Transport of Heat and Adsorbate

The computer modelling for transport of heat and adsorbate is based on the principle of the adsorption heat pipe coupled with the analytical method developed using EES programme. Vermiculite, impregnated with $CaCl_2$, was selected to predict the performance of THSS. The assumptions on governing the heat balance equation are according to previous modelling (Di et al., 2007; Miyazaki et al., 2009; Zhang et al., 2011) as listed below; -

i) The temperatures of the adsorbent and adsorbate are assumed to be the same at all times.

ii) A lump parameter approach is used in the present study to describe the energy and heat balance equations for each element of the adsorption systems.

iii) The pressure difference between the condenser and the evaporator was neglected.

iv) The refrigerant adsorbed uniformly in the adsorber and was liquid in the adsorbent.

5.8 Adsorption Isotherm

The numerical values in calculating this adsorption isotherm is based on the previous model developed by Miyazaki et al. (2009).

$$q^* = A(Ts)\left[\frac{P_S(T_w)}{P_S(T_S)}\right]^{B(T_S)} \quad (5.1)$$

Where,

Numerical value for A

$$A(T_S) = A_0 + A_1T_S + A_2T^2{}_S + A_3T^3{}_S \quad (5.2)$$

Numerical value for B

$$B(T_S) = B_0 + B_1T_S + B_2T^2{}_S + B_3T^3{}_S \quad (5.3)$$

The numerical values of $A_0 - A_3$ and $B_0 - B_3$ are provided in Table 5.2

Table 5.2: Value of Parameter used for the adsorption isotherm (Miyazaki et al., 2009)

Parameter	Value
A_0	-6.5314
A_1	0.072452
A_2	$-0.23951X10^{-3}$
A_3	$0.25493 X 10^{-3}$
B_0	-15.587
B_1	0.15915
B_2	$-0.50612 X 10^{-3}$
B_3	$0.5329 X 10^{-6}$

5.9 Adsorption rate

The adsorption rate for the present study is estimated according to Miyazaki et al.(2009) use of the Linear Driving Force Method (LDF) in equation (5) below.

$$\frac{dq}{dt} = k_s a_v (q^* - q) \quad (5.4)$$

Where, q^* is the possible equilibrium amount that adsorbs, for this study its numerical value will be 0.55 based on the experimental results from the vertical adsorbent pipe. $k_s a_v$ is the overall mass transfer coefficient of the adsorbent or refrigerant pair and can be written as:

$$k_s a_v = \frac{15 D_S}{R_P^2} \quad (5.5)$$

Where, R_p is the adsorbent particle radius and D_S is the surface diffusivity and can be expressed by an Arrhenius equation as shown below:

$$D_s = D_{so} \exp\left(-\frac{E_a}{RT}\right) \quad (5.6)$$

Where, D_{so} is the pre-exponential term, E_a is the activation energy of surface diffusion. One of the most important conditions for using Equation 5.6 is that D_s must be constant

(Chi. Tien, 1994). The value of D_{so} and E_a were reported as 2.54 x10^{-4} m^2/s and 4.2 x10^4 J/mol respectively (Sakoda & Suzuki,1986).

5.10 Mass Balance of Adsorbate

In this study water is used as the adsorbate. Since the quantity of water which exists in the gas phase is negligible in comparison with those in other phases, the mass balance of adsorbate (water) is described as follows (Sakoda & Suzuki, 1983):

$$M_s \frac{dq}{dt} + \frac{dM_w}{dt} = 0 \quad (5.7)$$

Where M_s is the weight of adsorbent in the adsorbent bed, M_w is that of water in the evaporator and *t* is time.

5.11 Heat Balance in the Adsorption Cycle

During the adsorption cycle, the movement of heat in the adsorption cycles was considered. Figure 5.4. & Figure 5.5 illustrate the vapour transport during the adsorption process. The heat balance of the adsorption pipe and that of adsorbent particles can be expressed as:

$$\frac{d}{dt}(C_s M_s T_s) = Qst \cdot M_S \cdot \frac{d_q}{d_t} - h_{stp} \cdot A_{stp} \cdot (T_s - T_p) \quad (5.8)$$

The left part of the model is the heat from the adsorption process through the adsorbent material. The first term from the right provides the heat generated due to the condensation of the desorbed water, while the second term provides the heat rejected to the reactor pipe. The isosteric heat of adsorption Qst, is thermodynamically derived from the adsorption equilibrium given in Equation 5.1. Due to the difficulty of the theoretical description of these phenomena and also for the simplification of this model,

Qst was considered constant in this study as 2.8 MJ/kg, which was given in the literature by Sakoda & Suzuki (1986).

For an adsorbent pipe with heat rejection to ambient, the temperature of the pipe is determined by;

$$\frac{d}{dt}(C_s M_s T_s) = h_{stp} \cdot A_{stp} \cdot (T_s - T_p) - h_a \cdot A_a \cdot (T_p - T_a) \quad (5.9)$$

Where C_s, M_s, T_s is the heat capacity, the mass and temperature of the adsorbent material respectively, and T_p is the temperature of adsorbent pipe, h_{stp}, A_{stp} are the heat transfer coefficient and area between the adsorbent bed and the adsorbent pipe wall, and $h_a \; and \; A_a$ are the heat transfer coefficient of the atmosphere and area between the atmosphere and adsorbent pipe wall. For this study, the Euler method is used for solving the numerical integration to determine the temperature of the adsorbent and evaporator pipe according to Nellis & Sanford (2009).

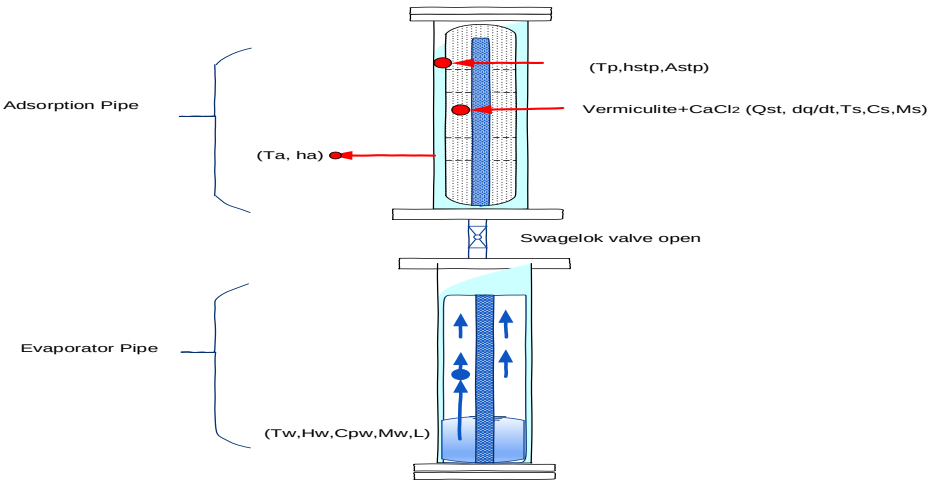


Figure 5.4: Heat transport of THSS during adsorption.

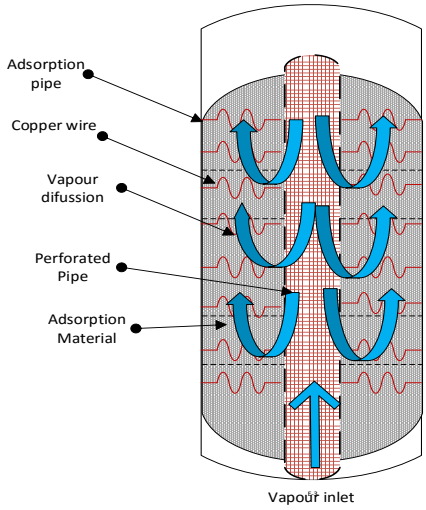


Figure 5.5: Detail of vapour diffusion in the adsorption pipe.

The average temperature of water in the evaporator pipe can be determined by:

$$\frac{d}{dt}(C_w M_w T_w) = h_w \cdot A_w \cdot (T_w - T_a) - L \cdot M_S \cdot \frac{d_q}{d_t} \quad (5.10)$$

Right hand side of the equation denote the heat from the evaporator and the left hand side denote the heat transfer from water to ambient. L is the latent heat of evaporation that is assumed to be equal to Qst (isosteric heat adsorption). It is necessary to calculate the heat transfer in the water tank, and thus h_w is determined by some experiments as the temperature drop of a typical water tank. The results showed that the effective heat transfer coefficient h_w is in the range of 400 - 600 W/m^{2}K (Riffat et al., 2013).

5.11.1 Parameters Adopted in the Simulation

The parameters used in this model can be divided into three categories (Table 5.3) which consist of adsorption properties, the design condition, and operation condition respectively, with the flowchart of the modelling process as per Figure 5.6.

The adsorbent particles in the adsorbent bed were assumed to transfer only through the heat transfer glass wall. Its corresponding heat transfer area A_{stp} was regarded as the total surface area of the glass pipe and the heat transfer coefficient, h_{stp} , was estimated by using the following equation as the approximation (Sakoda 1986):

$$h_{stp} = \frac{k_e}{d/2} \quad (5.11)$$

Where d is the average distance between the heat transfer copper wire and k_e is the effective thermal conductivity of the packed bed, which was estimated at 1.35 W/m^{2}K by Tanashev et al. (2013). The heat transfer coefficient between the ambient air and the container of the adsorbents (h_a), is taken as 1.23 W/m^{2}K, which is often used as a similar empirical value for composite materials (Miyazaki et al., 2009). The parameter for vermiculite + $CaCl_2$ is difficult to find in the previous literature. Therefore, some assumptions must be used for this modelling. The activation energy (E_a) for vermiculite+$CaCl_2$ was estimated based on experiments of the dehydration of vermiculite studied by R.Sh.Mikhail et al. (1970) with a reading of 3.7kcal/mole (15 kJ/mole). The isosteric heat adsorption (Qst) estimation was based on a previous study done by Aristov et al. (2000), with a reading of 39.4kJ/mole.

Table 5.3: Simulation physical Data for selected composite material

	Symbols	Vermiculite + $CaCl_2$ (VCC)	Units
Adsorption Properties	$q\infty$ (water uptake)	0.55	kg/kg
	Dso (pre-exponential term)	2.54 x 10^{-4}	m^2/s
	Ea (activation energy)	1.5 x 10^4	J/mol
	Qst (isosteric heat of adsorption)	3940	kJ/kg
	M_b (Mass of adsorbent pipe)	0.75	kg
	M_s (Mass of adsorbent material)	0.05	kg
	M_w (Mass of water)	0.1	kg
	M_e (mass of evaporator pipe)	0.90	kg
Physical Properties	Length (L)	0.26	m
	Internal Diameter	0.05	m
	Outside Diameter	0.055	m
	Adsorbent bed Cartridge (empty)	0.67	kg
	Copper pipe	25	Nos turns
	Fins Spacing	0.01	m
	A_{stp} (Area of adsorbent cartridge)	0.045	m^2
	A_a(Area of adsorbent pipe)	0.047	m^2
	A_w (Area of water cartridge)	0.045	m^2
	h_a(Heat transfer coefficient between adsorbent pipe and ambient)	1.23	W/m^2K
	h_w(Heat transfer coefficient in evaporator (water cartridge)	400	W/m^2K
	R_p (adsorbent particle radius)	2.0 x 10^{-3}	m
	Cp (specific heat)	3.06 (Aydin et al., 2015a)	kJ/kgK
Operating Conditions	T_a (ambient temperature)	10	° C
	$T_{in,ads}$ (initial temperature in adsorbent pipe)	20	° C
	$T_{in,w}$ (initial temperature in water pipe)	17	° C
	T_s (adsorbent material temperature)	60	° C
	T_{fsolar} (solar collector final temperature)	80	° C

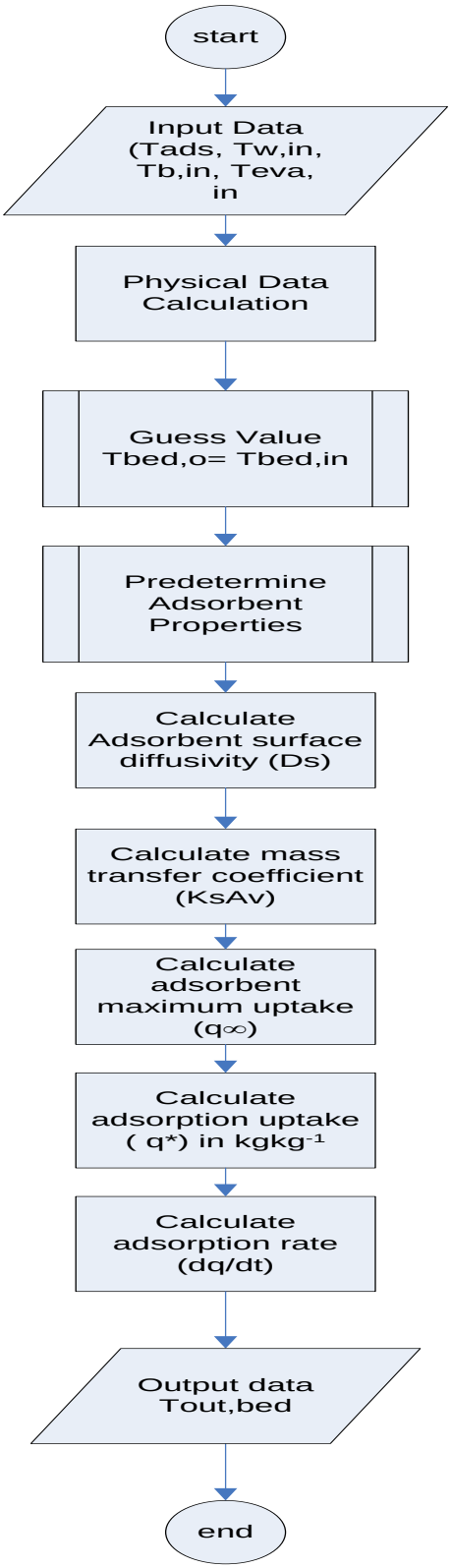


Figure 5.6 : Adsorbent pipe model flow

5.11.2 Heat Balance in Desorption Cycle

Heat balance in the desorption cycle was numerically investigated using three different heat sources consisting of an electrical clamp, a heat pump and solar thermal energy.

5.11.2.1 Desorption via Electric Clamp

In this numerical modelling, the regeneration via an electric heating clamp circuit is considered.

Assumptions

On governing the equation during the desorption/charging via a heating clamp plate, the systems have been formulated based on the following assumptions:

i. The temperature of the heating clamp is considered constant at all times.
ii. The ambient temperature is set at 25°C and is constant at all times.

The movement of heat in the desorption cycle is similarly considered as shown in Figure 5.7.

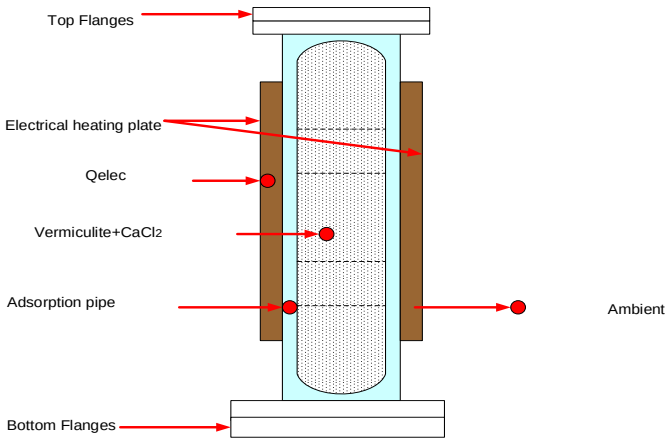


Figure 5.7: Desorption via electric heating clamp

$$\frac{d}{dt}\left(C_p M_p T_p\right) = -h_{stp} \cdot A_{stp} \cdot \left(T_s - T_p\right) - h_a \cdot A_a \cdot \left(T_p - T_a\right) + Q_{elec} \quad (5.12)$$

Where C_p, W_p, T_p are the heat capacity, the mass and temperature of the adsorption pipe respectively, h_a & A_a are the heat transfer coefficient of the atmosphere and area between the atmosphere and adsorption pipe, h_{stp}, A_{stp} are the heat transfer coefficient and area between the adsorbent material and the adsorbent pipe, and Q_{elec} is the electric clamp power.

5.11.2.2 Desorption via heat pump

In this numerical modelling, the regeneration via a heat pump circuit and pressure–enthalpy correlation points are considered (see example Figure 5.8).

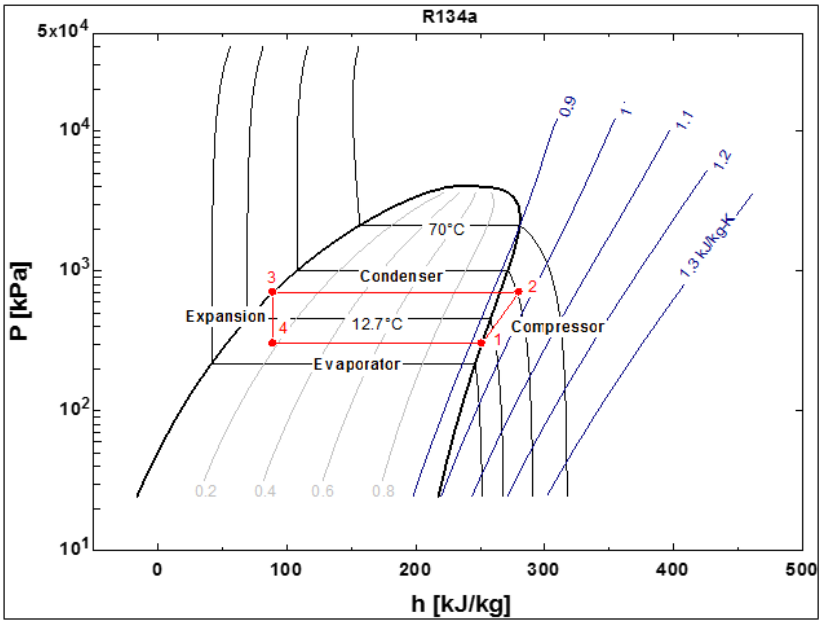


Figure 5.8: Pressure-enthalpy chart of the heat pump refrigeration cycle.

Assumptions

On governing the equation during the desorption/charging by means of a heat pump circuit, the systems have been formulated using the following assumptions:

i. The mathematical models are based on the single-stage R134a or R1234yf vapour- compression refrigeration cycle in quasi-steady state conditions within the investigative time interval.
ii. The refrigerant in the evaporator and condenser coils exists as saturated vapour and liquid respectively.
iii. Expansion of the refrigerant is considered to be isenthalpic.
iv. Pressure drops in the evaporator and condenser coil deemed to be less than 15kPa have a negligible effect on the thermal performance of the heat pump system.
v. Thermal losses in the evaporator, piping system, and condenser are insignificant.
vi. Compression of the refrigerant is considered to follow a polytropic process with the index of 1.05-1.18.
vii. The interaction between the principal components (evaporator, compressor, condenser and thermostatic expansion valve) of the THSS-R134a/R1234yf are considered.

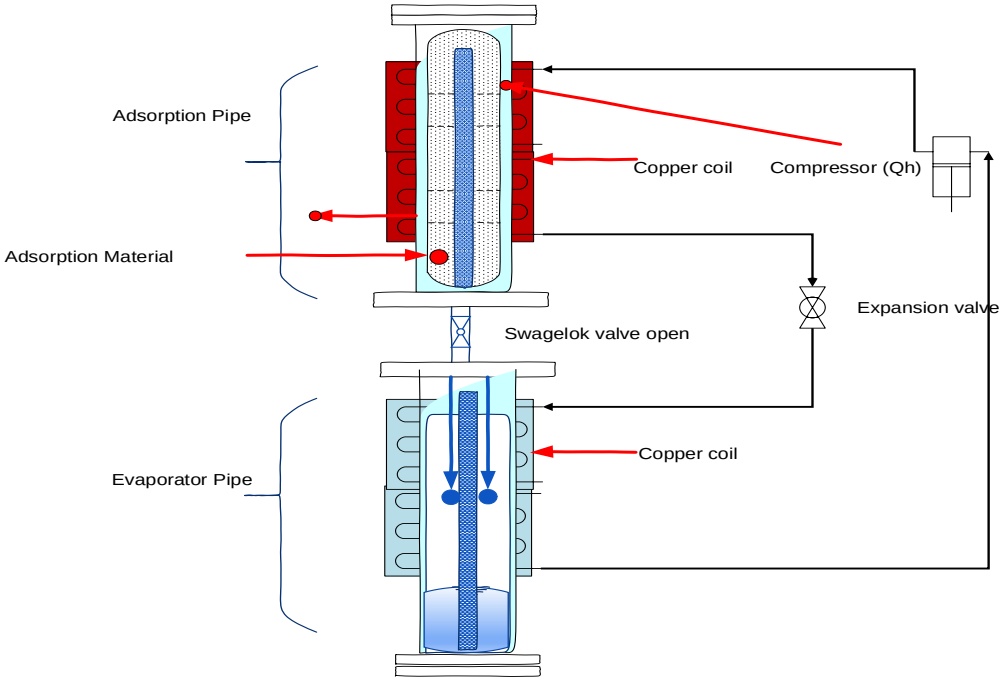


Figure 5.9: Heat transport of THSS-R134a/R1234yf

Movement of heat in the desorption cycle was similarly considered, as shown in Figure 5.9.

$$\frac{d}{dt}\left(C_{cp}M_{cp}T_{cp}\right) = Q_{st}Ms\frac{dq}{dt} - [h_a \cdot A_a \cdot \left(T_{cp} - T_a\right)] + Q_H \quad (5.13)$$

Where RHS denotes the heat in the adsorption pipe, and the first term of LHS is the adsorption heat and heat transfer from the adsorption pipe to ambient. Q_H is the heat from the heat pump as:

$$Q_H = \dot{m}(h_2 - h_3) \quad (5.14)$$

This equation is based on the heat pump Carnot cycle, where h_2 is the enthalpy from the refrigerant discharge temperature, h_3 is the enthalpy at the condenser temperature and $\dot{m}$ is the mass flow rate of refrigerant.

The compressor model

The compressor under consideration is a hermetic constant speed compressor, and the mass of refrigerant pumped and circulated by the compressor is given as (Mempouo, 2011):

$$\dot{m} = \eta_v \cdot \frac{V_d \eta_v}{V_1} \quad (5.15)$$

The pumped mass of the refrigerant by the compressor can also be expressed in terms of the rotary speed (N) of the compressor as follows:

$$\dot{m} = \eta_v \cdot \frac{N V_d \eta_v}{60 v_1} \quad (5.16)$$

Where V_d is the displacement volume rate, η_v the volumetric efficiency of the compressor, and v_1 the specific volume at the inlet of the compressor. The displacement volume (V_d) for a reciprocating-type compressor can be expressed as:

$$V_d = \frac{S_c \pi D_b^2}{4\ x\ 60} \quad (5.17)$$

The indicated power for compression can also be calculated in terms of the change of the enthalpy of the refrigerant from the inlet $h_1$to outlet h_2 of the compressor as follows:

$$W_{comp} = W_{oi} * \eta_{comp} = \dot{m}_r (h_1 - h_{2)} \quad (5.18)$$

Where W_{oi} is the total ideal input electric power to the compressor, and η_{comp} is the general efficiency of the compressor.

The Expansion Valves Model

The throttling process is regarded as the isenthalpic process. The mass flow rate is calculated as follows:

$$\dot{m}_r = k_{ex} \sqrt{2 \rho_{in} (p_c - p_{ev})} \quad (5.19)$$

Where, k_{ex} is a proportionality constant and is changed as required to maintain the mix of gas and liquid in the evaporator and p_c and p_e are the condensing and evaporating pressures (Pa) respectively. The thermostatic expansion valve is modelled as an orifice through which the liquid is expanded from condensing to evaporating pressures. The mass flow rate through it can be correlated according to the Bernoulli equation (Fu, 2014):

$$\dot{m}_r = C_d A\sqrt{2\rho_{in}(p_c - p_{ev})} \quad (5.20)$$

Where ρ_{in} is the density of the refrigerant (liquid) at the inlet of the valve (kg/m^3), and A is the minimum flow area across the orifice. C_d is the flow coefficient, which depends upon the aperture of the valve. The maximum value is reached when the valve is fully open. C_d is evaluated through the empirical equation (Fu, 2014):

$$C_d = 0.02\sqrt{\rho_{in}} + 0.63 v_{out} \quad (5.21)$$

Where v_{out} is the specific volume output of refrigerant.

The Adsorbent Pipe Model/Condenser Coils

During the regeneration/charging process, the heat from the condenser coils will be transferred to the walls of the adsorbent pipe. The heat in the condenser coils can be determined by the following equation:

$$Q_H = \dot{m}(h_{2_} h_3) \quad (5.22)$$

Where $\dot{m}$ is the mass flow rate of the refrigerant (m^3/s), h_2 is the enthalpy heat refrigerant from the discharge pipe of the compressor (kJ/kg), and h_3 is the enthalpy of refrigerant from the outlet of the condenser coils of the system. The enthalpy heat is determined via thermo-physical properties libraries available in the EES software.

The Evaporator Coils

The heat from the evaporator coils transferred to the evaporator pipe walls can be determined by:

$$Q_e = \dot{m}(h_1 - h_4) \quad (5.23)$$

Where $\dot{m}$ is the mass flow rate of the refrigerant flow in the evaporator (m^3/s), h_1 is the enthalpy heat from the outlet of the evaporator coils to the compressor (suction) (kJ/kg), and h_4 is the enthalpy heat from the outlet of the expansion valve to the evaporator coils (kJ/kg).

5.11.2.3 Desorption via Solar Heat

Methodology

The regeneration using solar energy as a heat source is described in the schematic drawing in Figure 5.10. Firstly, the adsorption/discharge process will take place between the sorption heat storage and evaporator/condenser through pressure differences under vacuum conditions. The heat from the adsorption process will be transferred to the domestic hot water storage. The useful heat will be used for domestic hot water or space heating at the same time. After the discharge process is completed, the solar loop is activated for the regeneration. The solar energy will be transferred the heat to the adsorption pipe and will disassociate water vapour from the adsorbent material and condense in the evaporator/condenser. In this system, a separate water vessel is used for the desorbed and condensed purposes. In addition, the ground heat source loop will be activated as a low-temperature heat source and heat sink for the evaporator/condenser. This is also to ensure that the water vapour fully condenses during the desorption process. The solar thermal collector will be charging the sorption storage and domestic hot water storage if solar energy is accessible. For the working

pair of vermiculite+$CaCl_2$, the charging temperature is between 40 to 60°C. This charging temperature can be achievable by using an evacuated collector.

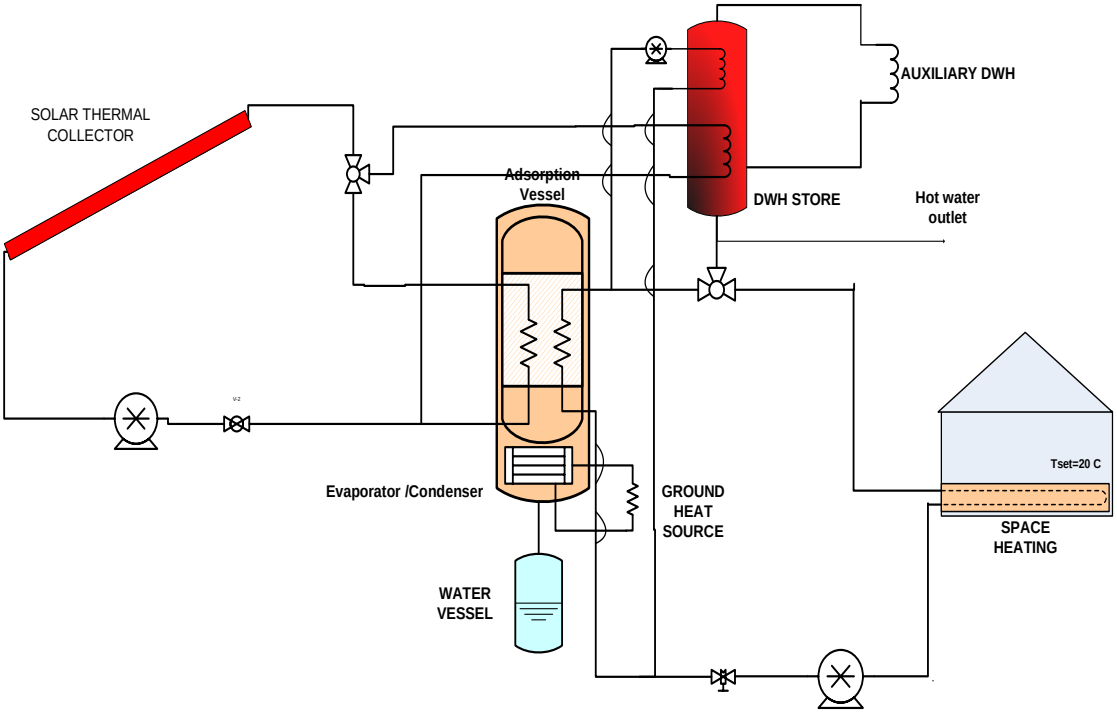


Figure 5.10: Schematic drawing of THSS-SOLAR

The energy balance of the evacuated tube collector can be expressed as (Duffie and Beckman, 2013):

$$Q_{solar} = A_c \cdot F_r \cdot [(H_t \cdot (\tau\alpha)_{net} - U_L \cdot (T_f - T_a)] \quad (5.24)$$

Equation 5.25: Energy balance in the evacuated tube and evaporation heat.

$$Q_{st} Ms \frac{dq}{dt} + [h_a \cdot A_a \cdot (T_{cw} - T_a)] = \mathrm{A_c} * \mathrm{F_r} * [(H_t) * (\tau\alpha) - \mathrm{UL} * (\mathrm{Tf} - \mathrm{Ta})] \quad (5.26)$$

The right part of the equation denotes the adsorption heat and the heat transfer through the adsorption pipe glass/wall. The left part of the equation is solar energy through the evacuated tube collectors. Where A_c is the collector area (m^2), H_t is the solar radiation

per m^2 (kW/m^2), $\tau\alpha$ is the absorption-transmission coefficient of solar collectors, U_L is the heat loss coefficient of solar collectors (W/m^2K), T_f is the collector surface temperature, and T_a is ambient temperature (°C). The assumptions used in this simulation are given in Table 5.4. The collector area in this simulation varied from $10m^2$ to $50m^2$ depending on the availability of solar intensity.

Table 5.4: Assumptions for solar heat regeneration

Constant	Symbol	Value
Total collector area	A_c	$10m^2$ to $50m^2$
Collector heat exchanger efficiency	F_r	0.86 (Aydin et al., 2014)
Absorption – transmission coefficient	$\tau\alpha$	0.8 (Aydin et al., 2014)
Heat loss coefficient	U_L	6.9 W/m^2K (Aydin et al., 2014)
Final temperature of solar collector	T_f	80°C

5.12 System performance Equation

The system performance of this small prototype was simplified as;

i. COP of the systems via electrical clamp for desorption

$$COP_1 = \frac{Q_{ads}}{Q_{electric}} \quad (5.27)$$

ii. COP of the systems via heat pump circuit for desorption

$$COP_2 = \frac{Q_{ads}}{Q_h} \quad (5.28)$$

iii. COP of the heat pump circuit

$$COP_{hp} = \frac{Q_h}{W_c} \quad (5.29)$$

iv. COP of the systems via solar thermal for desorption

$$COP_3 = \frac{Q_{ads}}{Q_{solar}} \quad (5.30)$$

Where Q_{ads} is the heat generated due to the adsorption heating process at any time (td), COP_1 is the regeneration/desorption via the heating element, COP_2 is the desorption via the heat pump heating power, COP_{hp} is the heat pump circuit and COP_3 is the desorption via solar heat. The performance of the systems was calculated by assuming that the heat extraction from the adsorption pipe and evaporator pipe happened during the adsorption and desorption process. The heat transfer fluid was not included in this numerical modelling.

5.13 Numerical result and discussion

The simulation for the THSS was based upon the adsorption heating process of using the vermiculite+$CaCl_2$ conducted through an EES numerical calculation. The calculation was analysed independently within the adsorption and desorption cycles

5.13.1 Adsorption Process

In this section, the results and discussion are mainly focused on the adsorption process of the TCM materials and their behaviours under the influence of change in saturation pressure (P_s) and adsorption uptake (d_q/d_t).

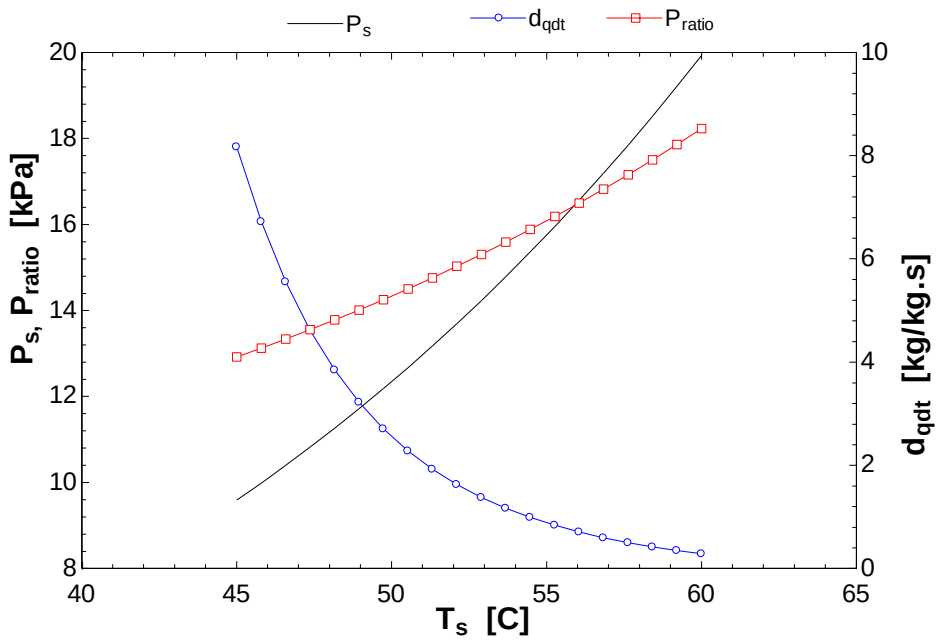


Figure 5.11: The effect of adsorption temperature vs. adsorption uptake and saturation pressure and pressure ratio.

Figure 5.11 exhibits the effect of increasing the adsorption material temperature (T_s) on saturation pressure and adsorption rate (d_q/d_t). As can be seen from these results, the increase in the adsorption temperature will decrease the adsorption uptake from 8.5kg/kg to 0.28kg/kg. However, the saturation pressure rises from 9kPa to 20kPa. These results suggest that the increase in adsorption temperature will increase the pressure ratio from 9kPa to 20kPa and the adsorption rate will decrease from 8kg/kg to 0.25kg/kg. This is because the reaction will take place during the adsorption cycle when the water vapour is absorbed by the adsorbent material. Therefore, it could be predicted that the adsorbent material temperature will be increased by the increase in adsorption rate during this period.

5.13.2 Desorption Process

The desorption method in this simulation has been described in section 5.11.2

5.13.2.1 Desorption performance of VCC using electrical heat clamp as heat source

The desorption performance on TCM material of VCC of using electrical heat clamp as a heat source has been analysed. Two possible parameters that affected the performance consisting of the heating temperature and desorption time was analysed and discussed below.

i. Heating Temperature Effect

The desorption method using an electric heating clamp has also been numerically analysed for VCC material, and Figure 5.12 illustrates the effect of the heating temperature on the chosen parameters: heating power (Q_{elec}), temperature of the adsorbent material (T_s), adsorption heat (Q_{ads}), and COP_1. The increase of the heating temperature will increase the adsorption material temperature (T_s) from 37°C to 41°C, a change that is an inverse proportional correlation with the COP_1. The COP_1 decreases from 11.85 to 0.04. This phenomenon is predictable in this system as the work/heating power, according to the product/fuel principle, cannot be higher than the heat generated by the adsorbent material. This would reduce the COP of the whole system.

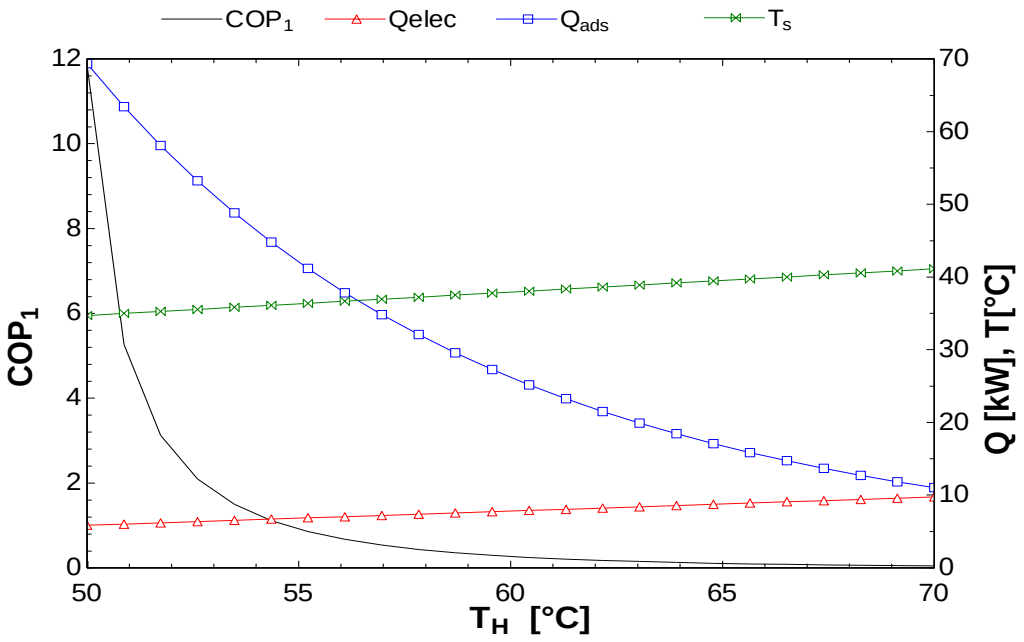


Figure 5.12: Effect of heating temperature (T_H) on heating power ($Q_{electric}$), adsorption heat (Q_{ads}), adsorbent bed temperature (T_s) and COP_1.

ii. Desorption Time Effect

Figure 5.13 depicts the effect of the desorption time on the temperature of adsorbent material (T_s), heating temperature (T_H), adsorbent heat (Q_{ads}) and COP_1. The heating temperature was set at a constant of 60°C. It can be seen that within five hours of the desorption period, the adsorbent bed temperature (T_p) increases from 47°C to 60°C and plateaus throughout the remainder of the process. However, the adsorption heat (Q_{ads}) and COP of the systems decrease from 0.38 to 0.02 and 0.28 to 0.01 respectively. These results indicate that as time passed, the adsorbent material was in a state of semi-equilibrium, and this will affect the performance of the THSS. Therefore, the desorption time is needed to be optimised to increase the performance of the

system. Again, prolonging of the desorption time needs to be avoided as it would decrease the COP of the systems.

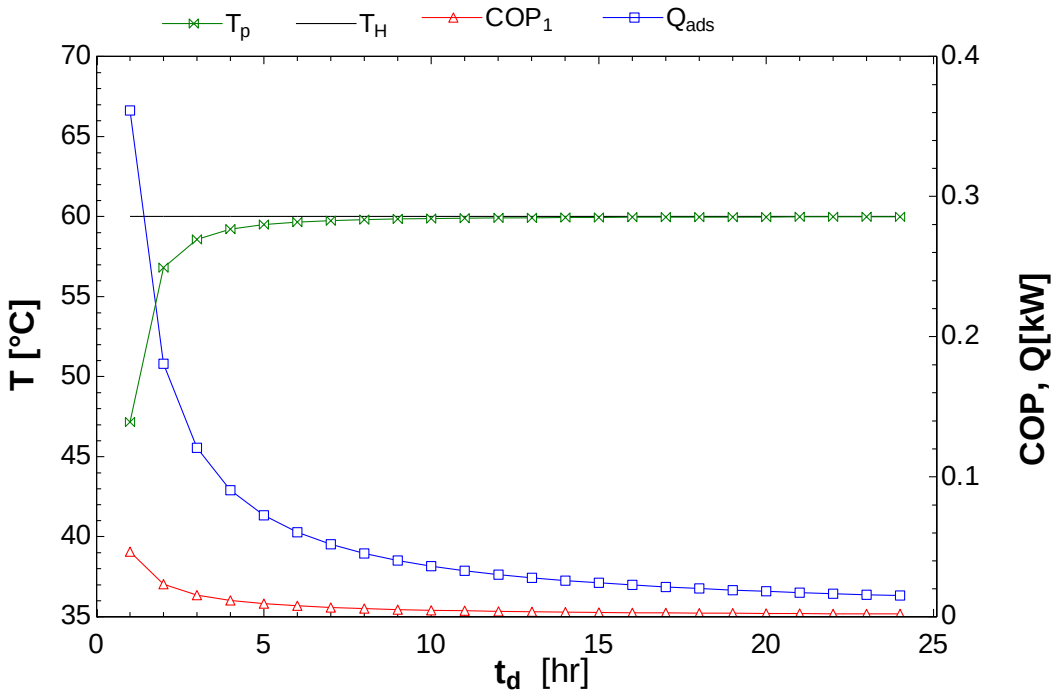


Figure 5.13: Effect of time to adsorbent bed temperature, heating temperature, adsorption heat and COP_1.

5.13.2.2 Desorption Performance of VCC using a Heat-Pump Circuit with R134a as Refrigerant Gas (THSS-VCC-R134a)

An analysis has been conducted on the performance of the THSS during desorption for VCC using a heat-pump circuit incorporated with the refrigerant gas R134a. Four possible influential parameters that may affect the THSS performance are: the heating temperature effect, the mass of material effect, desorption time effect, and solar collector area and they have been investigated and discussed below.

i. Heating Temperature Effect

Figure 5.14 shows the effect of heating temperature (T_H) (R134a) on the adsorption heat and the compressor work. With the assumption that the constant dry mass of VCC is 50g and with 60g of water, the compressor work increases in a positive correlation with the heating temperature. However, the adsorption is expected to be constant throughout the desorption process as no reaction will occur. The heating temperature would also affect the COP system and the COP the heat pump. With the assumption of an ambient temperature (T_a) of 10°C, it would be expected that the COP_{hp} would decrease from 6.15 to1.33 with the increase in heating temperature rising from 30-60°C, whereas it is expected the COP_2 would rise from 1.44 to 1.98. It can be predicted that as the heating temperature increases, the hydrated composite material will reach semi-equilibrium and lower energy levels will be required to disassociate the water vapour.

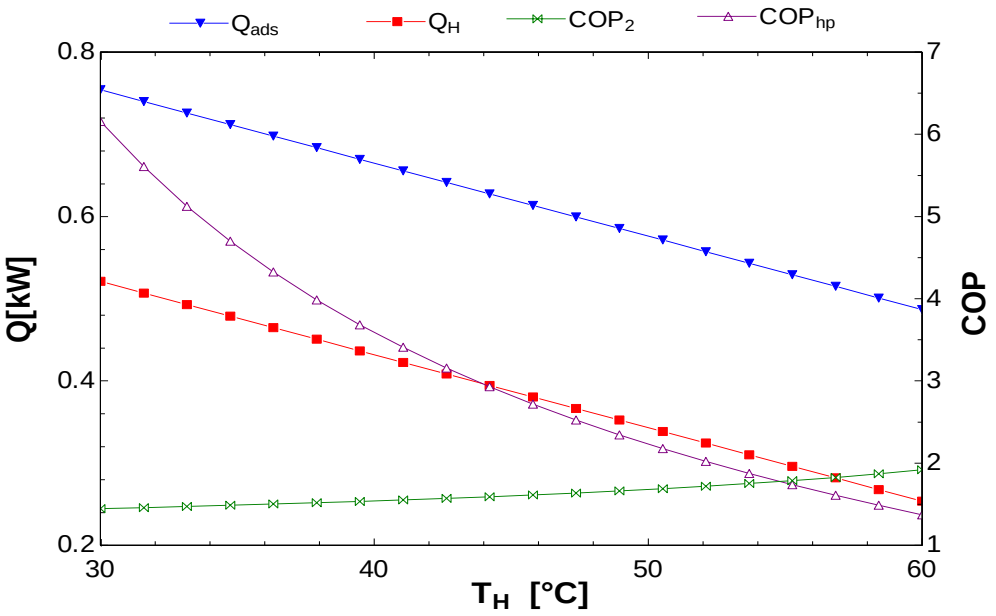


Figure 5.14: Adsorption heat, condenser heat, COP_2 and COP_{HP} vs. heating temperature (VCC-R134a).

ii. Mass of Material Effect

Figure 5.15 illustrates the effect of mass adsorbent material effect and predicted that with the assumptions of a heating temperature (T_H) of 60°C and an ambient temperature (T_a) of 10°C, the heat pump heating power (Q_H) and the COP of the heat pump will remain constant at 0.026kW and 1.41 respectively. However, the adsorbent heat (Q_{ads}) and COP of the systems increased from 0.27 to 17kW and 0.042kW to 2.75kW respectively.

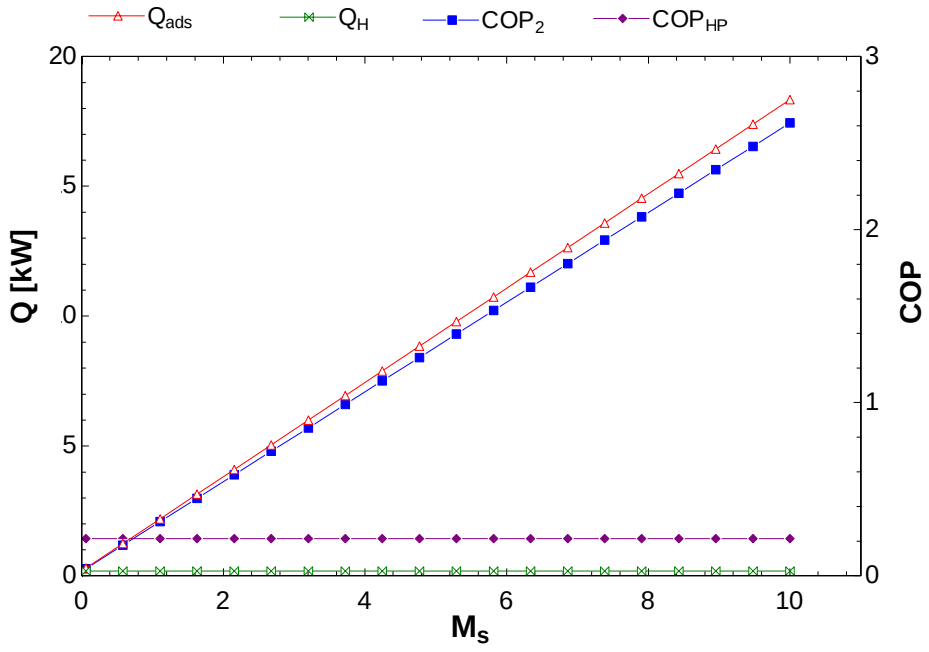


Figure 5.15: Effect of mass change to heating power and the COP of the heat pump.

iii. Desorption Time Effect

Time dependence during desorption will also have an effect on the COP_{hp} and COP_2 as shown in Figure 5.16. With the assumption of the mass of VCC at 0.05kg, the mass of water at 0.06kg, and with a heat source temperature of 60°C,

the COP of the systems (COP_2) and COP of the heat pump (COP_{hp}) decreased from 0.92 to 0.03 and 1.4 to 0.02 respectively. In this case, the COP of the systems is higher than the COP of the heat pump. Furthermore, the adsorption heat (Q_{ads}) decreased from 0.233kW to 0.009kW; as time passed the heat will have been lost to the immediate environment.

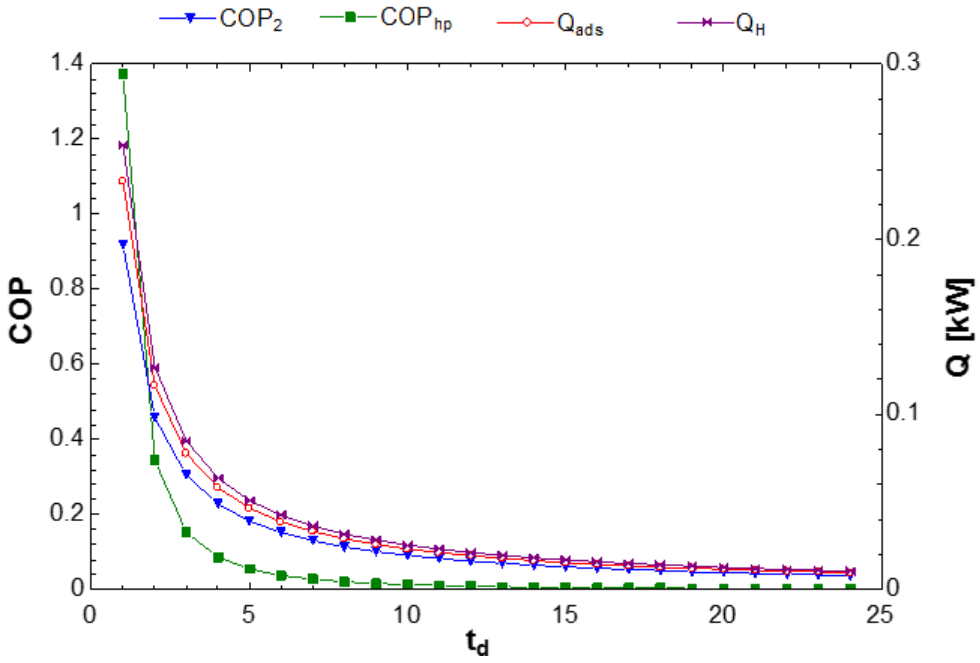


Figure 5.16: Effect of time on adsorption heat (COP_2) and the COP of the heat pump (R134a).

5.13.2.3 Desorption Performance of VCC using a Heat-Pump Circuit with R1234yf as the Refrigerant Gas (THSS-VCC-R1234yf)

In this section, an analysis has been conducted on the performance of the THSS during desorption using a heat-pump circuit incorporated with the refrigerant gas of R1234yf. Three possibly influential parameters that will affect the THSS performance are the

heating temperature effect, the mass of material effect and the desorption time effect, all of which have been investigated and discussed below.

i. Heating Temperature Effect

Figure 5.17 shows the effect of the heating temperature (T_H) (R1234yf) on adsorption heat, heat pump heat, the COP of the heat pump (COP_{hp}), and the COP of the system (COP_2). We can see that the effect of this on the COP_{hp} is a decrease from 2.66 to 0.93, whereas the COP_2 has increased from 0.32 to 0.48. A higher COP_{hp} compared to the lower COP_2 is due to the small amount of adsorbent materials using lower heating power than was estimated to be required for the desorption process.

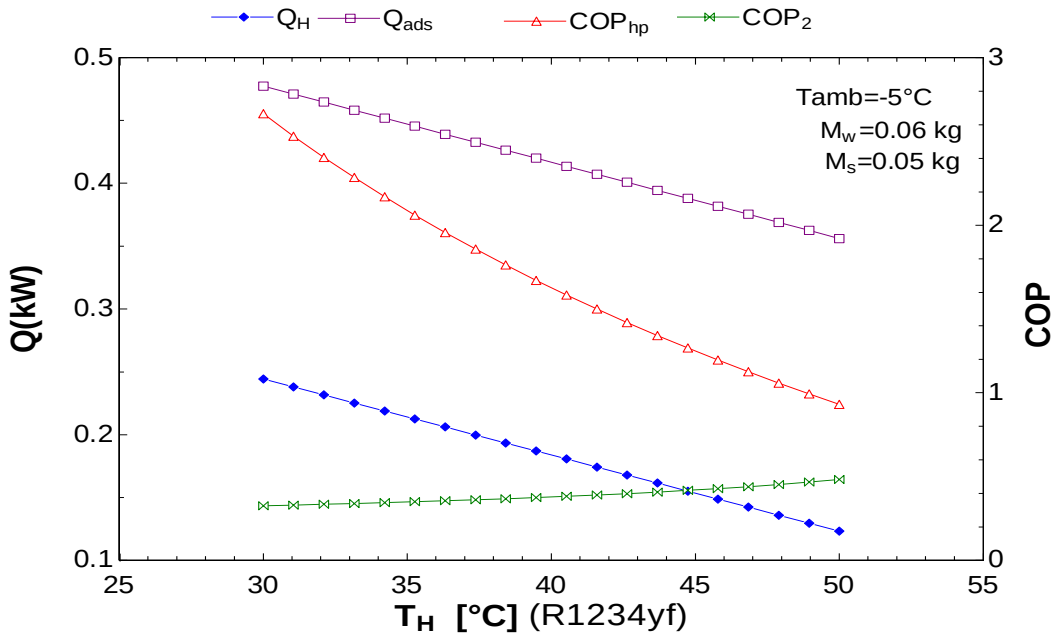


Figure 5.17: Effect of heating temperature on adsorption heat and compressor work.

ii. Mass of Composite Adsorbent Effect

The increase of the VCC mass will increase the adsorption heat due to the increase of potential energy to be extracted from this material. Therefore, as

can be seen in Figure 5.18 with the mass increase, the adsorbent heat (Q_{ads}) and the COP of the systems increase between the ranges of 0.28 to 46.6kW and 0.006 to 1.05 respectively. The COP of the heat pump (COP_{HP}) and the condenser heat (Q_H) remain constant because it is assumed that the heating temperature (T_H) and ambient temperature (T_a) are constant. However, during desorption, no reaction occurs. Therefore, we can only use this result to compare the effect of a mass increase in the systems quantitatively. However, we predict that if the mass of adsorbent material increases, it will increase the heating power that is required for disassociating the water vapour from the adsorbent material.

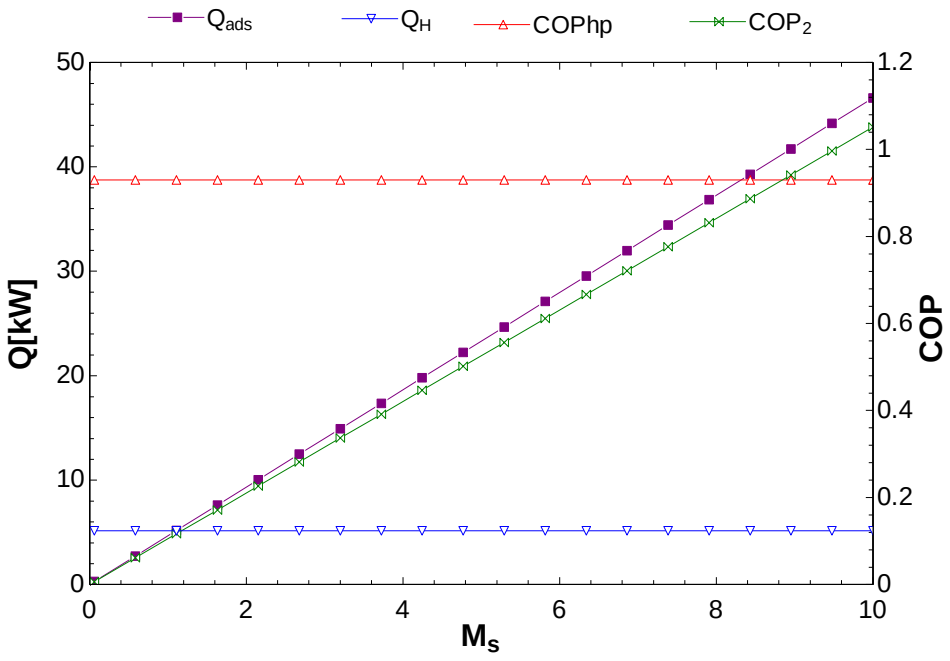


Figure 5.18: Effect of mass change on adsorption heat and COP_2.

iii. Desorption Time Effect

Time dependence will also have an effect on the COP_{hp} and COP_2 as shown in Figure 5.19. With the assumption that the mass of the VCC is 0.05kg and the mass of water is 0.06kg, the COP of the systems (COP_2) and the COP of the heat pump (COP_{hp}) are decrease from 9.4 to 0.005 and 0.92 to 0.08 respectively. From this result we can see that the COP of the systems is higher than that of the heat pump. The adsorption heat (Q_{ads}) and the condenser heat (Q_H) have decreased because as time passes the heat is lost to the immediate environment. As is similar to the TCM SGCC, five hours is considered an appropriate amount of time for desorption, as the system will not be effective for longer periods.

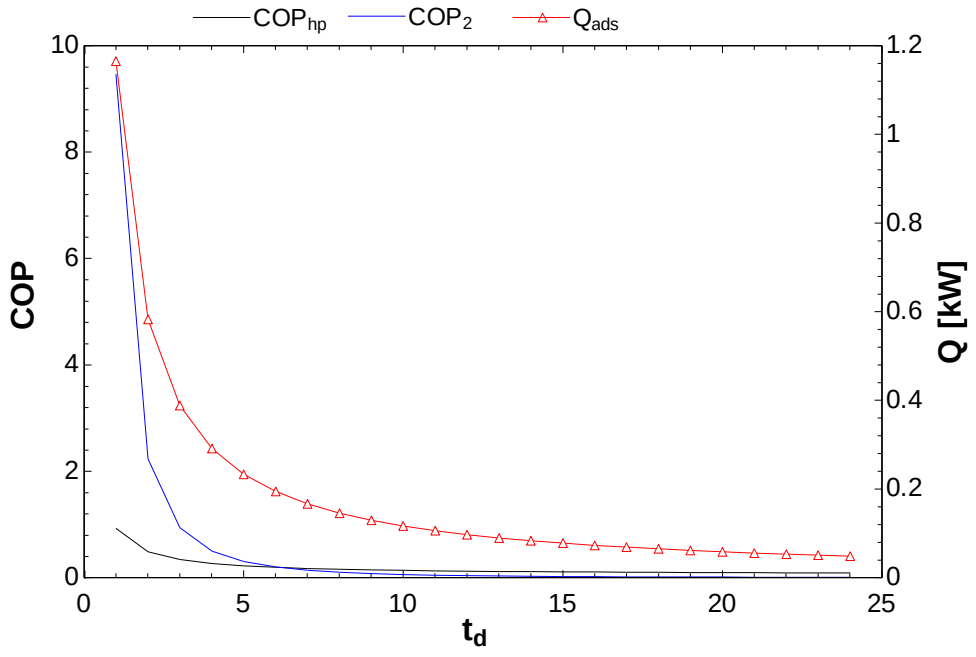


Figure 5.19: Effect of time on COP_2 and COP_{hp}.

5.13.2.4 Desorption Performance of VCC using the Solar Thermal as the Heat Source

The analysis conducted using solar thermal energy for the VCC desorption process is similar to that using the SGCC material. June was the month selected for the evaluation of the THSS performance via solar thermal energy because the maximum solar intensity was estimated to occur in this month.

i. The Effect of the COP will Increase with the Expansion of the Solar Collector Area

Technically, the larger solar collectors will increase the solar thermal energy gain and Figure 5.20 shows this influence. The results demonstrate that with the increase in collector size from 10 m^2 to 50 m^2, the solar thermal heat gain increased from 1.1 to 5kW. As a consequence of this, the COP_3 will also increase from 0.01 to 0.35. The adsorbent heat remains constant because of the constant mass of material used in the simulation, and it was assumed that there is no reaction during the desorption process. The peak COP occurrence in this result indicates that the solar thermal adsorbent heat is more than that the solar intensities available and a constant COP occurs when the adsorbent heat is relatively equal to the solar gain in the systems.

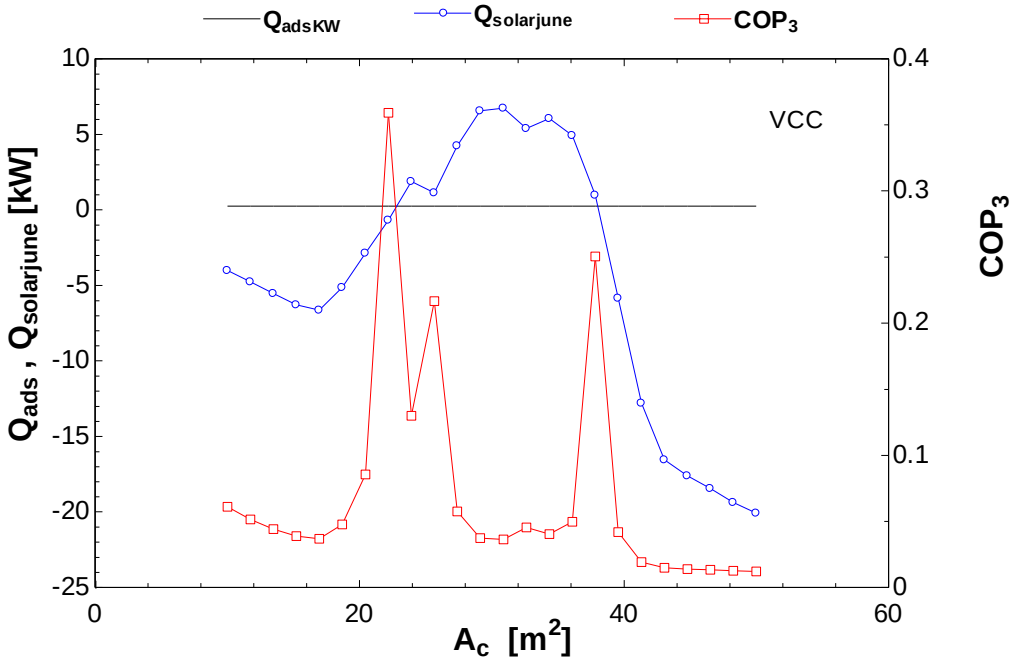


Figure 5.20: Effect of solar collector size on the COP of the systems.

Table 5.5: Summary results of adsorbent heat (Q_{ads}) from the numerical analysis

Influence Factors	Changing Rate	Q_{ads}			
		Electric clamp	R134a	R1234yf	Solar
Heating temperature	50-70°C	12→10	-	-	-
Heating temperature	30-60°C		0.75→0.5	0.55→0.25	-
Mass Change	2-10kg	-	0.27→ 17	0.28→46.6	-
Desorption time	1-24hr	0.38→0.02	0.23→0.009	1.18→0.02	-
Solar Collector area	$10m^2$ -$50m^2$	-	-	-	0.245

Table 5.6: Summary results of all COP from the numerical analysis

Influence Factors	Changing Rate	COP			
		Electric clamp	R134a	R1234yf	Solar
		COP_1	COP_2	COP_2	COP_3
Heating temperature	50-70°C	11.85→0.04	-	-	-
Heating temperature	30-60°C	-	1.44→1.98	0.33→0.48	-
Mass Change	2-10kg	-	0.27→17	0.06→48	-
Desorption time	1-24hr	0.28→0.01	0.92→0.03	9.4→0.05	-
Solar Collector area	$10m^2$ -$50m^2$	-	-	-	0.01→0.35

5.14 Conclusions of the Chapter

The modelling based on the composite materials of vermiculite+$CaCl_2$/water was numerically analysed and discussed to evaluate which TCM has the most potential for use in a THSS. Within this context, four parameters that influence the performance of a THSS were investigated. These parameters were: heating temperature (T_H), the mass of adsorbent material (M_s), desorption time (T_d) and solar collector area (A_c). Furthermore, three methods of desorption were analysed in this study, consisting of the heating element, heat-pump circuit and solar thermal energy. For the method of using heat pump circuits as the heat source, two different refrigerant gases were evaluated, namely R134a and R1234yf.

Table 5.5 summarises the simulation results of adsorbent heat (Q_{ads}) with all influence parameters assessed in this study. The desorption method of using a heat pump circuit will have affected the Q_{ads} when the heating temperature is increasing. The Q_{ads} of using electric heat clamp has higher than that of using the heat-pump circuit when the heating temperatures were increased. The mass of materials increase had also affected the Q_{ads}.

When the mass of composite material were increases, the Q_{ads} will increased. The Q_{ads} of using R1234yf was higher than that of R1234a ranges from 0.28 to 46.6kW and 0.27 to 17kW respectively. Q_{ads} behaviour is also highly dependent on desorption time. When the time was increased, VCC of using R1234yf has the highest Q_{ads} compared to other desorption heat source method ranges from 0.02 to 1.18kW. Other than that, all the desorption heat had decreased when the desorption time was increased for all heat source methods.

Table 5.6 summarises the result of COP for all desorption heat source. It can be seen that the increased of heating temperature will increase the COP of the THSS system. According to product/power theory we predicted that the higher power input would have an adverse effect on the COP. Therefore, the increase in the COP when the heating temperature was increased was due to the small amount of mass (0.05kg) applied in the simulation and thus less energy was required for the desorption process. VCC has higher COP when using R1234yf compared to R134a ranges from 0.05 to 9.4 and 0.03 to 0.92. Nonetheless, the small-scale investigation shall need to be entail to realise the THSS performance. Hence, this will be discussed further in the next chapter.

6. BUILD UP AND EXPERIMENTAL INVESTIGATION OF A SMALL–SCALE THERMOCHEMICAL HEAT STORAGE SYSTEM (THSS)

6.1 Introduction

The aim of this Chapter is to carry out a preliminary investigation of a small scale Thermochemical Heat Storage Systems (THSS-R134a) using a heat pump circuit for the regeneration heat source. The working pair for this prototype is the composite of vermiculite impregnated with calcium chloride and water as the refrigerant in the evaporator pipe. The rig was reconstructed during from vertical glass rig used for the materials synthesising experiments. However, in this experiments, this rig is modified with a heat pump circuit using a mini compressor for transporting the refrigeration gas as a heat source for desorption cycle. The system was also incorporated with the condenser coils, evaporator coils, and an expansion valve. The integration with a heat pump circuit is to analyse the performance of a THSS-R134a using an off-peak power in desorption/charging cycle and utilising renewable energy sources to minimise energy demands from fossil fuels (Wajid et al., 2016).

6.2 Equipment and Instrumentations

6.2.1 Adsorption Pipe

The adsorption pipe provided with a thermocouple and pressure transmitter for the pressure and temperature measurement. Additionally, this pipe was also connected with a vacuum pipe for the vacuum process before the adsorption process start. The

adsorption pipe receives heat from the coil pipe filled with the refrigerant gas from the compressor and then transferred the heat to adsorbent material while charging process. During the adsorption/discharge process, the water vapour from the evaporator pipe below will flow from the connecting Swagelok valve. The condenser used in this study is the cylindrical type made of glass with a transfer area of about 448 cm^2. The length of glass pipe is 250mm and 50mm diameter (see Figure 6.1).

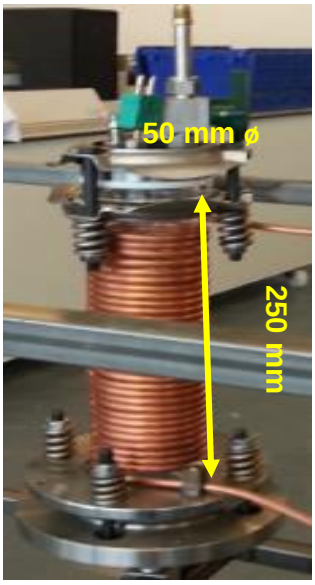


Figure 6.1: Adsorption pipe with Condenser coil R134a circuits

6.2.2 Evaporator Pipe

The evaporator pipe is located below the condenser pipe that separated with Swagelok ball valve and flanges (see Figure 6.2). Inside of the evaporator pipe consist of cotton wick, perforates aluminium pipe and a Perspex pipe as a water container. The length and diameter of evaporator pipe are similar to the condenser pipe. The evaporator pipe is connected with vacuum pipe for vacuuming, thermocouple and pressure transmitter for measuring the temperature and pressure.

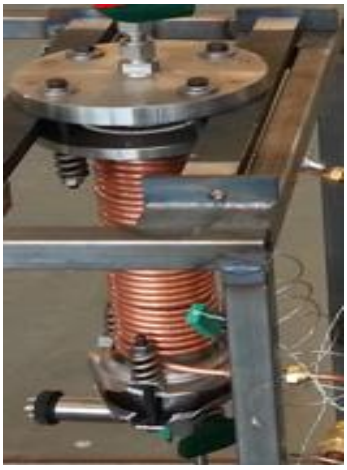


Figure 6.2: Evaporator Pipe with evaporator coil (R134a circuits)

6.2.3 Data Acquisition and Processing Systems

The data logger used was a dataTaker (DT500 series). It was used as an interface between a Desktop computer and pressure sensors & temperature sensors. It is an instrument that acquires data from the thermocouples and transfers the data via a serial link to a control programme in the PC that it records the data using DeLogger™ 4 Pro software an enhanced graphical package that allows reporting to a database and offers remote dataTaker management features. Data collection through data-logging was carried out, and the results were analysed to evaluate the THSS-R134a performance.

For this particular rig, the K-type thermocouple was chosen and all thermocouples were connected to DT500 data logger and tested for calibration before the testing commenced. Figure 6.3 indicates the location of all thermocouple & pressure sensors positions. Pressures were measured with UNIK 5000 GE pressure transmitter with a pressure range of -1 to 1.6bar.

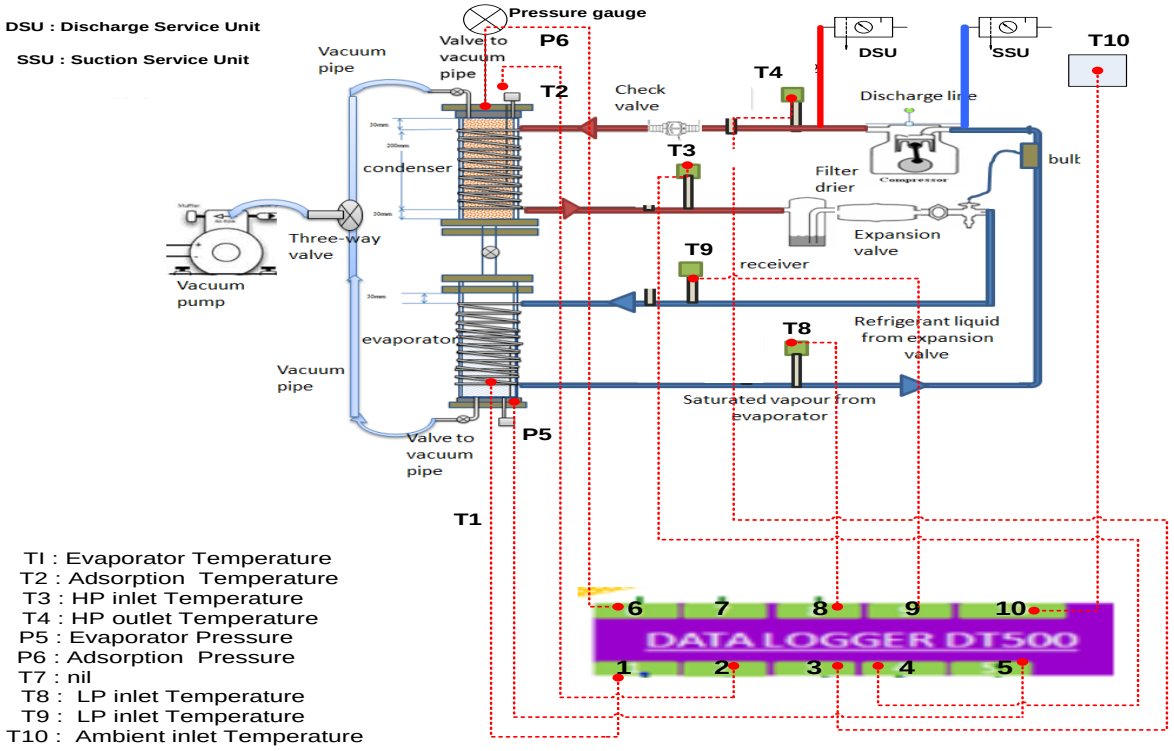


Figure 6.3: Temperature & pressure sensor position

6.2.4 Experimental Uncertainty

Any experiment incurs measurement errors, and when these are extrapolated, the uncertainty is increased. Therefore, careful calibration of equipment can minimise the error. Because of the errors and inaccuracies in equipment, measurement uncertainties must be computed and maintained as low as possible to provide an accurate value of the experimental parameters after calibration of the sensors. The basic equipment uncertainties summarised in Table 6.1.

Table 6.1: Sensor uncertainties

Sensor	Percentage Error
Thermocouple	±1.5
Pressure transducer	±0.25
Vacuum gauge	±0.01

6.3 Methodology of the Investigation

The experiment was conducted in two different processes namely the adsorption/discharge process and desorption/charging process. The discharge process would only involve the vacuum pump and the adsorption pipe and evaporator pipe. While, the heat pump circuit was not activated during this period. In addition, Swagelok ball valve that separates both pipes is open for the water vapour transport to the adsorption pipe. Then, during the desorption process, the heat pump circuit is activated to evaluate the heat pump efficiency (COP) and the heat gain at the adsorbent pipe. The basic equipment involves at this stage and the way they were set-up illustrated schematically in Figure 6.5.

The heat gain in adsorbent pipe can be measured by mean of mass flow rate of the refrigerant R134a through the copper pipe and the enthalpy change. The enthalpy was determined from PH-diagram (pressure–enthalpy diagram) for the specific gas that retrieved from EES software (see Figure 6.4). Data-taker was used to record temperatures and pressures at the key points in the circuit (see Figure 6.5), and the compressor power consumption (W_C) was recorded. Then these data were then analysed using Microsoft Excel. The experiment performances obtained is compared with simulation results. The constructed THSS is shown in Figure 6.6, and the details of each component are summarised in Table 6.2.

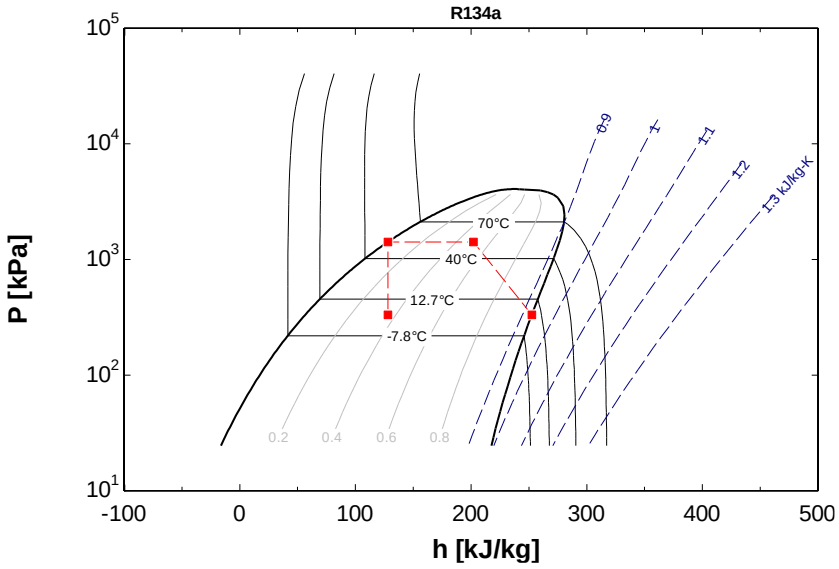


Figure 6.4: Pressure-Enthalpy (P-H) diagram for R134a circuits

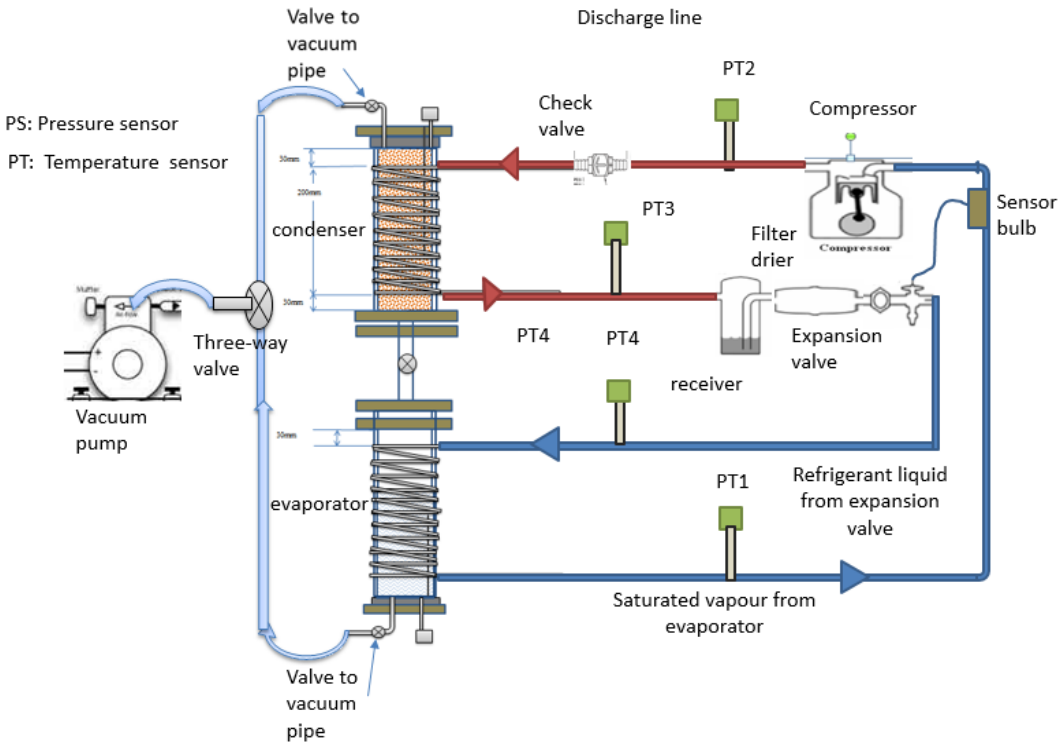


Figure 6.5: Schematic of THSS-R134a system

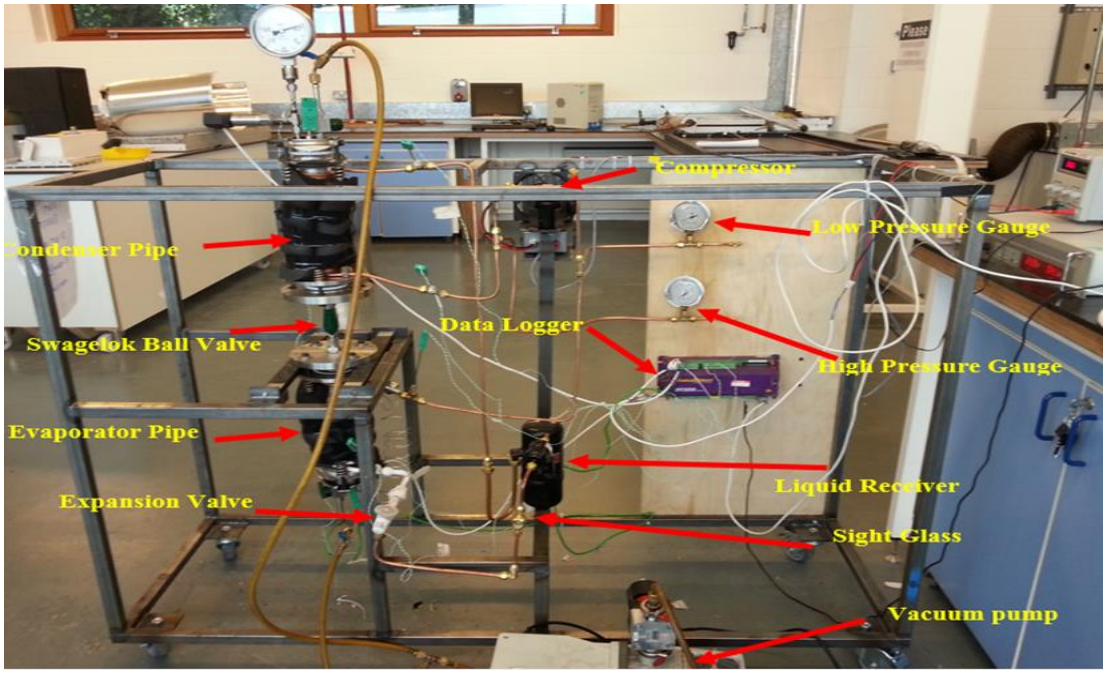


Figure 6.6: Photo showing the constructed THSS-R134a

Table 6.2: Specification of main components in the THSS-R134a system

No	Name	Type	Description
1	Compressor	Closed rotary hermetic	miniature DC inverter compressor (ZH2024, Greatcool) displacement rate of 1.9cm^3/rev, maximum input power of 135W
2	Condenser	Cylindrical borosilicate Glass	QVF glass, ID 50mm, L: 250mm, maximum pressure 4 barg, maximum temperature :200°C, heat transfer area: 448 cm^2,0.00196m^3, thermal conductivity (λ: 1.2 W/m.K), Density: 2.23 kg/dm^3, specific heat : 0.8 KJ/kg.K
3	Evaporator	Cylindrical borosilicate Glass	QVF glass, ID 50mm, maximum pressure 4 barg, maximum temperature :200° C, heat transfer area: 448 cm^2, thermal conductivity (λ: 1.2 W/m.K), Density (ρ): 2.23 kg/dm^3, specific heat (cp): 0.8 KJ/kg.K
4	Expansion Valve	Thermostatic Expansion Valve (TXV)	Universal, TN2 Danfoss, Control device, it has a sensing bulb attached to the outlet of the evaporator

6.5 Experimental Procedure

In this experiment, two different modes allocated for the THSS-R134a systems namely the adsorption/discharging and desorption/charging. On evaluating the thermal performance of the THSS-R134a, a series of experiments were conducted at the Sustainable Research Building Laboratory, Department of Architecture & Built Environment, Nottingham University. The procedures that followed to carry out the experiment were described as below.

6.5.1 Adsorption/Discharge Mode

Preparation

i. Make a note of the starting time

ii. Put the dry material in the wick and put the wick in the adsorbent bed (Adsorption section).

iii. Close the adsorption and evaporator pipe using flanges.

iv. Leakage test in conducted before the material is loading in the rig to make sure that the adsorbent pipe is under the vacuum condition.

v. Vacuum the system using the vacuum pump.

vi. Make sure that the system is in perfect vacuum by monitoring through the DataTaker Software.

vii. All sensors were calibrated before the experiment conducted.

Testing Period

i. Close the vacuum valve for adsorbent and evaporator pipe

ii. Stop the vacuum pump

iii. Release the Swagelok ball that connects adsorbent and evaporator pipe.

iv. Monitored the temperature rise through data taker software, when there is no more temperature rise and the adsorbent material is considered in the equilibrium stage, then stops the test by closing the separator valve.

v. Dismantle both pipe and weight the hydrated adsorbent material and water quickly and installed back the Rig.

6.5.2 Charging/Desorption Mode

Preparation

i. Make a note of starting time;

ii. Repeat the leakage test again to confirm that the system is in perfect vacuum condition.

iii. Close the vacuum valve and turn off the vacuum pump;

Testing Period

i. Activate the compressor and wait for the temperature from the discharge line is increase to 60°C;

ii. Run the refrigerant compressor and control the sight glass to ensure that there is enough refrigerant in the circuit and that the system is functioning properly;

iii. Let the experiment warm up for approximately 10 minutes; this brings the compressor up to its operating temperature and pressure, then check the temperature and pressure gauges on the low pressure and high pressure of the

compressor for correct refrigerant charge and confirm the values with the vapour compression properties of the R134a;

iv. When the temperature is in steady state open the Swagelok ball valve that connects adsorption pipe and evaporator pipe;

v. Monitored the temperature and the pressure through the Data Taker software;

vi. Continue the desorption up to 5hours at a constant temperature;

vii. When completed, dismantle the rig and quickly weight the mass of water and the adsorbent material using a digital weight machine.

6.6 Performance equations

The equations used for analysing the experimental results are given in Table 6.3 below;

Table 6.3: Equations used in the analysis (Wajid et al., 2016)

Equation No	Equation	Definition	Units
6.1	$E_{d,m} = \frac{Q_{THSS}}{\Delta m}$	Energy storage density per unit mass	kWh/kg
6.2	$E_{d,v} = \frac{Q_{THSS}}{V_{ad}}$	Energy storage density per volume unit	kWh/m^3
6.3	$\Delta m = M_{w,v} = M_w - M_d$	mass increase	kg
6.4	$Q_{THSS} = M_s \cdot C_{ps} \cdot \Delta T$	Thermal energy releases in adsorption pipe	kWh
6.5	$\dot{m} = \eta_v \cdot \frac{NV_d\eta_v}{60v_1}$	mass flow rate of the refrigerant by the compressor in term of rotary speed	kg/s
6.6	$W_{comp} = W_{oi} * \eta_{comp} = \dot{m_r}(h_1 - h_{2)}$	Compressor works with enthalpy flow	(kW)
6.7	$Q_{hp} = \dot{m}(h_{2-} h_3)$	Heat from heat pump	(kW)
6.8	$COP_{THSS} = \frac{Q_{THSS}(t)}{Qhp(t)}$	COP_{THSS}	(-)

6.7 Result and Discussion

6.7.1 Temperature variation of Adsorption Test

In this study, the primary objective is to investigate the temperature lift in the adsorption pipe during adsorption test shown in Figure 6.7 to Figure 6.13. Other than that, the effect of changing the mass of VCC and water were also being monitored, and the TCM weight was measured before and after the experiments.

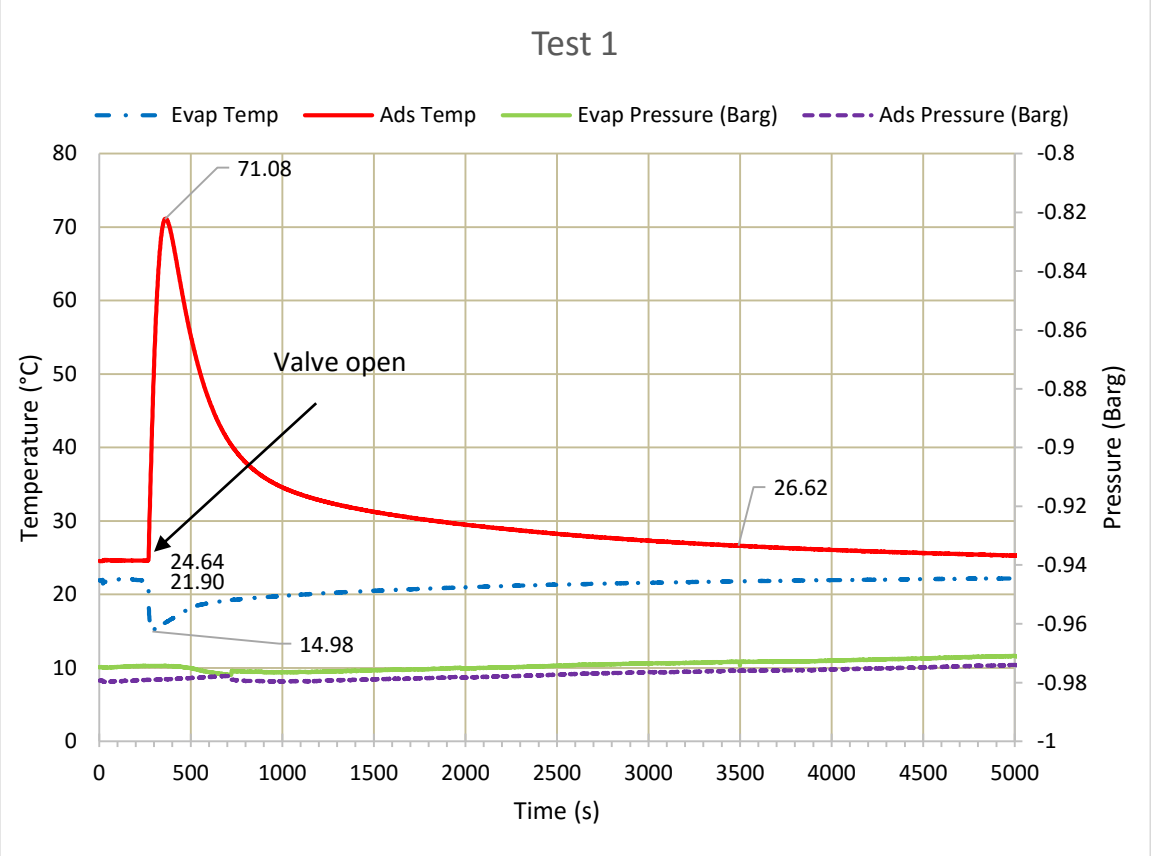


Figure 6.7: Temperature Variations of Test 1

The experiment result of (Test 1) of using the mass of VCC of 50 and mass of water 100g shown in Figure 6.7. The amount of mass of VCC and mass of water used was to test the experiment in a weight ratio of 1:2. We could see that the temperature rises sharply in 360s of starting the adsorption process. The temperature lift achieved is

71.10°C from its initial temperature of 24.60°C (ΔT of 46.50°C). The adsorption temperature drops sharply after 360s and returns to its initial temperature at the end of the test. The temperature drop sharply due to the adsorption pipe was not insulated when the 1st test was conducted. The evaporator temperature had shown a temperature drop at 15.0°C from its initial of 21.90°C (ΔT of 6.90°C). The evaporator temperature was also shown a temperature rise at 360s and return to its initial temperature at the end of the test. This results demonstrated a positive effect of using a mass ratio of 1:2 on the temperature lift in the adsorption temperature. However, the temperature drop is unavoidable due to the uninsulated pipe.

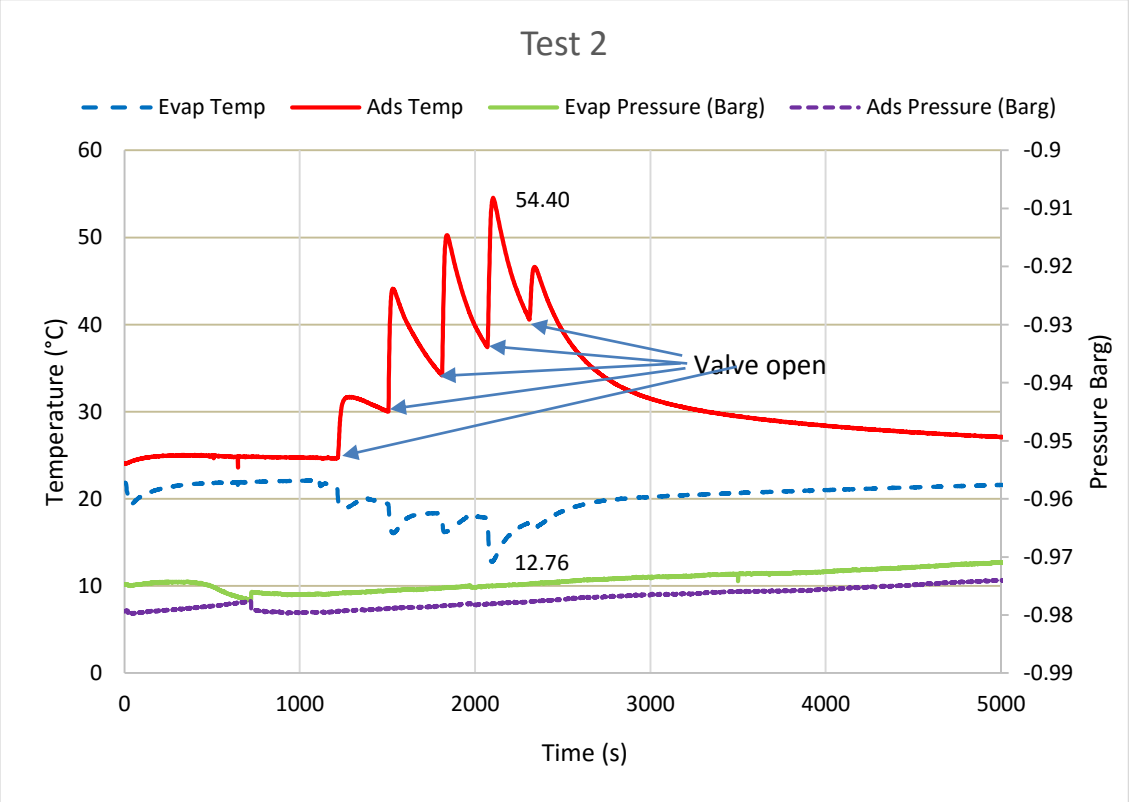


Figure 6.8: Temperature variation of Test 2

Adsorption test carried out using a mass ratio of 1:1 (Test 2) and the results of temperature variations at the adsorption and evaporation vessels of the rig shown in

Figure 6.8. At this point, the adsorption pipe was insulated to prevent temperature loss in the systems. The temperature in the adsorption pipe fluctuated from an initial temperature of 24.6°C to the highest temperature of 54.40°C. The temperature was noticed to be drop sharply from 54.60°C to 45°C in 8 minutes and gradually drop to its initial temperature (22.00°C) in the 75th minute of the whole adsorption process. Hence, from this result, we can see that the adsorption vessel required multiple vacuumed to increase to the highest temperature. For an efficient adsorption process, this should be avoided due the increase of input power from the vacuum pump that will affect adversely to the COP of the systems.

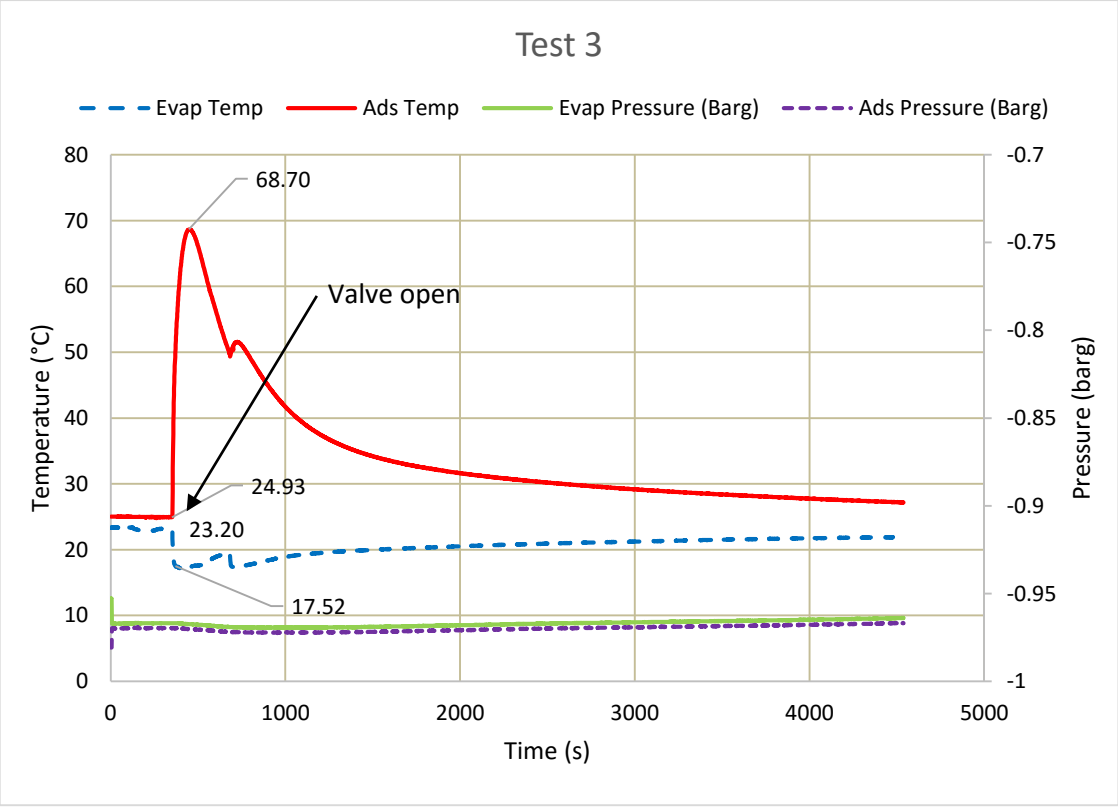


Figure 6.9: Temperature variation of Test 3

Another test conducted on using a mass ratio of 1:2 is being repeated as the result is shown in Figure 6.9. From this results, it can be seen that the adsorption temperature rises sharply when the valve open. The temperature rises to 68.70°C from its initial

temperature of 24.90°C and temperature difference at 43.80°C (ΔT) achieved. The adsorption temperature returns to its initial temperature at the end of 4500s of the adsorption test. The temperature lost to the ambient is gradually dropped when compared to the same weight ratio in Test 1. Hence, with the help of insulation on both vessel, the temperature loss can be reduced. The evaporator pipe showed temperature drop at 17.50 °C from its initial temperature of 23.0°C. The higher temperature in the evaporator pipe indicates that the water inside evaporator section was not fully evaporated or successfully being transported during the adsorption process.

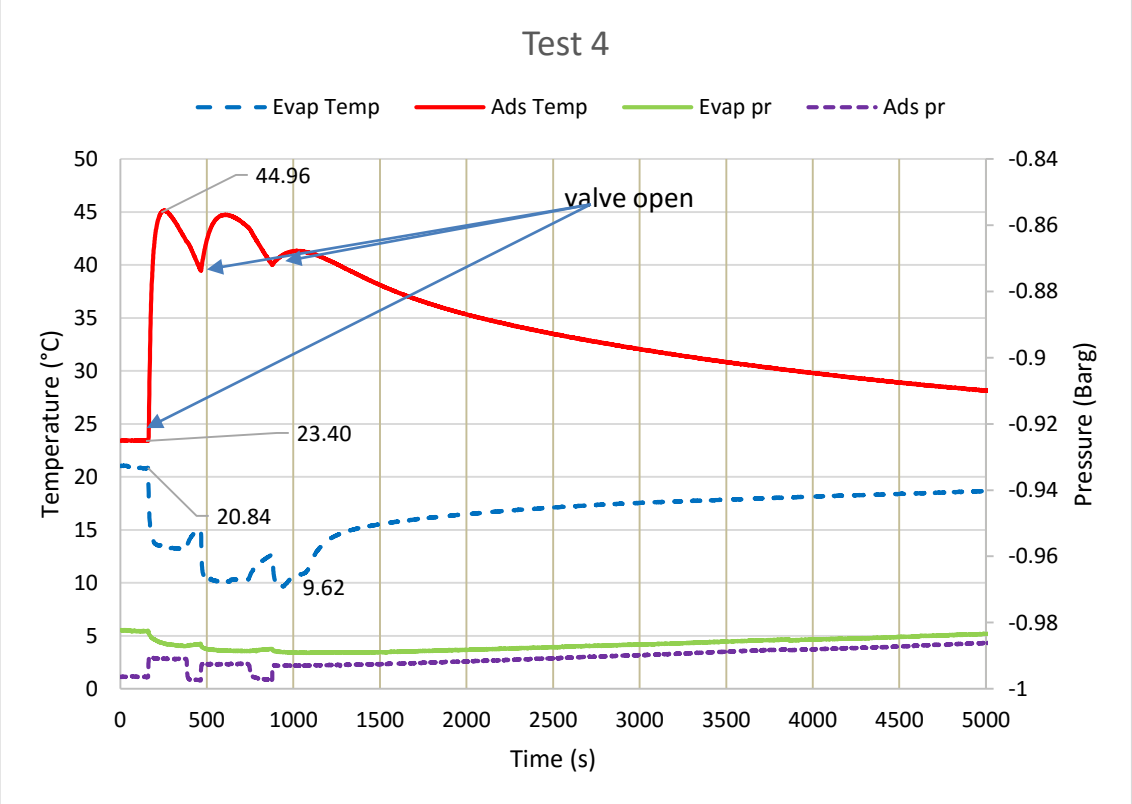


Figure 6.10: Temperature variation of Test 4

Additionally, Test 4 conducted on repeating the weight ratio of 1:1 and the results are shown in Figure 6.10. This result shows that the temperature rise in adsorption pipe is lower than Test 2 that is 44.95 °C and 54.42 respectively. However, the temperature drop in the evaporator pipe is higher than Test 2 that is 9.62°C and 12.76°C respectively.

Hence, from this result, we could say that the mass ratio of 1:1 has shown a lower temperature rise from the adsorption process.

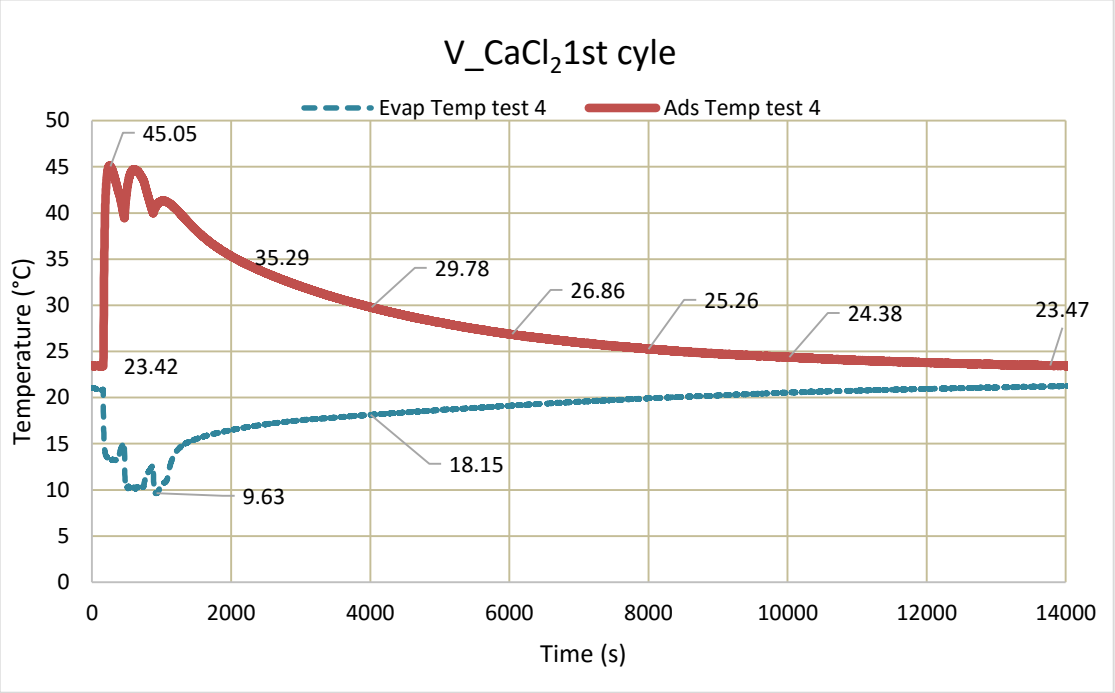


Figure 6.11: Temperature variation of the 1st cycle on Test 4

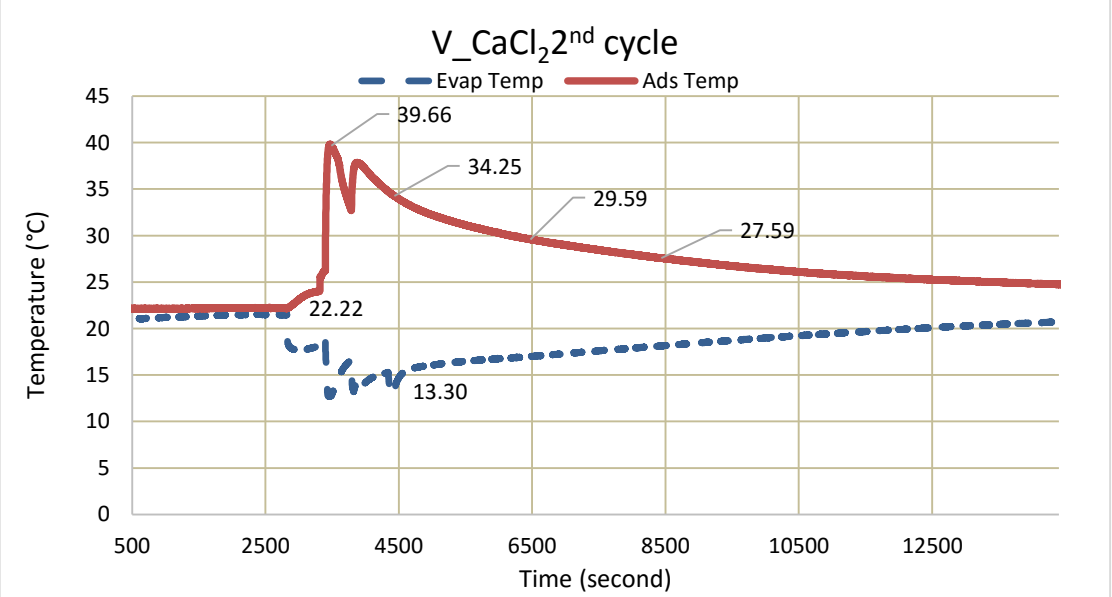


Figure 6.12: Temperature variation of the 2nd cycle for Test 4

Additionally, to investigate the performance of THSS cyclic condition Test 4 repeated using the same VCC in the 1st cycle. The results of this effect shown in Figure 6.11 & Figure 6.12. This result indicates that, in the second cycle of adsorption, the temperature rise is 39.6°C from its initial temperature of 22.2°C (Figure 6.12). Thus, this is evidence that this adsorbent material could be use in the multiple cycles with only 0.18% temperature deteriorate in the systems. Furthermore, in the 2nd cycle of the adsorption process, the temperature rise would be a sufficient to utilise as room heating systems in a building.

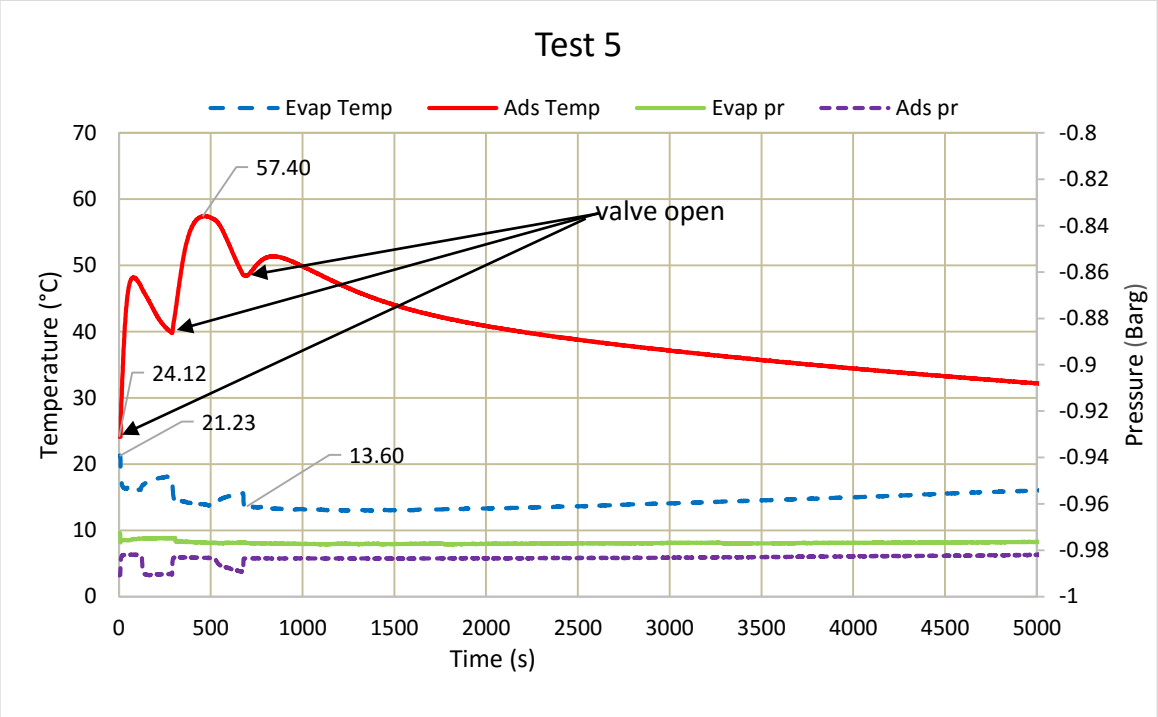


Figure 6.13: Temperature variations of Test 5

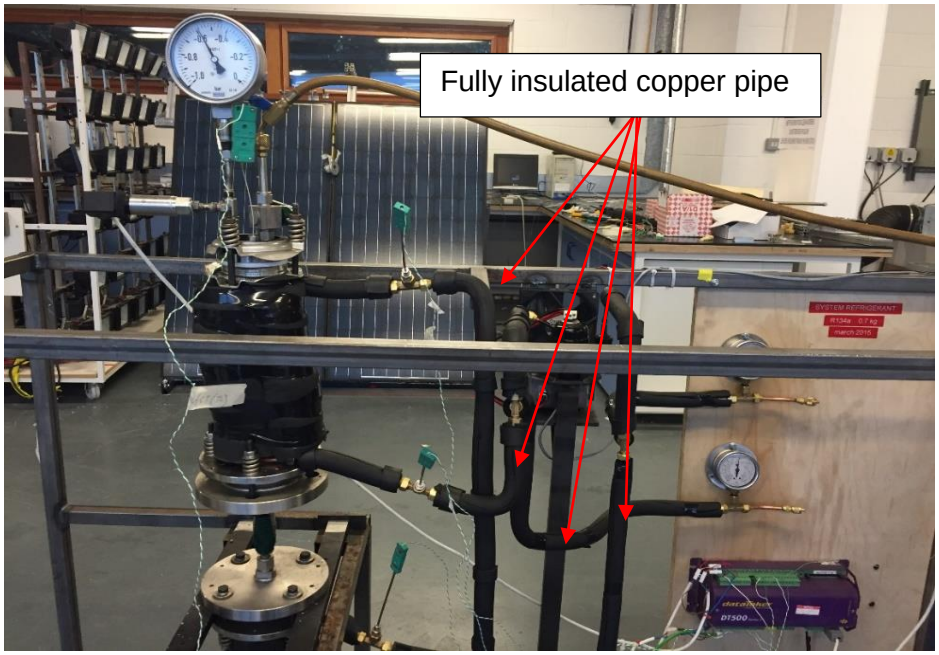


Figure 6.14: The THSS-R134a (fully insulated)

Another set of adsorption and desorption test carried out in Test 5 using the weight ratio of 1:2 and the result is shown in Figure 6.13. The objective of repeating this test is to investigate the performance of desorption test with fully insulated R134a circuit (see Figure 6.14). As can be seen from the results, the temperature rise in adsorption pipe is lower than that of Test 1, which is 57.40°C and 71.08°C respectively. Some limitation in this system is that after a few repeated test, pressure loss ensued due to frequent dismantling. This will affect the reaction and hence the temperature rise in adsorption pipe.

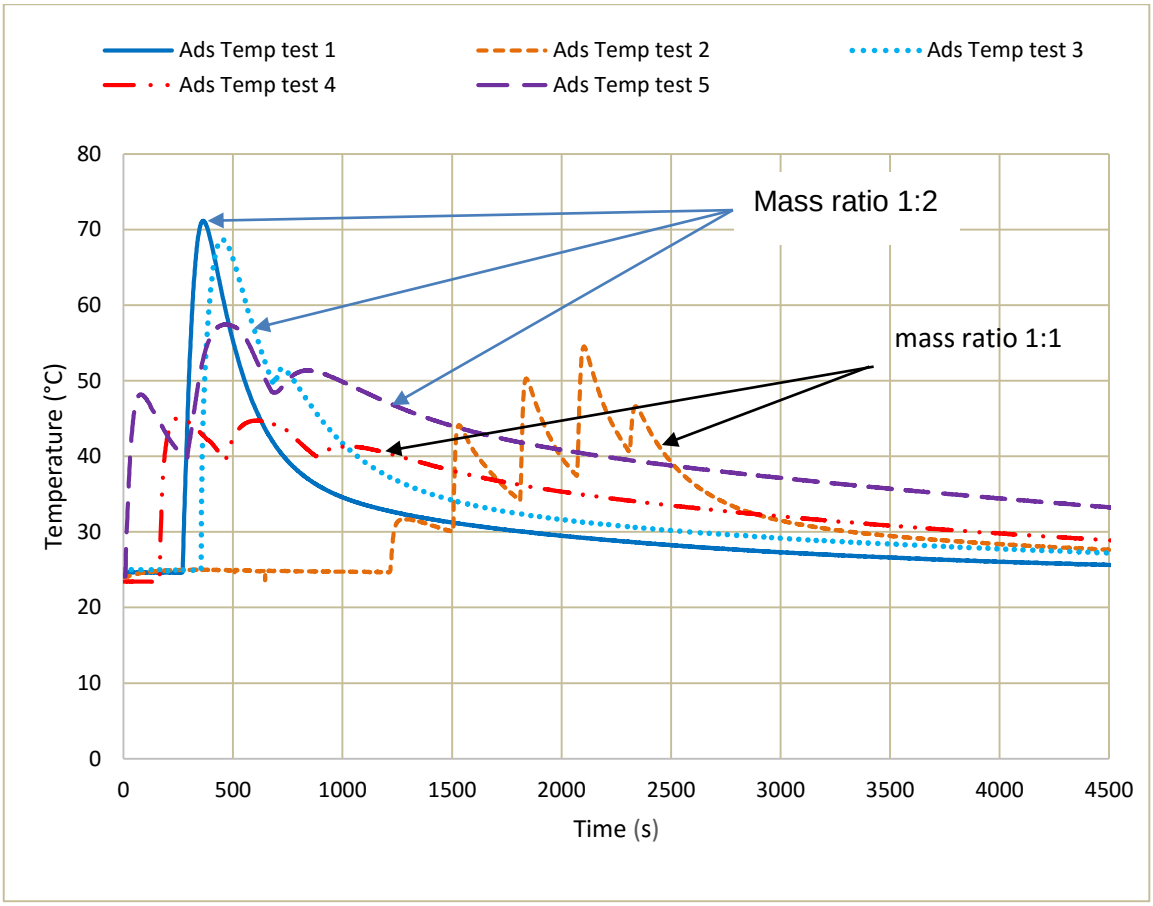


Figure 6.15: Comparison of Adsorption temperature for all test

Figure 6.15 shows a comparison of adsorption pipe temperature for all test. These results indicate that, the weight ratio of 1:2 (Test 1, Test 3 & Test 5) has higher temperature lift compared to weight ratio of 1:1 (Test 2 & Test 4). Test 1& Test 3 can achieve a higher temperature, without the help of vacuumed pump. However, Test 2, Test 4 and Test 5, showing the fluctuation in the adsorption temperature due to repetition in of vacuuming the systems during the test.

Table 6.4 showing the summary of all test and their performance during the adsorption process. The 1st test conducted showing a positive increased in the temperature lift (71.10°C), however, less efficient of maintained the temperature due to temperature loss in the systems (average 15°C @ 3mins). With the result of this, the temperature

maintained in 98 seconds of the adsorption Test. From Test 2 to Test 5, the adsorption and evaporator pipe were insulated. Hence, from this point onwards the temperature loss is in the range of 3 to 9°C in an average of 5 minutes of adsorption test. Hence, proper insulation and vacuumed condition are vitally important to achieve high adsorption temperature in these investigations.

Table 6.4: Summary of Temperature Variations of Vermiculite-$CaCl_2$

Test	T_{in} Ads (°C)	T_{in} Eva (°C)	T_F Ads (°C)	T_F Eva (°C)	Ambient (°C)	Temperature Drop	Δ T Ads (°C) @ duration	Remarks
Test 1	24.62	21.90	71.10	15.10	23±2	Average 15°C @ 3mins	98 s	Not insulated
Test 2	24.65	21.80	54.60	13.35	23±2	Average 9°C @ 8mins	893 s	Insulated
Test 3	25.01	23.30	68.70	17.35	23±2	Average 5°C @ 8mins	115 s	Insulated
Test 4 (cycle 1)	23.41	20.80	45.00	9.74	23±2	3°C @ 5mins	100 s	Insulated
Test 4 (cycle 2)	22.2	22.2	39.6	13.3	23±2	3°C @ 5mins	145 s	Insulated
Test 5	24.10	20.60	57.20	13.30	23±2	2.5@ 5mins	494 s	Fully insulated heat pump circuits

Table 6.5 shows the mass change during the adsorption and desorption process. The results of Test 1 indicate that the amount of VCC increased from 49g to 56g, which gives 7g of water being adsorbed during the adsorption process. Hence, this shows that less water vapour needed to increase the temperature during the adsorption process. Despite vapour transport is not entirely successful during the adsorption process, the temperature rise at 71.10°C was relatively sufficient for hot water and room heating applications. The highest water uptake is in Test 5 (0.37g/g), and the lowest water uptake is in Test 2 (0.06g/g). The results are also showing that the mass ratio of 1:2 gives higher water absorption (84% more) compared to the mass ratio of 1:1.

Table 6.5: Result of mass change for the adsorbent and water

Test Date	Materials			M (Before Ads/des)	M (After Ads/des)	Δ M (Ads/des)	water uptake (g_{H20}/g_{dryads})
21/04/2015	Adsorption	Test 1	V_$CaCl_2$	50	56	6	0.14
			Water (H_2O)	100	93	6	
22/04/2015	Desorption		V_$CaCl_2$	56	57	1	
			Water (H_2O)	79	79	0	
06/05/2015	Adsorption	Test 2	V_$CaCl_2$	60	67	3	0.06
			Water (H_2O)	60	65	3	
07/05/2015	Desorption		V_$CaCl_2$	67	64	3	
			Water (H_2O)	65	60	3	
12/05/2015	Adsorption	Test 3	V_$CaCl_2$	40	50	10	0.18
			Water (H_2O)	80	70	10	
13/05/2015	Desorption		V_$CaCl_2$	50	47	3	
			Water (H_2O)	88	91	3	
20/10/2015	Adsorption	Test 4	V_$CaCl_2$	60	66	6	0.07
			Water (H_2O)	60	54	6	
21/10/2015	Desorption		V_$CaCl_2$	62	60	2	
			Water (H_2O)	54	56	2	
10/11/2015	Adsorption	Test 5	V_$CaCl_2$	50	67	17	0.37
			Water (H_2O)	100	83	17	
11/11/2015	Desorption		V_$CaCl_2$	67	75	8	
			Water (H_2O)	82	90	8	

6.7.2 Temperature variation during desorption Test

In this investigation the mass ratio effect on the desorption process also being investigated. Figure 6.16 to Figure 6.20 exhibit the temperature variation during desorption via a heat pump circuit (R134a).

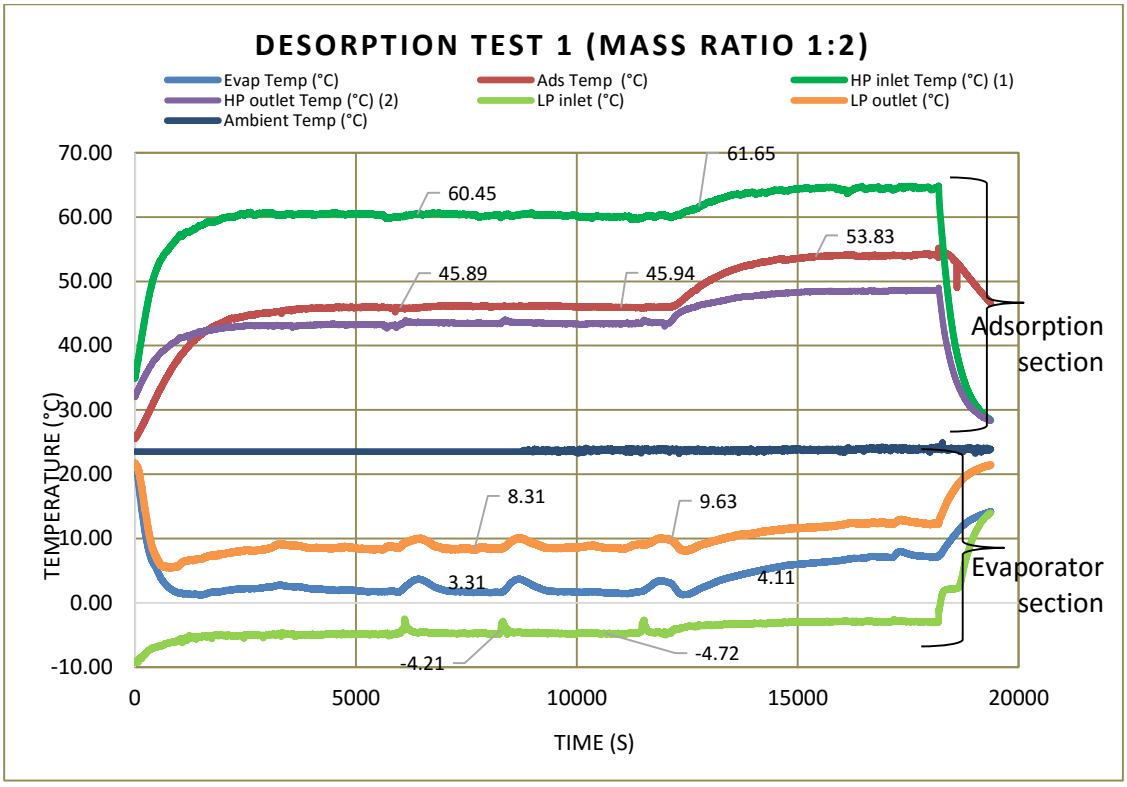


Figure 6.16: Temperature variations of adsorption pipe, evaporator pipe, inlet & outlet of the high-pressure loop, inlet & outlet of the low-pressure loop of the heat pump for desorption Test1.

It can be seen in Figure 6.16, the discharge temperature (HP outlet – dark green line) from the compressor is taking nearly 30 minutes to reach the desired desorption temperature of 60°C for Test 1. The discharge temperature then maintained at 60°C in 3.3 hours of desorption period. There were slightly increased for the HP inlet temperature from 3.3 hours onwards due to sudden changes in the compressor flow rate. Ads Temp (red line) showing the temperature in the adsorption pipe. This temperature indicates the heat transferred from the R134a circuits to the adsorption pipe. Additionally, temperature difference (ΔT) at 14.56°C observed from the copper pipe to the VCC inside the adsorbent pipe. This is because of low thermal conductivity of the glass vessel (λ: 1.2 W/m.K). Other than that, at this point, both vessels were not insulated and the temperature likely to lose to the ambient temperature. The lower part of the graph showing the heat transfer from the evaporator circuits of R134a the evaporator pipe

(water cartridge). It can be seen that the LP inlet (light green) (temperature of low-pressure liquid discharge from the evaporator of R134a) and the temperature of evaporator pipe had an average temperature difference (ΔT) of 7.40 to 8.80 °C. Hence, the temperature loss in the evaporator section is 40% lower than the adsorption section.

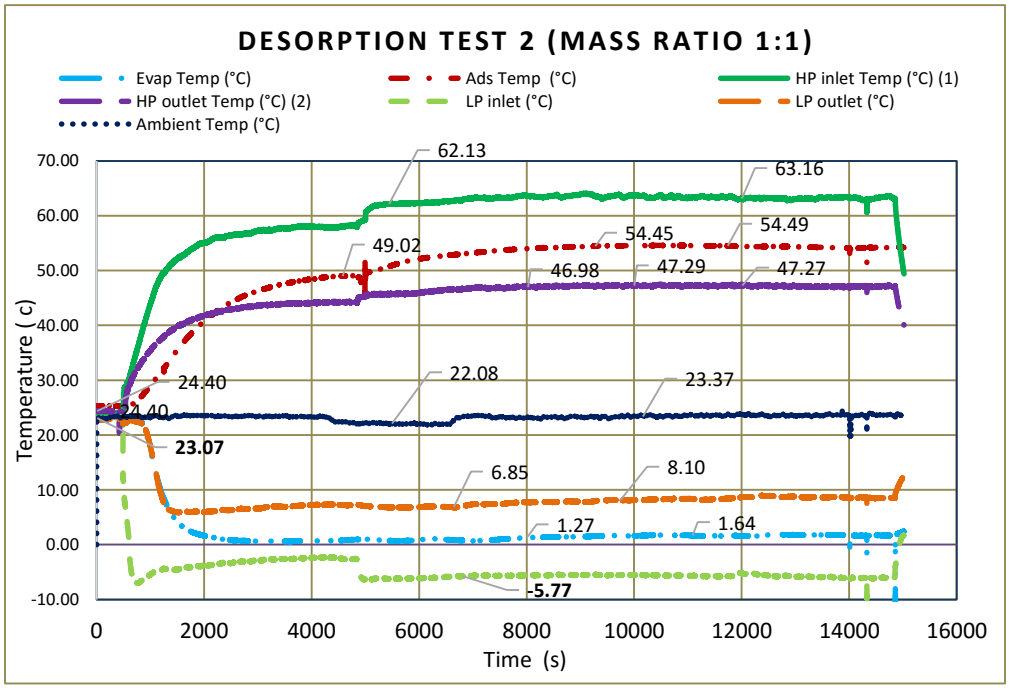


Figure 6.17: Temperature variations of adsorption pipe, evaporator pipe, inlet & outlet of the high-pressure loop, inlet & outlet of the low-pressure loop of the heat pump (Test 2)

Figure 6.17 exhibits, the result from desorption Test 2 of using the mass ratio of 1:1. The HP Inlet Temp, (discharge temperature of R134a from the compressor) marginally increased from 1000s of the test and reached 58°C. Then, from 5000s second onwards the temperature rose from 58 to 63°C and remain plateau throughout the desorption process. The sudden increase in the temperature at 5000s is due to a slight increase in compressor flow rate. The temperature difference (ΔT) from the HP inlet (light green line) to the adsorbent material at 8.8°C on average. Some improvement showing a lower temperature loss in the systems due to the pipe was insulated during this test. Other

than that, the temperature different at the evaporator section at 7.0°C on average. Hence, both sections have shown improvement on maintaining the temperature through the desorption process.

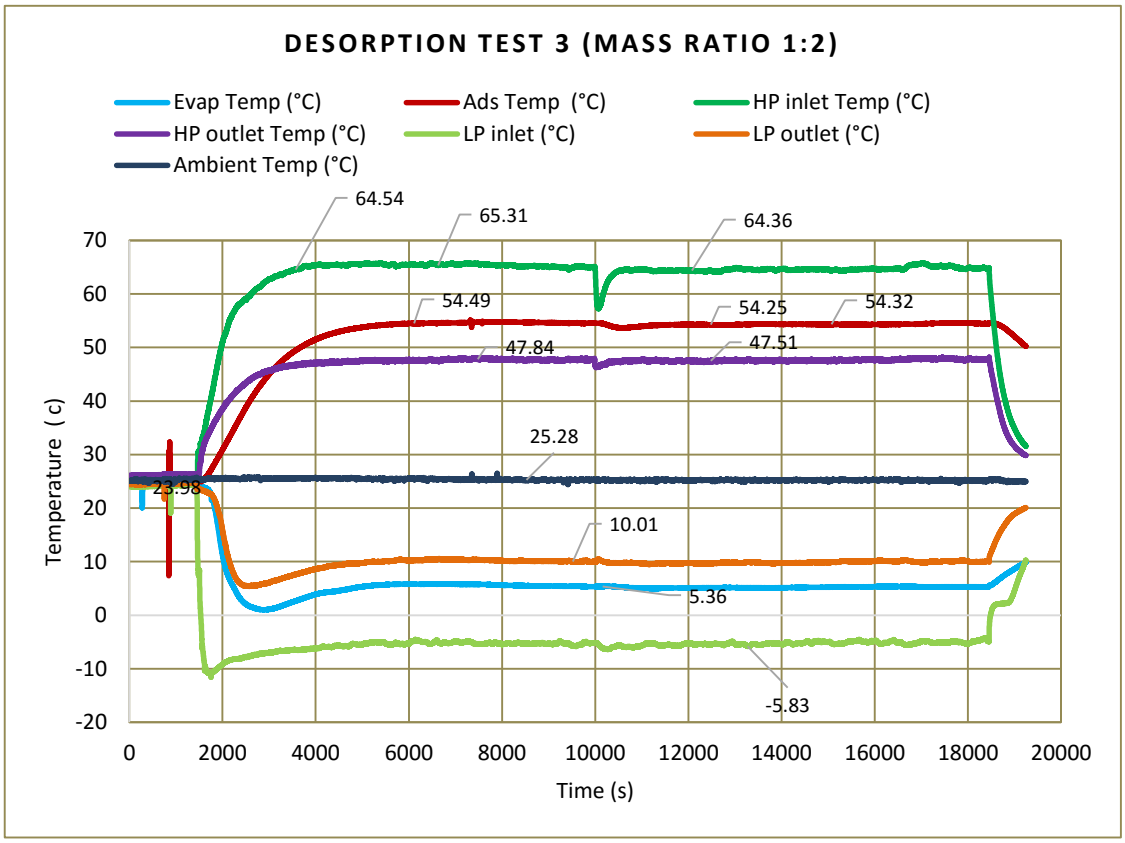


Figure 6.18: Temperature variations of Adsorption pipe, Evaporator pipe, inlet & outlet of the high-pressure loop, inlet & outlet of the low-pressure loop of the heat pump (Test 3).

The result of temperature variation from desorption process of Test 3 showed in Figure 6.18. Similar temperature rises from the start of the test when compared to Test 1 and Test 2, however, at this point, the temperature of HP inlet reached a maximum at 65.30°C and plateau throughout the desorption test. This was due to the constant flow rate of the compressor, and sudden stop of the compressor does not occur throughout the process.

The temperature difference from the HP inlet to the VCC at 10.0°C on average and from the LP inlet to the evaporator pipe at 10.70°C on average.

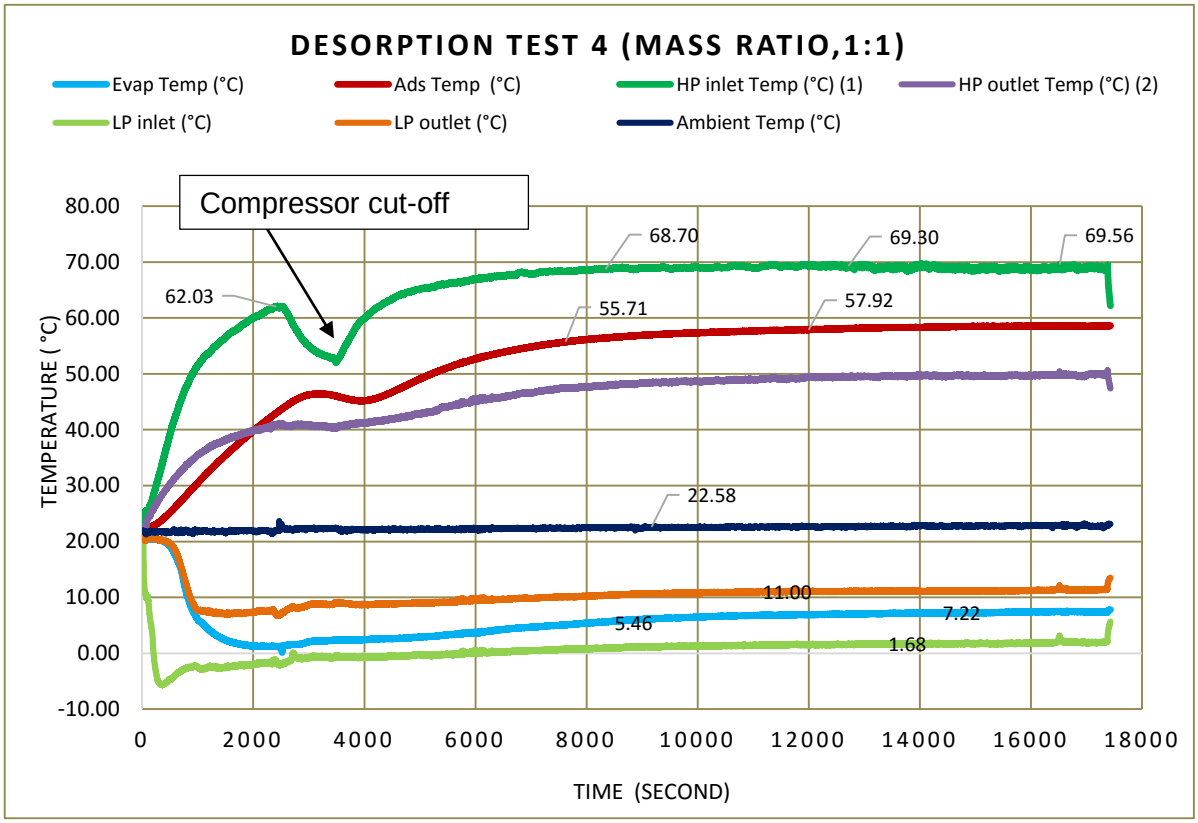


Figure 6.19: Temperature variations of Adsorption pipe, Evaporator pipe, inlet & outlet of the high-pressure loop, inlet & outlet of the low-pressure loop of the heat pump (Test 4).

Figure 6.19 illustrates the temperature variation during desorption of Test 4. From this results, it can be seen that the HP inlet (dark green line) marginally increased from the start of desorption test and reached to 62.0°C at the 2500s. At this point, the compressor is running at full speed (6000rpm) and the compressor was automatically cut-off from the 2500s to 4000s due to a technical problem. With the result of this, sudden temperature drop occurred during this period. The compressor was turn on again, and HP inlet temperature increased up to 69.30°C throughout the process. This was 6%

higher than the manufacturer specification. The temperature different from HP inlet to VCC (ads Temp – dark red line) was 11.40°C on average, whereas lower temperature difference at the evaporator section which was at 3.90°C on average.

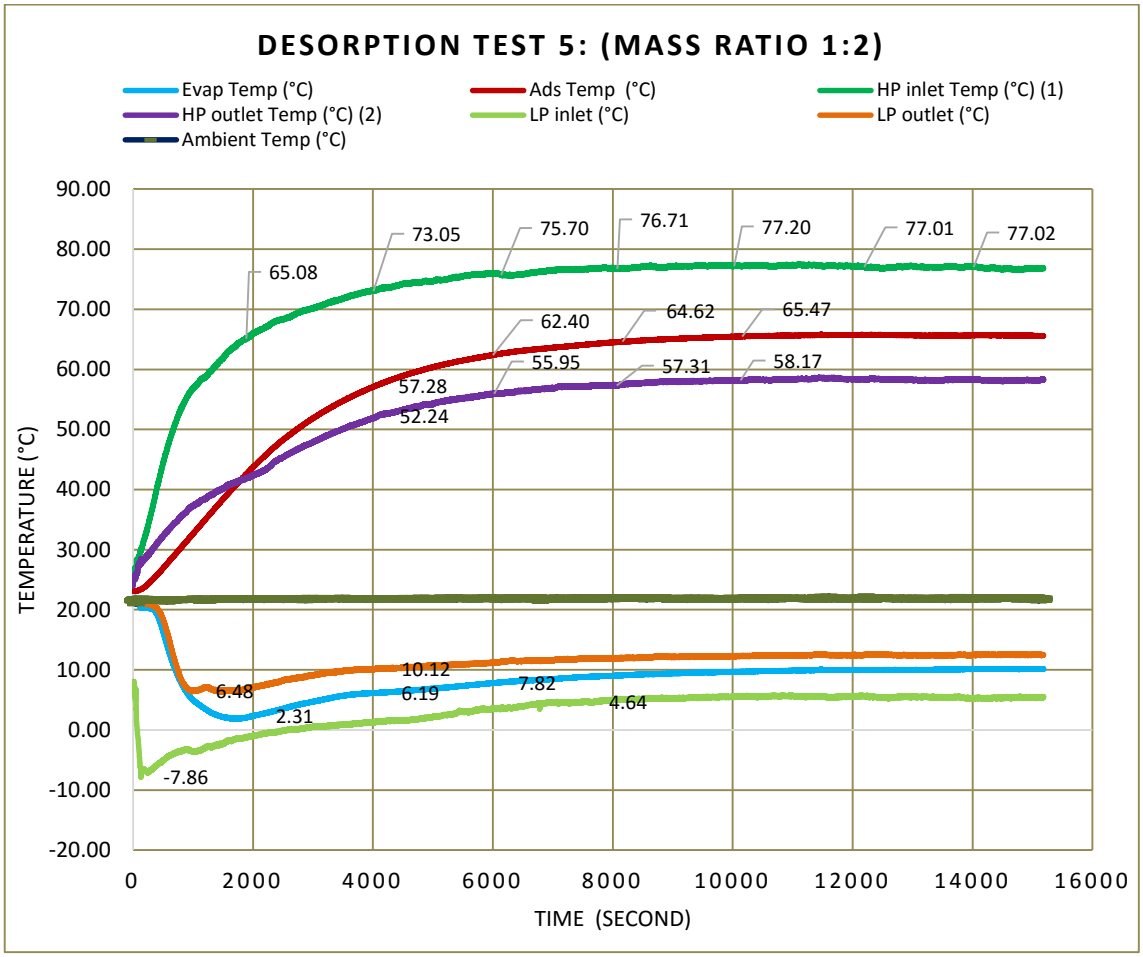


Figure 6.20: Temperature variations of Adsorption pipe, Evaporator pipe, inlet & outlet of the high-pressure loop, inlet & outlet of the low-pressure loop of the heat pump (Test 5 fully insulate the heat pump circuit).

Additionally, Test 5 was conducted to investigate the performance of the heat pump with a fully insulated heat pump circuit. Figure 6.20 showed the result of temperature variations for Test 5. It can be seen that, using a maximum compressor speed of 6000rpm and fully insulated copper pipe, a high at 77.20°C achieved at the HP inlet

temperature. The temperature at VCC reached a maximum at 65.50°C from 6000s throughout the remaining of desorption test. This is equal to the material synthesising experiments in Chapter 3 of using an electrical heat-clamp as the heat source for desorption. Consequently, the temperature of the suction line (LP inlet) was at 7.8°C is sufficient enough to create a temperature difference inside the evaporator pipe and to condensed the water vapour during desorption. Furthermore, the same amount of water condensed back to the evaporator during in 4 hours of desorption process (see Table 6.5).

6.7.3 Compressor performance

Figure 6.21 exhibits the effect of a change in condenser temperature to COP and heat gain in the condenser coils (Q_h). With a constant refrigerant flow rate, it can be seen that the COP decreased by the change of condenser outlet temperature. Therefore, optimisation of condenser temperature outlet needs to be considered to achieve the performance of R134a circuit. Figure 6.22 shows that the COP decrease with the increase in the condenser temperature. However, these changes increase the compressor work. This result indicates that the temperature of condenser temperature would affect adversely with the COP.

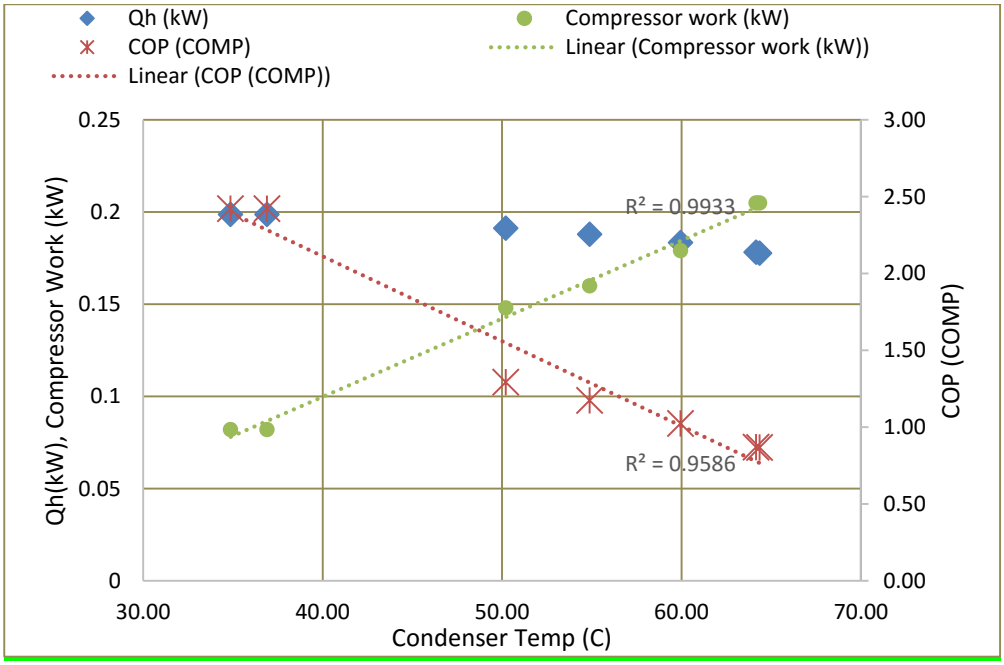


Figure 6.21: The effect of COP with the increase in condenser temperature.

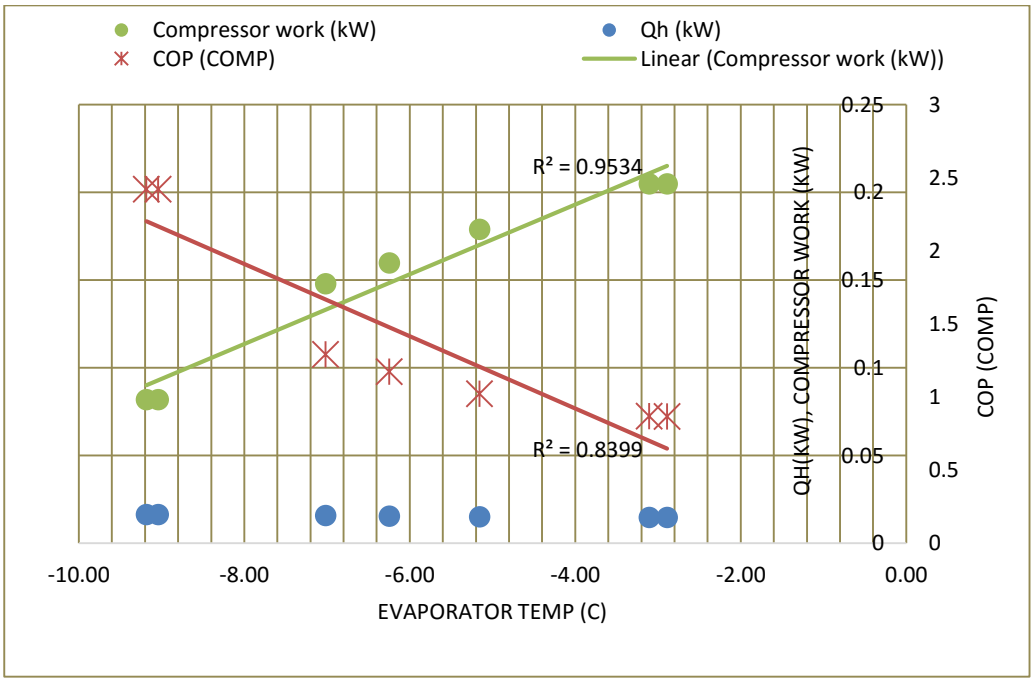


Figure 6.22: The effect COP (comp), Heat gain, on the condenser pipe (Qh) versus the evaporator temperature.

Table 6.6 indicates the temperature variation during the desorption process. It can be seen within 35 minutes of the desorption test; the compressor could attain temperature rise of nearly 60°C. The temperature from the compressor outlet to the adsorption pipe considered an appropriate temperature for the desorption process. The effect of COP of R134a circuit would also be a temperature dependent. Additionally, temperature variation in the condenser coil effect the COP and the heat gain (Q_H). Furthermore, there was relatively large variant between the measured compressor works (W_c) with manufacturer data. The COP calculated from the experimental data was in the range of 1.38 to 2.88, while the COP calculated using the specification ranges from 0.87 to 2.42. This result indicates that the experimental compressor work and manufacture data well agrees.

Table 6.6: Temperature variations and compressor performance during desorption process.

Time (minutes)	Eva. Temp (°C)	Ads. Pipe Temp (°C)	HP inlet (°C) (T3)	HP outlet (°C) (T2)	LP inlet (°C)	LP outlet (°C)	Ambient (°C)	Compressor (kW) (exp)	Refrigerant mass flowrate ($\dot{m}$) (m^3/s)	Compressor work (kW) (supplier data)	Heat gain Qh (kW)	COP(HP) (Supplier Wc)	COP Exp Wc	% copHP variant
1	21.77	25.49	34.88	31.99	-9.18	21.61	23.50	0.06902	0.000664	0.082	0.198	2.42	2.88	0.16
10	20.14	26.06	36.90	32.79	-9.04	21.19	23.50	0.0833	0.000664	0.082	0.19	2.42	2.38	0.02
15	6.25	30.92	50.21	37.44	-7.02	8.36	23.50	0.0833	0.000664	0.148	0.191	1.29	2.30	0.44
30	2.49	35.45	54.88	39.79	-6.25	5.60	23.50	0.0833	0.000664	0.16	0.187	1.17	2.25	0.48
35	1.93	43.93	59.95	42.82	-5.16	7.69	23.50	0.0833	0.000664	0.179	0.183	1.02	2.20	0.53
240	5.58	53.44	64.17	48.12	-3.10	11.38	23.78	0.0999	0.000664	0.205	0.178	0.87	1.78	0.51
360	6.55	54.03	64.36	48.47	-2.89	12.07	23.76	0.0999	0.000664	0.205	0.177	0.87	1.78	0.51

6.8 Overall performance of all test

Table 6.7, showing the overall performance of the THSS-R134a of the different mass ratio, which is 1:1 and 1:2 respectively. Technically, heating storage with a $5.11X10^{-4}m^3$ volume of this THSS calculated ranges from 0.095~0.237kWh/m^3 with a corresponding COP of 0.53~1.34 respectively. Therefore, the overall performance of the system is highly dependent on the mass of the working pair and the temperature lift during the adsorption process. Thus, these experiments suggest that actual scale systems should use a most appropriate mass for working pair to enhance the heat store and COP the whole systems. Additionally, the heat-source pipe should be installed in the reaction vessel (adsorption pipe) to enhance the heat transfer and improve the dissociation of water vapour during the desorption process (Wajid et al., 2016).

Table 6.7: Performance comparison of all test

	TEST 1	TEST2	TEST 3	TEST 4	TEST 5
Mass ratio (mass of dry adsorbent: mass of water)	1:2	1:1	1:2	1:1	1:2
Maximum Adsorption Temperature (°C)	71.10	54.55	68.10	45.10	57.20
$E_{d,m}$**(kWh/kg)**	0.237	0.127	0.186	0.095	0.1405
$E_{d,v}$ **(kWh/m^3)**	474	254	372	190	281
COP THSS	1.34	0.71	1.05	0.53	0.8

6.9 Validation of the simulation of the adsorbent temperature vs experiment results for VCC

As can be seen in Figure 6.23, the numerical model fitted well with the experimental data. Therefore, the numerical model had shown good agreement with experimental data. Additionally, these results indicate that the adsorption temperature increased during 140 seconds from starting the process and the temperature drops marginally after 250 seconds. Hence, this result indicates that proper insulation is crucial during the adsorption process to retain the maximum temperature for heating purposes in the building.

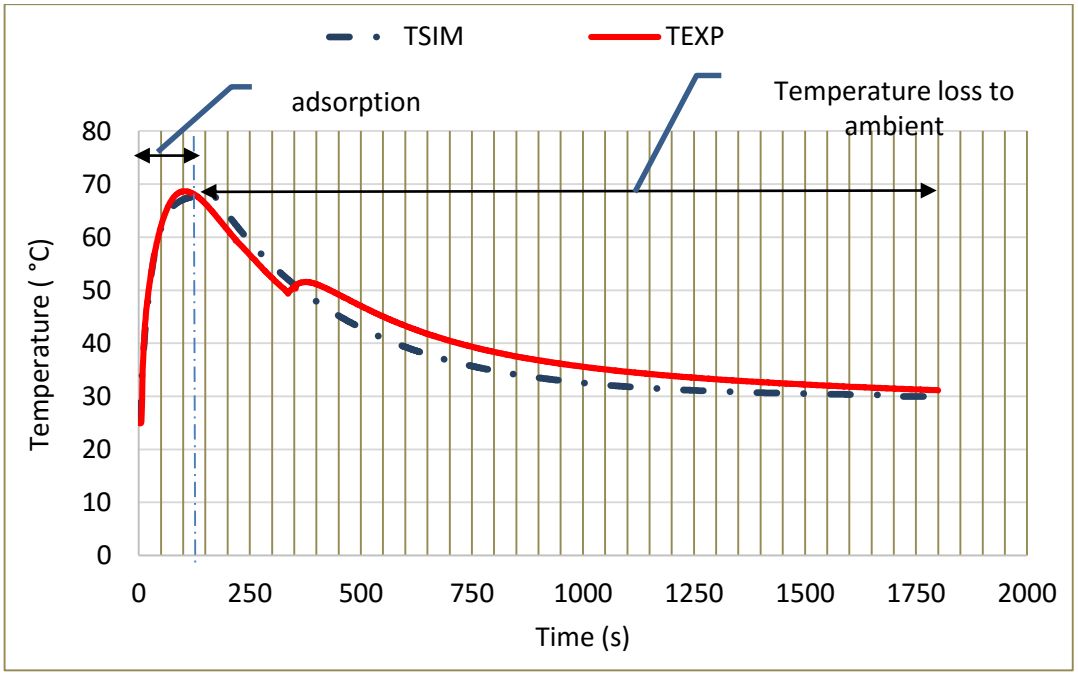


Figure 6.23: Theoretical versus experimental results of adsorption pipe temperature (Tp) during the adsorption cycle of vermiculite+$CaCl_2$

6.10 Conclusions of the Chapter

From this experiment some key findings can be made such as;

- The overall performance of this storage system is highly dependent on the temperature lift in the adsorption process. Hence, to achieve this, it does not only depend on the mass of the water. However, the water vapour transport is also crucially needed to be optimised. Good water vapour transport will achieve if the systems are fully vacuumed throughout the cycle. Therefore, a leakage test is crucially needed to be entail before the experiments conducted.
- Another important key finding in this experiments is that, the distance of transporting water vapour need to be optimised to make sure that, the distance between the adsorption pipe/reactor and the evaporator is close enough for the reaction took place. Long distance for each pipe should avoided, as the water vapour hypothetically transported via pressure different between adsorbent material and water, and no force convection available in the systems.
- The amount of water left in the evaporator pipe after the adsorption cycle shows that the water does not evaporate well, and the temperature drop is much lower and need to avoid. Therefore, the amount of water used to need to be carefully optimised to improve the systems. Furthermore, lower temperature drop in the evaporator pipe shall be useful to utilise as the cooling in the building during summer months.
- Limitation occurs in these experiments with a maximum weight of the adsorbent material of 60g. Therefore, it was difficult to make further analysis on the weight ratio of the systems. However, this system shall be a good prototype example for a real-

scale prototype, which would be more realistic for the real scale of heat storage systems.

- To maintain a constant adsorption temperature proper insulation is crucially considered during the adsorption and desorption cycle. Therefore, proper insulation for the systems design needed to be resolved before the experiments taken place.
- The overall performance of using a miniature compressor proved that the small scale THSS has COP range from 0.53~1.34 which is almost half as a commercial heat pump available in the market. Furthermore, with the maximum condensing temperature of 77°C & evaporating temperature of 4°C, this miniature heat pump circuit can be utilised for many applications such as in an aircraft computer, portable cooling or heating systems, miniature refrigeration or mini chilled water systems.

7. PERFORMANCE INVESTIGATION OF SOLAR HEAT STORAGE COLLECTOR (SHSC)-THEORETICAL, BUILD –UP AND EXPERIMENTAL TESTING.

7.1 Introduction

Renewable energy technologies such as wind turbines, biomass boilers, and solar PV/Thermal systems were widely being investigates to overcome the problems relates to the scarcity of fossil fuel, global warming, and climate change. While the energy resources these technologies are theoretically inexhaustible and abundant, there is often a large barrier to their successful implementation, namely a mismatch between the production of and demand for the energy they generate (Arteconi et al., 2012). Consequently, solar energy currently seen as one of the most promising alternatives to more conventional energy resources but require some energy management (i.e. gas and electricity). The use of solar thermal energy has been broadly researched, accepted publicly and adopted for heating, ventilation and air-conditioning in both domestic and commercial buildings (Aydin et al., 2015b). Moreover, thermochemical energy storage was widely being investigated towards the alleviation of the use of electricity or gas for heating and cooling in buildings. However, the system could not commercially implement due to complicated in the system design. To enhance the systems design and to be more environmentally friendly, the abundant solar energy can be used for the regeneration of the sorption systems.

The integration of using solar thermal with energy storage systems has been investigating by many researchers on using PCM energy storage (Enibe, 2002; Kürklü et al., 2002; Mettawee & Assassa, 2006). However, most of these studies were using a concept from flat plate solar collector integrated with PCM as the heat source for the charging cycle.

These authors applying a concept of flat plate collectors in the design due to the reason of PCM material needs to be enclosed and conceal during the phase change. However, the limitation occurs in their investigation that the flat plate is relatively low efficient when compared to an evacuated tube. Furthermore, some of the inorganic PCM could be toxic and have complex melting behaviour. However, composite materials are thought to become more stable, high energy storage density and require low regeneration temperature (Daou et al., 2008; Fujioka et al., 2008; Wu et al., 2009). This material will overcome the problem associated with complexity in PCM as an energy storage system. However, most of this literature were focussing on experimentally studied on a close sorption system. By far the close sorption systems has their limitations such as low COP & complicated systems configuration, which make the systems difficult to compete with the conventional heating systems.

Some of the researchers have studied experimentally and theoretically the integration of the solar collector as a reactor/generator using a solid adsorbent material. In Nigeria, Anyanwu & Ezekwe (2003), designed and constructed a solid adsorption solar refrigeration systems using activated carbon/methanol as working pairs. These researchers using a flat plate as the reactor/generator for the system. From their experiments, they had found that the refrigerator had yielded the evaporation temperature of 1.0~8.5°C with the useful cooling produce of 266.8kJ/m^2 of collector area. However, due to pressure in the systems is not constant and desorption was partially completed and hence affected the whole system performance. In this experiment, the evacuated tube solar collector has been chosen to integrate with Thermochemical energy storage (Vermiculite+$CaCl_2$). Hence, this exercise is to analyse through modelling and experimental the integration solar thermal energy of the adsorption heat storage systems.

7.2 The Mathematical modelling of SHSC

In this study, a thermodynamics analysis of an open solar heat storage collector system is presented. The numerical analysis was carried out assuming UK climate conditions. The composite adsorbent material chosen is vermiculite + $CaCl_2$ based on the extensive material synthesising done by (Casey et al., 2014; Casey et al., 2015; Aydin et al., 2015b). This material has promising properties when compared to other composite materials such as Vermiculite + $MgSO_4$, Vermiculite+ $LiNO_3$, and Vermiculite + LiBr. The properties such as high heat storage capacity, reaction advancement, high heat and mass transfer, good cyclic ability, low toxicity, low regeneration temperature and low cost which will think to be the most promising candidates to be adopted for adsorption heat storage systems in a long-term run.

The EES software has been used to perform the analysis. The different between this model, when compared to Chapter 5 is that this numerical modelling using open sorption storage system concept. Therefore, the reaction rate of adsorption process will be considered as reaction advancement instead of adsorption isotherm as applied in the close sorption systems. The formula of reaction explained in the discharging and charging model.

All assumptions used in the modelling are listed in Table 7.1. To analyse the mass and energy balance of the solar collectors, and fan, the manufacturer design data chosen as constants. To analyse the reactions during the charging and discharging periods, the properties for Vermiculite+$CaCl_2$ were taken from experimental studies and literature sources (Jänchen et al., 2005; Balasubramanian et al., 2010; Casey et al., 2014; Barreneche et al., 2015; Aydin et al., 2015a). The amount of absorbent for the reactions chosen as 10 kg and the total weight of the SHSC selected was set at 5 kg, which made up of the glass material.

Table 7.1: Assumptions use in modelling

Solar Adsorption collectors & materials		**General Assumptions**	
I	0.5kW/m^2 (Aydin et al., 2015a)	T_a	25°C
F_r	0.93 (Aydin et al., 2015a)	$C_{p,w}$	4.18 kJ/kgK
τα	0.75 (Aydin et al., 2015a)	$C_{p,a}$	1.008 kJ/kgK
Ul	$4x10^{-3}$ kW/m^2C (Aydin et al., 2015a)	$M_{,w}$	0.018 kg/mol
M_{col}	5kg	**Fan**	
Cp_{col}	0.84 kJ/kgK	W_f	0.05kW
Material (V-$CaCl_2$)		W_{pump}	0.05kW
ΔH_r	47kJ/mol (Casey et al., 2014)		
ΔH_w	435.1kJ/kg (Casey et al., 2014)		
M_s	10 kg		
$C_{p,s}$	3.06kJ/kgK (Casey et al., 2014)		
$\boldsymbol{\rho}$ $CaCl_2$	2100kg/m^3 (Balasubramanian et al., 2010)		
$\boldsymbol{\rho}$ vermiculite	80kg/m^3		
$\boldsymbol{\rho}$ avg	175kg/m^3		

7.3 Option 1: SHSC heat transfer through fan (air to air heat exchange)

The principal objective in this investigation is by integrating the solar collector as the thermal storage for heating the building. The discharging cycle of a solar heat storage collector (SHSC) depicts in Figure 7.2 showing that the cycle start with the humid air flows with the help of small fan through the solar adsorption collectors. As the humid air enter the adsorption collector, the reaction occurs, and this will create hot air exits from the collectors. The hot air then will flow to the fan coil unit to heat the building. The air then enters the dehumidifier where cold water is sprayed on for evaporates the vapour. After this, a fan blows the air to the solar adsorption collector unit to complete the cycle.

While in charging cycle, as depicted in Figure 7.1, the dry air will enter the dehumidifier and the water sprayed will condensate the vapour. The dry air will exit from the dehumidifier and enters the solar adsorption collectors. The heat from the solar collectors will disassociate the water vapour from the adsorption materials. The charged (fully dried) adsorbent is then kept dry, separate from the humidification unit (storage phase) for use in the next system discharge cycle. A well-insulated typically sized 100m^2 house under the UK climate conditions was considered in the present numerical study.

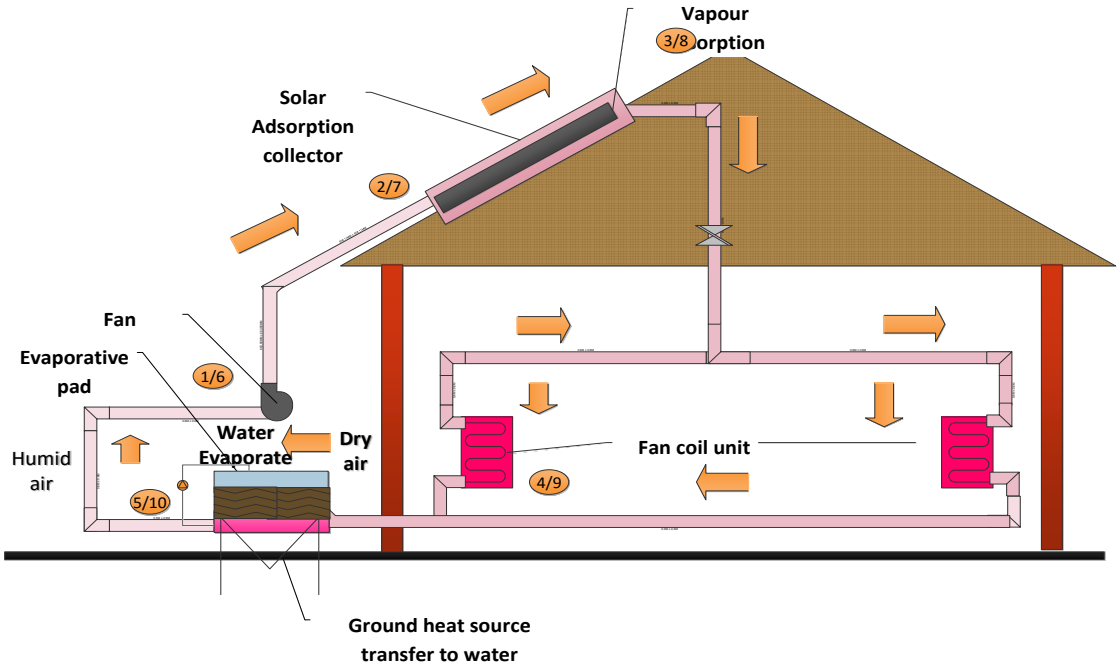


Figure 7.1: The SHSC in discharging cycle (Option 1)

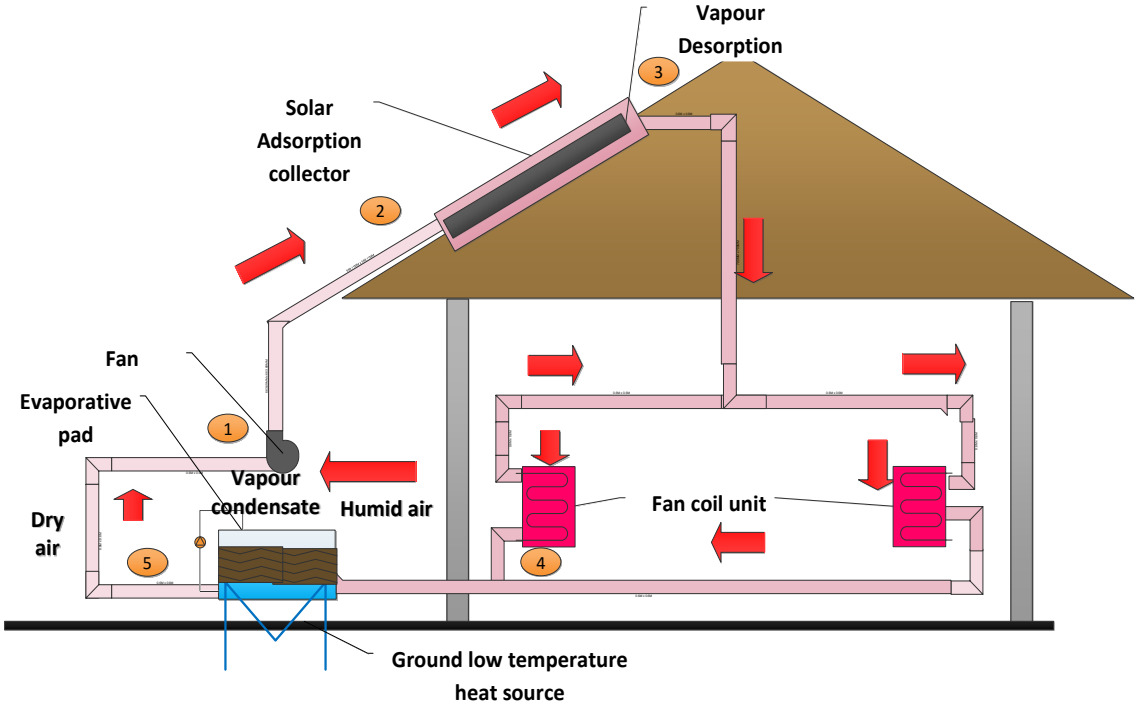


Figure 7.2: The SHSC in charging cycle (Option 1)

7.3.1 Analysis for charging process for Option 1

In the charging cycle, the fan blows inlet air to the solar adsorption collector. The energy balance of the fan given in Equation 7.1 (Aydin et al., 2015a).

$$W_f = \dot{m}_a \times C_{p,a} \times (T_2 - T_1) \quad (7.1)$$

Where, $\dot{m}_a$ is the mass flowrate of air and $C_{p,a}$ is the specific heat of the air. The total solar heat gained by the collectors using Equation 7.2 (Aydin et al., 2015a)

$$Q_{us} = A_{col} \times F_r \times [I \times \tau\alpha - U \times (T_{f,s} - T_{a,s})] \quad (7.2)$$

Where A_{col} is the total collector area, F_r, the collector heat exchanger efficiency, I, the total solar radiation, $\tau\alpha$, the absorption/transmission coefficient and U the heat loss coefficient

of solar collectors. $T_{f,s}$,$T_{a,s}$ are the solar collector and ambient temperature, respectively. The collector efficiency, η_{col}, calculated by using the equation below;

$$\eta_{col} = \frac{Q_{us}}{I \times A_{col}} \quad (7.3)$$

The heat transferred to the adsorbent is equal to the difference of the energy carried by the inlet and outlet air and heat from the solar collectors. Other than that, heat loss to the surrounding also considered in this model, which derived in the equation below;

$$Q_{tr} = \dot{m}_a \times C_{p,a} \times (T_3 - T_2) + Q_{us} - Q_{loss} \quad (7.4)$$

Total energy transferred to the adsorbent material in any time span, t_c, will be equal to the energy to provide dehumidification of the adsorbent where Equation 7.5 depicted. Here, the first part of the equation represents the reaction energy, while the second part is the sensible heating of the adsorbent in the solar collector.

$$Q_{char} = n \times X_c \times \Delta H_r - \left\{\int_{t0}^{tc} m_s \times C_{p,s} \times (T_s - T_{a,s})dt + \int_{t0}^{tc} m_{col} \times C_{p,col} (T_{fcol} - T_{a,s})d_t\right\} \quad (7.5)$$

The ratio of temperature to absolute humidity difference of input-output air at any time, t_c, calculated using Equation 7.6. Inlet temperature to the reactor calculated using Equation 7.1 & Equation 7.4. The outlet temperature of the air simulated according to the humidity difference between the inlet and outlet air streams as according to Equation 7.6 (Aydin et al., 2015a).

$$\left[\frac{T_3 - T_2}{w_3 - w_2}\right]_{tc} = \frac{\Delta H_w}{Cp,a + (w_3 \times C_{p,w})} \quad (7.6)$$

The charging reaction advancement X_c is the ratio of total water vapour removed from the adsorbent to the multiplication of the reaction stoichiometry coefficient, total mole of adsorbent and molar weight of water, as depicted in Equation 7.7 (Aydin et al., 2015a).

$$X_c = \frac{\dot{m}_a \times \int_{to}^{tc}(w_3 - w_2)dt}{v \times n \times M_{m,w}} \quad (7.7)$$

According to the product/ fuel principle as according to (Dincer, 2002; Zondag et al., 2013; Utlu et al., 2014; Aydin et al., 2015a), the charging process efficiency can be calculated as the ratio of heat transferred to the adsorbent to the energy supplied to the system as depicted in Equation 7.8.

$$\eta_c = \frac{Q_{tr}}{(Q_u + W_f) \times t_c} \quad (7.8)$$

7.3.2 Analysis of Discharging Process for Option 1

The discharge process can be analysed similarly to the charging process by considering the inverse of the same reaction. Therefore, the fan energy consumption calculated using Equation 7.9 (Aydin et al., 2015a).

$$W_f = \dot{m}_{ad} \times C_{p,a} \times (T_6 - T_7) \quad (7.9)$$

Total energy generation in the reactor as the result of water adsorption independent on the temperature lift (ΔT) of air and heat loss to the environment calculated according to Equation 7.10.

$$Q_{gen} = \dot{m}_{ad} \times C_{p,a} \times (T_7 - T_8) + Q_{loss} \quad (7.10)$$

The reaction advancement X_d for discharging is a function of the amount of adsorbed moisture as depicted in Equation 7.15. During the discharge process, the adsorption ratio will approach saturation point and the instantaneous moisture transfer to the adsorbent material will be decreases. Hence, the X_d is crucially important for the solar heat storage system (discharge from the SHSC) and reaction can be calculated in Equation 7.11

$$Q_d = n \times X_d \times \Delta H_r - \left\{\int_{t0}^{td} m_s \times C_{p,s} \times (T_s - T_{a,w})dt + \int_{t0}^{td} m_{col} \times C_{p,col} (T_{fcol} - T_{a,w})dt\right\} \quad (7.11)$$

$$\left[\frac{T_8 - T_7}{w_7 - w_8}\right]_{tc} = \frac{\Delta H_w}{C_{p,a} + (w_7 \times C_{p,w})} \quad (7.12)$$

$$\Delta T = T_8 - T_7 \quad (7.13)$$

$$\Delta w = w_8 - w_7 \quad (7.14)$$

$$X_d = \frac{\dot{m}_{dt} \times \int_{to}^{td} (w_8 - w_7) dt}{v \times n \times M_{m,w}} \quad (7.15)$$

The energy transferred to the fan coil in the room calculated from Equation 7.16 below,

$$Q_{room} = \dot{m}_a \times C_{p,a} \times (T_8 - T_9) \quad (7.16)$$

Consequently, the energy balance in the room calculated by analysing heating load required by Equation 7.17

$$Q_{room} = U \times A \times (T_d - T_a) \quad (7.17)$$

The heat loss coefficients (U-Value) and total area (A) of the individual building components given in Table 7.2. Air changes per hour (ACH) are set at two for the ventilation heat loss calculation (see: Equation 7.18). The total heat load of the building, Q_T (kW) calculated according to Equation 7.19.

Table 7.2: Heat loss coefficients and surface areas of building components

Component	U(W/m^{2}C)	A(m^2)
Window	2.8	25.83
Block Work	0.353	153.59
Floor	0.250	53.3
Roof	0.13	54.5

$$Q_T = Q_w + Q_b + Q_f + Q_r + Q_v \quad (7.18)$$

$$Q_v = ACH \times V \times c_{p,a} \times (T_d - T_a) \quad (7.19)$$

The total amount of water transferred from the air in the humidification unit calculated using Equation 7.20.

$$\dot{m}_w = \dot{m}_{ad} \times \left\lfloor \frac{W_9 - W_{10}}{1000} \right\rfloor \quad (7.20)$$

The efficiency of the discharging process defined as the ratio of net heat gain (recovered heat) to the total energy supplied to the system by the fan and adsorbent material (inside the collector) during the process (see Equation 7.21). Similarly, the coefficient of performance, COP, of the system defined as the thermal energy gain per kWh electrical power consumption of the fan only (see Equation 7.22).

$$\eta_d = \frac{Q_d}{(Q_{gen} + W_f) \times t_d} \quad (7.21)$$

$$COP = \frac{Q_d}{W_f \times t_d} \quad (7.22)$$

7.3.3 Result and Discussion from the modelling for Option 1

In this study, SHSC were investigated experimentally and numerically. The concept of this numerical analysis is using a theory of an open sorption storage system. Therefore, the reaction of advancement (X_d), is used to calculate the adsorption isotherm instead of adsorption rate in the close system in the previous chapter. The heat and mass transfer considered in the adsorption and desorption process, and the modelling was carried out separately. In the charging process, the mass flow rate, the collector size and time dependence were shown in Figure 7.3~Figure 7.6 respectively. As for the desorption process, a simulation was carried out independently of the effect of mass flow rate change, (Δw) and (t_d) respectively as shown in Figure 7.7~Figure 7.9.

a) Charging results

The rise in mass flow rate of air inlet $\dot{m}_c$ has significantly increase the solar heat (Q_{us}) and heat transfer in solar heat storage collectors (SHSC) (Q_{tr}) as shown in Figure 7.3. The increase of solar heat effect positive linearly with the rise of mass flow rate. Apart from that, the outlet temperature (T_3) of SHSC has significantly decrease from 150°C to 90°C. This might be due to the decrease in the final temperature in the solar surface collector $(T_{f,s})$ which assumed from 100°C to 90°C to simulate the regeneration temperature of chosen for the TCM. Other than that, the efficiency of charging and the efficiency of solar collector is also increase by the rise of mass flow rate as well (see Figure 7.4).

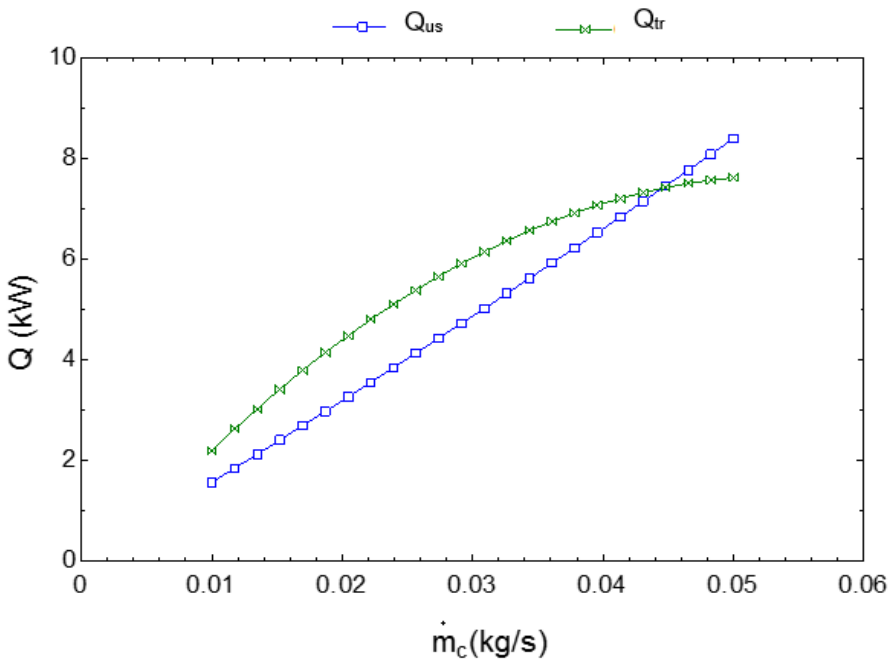


Figure 7.3: Results showing the effect of mass flow rate on collector heat gain and heat transferred to the material for the charging cycle.

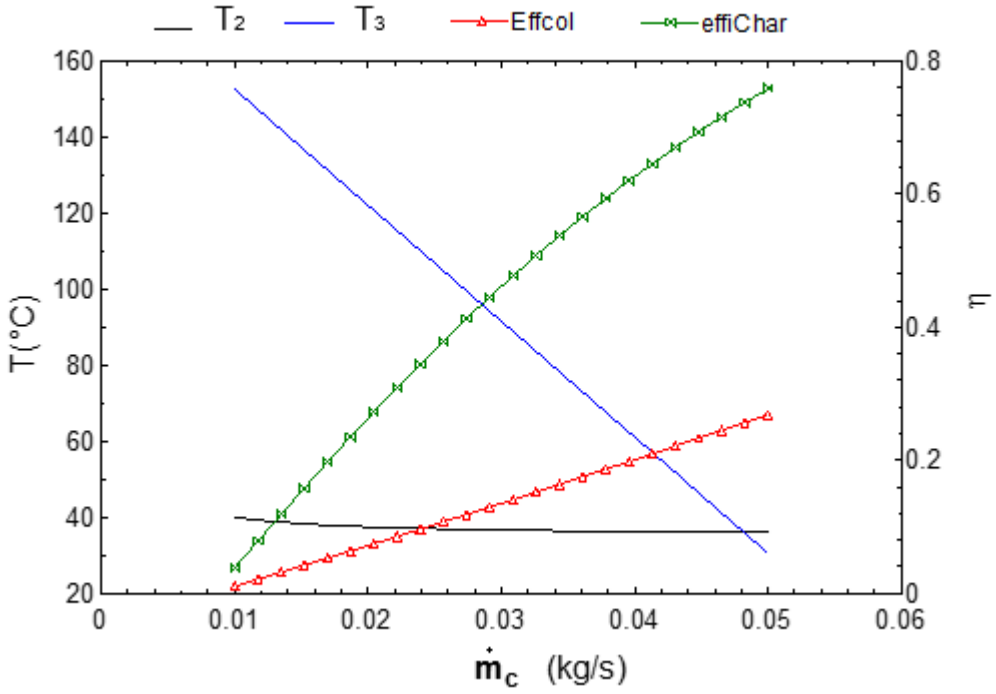


Figure 7.4: Results showing the effect of charging cycle mass flow rate on inlet–outlet temperatures, charging and collector efficiency.

Apart from this study, the effect of mass flow rate, the changes in the collector area also being investigate using a quasi-stationary state condition on the mass flow rate of 0.07kg/s. Figure 7.5 Illustrated of this effect and it was shown that the outlet temperature (T_3), the heat transfer in the SHSC (Q_{tr}), the solar heat (Q_{us}), increases linearly by the increase in solar collector area. Thus, this modelling suggests that, there were no heat waste by increasing the area of collector size. However, the size need to be optimise and the available surplus heat could be stored for hot water during night-time. Other than that, the inlet temperature (T_2) does not affected by the increase of solar collector area, due to the heat of heat transfer to the inlet temperature were from the humidifier that assume to have a lower temperature compare to solar thermal.

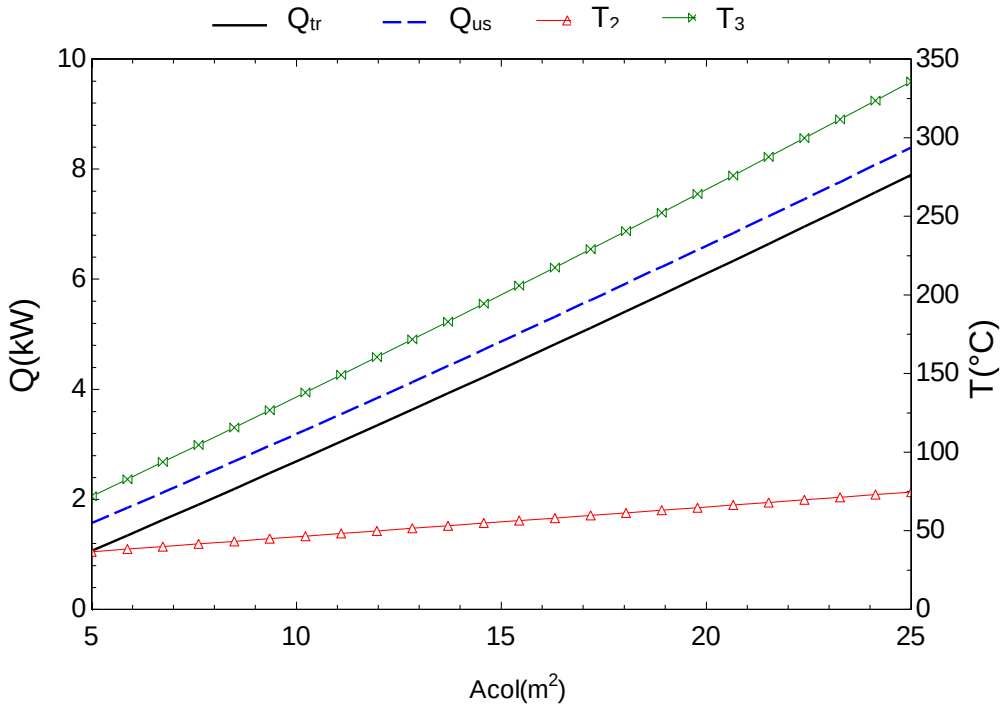


Figure 7.5: Illustrations showing the effect of collector area on inlet–outlet temperature, heat gain from collectors and transferred heat to the adsorbent for the charging cycle

Other than that, the time-dependent analysis also has been carried out for the parameter such as $(Q_{us}, Q_{tr}, T_2, T_3, X_c, \eta c)$ as depicted in Figure 7.6. By assuming solar intensities of 0.5kW/m^2 (I) and collector area is 5m^2 that give approximate equivalent to 1.58kW of solar power (Q_{us}). This result shows that, the outlet temperature (T_3) has decreased in 5hours of charging from 130°C to 0°C as the time passed. However, the heat collected from the solar intensities (Q_{us}) and heat transfer in the collectors (Q_{tr}) decreased ranges from 1.6 to 0.64 and 1.06 to -0.42 respectively. The negative value of heat transfer to the collector indicates that the most effective charging periods is in the first 5 hours. Other than that, the efficiency of charging (Π_c) has decreased by the time change. As the material has reach its equilibrium point, this give the reaction advancement (X_d) of 0.64(64%) and efficiency (ηc) of 0.13 (13%) until the end of charging period (24hrs).

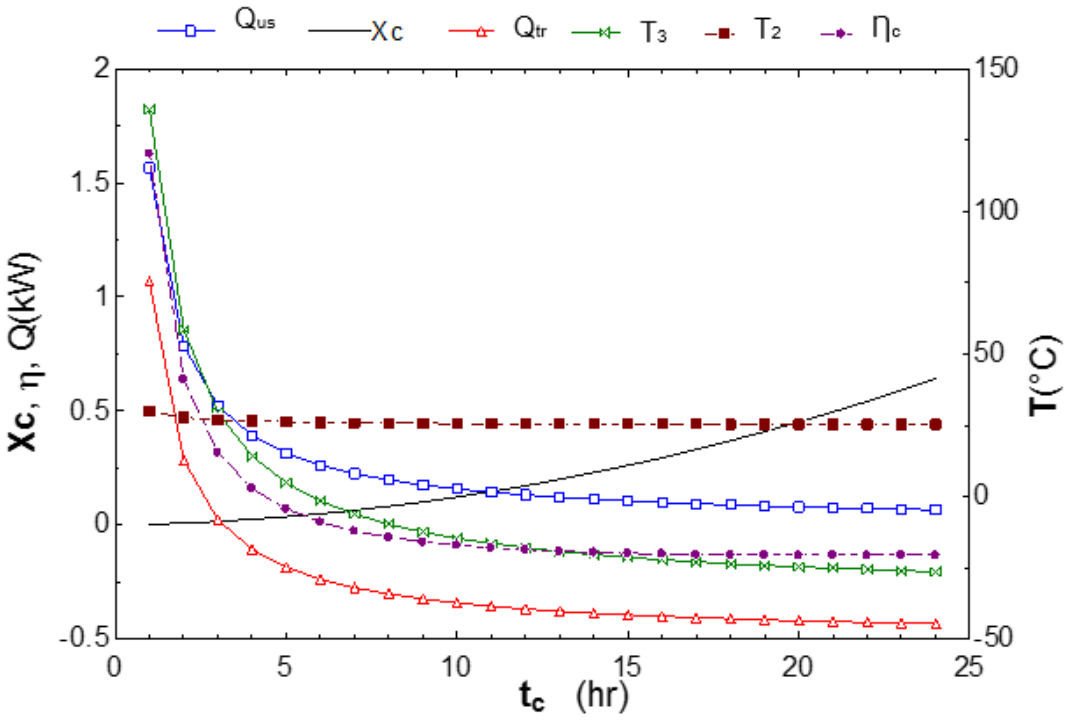


Figure 7.6: Illustrations showing the effect of time on inlet–outlet temperature, heat gain from collectors, heat transferred to the absorbent, reaction advancement and charging efficiency for the charging cycle.

a) Discharging result

In an open sorption, the performance of the systems is affected by the change in mass flow rate. The increase in mass flow rate will affect positively in the efficiency of discharging (η_d) and instantaneously the heat generated (Q_{gen}) and the reaction (X_d) (see Figure 7.7). From this results, it can be seen that the Q_{gen} increased from -0.6 to 6.12. The efficiency of discharge fluctuated at the beginning of the process due to heat transfer to the collector does not occur when the mass flow rate of water is at 0.03kg/s.

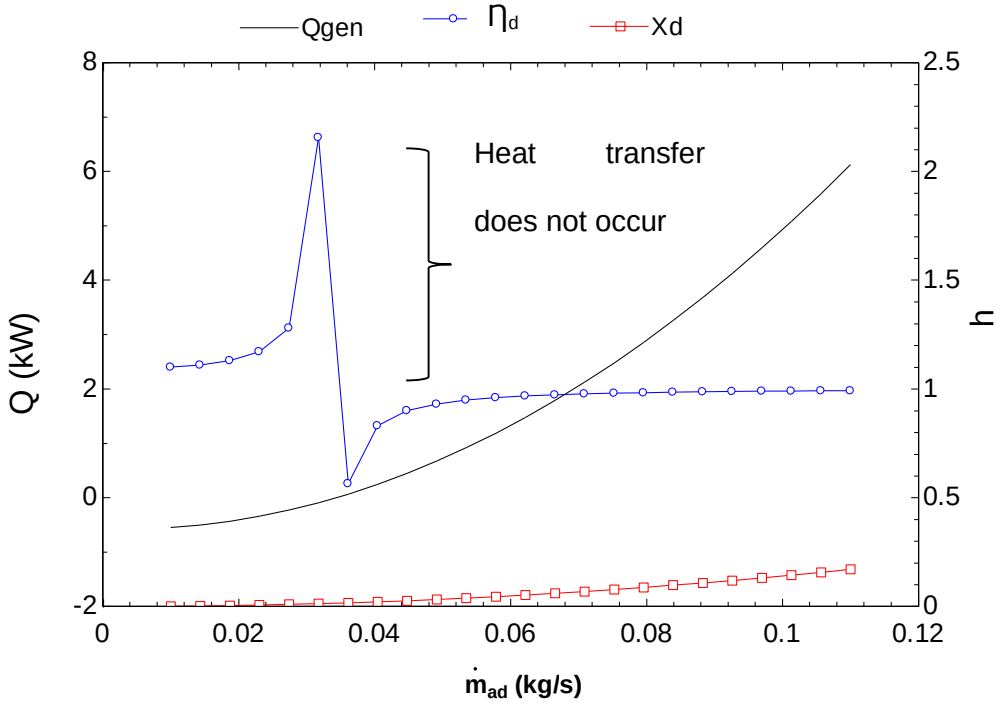


Figure 7.7: Illustrations showing the effect of mass flow rate on discharging efficiency and heat generation for the discharging cycle.

Other than that, the amount of water vapour transferred in the reactor/solar heat collector is crucially need to be optimised to get high efficiency in the system. The quantity of water vapour transfer in the systems will lead to an exothermic reaction in the systems. Hence, this will result in a temperature lift in the reactor/solar heat collector. Figure 7.8, exhibits the correlation between of absolute humidity change (Δw) and the temperature lift (ΔT) of the systems. This result indicates that with the change of absolute humidity of 1g/kg to 10g/kg will give a temperature difference from 185°C. This effect would also increase the heat generated (Q_{gen}) from 0.8kW to 25kW. The efficiency discharge (η_d) has also increased ranges in -0.2 to 0.1. However, this simulation suggests that there is evidence that the increasing amount of absolute humidity will positively increase the heat generated in the systems.

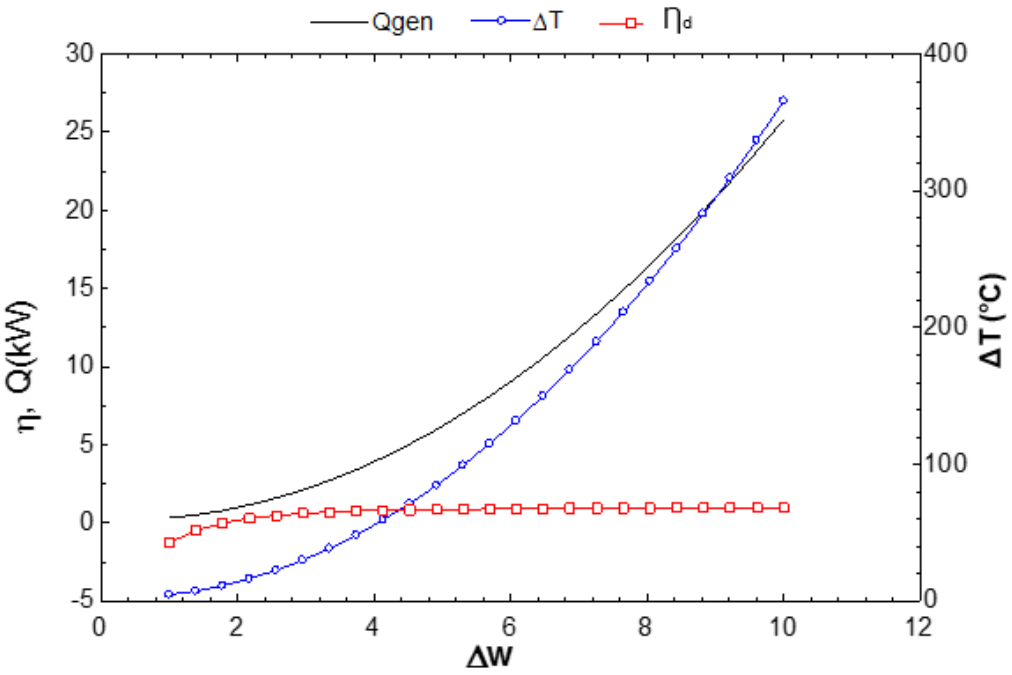


Figure 7.8: Illustrations showing the effect of absolute humidity on discharging efficiency generated heat and temperature lift for the discharging cycle.

Consequently, time-dependent has also an important parameter that affects the performance of the SHSC. Dependent variables chosen to analyse the impact of the change in discharge time (t_d) were output temperature (T_8), temperature lift (ΔT), COP, generated heat (Q_{gen}) and reaction advancement (X_d). As can be seen in Figure 7.9, the output temperature (T_8), temperature lift (ΔT) and COP decrease in the first 5 hours of discharge time and remain constant until the end of the cycle (t=24hr). With a constant mass flow rate of 0.07kg/s, the heat generated (Q_{gen}) decreased from 0.35kW to -0.26kW. Furthermore, the decreased on outlet temperature is insignificantly affected the heat generated because it is assumed that the discharge heat (Q_d) transferred the heat directly to the SHSC. Apart from that, the temperature outlet to the room (T_9) decreased from 42.55°C to 14.86°C as time passed. Therefore, this simulation suggests that the first 5

hour of discharging is the most productive period for the heat storage. Although the COP of the systems has decreased from 7.8 to 0.78, this considers high compared to the conventional heat pump systems.

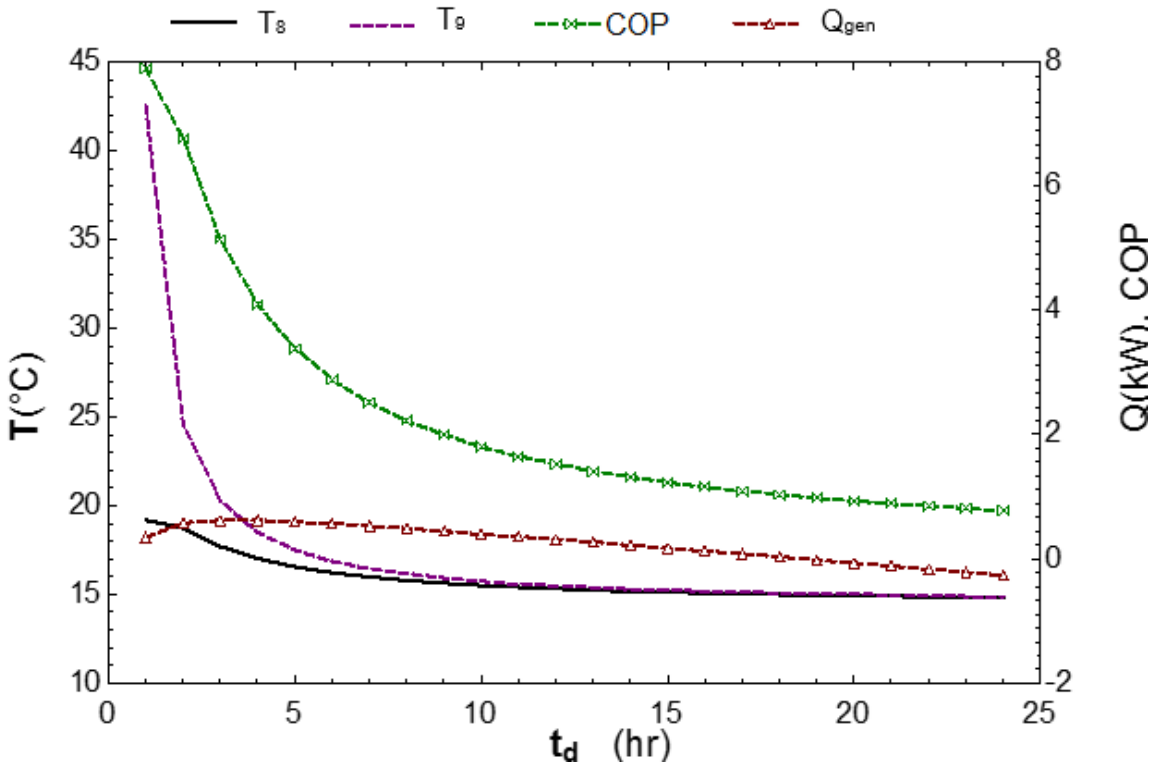


Figure 7.9: Illustrations showing the effect of time on output temperature, COP & generated heat for the discharging cycle.

7.4 Option 2: SHSC heat transfer through heat pipe and water (air to water heat exchange)

Option 2, involve the heat transfer from the adsorbent material to the heat pipe heat and heat sink to inlet and outlet of domestic water systems. The schematic of this option shown in Figure 7.10 & Figure 7.11. The charging cycle is similar to Option 1. However, the domestic cold water stops at this point.

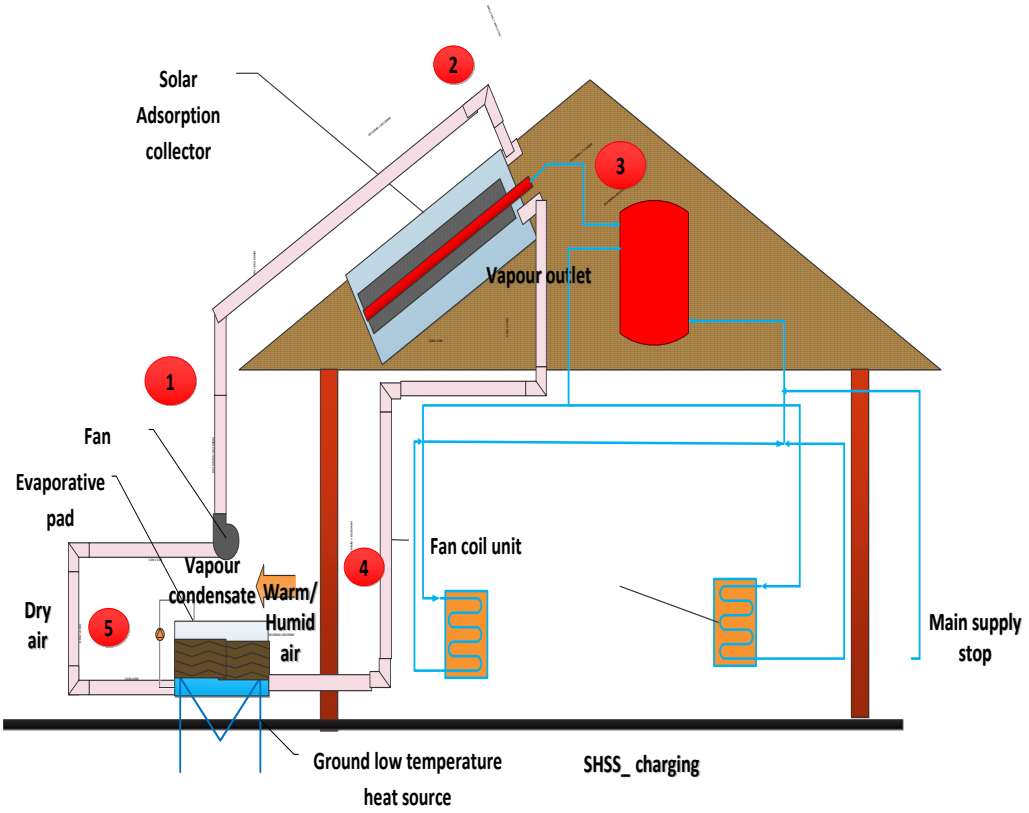


Figure 7.10 SHSS charging cycle (Option 2)

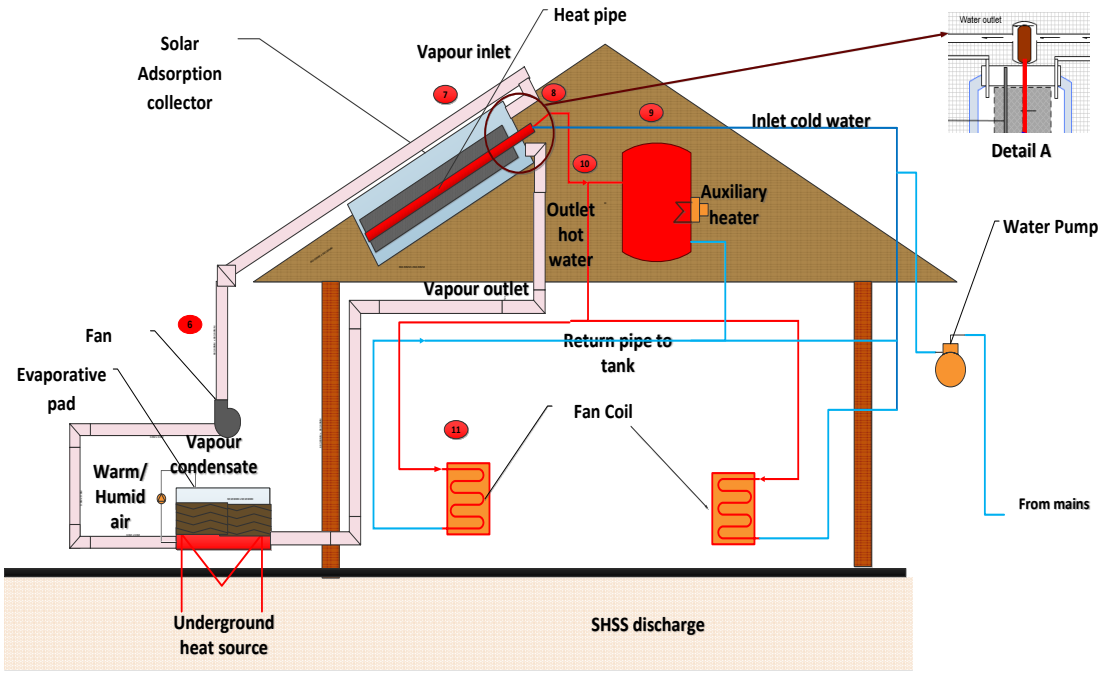


Figure 7.11: SHSS discharge cycle (Option 2)

7.4.1 Analysis for charging process for Option 2

In the charging cycle, the analysis is similar to the systems using air as the heat transfer media (see Figure 7.10). To simplify the modelling, the assumption made that there is no water flow through the heat pipe. Therefore, during this cycle Equation 7.1 to Equation 7.9 can be repeated and duplicating the analysis is unnecessary at this point.

7.4.2 Analysis of Discharging Process for Option 2

The discharge process can be analysed similarly to the charging process by considering the inverse of the same reaction (see Figure 7.11). However, in option 2, the heat from the adsorbent material is transfer through a heat pipe inside the solar collector. Then, the heat will be transfer through the end of the heat pipe (normally known as the bulb of the heat pipe) to the inlet/outlet of the cold water (see Detail A). The analysis of the air from the humidifier enters the solar collector are similar to Equation 7.9~Equation 7.15. The heat transfer from heat pipe to inlet and outlet of the domestic water written as;

$$Q_{hp} = \dot{m}_w \times C_{p,w} \times (T_8 - T_7) \quad (7.23)$$

The energy balance of the water pump written as;

$$W_{pump} = \dot{m}_w \times C_{p,w} \times (T_{10} - T_9) \quad (7.24)$$

The energy transferred to the fan coil in the room written as;

$$Q_{room} = \dot{m}_w \times C_{p,w} \times (T_{11} - T_{10}) \quad (7.25)$$

Consequently, the energy balance in the room calculated by analysing heating load required by Equation 7.17. The heating load inside the room is similar to Option 1 as depicts in Equation 7.17~Equation 7.19.

Similarly, the efficiency of discharge process and the COP of the system is defined as the thermal energy gain per kWh electrical power consumption of the fan and water pump (see Equation 7.26 & Equation 7.27)

$$\eta_d = \frac{Q_d}{(Q_{gen} + W_f + Wpump) \times t_d} \quad (7.26)$$

$$COP = \frac{Q_d}{(W_f + Wpump) \times t_d} \quad (7.27)$$

7.4.3 Result and Discussion from the modelling (Option 2)

a) Charging Results

The charging result for this option is similar to Option 1. Therefore, no repetition analysis was carried out at this point as was assume that the results will be similar.

b) Discharge Results

The analysis of discharge has calculated by evaluating the change in mass flow rate ($\dot{m}_w$) and time change (t_d) to parameters ($T_8, T_{10}, T_{11}, \eta_d$ & COP). In this analysis, the fan flow rate assumed as constant at 0.1 kg/s. It can be seen from Figure 7.12 that the increase of water flow rate will increase the temperature of the room fan-coil unit (T_{11}) from 5°C to 40°C. Similar pattern effected the discharge temperature from the collector (T_8) which is increasing from 10°C to 90°C. This would also positively have affected the COP of the systems which is increasing from -5.4 to 5.14. However, the discharge efficiency (η_d) is decrease from 1.2 to 0.04.

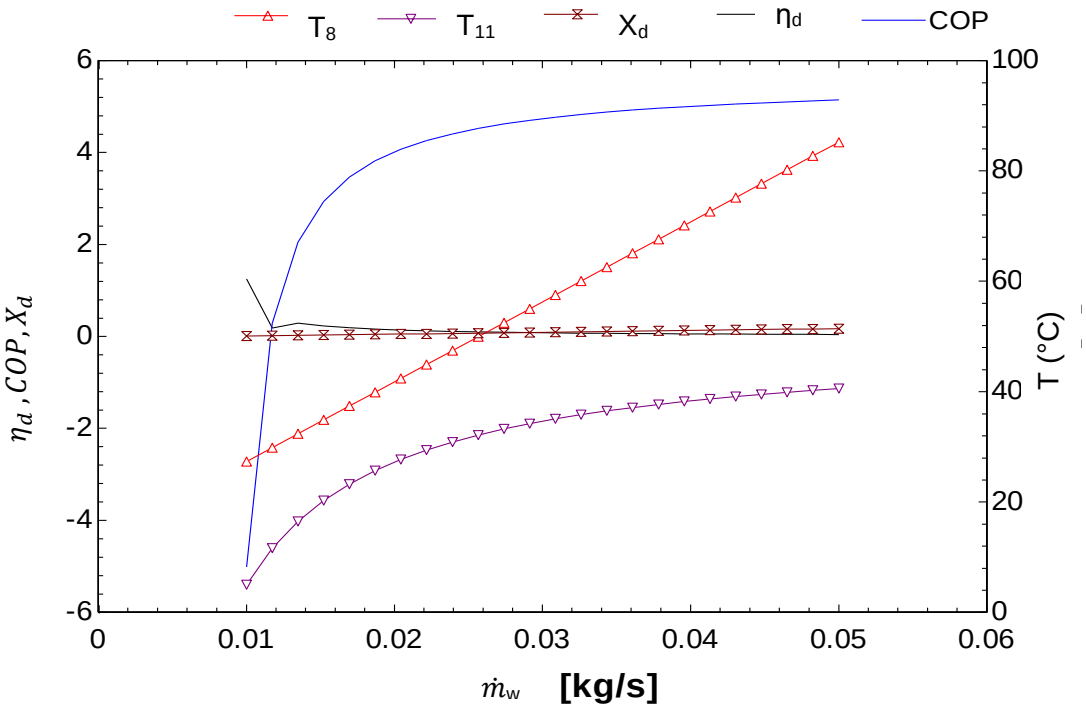


Figure 7.12: Result showing the effect of mass flow rate ($\dot{m}_w$) to discharge temperature (T_8), fan-coil outlet temperature (T_{11}), the efficiency of discharge (η_D), reaction advancement (X_d) and COP of the system.

Figure 7.13 exhibits the effect of discharge time (t_d) to parameters of ($T8, T10, T11, \eta_d$ & COP). With a constant mass flowrate from the collector side ($\dot{m}_a = 0.07\ kg/s$) and constant fan coil mass flowrate of ($\dot{m}_w = 0.3\ kg/s$), the discharge temperature and room fan coil temperature is decreasing from 41.2 to 35.6°C & 41.0 to 25.09°C respectively. Furthermore, these temperatures were starting to decrease from 5 hour of discharging time. Therefore, these changes will also influence the efficiency of discharge and the COP of the system to decrease from 0.83 to 0.03 & 4.9 to 0.83 respectively.

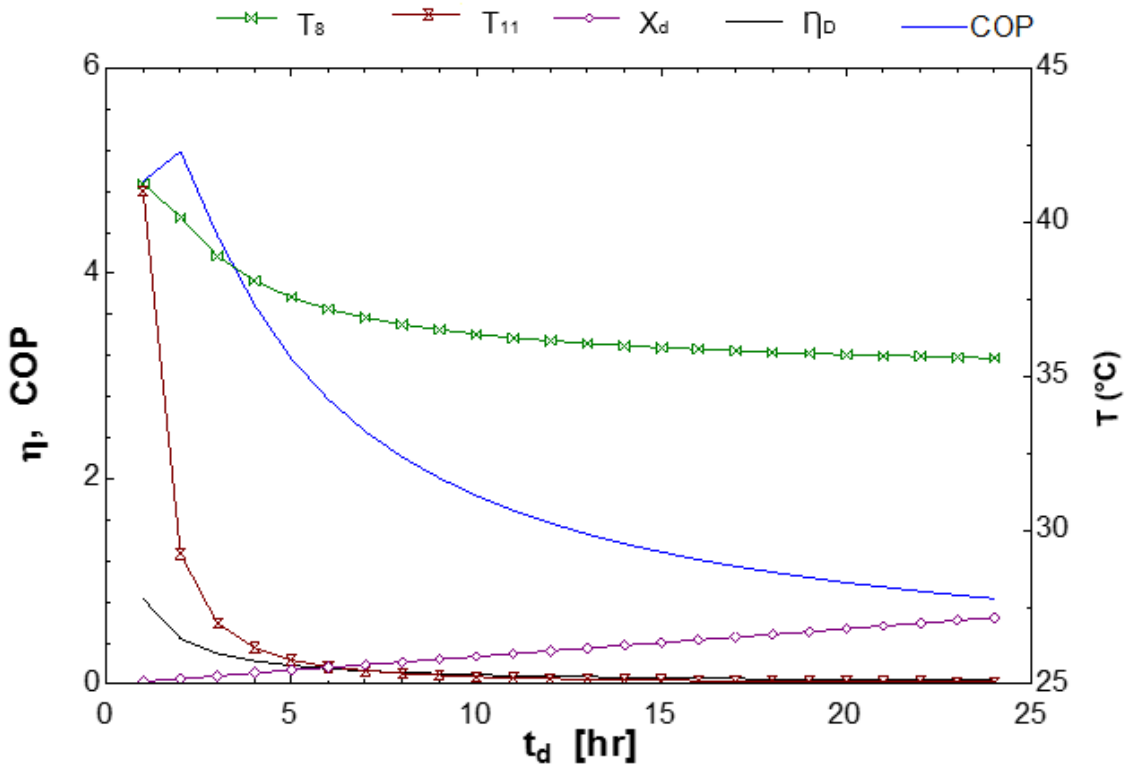


Figure 7.13: Results showing the effect of discharge time to discharge temperature, fan-coil outlet temperature, the efficiency of discharge and COP of the system.

7.5 Experimental investigation on small-scale prototype of SHSC

7.5.1 Material and Method

A novel adsorption pipe integrating with evacuated tube collector is developed and tested in the Sustainable Research Building, University of Nottingham, UK. A schematic of SHSC for discharge and charging process illustrated in Figure 7.14 & Figure 7.15. First, the experiment starts with an adsorption process. The material was dried in the electrical oven for 24 hours at 150°C. Then the materials were inserted in the evaporated pipe which attached with the heat pipe in the middle of the semicircle perforated pipe (see detail A-A). The ultrasonic humidifier was used to provide water vapour for charging process. In

this cycle, the water vapour/mist will be sprayed inside the collector until the material reaches approximately 70~80% absolute humidity. Instantaneously, as the water sprayed inside the collector, VCC generated heat from the exothermic reaction. The adsorption heat from the material transferred to the heat pipe inside the collector and water inlet on the top of the collector. The temperature rises from VCC, inlet and an outlet temperature of water flow through the heat pipe bulb measure though a K-type thermocouple every one-second interval. The relative humidity in measured using a handheld digital relative humidity meter every 15 minutes as the adsorption process started. When there is no more temperature rise, the materials were weighed again to measure the absolute humidity during the adsorption process. Then desorption process will be conducted to completed the cycle. During desorption, a solar light simulator was used as the heat source. The water inlet and outlet from the domestic waste sink was closed during this process. The vapour outlet will be kept open, and the humidity of the water vapour measured during this process. After 2 hours of the procedure, the materials were weigh again to analyse the absolute humidity of VCC from desorption. The main concern in this open or closed system is to get the lowest possible absolute humidity of the material during desorption. Because this will affect the whole systems in the next cycle. However, in this study, the water vapour sprayed inside the collector to create maximum reaction during adsorption which is hard to achieve via a closed sorption system.

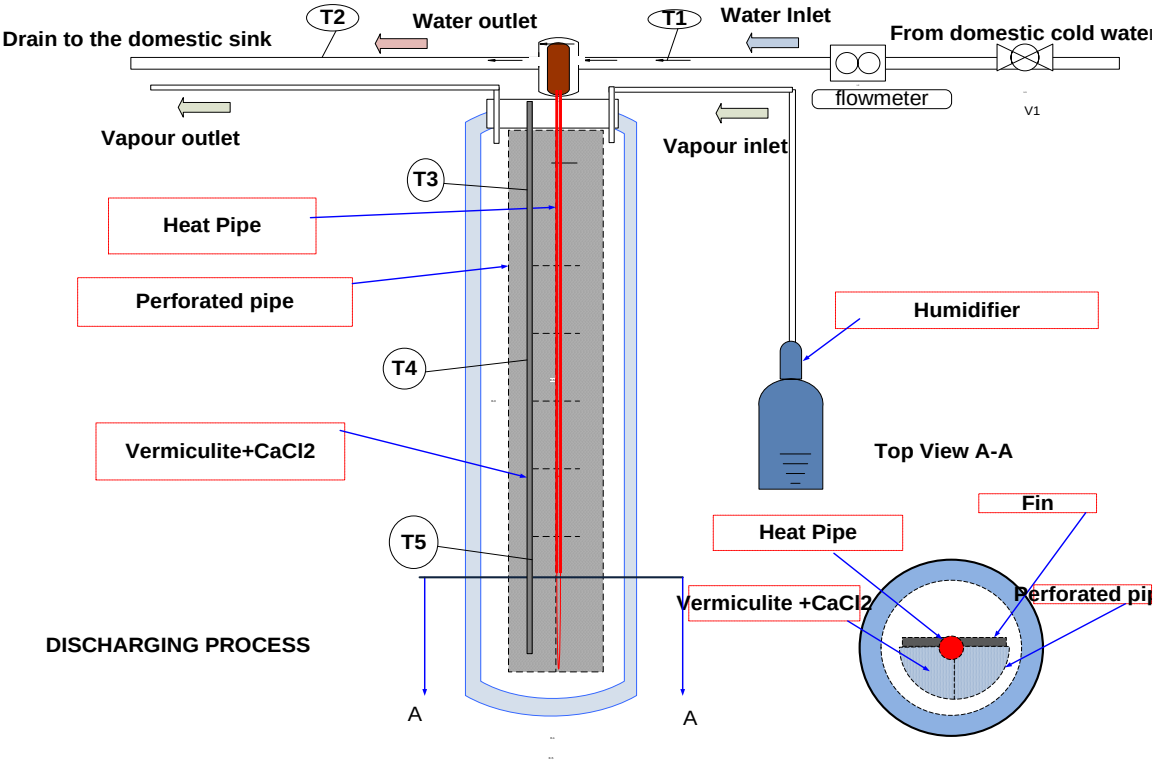


Figure 7.14: Schematic of SHSC (discharging process)

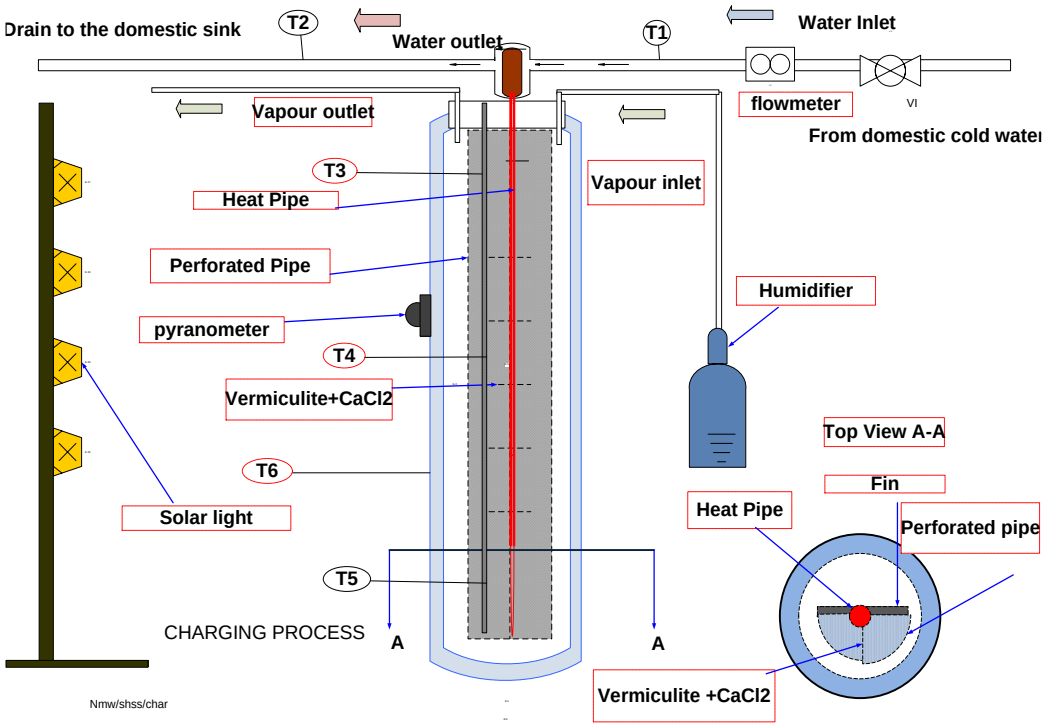


Figure 7.15: Schematic of SHSC (charging process)

7.5.2 Installation of the prototype systems

The construction of a lab-scale of a prototype SHSC is according to Figure 7.16. As can be seen that a single evacuated tube used with the length of 2200mm and 70mm inside diameter installed with a tilt angle of 45°. Four (4) halogen solar simulator (each 500W maximum) was installed parallel with the solar collector to get the maximum heat from the light (Figure 7.17). Inside of the collector, the perforated pipe was installed in front of a heat pipe fins (Figure 7.19). This perforated pipe used for the storage of adsorption material. The length of perforated pipe is 1400mm with semicircle diameter of 40mm. The fin was painted with a solar paint to enhance solar absorption (Figure 7.18). The heat pipe inserted through the heat pipe fins, and adsorption heat will be transferred during the adsorption process (see Figure 7.19 & Figure 7.20).

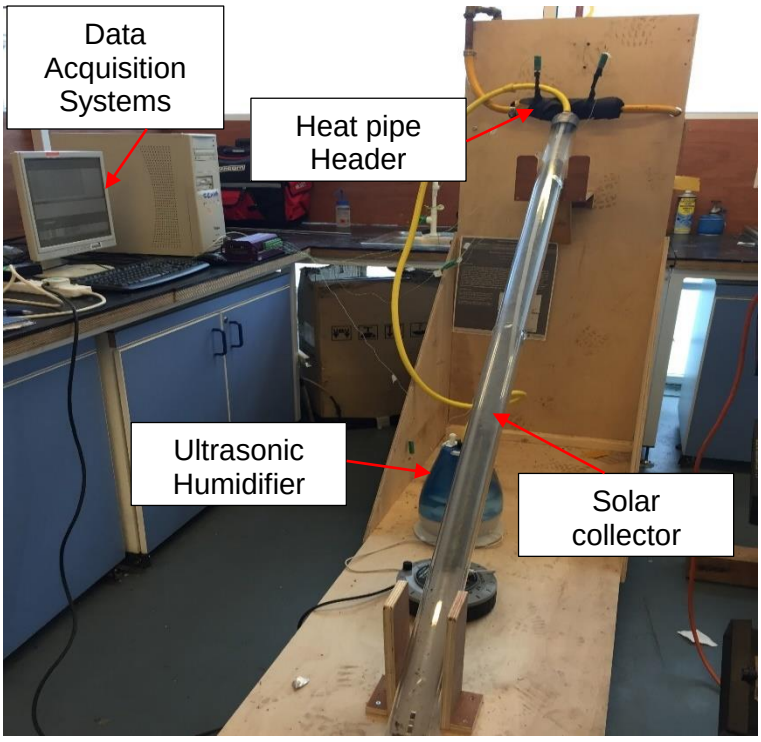


Figure 7.16: The construction small scale of SHSC

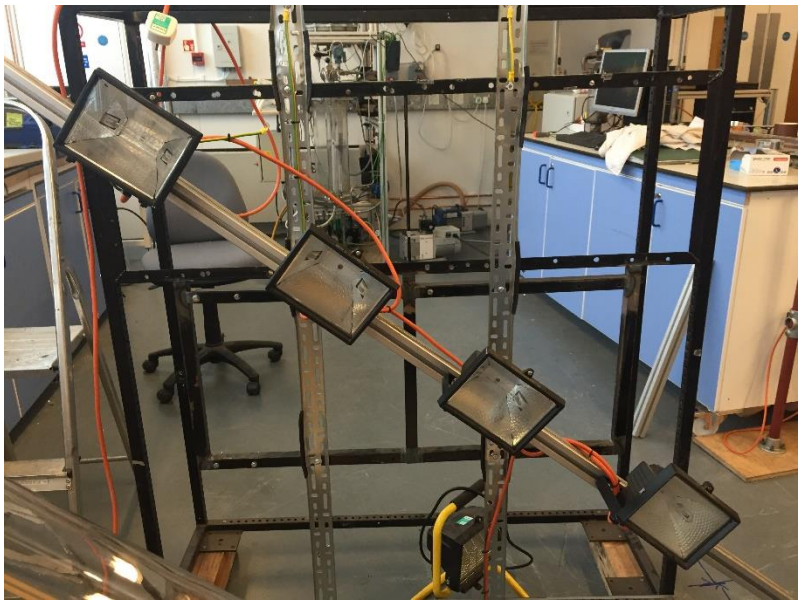


Figure 7.17: Halogen lights



Figure 7.18: Solar coating on the heat pipe

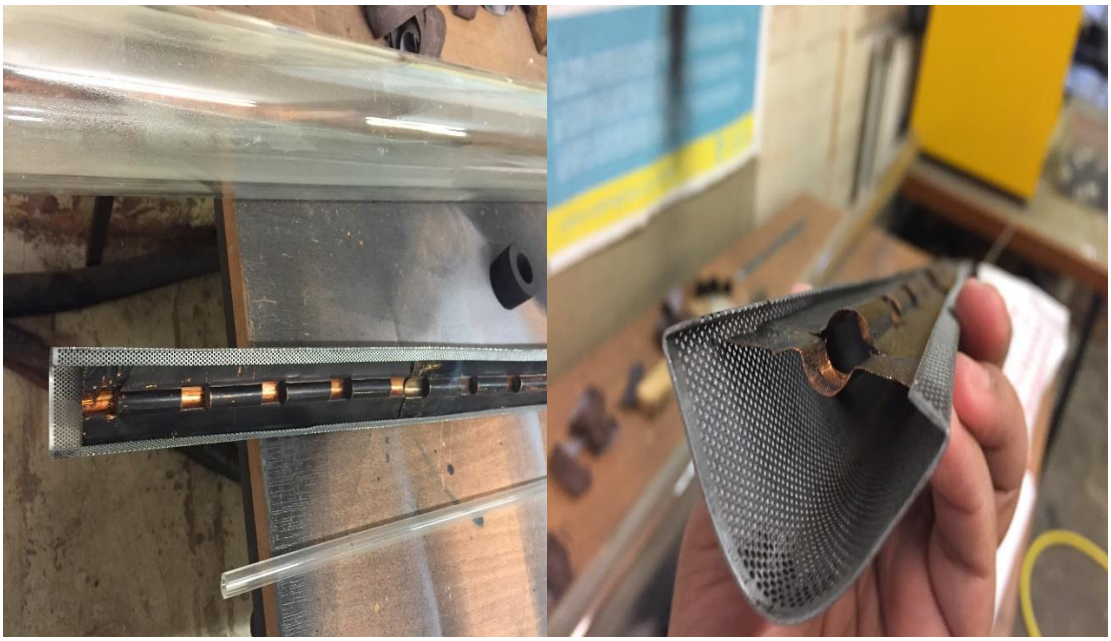


Figure 7.19: Removable perforated pipe for the adsorbent material installed inside the collector (right: plan view, left: top view)

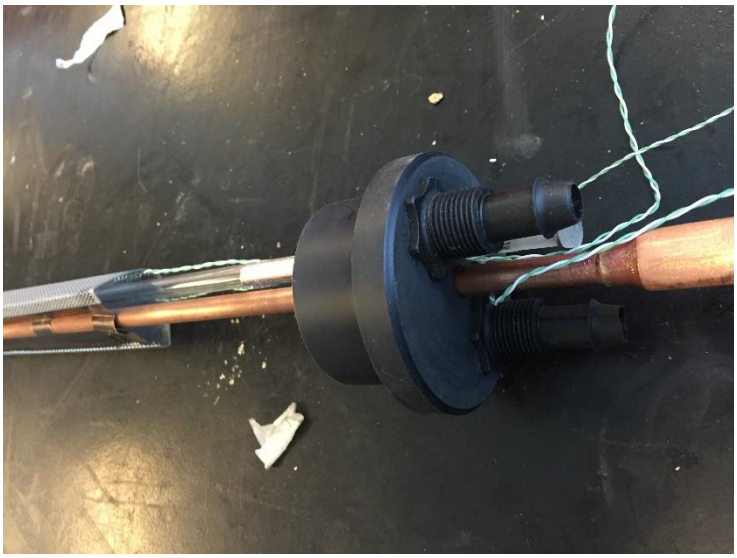


Figure 7.20: The heat pipe inserted through the fins

7.5.3 Measurement procedure

The important parameter that needs to be determined in these experiments is the temperature, the flow rate of water, solar intensities, humidity, and weight of the materials.

Temperature measurement

The temperature was measured using a K-Type thermocouple and the position of the thermocouples was listed Table 7.3. All thermocouple and solar radiation intensities connected to the data logger DT500. All thermocouples were tested for calibration before the testing commenced.

Table 7.3: Thermocouple position

Number	Descriptions
T1	Water inlet temperature (°C)
T2	Water outlet temperature (°C)
T3	Top material temperature (°C)
T4	Middle material temperature (°C)
T5	Bottom material temperature (°C)
T6	Collector surface temperature (°C)
T7	Ambient Temperature (°C)

Pyranometer

The solar simulator was used to gain a solar thermal power, and the measurement was using Kipp and Zonen CMP 11 pyranometer with the sensitivity of 9.27 x 10^{-6} V/Wm^{-2} (see Figure 7.21). This pyranometer was mounted parallel to the angle of the solar collector. Table 7.4 describes the details specification of CMP 11.



Figure 7.21: Kipp & Zonen pyranometer

Table 7.4: Specifications for CMP 11

Spectral range (overall)	**285 to 2800 nm**
Sensitivity	7 to 14 µV/W/m²
Response time	< 5 s
Temperature dependence of sensitivity (-10 ºC to +40 ºC)	< 1 %
Operational temperature range	-40 °C to +80 °C
Maximum solar irradiance	4000 W/m²
Field of view	180 °

The flowmeter

The vertical flowmeter was used to measure the flowrate from the domestic water pipe to the inlet and outlet of the heat pipe bulb. The range of flow rate is 3l/min~22l/min. The flow rates tested in this experiment are 3l/min. The flowmeter was installed at the back of the rig to ease the inlet pipe from the nearest domestic sink (see Figure 7.22).



Figure 7.22: Installation of flowmeter

7.5.4 Performance equations

The experimental analysis of this study was according to the equation below;

Energy storage density per mass unit

$$E_d = \frac{E_{cum,dr}}{\Delta m} \quad [\text{Wh/g}] \tag{7.28}$$

Energy storage density per volume unit

$$E_{d,dr} = \frac{E_{cum,dr}}{V_{ad}} \quad [\text{kWh/m}^3] \tag{7.29}$$

Mass increase

$$\Delta m = M_{w,v} = M_w - M_d \text{ [g]} \tag{7.30}$$

Cumulative thermal energy generation

$$Q_{SHSC} = \dot{m}_{dr} \cdot C_p(T_o - T_i) \quad [\text{kWh}] \tag{7.31}$$

COP of the systems;

$$COP_{THSS} = \frac{Q_{shsc}(t)}{Q_{solar}(t)} \quad (7.32)$$

7.5.5 Experimental Results and Discussion

This experimental result will predict the actual performance of SHSS systems in laboratory scale on single evacuated tube collector. Two set of a test conducted which was involving the adsorption and desorption process known as Test 1 & Test 2. The different parameters involve in these two test are the weight of dry VCC and water vapour supply location which shown the Figure 7.23 ~Figure 7.26.

Result on Adsorption and Desorption for Test 1: Water vapour supply at the bottom of material

Figure 7.23, illustrates the temperature variation of the adsorption process on Test 1. In this test, the water vapour supply was installed at the end of perforated pipe containing VCC. Three thermocouple positions installed and monitored which were located at the Top, Middle, and Bottom of the material. The first 1000s the domestic water supply valve was open. However, there was no heat transfer observed from the collector to the water, and therefore, the valve was closed at 1000s. When the water vapour sprayed at the bottom of the material, there were temperature increases at the bottom and the middle of material from its initial temperature from 24°C to 28°C. Conversely, the temperature starting to increase from 3000s at the top of the material with maximum temperature at 26°C. This result showed that the temperature increase in highly depending on the water vapour transfer from the humidifier. Furthermore, the amount of material is insufficient to obtain the desired temperature similar to the closed sorption systems. Hence, due to low-temperature lift in this experiment, the heat transfer to the domestic cold water would be

unlikely to achieve. However, at the end of the experiments, the weight material increases 213g from its initial dry weight of 168g.

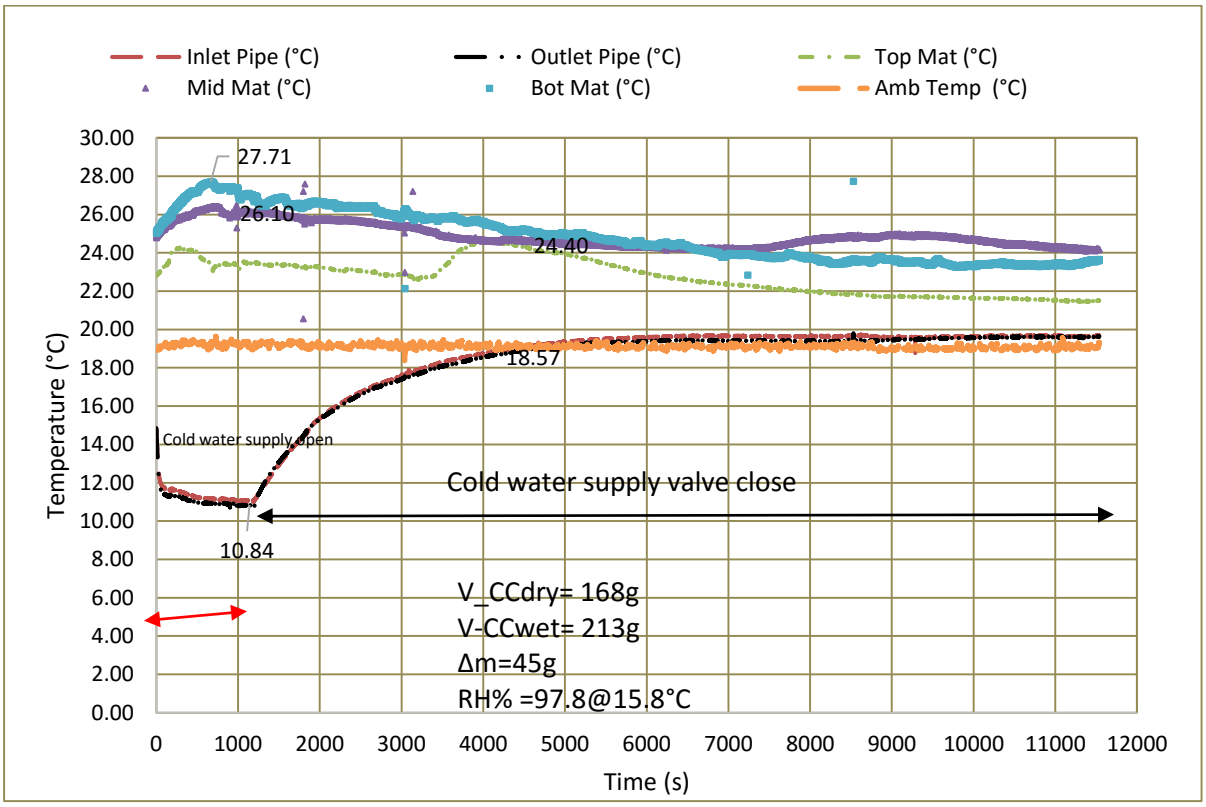


Figure 7.23: Temperature variations of inlet and outlet of domestic water and material in the perforated pipe for Adsorption Test 1

To complete the process cycle, desorption test was conducted, and the results are shown in Figure 7.24. Despite the low-temperature lift in from adsorption cycle, desorption cycle indicates that the solar light effectively transferred the heat to the solar collector. In just one hour of desorption cycle, with average solar intensities of 950W/m^2, the temperature reaches its maximum at 64°C in the middle of material (purple line). The top and bottom of the materials have the similar maximum temperature increase was 50°C, which gives the average temperature increased at 54.3°C. Furthermore, at the end of experiments, the desorbed moisture is 22g, which gives water desorption at 0.5g/g of hydrated adsorbent.

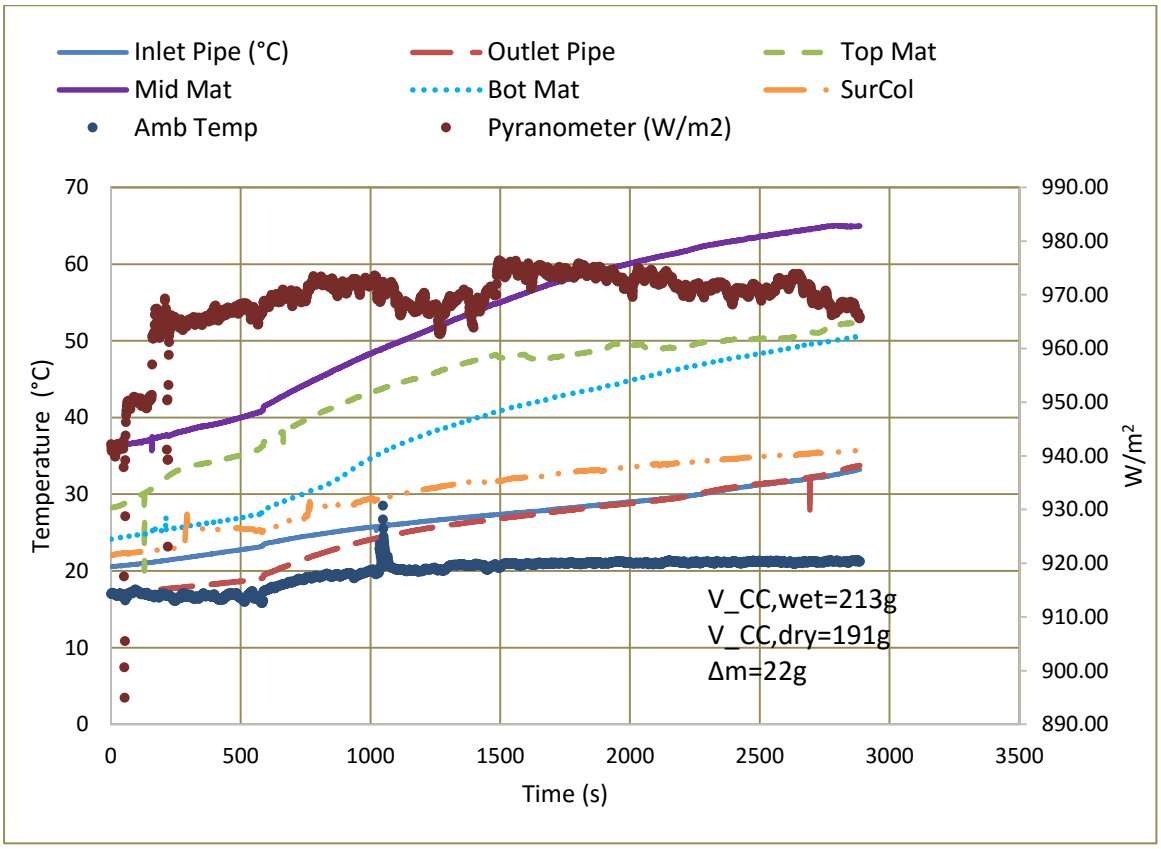


Figure 7.24: Temperature variations of inlet and outlet of domestic water, material in the perforated pipe & solar intensities for Desorption Test 1

Result for Adsorption and Desorption Test 2: Water vapour spray at the middle of material

As mentioned before, in Test 2, the water vapour sprayed in the middle of the perforated pipe. Therefore, it shown in Figure 7.25, the middle material (purple line) has temperature lift higher than that of the top & bottom of the material. This phenomenon was expected to occur, as the reaction will start in the middle as the water vapour supply was in the middle of the material. The temperature lift achieved in the middle of material was 30°C, which was 2°C more than Test1. This was likely to happen as the water vapour was difficult to move upward in Test 1. Conversely, the water vapour reacts immediately in the middle of material for Test 2 as the contact point of material and water vapour was rather near.

Therefore, from this analysis, it can be predicted that the vapour transport is crucially needed to be controlled to the material as it would influence the reaction and hence, the temperature lift in the systems. Interestingly, although the dry material in Test 2 is lower by 35% from Test 1, the moisture uptake (Δm) is 55% higher (see Figure 7.24). This may be because the different percentage of $CaCl_2$ solution used in Test 1 and Test 2. In Test 1, the solution was prepared in 130%wt (2 litres of water, 1500g dry $CaCl_2$) ratio between dry $CaCl_2$ and water. However, in Test 2, the solution material was prepared in 100% wt. Therefore, due to a higher percentage of $CaCl_2$ used in Test 1, the salt might have blocked the pores of Vermiculite. Hence, in preparing the material, using a large volume of the salt solution not advisable because it will influence the absorption of water vapour in the host matrix. Furthermore, it will lead to agglomeration between the host matrix and salt solution which lowering the heat and mass transfer in the systems

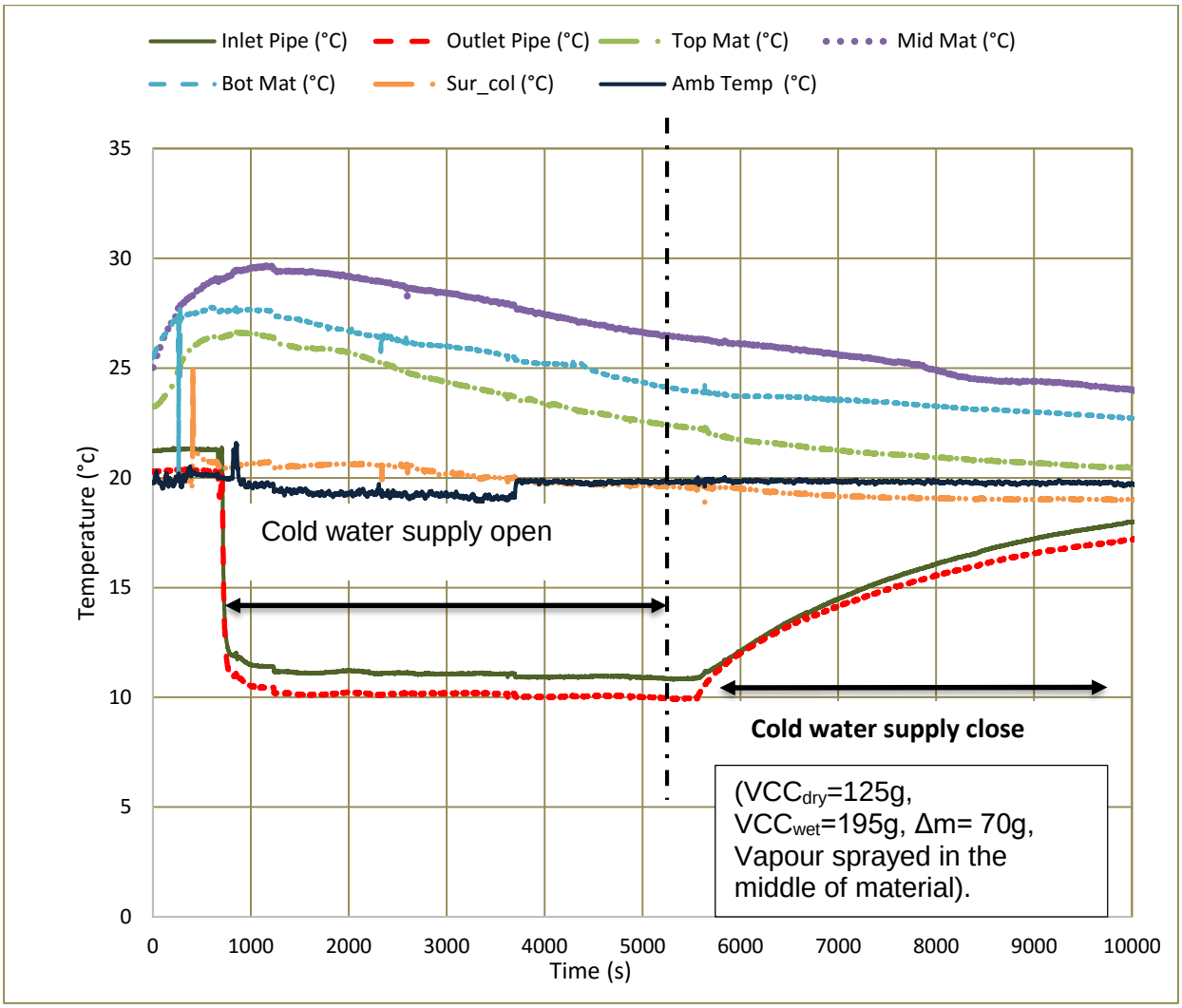


Figure 7.25: Temperature variations of inlet and outlet of domestic water, material in the perforated pipe for Adsorption Test 2

Figure 7.26, illustrates the result during desorption cycle for Test 2. It can be seen that the solar intensities have dropped from start to 1000s of the experiments. This was due to the modification of pyranometer during this period. However, the light intensities managed to maintain on average at 850W/m^2. As the result of this, 35g of moisture desorb from the total weight of wet VCC of 195g which gives 0.18 g/g wet VCC. Despite the temperature, lift is still low when compared to closed adsorption systems. However, the SHSC has

proved that the integrating the solar thermal energy will improve the water desorption percentage.

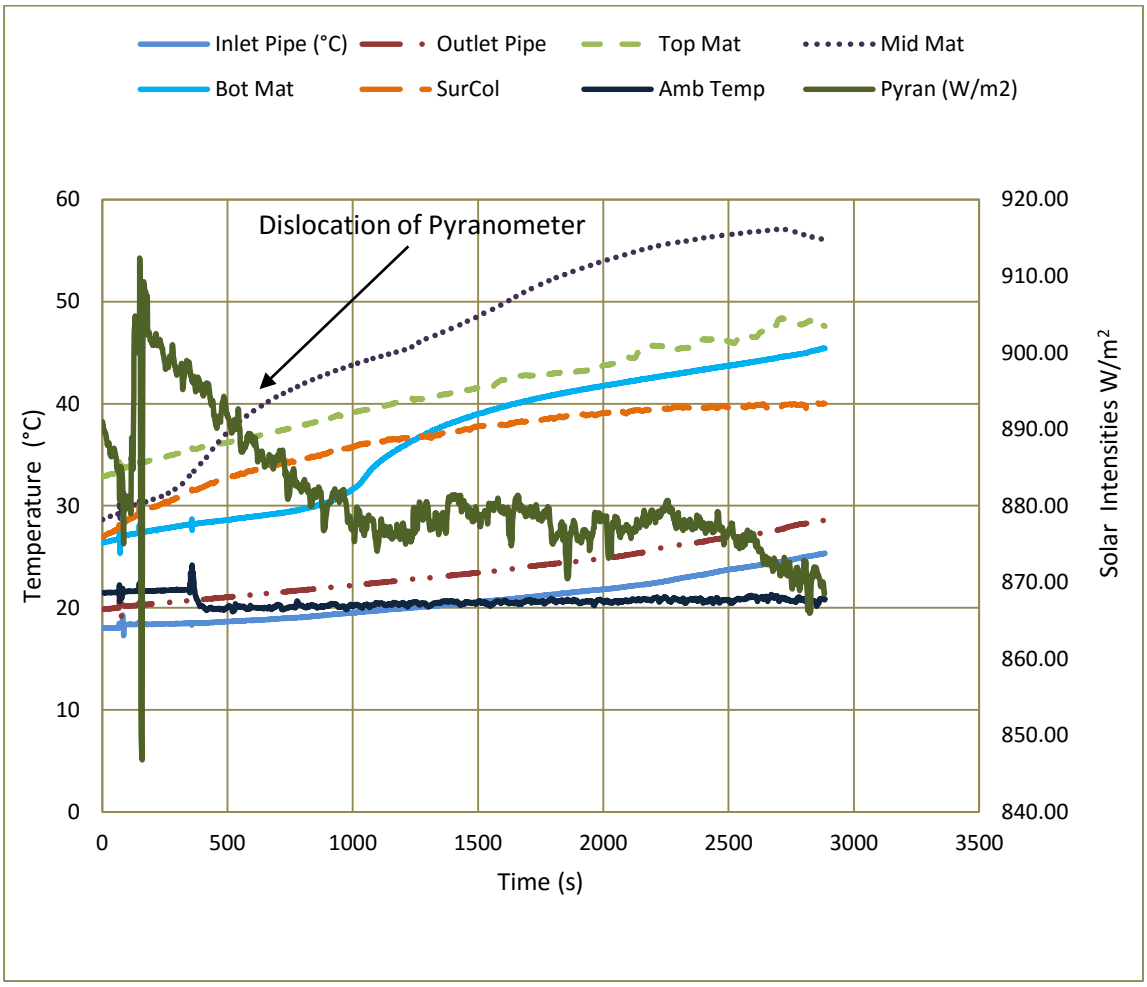


Figure 7.26: Temperature variations of inlet and outlet of domestic water, material in the perforated pipe & solar intensities for Desorption Test 2

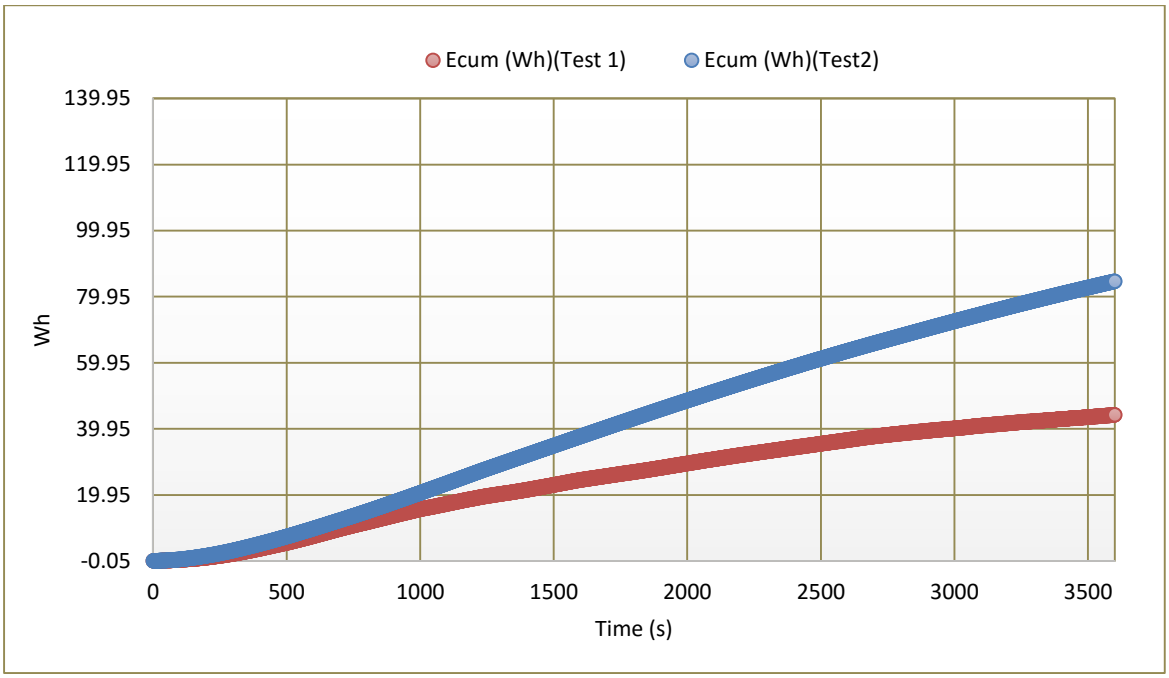


Figure 7.27: Cumulative energy for Test 1&Test 2

Figure 7.27 depicts the cumulative energy on Test 1& Test 2 in one or of the adsorption process. From these results, it can be seen that the cumulative energy of Test 2 is higher than Test 1, which were 79.95 Wh and 39.95 Wh respectively. Test 2 has higher cumulative energy because of higher temperature lift (ΔT) at °5C and higher water sorption (35% more than Test 1). With the result of this, the COP of Test 2 is greater that Test 1 ranges from 0.3 to 0.55 and 0.1 to 0.52 (see Figure 7.28). Other than that, it can be predicted that the adsorption process is effective in the range of 1000 seconds and further up to this period the COP is low due to no reaction occurred. Consequently, when compared to previous experiments in Chapter 4 & 6, lower temperature lift occurred in this experiments were due to low water uptake and low water vapour transport during the adsorption process.

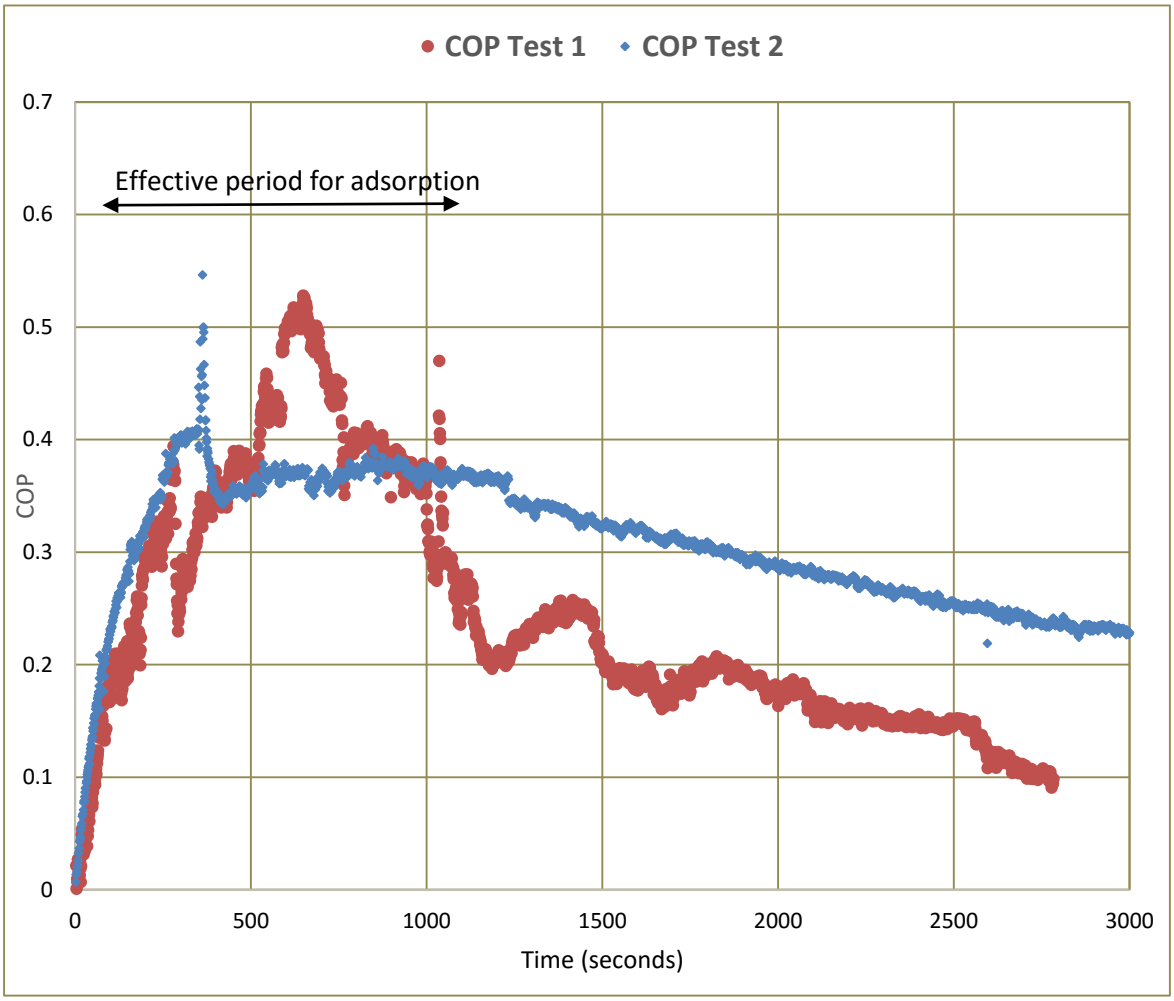


Figure 7.28: Comparison of COP Test 1 and Test 2

Table 7.5: Comparison between numerical and experimental results

Parameters	Option 1 (Numerical)	Option 2 (Numerical)	Experimental
Acol (Collector area) (m^2)	5	5	0.49
$m_{,s}$ (mass of Thermochemical material) (kg)	10	10	0.125-0.213
COP	7.89-0.78	5.6-0.83	0.1-0.55

7.6 Conclusions of the Chapter

In this study, a small scale of SHSS numerically & experimentally investigated. The main aim of this study is to investigate the alternative method of using a solar thermal energy incorporated with TES system. In the experimental investigations, it was also aiming to identify the temperature lift in adsorption process of a single evacuated tube.

Modelling results in Option 1

The theoretical simulation of SHSC with the change in several parameters has demonstrated in this study. This simulation suggests that with a constant mass flow rate of 0.07kg/s, 5m^2 of the solar collector area, and solar intensities *(I)* of 0.5kW/m^2 efficiently would generate a heat storage for 100m^2 house with a heating temperature of 42°C. In open systems, the water vapour transport which transferred by fans helps to improve the reaction and hence the heat storage in the systems. Therefore, the increase in mass flow rate of the system, it will instantaneously increase the heat transferred to the reactor/solar heat collector. However, some limitation occurs on the decreasing of outlet temperature in the process, which need to avoid. Therefore, the reactor design/SHSC design is crucial to achieving high-temperature lift with a low-temperature loss in the systems. Apart from that, this simulation suggested that the optimum mass flow rate is 0.07kg/s and the

reaction time is in the first 5 hours of the process. Consequently, to make an up most efficient and benefitting heat storage systems; hence, this is the period where the optimisation is crucially needed to attempt. Other than that, for open systems, the inlet temperature also crucially needs to be optimised to avoid the vapour condensate along the ductwork, and this will affect the output temperature in the systems.

Modelling Results Option 2

The different modelling in Option 2 is the heat transfer from the collector to the domestic cold water and then to the fan-coil unit in the room. From the discharge analysis, the simulation results suggest that with air mass flow rate of ($\dot{m}_a = 0.07\ kg/s$) & water mass flowrate ($\dot{m}_w = 0.3\ kg/s$) & 10 kg of adsorbent material will sufficient to heat 100m^2 house with fan-coil temperature of 41°C. Other than that, the optimum time for discharge would be in the range of 5 hours. However, this would be the predicted performance as suggested from the modelling result.

Comparison Modelling Results and experimental result

In the numerical study, it can be predicted that the temperature lift of 48°C could achieve. However, in the experiments, the highest temperature increase was only 30°C (see Figure 7.25). This is because only 0.125-0.213kg of the composite material was used in the experiments when compared to the numerical study of 10kg. Furthermore, the collector area utilisation in the numerical study are 5m^2 compare to only a single tube of the collector in the experiments. Other than that, in the numerical study, the water vapour transport via a fan, however, in the experiments the water vapour was transferred through an ultrasonic humidifier with a low mass flow rate. Thus, this will influence the water uptake and the

reaction. Thus, further investigation needs to be entailed on improving the water vapour transport which vital in close/open thermochemical energy storage systems.

According to the experimental results 79.95 Wh thermal energy is achieved using 0.026 m^3 of absorbent corresponding to 3075 Wh/m^3 energy storage density. In 2hr of desorption cycle, nearly 50% of moisture was disassociated from the hydrate composite materials. Thus, these experiments indicate that the composite material can be 50% dehydrate with an average of 850W/m^2 solar intensities.

Comparison between the numerical result and experimental result summarised in Table 7.5. From this analysis, it can be seen that option 1 has a higher range of COP compared to Option 2, which were 0.78 to 7.89 and 0.83 to 5.6 respectively. However, the experimental result shows lower COP range of 0.1 to 0.55. The COP in experimental has given a lower range because small amount mass for VCC (98% less) was used in the experiments hence, lowering the reaction during for adsorption process. Furthermore, only single evacuated tube solar collector used in the experiments. Hence, a large-scale of SHSC needed to be entailed to realise the actual performance of the systems.

From the numerical and experimental results, further improvement of the design on small-scale SHSS needed to be entailed to achieve higher temperatures of the absorbent. Thereby full dehydration could be achieved and improved the cyclic operations of the systems. Apart from that, this study shall be an alternative sustainable technology and affordable for space heating applications. However, these experiments considered a small scale of TES systems involving solar heat storage collector. A domestic scale of THSS will be discussed further in the next chapter of this thesis.

8. DOMESTIC SCALE PROTOTYPE OF THSS: BUILD-UP, EXPERIMENTAL INVESTIGATION, ECONOMIC & ENVIRONMENTAL ANALYSIS

8.1 Introduction

Designing a high heating capacity and efficient Thermochemical Heating/cooling storage system is an important challenge in sorption technology. Few parameter has identified on improving the design such as such as the high water uptake, good vapour transport, good heat and mass transfer, no heat loss and low energy regeneration. In considering on harnessing the availability of solar power, this will alleviate the energy required for desorption/regeneration process. Previously, most of the closed thermochemical storage systems that have been investigating were mainly using solar thermal as the heat source for the regeneration/desorption process. Most these applications were focused on cooling for buildings (Wang et al., 2008; Ogueke & Anyanwu, 2008; Louajari et al., 2011; Hassan & Mohamad, 2013; Alam et al., 2013). Using solar thermal as regeneration energy might be beneficial to hot climate countries. However, it may be difficult to realise in cold climate countries with lower solar energy availability. Therefore, using the heat pump as a heat source may become more economical to be adopted in cold climate countries. Many researchers have been taking effort investigating the integration of sorption storage system with heat pump (Banker et al., 2008; Banker et al., 2009; Cyklis 2014). However, a major disadvantage of this system is that the mechanical and adsorption segments have largely varied the cycle time. The mechanical compressor has a cycle time of a few milliseconds, while, the adsorption segment requires several minutes to complete a cycle of the

compression process. Hence, sufficiently large adsorbers will be necessary to ensure that the mass flow rate through each of the compressor is simultaneous. Therefore, this limitation will lead into a more detailed investigation for more efficient heat storage. More importantly, compactness of system design will result in more economical and feasible to adopted in residential housing.

Objective

In the literature review, most studies in the field of thermochemical adsorption systems focussed on the application of air-conditioning, refrigeration, and ice-making systems. The experimental investigation of THSS is still minimal or difficult to find in the literature. Therefore, the aim of this chapter is to investigate the performance of a domestic-scale THSS prototype that could utilise for space heating or hot water systems in the buildings. This investigation also implicates of analysing the performance of using the heat pump as a heat source on desorption period. Other than that, to minimise the electrical consumption for the heat-pump, low-grade energy was used as a heat source on the evaporator side. This alternative will simplify the concept of ground source heat-pump which commonly available in the market. Although substantial studies have carried involving a close Thermochemical heat storage system, however, using the heat pump as a heat source for the desorption process as yet to be discovered. More importantly, the most efficient Thermochemical heat storage design is vital to retain the heat stored in the systems and utilising it in the next cycle. Therefore, in this study several design option discussed in considering the factors that affected the performance of the systems.

8.2 Experimental set-up

The initial arrangement of a domestic-scale THSS shown in Figure 8.1. As can be seen that, the THSS was constructed in a vertical arrangement. This structure is similar to the

small-scale prototype. However, the evaporator section is located at the top of the adsorbent pipe, whereas, the small-scale THSS the evaporator was at the bottom. The current configuration was different due to the weight of adsorbent bed was 50% higher than the evaporator section which required additional structure if the condenser section was on the top. Other than that, this THSS has also incorporated with heat transfer fluid (HTF) using water inside both sections which make the current configuration can be manufactured easily. The adsorption section filled with 10kg of vermiculite+$CaCl_2$ and in evaporation section filled with 5kg water to create a 1:2 mass ratio. The weight was estimated to meet the demand of hot water boiler on typical diurnal of 24kW.

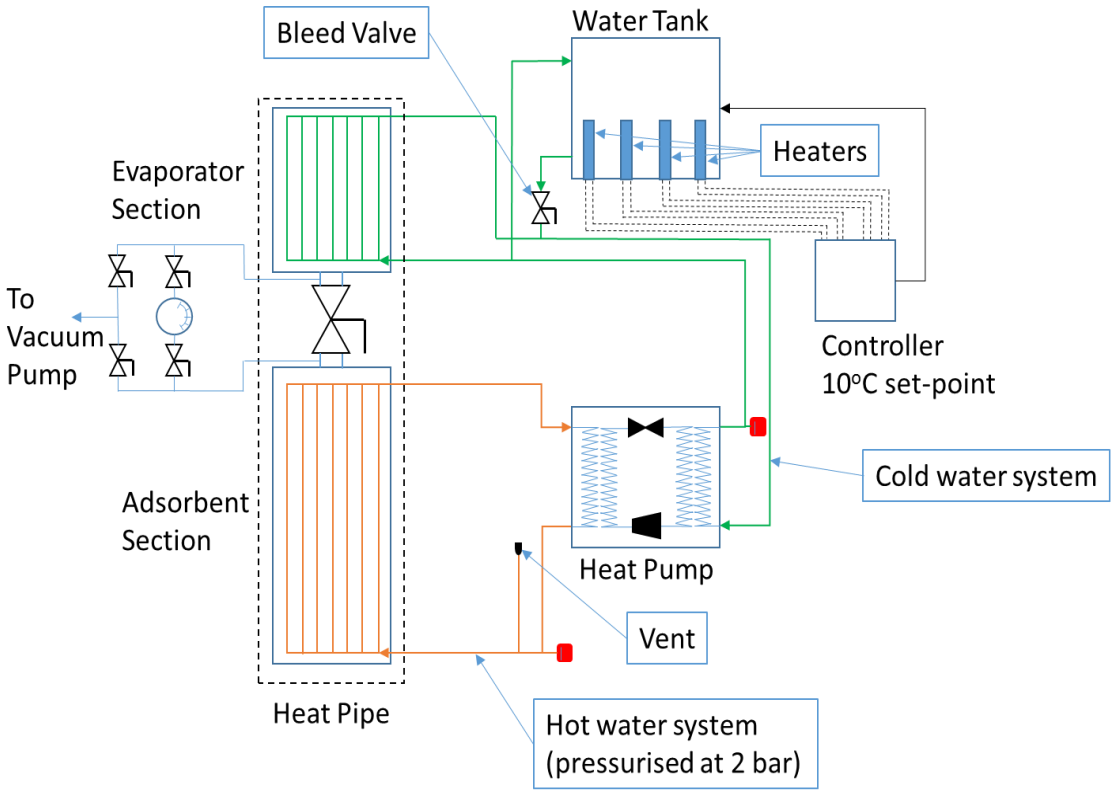


Figure 8.1: Initial Arrangement of the Heat Pipe Assembly for Testing

The main structures & operations of THSS describes as follows;

i. The water tank simulates as a low-grade heat source (ground source) for the evaporator section.
ii. Pipe arrangements through both evaporator and adsorbent sides of the THSS are connected in parallel to optimise flow rate of HTF (heat transfer fluid).
iii. On desorption/charging cycle, the heat pump provides a heat source via an HTF across the heat-pipe, which is designed to allow the adsorbent in the adsorbent section to dissociate Vermiculite +$CaCl_2$ and water vapour.
iv. The water vapour was condensed at the low temperature inside evaporator section. The ball valve on the heat pipe remains open during this operation.
v. Between charging and discharging the ball valve on the heat pipe is closed to protect the adsorbent material from any contact with water.
vi. During discharge of the system, the heat pump is turned off, and the temperature difference between the hot water and the cold water systems is allowed to reduce to zero. The ball valve on the heat pipe opened.
vii. Water vapour from the evaporator section is allowed to move into the adsorbent section where it will react with the dry adsorbent material to generate heat. This heat will increase the temperature of the water in the hot water system that can be monitored via a data logger.
viii. Both hot and cold water systems filled with water/33% glycol mix to minimise freezing inside the pipe.

8.2.1 Construction of THSS

The assembly design of the heat pipe shown Figure 8.2 below. As can be seen that, the adsorbent and water cartridge arranged in hexagonally for easy fitting inside the evaporator

and adsorbent section. The heat pipe system was constructed in stainless steel. The full construction of THSS is shown in Figure 8.3 & Figure 8.4. As can be seen in Figure 8.3, the THSS is integrated with the heat-pump circuit and a low-grade temperature heat source to simulate as a ground heat source temperature for the heat-pump. Other than that, a load (in the form of a car radiator) was added to the hot water system to ensure that the heat pump would operate constantly. A 3kW inline Willis heater was also added to the hot water circuit.

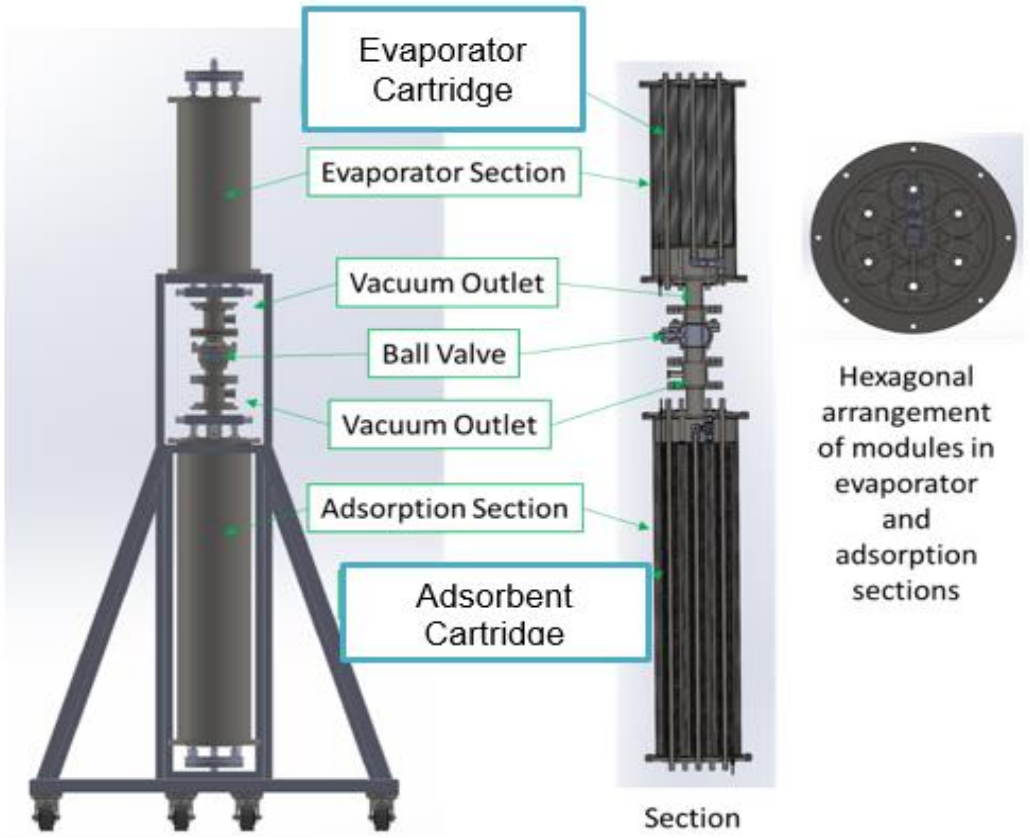


Figure 8.2: THSS Design

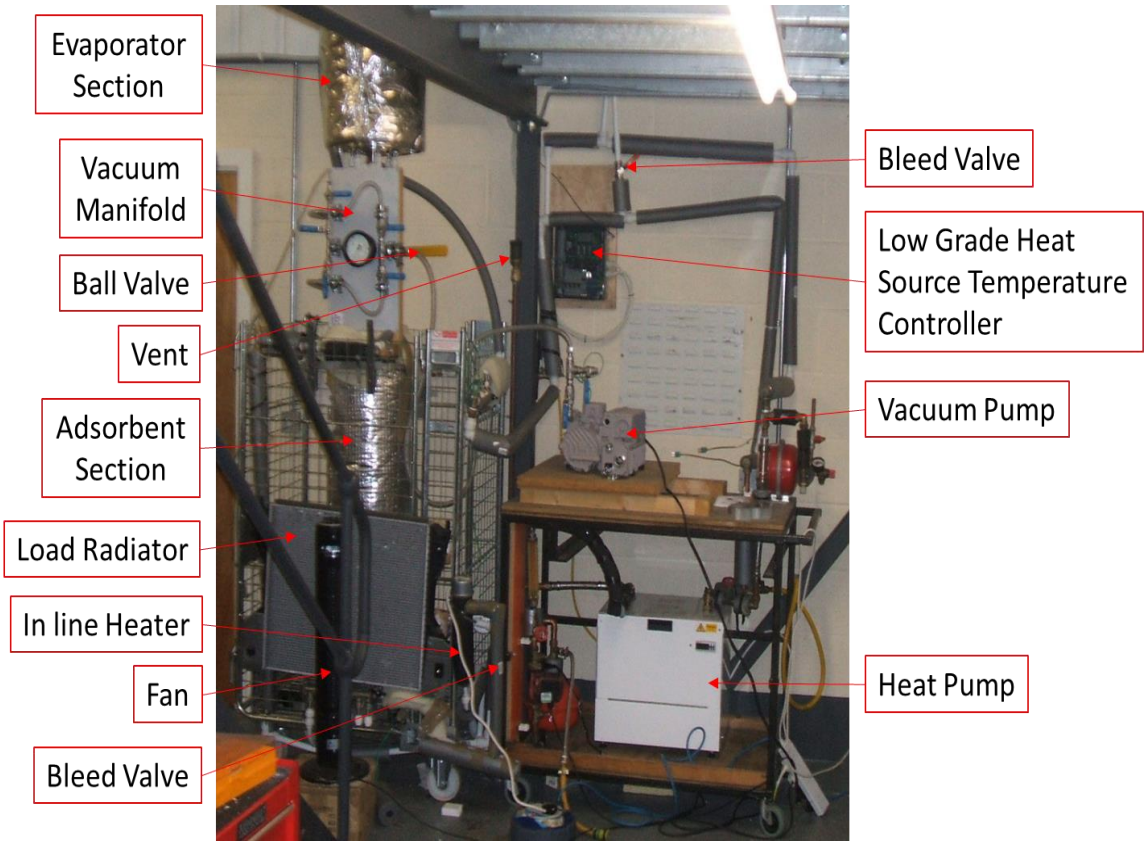


Figure 8.3: Constructed THSS System

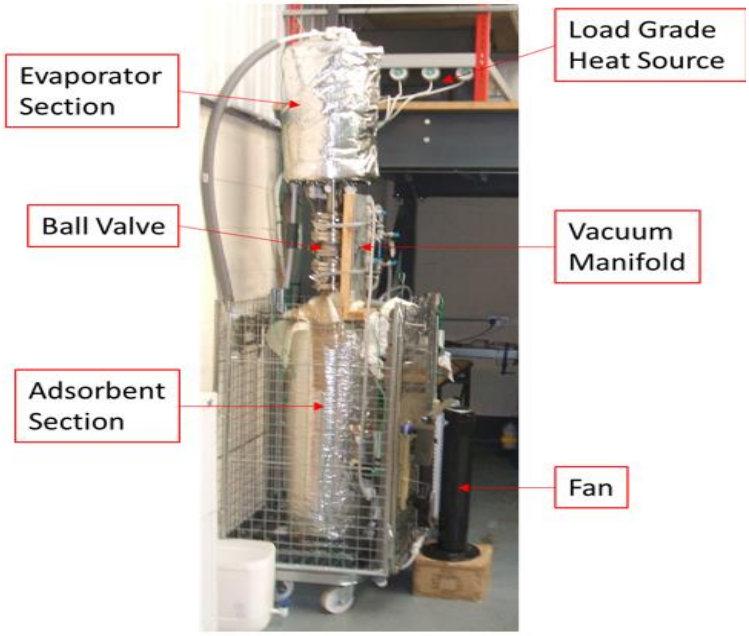


Figure 8.4: Heat pipe section of constructed THSS

8.2.2 Construction of Adsorbent & Evaporator cartridge

Figure 8.5 exhibits the adsorption section of the heat-pipe. As can be seen that, seven number of pipe was extruded outside of the adsorption section to ease the connection with the heat-pump circuits. Other than that, a K-type thermocouple was inserted into the pipe before the full assembly taken place. The evaporator section has a similar construction with the adsorbent section. However, the size of evaporator section is approximately half of the adsorption section. Figure 8.6 illustrates the adsorbent cartridge construction using a copper wire and aluminium wick similar with the small-scale prototype THSS. This construction and the material was choosing to enhance the heat and mass transfer in the systems. Other than that, evaporator sections in Figure 8.7 & Figure 8.8 showed that this section has similar construction with the adsorption section, whereas, the evaporator section cartridge using a cotton wool to ease the evaporation process. As mentioned in the experimental set-up the cartridge was arranged hexagonally. Hence, Figure 8.9 indicates the arrangement of cartridges inside the evaporator sections. Both sections were insulated before connected with a ball valve as shown in Figure 8.10 & Figure 8.11.

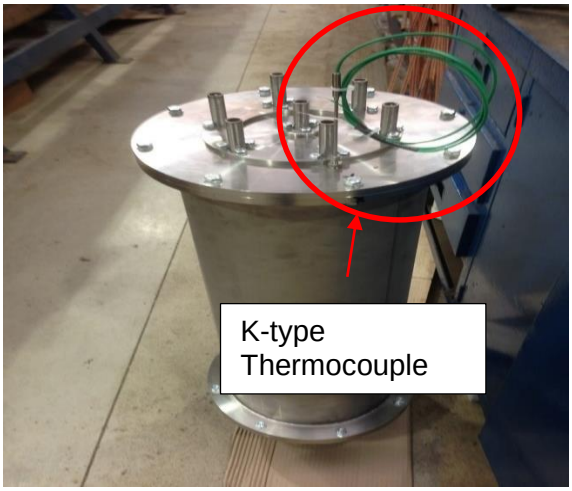


Figure 8.5: Adsorption section



Figure 8.6: Adsorbent cartridge for the adsorption section



Figure 8.7: Water cartridge for the evaporator section



Figure 8.8: Cotton wool installed in water cartridge in evaporator section



Figure 8.9: Water cartridge installed inside the evaporator section



Figure 8.10: Side view of adsorbent section (Fully insulated)



Figure 8.11: Ball valve connecting both sections

8.2.3 Thermocouple Type and Position

A K-type thermocouple used for this THSS and Figure 8.12 illustrates the thermocouple position for each section. The thermocouples were inserted at 156mm from top and bottom of the flanges to ensure the temperatures inside both adsorption and evaporator section was monitored through the data logger.

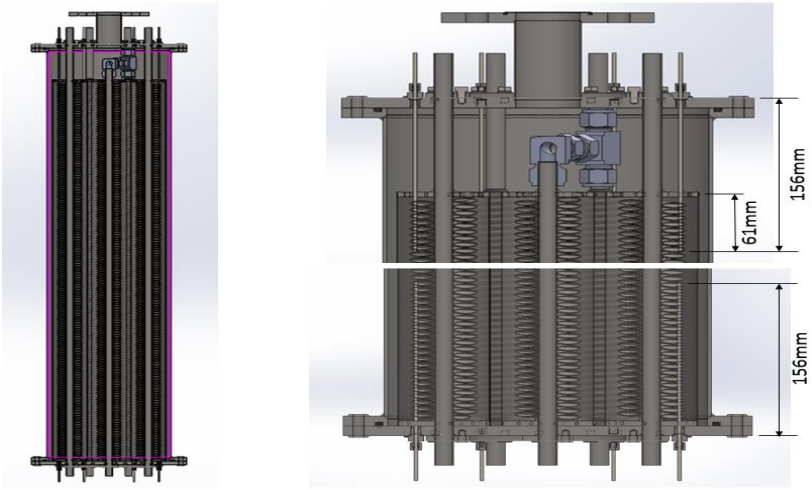


Figure 8.12: Cross section of Thermocouples position

8.2.4 Heat Pump

The heat pump used in this THSS is the Kensa Shoebox 3kW, which operates on a single compressor using R134a with a maximum delivered water temperature of 65°C. This temperature is considered sufficient for desorption process for vermiculite+$CaCl_2$ based on the experimental result for small-scale THSS. Other than that, to overcome with the automatic cut-off operation with the heat-pump, the THSS was installed with a 3kW in-line heater to maintained the hot water temperature during desorption.



Figure 8.13: 3kW Kensa Heat Pump

8.3 Analysis equations

The equations used for analysing the experimental results are given as below;

8.3.1 Adsorption process

Thermal energy release in adsorption pipe can be calculated as below equation;

$$Q_{THSS} = M_s \cdot C_{ps} \cdot \Delta T \quad (8.1)$$

8.3.2 Desorption process

The heat source for desorption process gained from the heat-pump. Hence, the heat gained from heat-pump is calculate using similar formulae in the mathematical modelling as depicts below;

$$Q_{hp} = \dot{m}(h_{2-} h_3) \quad (8.2)$$

8.3.3 Performance

The COP of THSS circuit at any time (t) instant calculated as;

$$COP_{THSS} = \frac{Q_{THSS}(t)}{Qhp(t)} \quad (8.3)$$

8.4 Experimental result and discussions

8.4.1 Initial trial issues and piping modification

A few trial has been conducted and found that the heat transfer from the water pipe to the adsorbent material is weak, and affected the desorption process. The disassociation of water particle from the hydrated adsorbent material was unsuccessful. This affected the adsorption process in the next cycle, where it was also found that there a no temperature different in the adsorption section. Hence, modifications were made to the heat pipe system

to improve the performance for desorption. The piping through the adsorbent and evaporator sections modified to a serial arrangement. This will reduce the flow rate of the hot water through the adsorbent section and gave a longer path for the heat transfer. Other than that, as the heat pump operates with automatic shut-off control systems, the heat-pump was found to stops in the middle of desorption process. Hence, this will affect the performance during desorption. Therefore, a heating load (in the form of a car radiator) was added to the hot water system to ensure that the heat pump would operate over a longer period and maintained a constant temperature. The revised arrangement is shown in Figure 8.14 and the thermocouple position illustrated in Figure 8.15. Table 8.1 indicates the thermocouples number and descriptions.

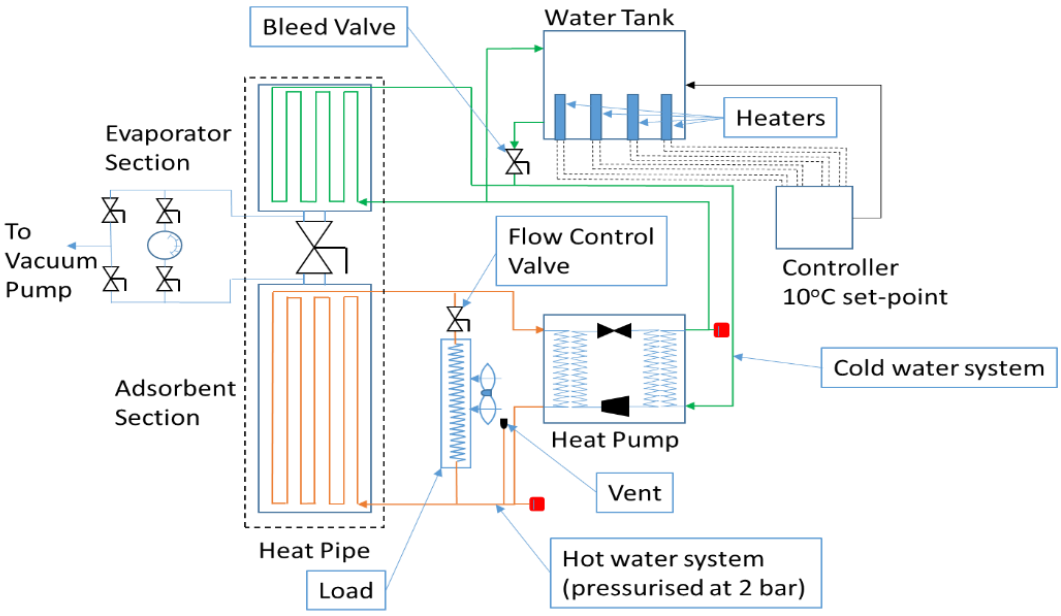


Figure 8.14: Revised Heat Pipe Arrangement

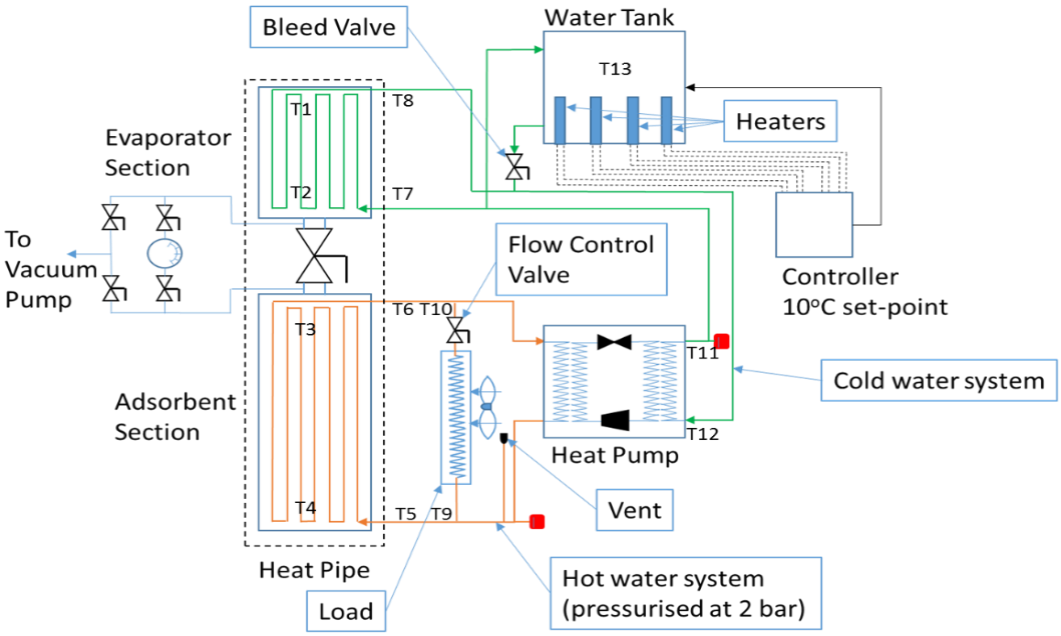


Figure 8.15: Final Schematic Arrangement for the THSS & Thermocouples position

Table 8.1: Thermocouple position and descriptions

Number	Descriptions
T1	Top of Evaporator section temperature
T2	Bottom of evaporator section temperature
T3	Top of adsorption section temperature
T4	Bottom of adsorption section temperature
T5	Inlet temperature of adsorbent section
T6	Outlet temperature of adsorbent section
T7	Inlet temperature of evaporator section
T8	Outlet temperature of evaporator section
T9	Inlet temperature of radiator
T10	Outlet temperature of radiator
T11	Inlet temperature of heat-pump evaporator
T12	Outlet temperature of heat-pump evaporator
T13	Water tank temperature

8.4.2 Overall performance

The system has shown improvement when tested using a new piping arrangement. At the adsorption process, the temperature of the adsorbent material reached 57˚C and the

temperature in the evaporator reached at 13°C. The temperatures at various points in the system during desorption showed in Table 8.2. The calculated overall performance of the systems shown in Table 8.3. The calculated heat gained from the adsorption process is 1407.6 kJ/kg with a corresponding COP of 0.13. The overall performance of THSS estimated based on the temperature lift from the adsorption and desorption process. Lower COP calculated is due low-temperature lift during the adsorption process. Nevertheless, this system has the heat storage capacity of 364 kWh/m^3 calculated based on the density of VCC (175 kg/m^3)(Aydin et al., 2015a).

Table 8.2: Steady-State Temperatures Monitored in the Pipe System during desorption

Temperatures (°C)										
T1	T2	T3	T4	T5	T6	T7	T8	T9	T10	T11
8.3-8.9	11.9 - 14.1	60.3-62.1	Not monitored	59.2-85.8	64.2-66.4	6.3-9.3	3.4-4.0	52.0-55.2	40.6-52.7	4.4-7.9

Table 8.3: Overall performance of Domestic-Scale THSS

DESCRIPTION	**Result**
Maximum Adsorption Temperature (°C)	57
Q_{THSS}(kJ/kg)	1407.6
Q_{THSS}(kWh/m^3)	364
COP THSS	0.13

8.5 Economic Analysis

A simple economic analysis and environmental analysis presented in this section, including sensitivity analysis methods of net present value (NPV) and internal rate of return (IRR) using Single Payment present worth factor (SPPWF). The equation for SPPWF shown as below:

$P = F[1/(1+i)\text{^}n]$ (Apostolakis, 2007) (8.4)

The factor $\frac{1}{(1+i)^n}$ in equation 8.4 is known as SPPWF, where (F) represent the future worth, n is years, (P), Present worth at interest of 'i' (per year).

8.5.1 Impact on energy price with inflation rate of 7%

Before the estimation of running cost being analysed, the energy price increased calculated by using the assumption of the inflation rate of 7% each year. The energy price in this analysis is referring to DECC (2015) and E.ON (2015) websites as below tariff:

i. Gas: 7.29p/kWh for the first 2680kWh per year and then 4.79p/kWh
ii. Electricity: the day units: 24.64p/kWh for the first 900kWh per year and then 15.88p/kWh, night units: 7.12p/kWh

Figure 8.16 illustrates the impact of the inflation rate to the energy prices. It is clearly shown that, in 20 years of time, the gas price increased 17p/kWh and the electricity price increased 60p/kWh. Hence, this price increased will use to analyse the economic viability of THSS in the next 20 years.

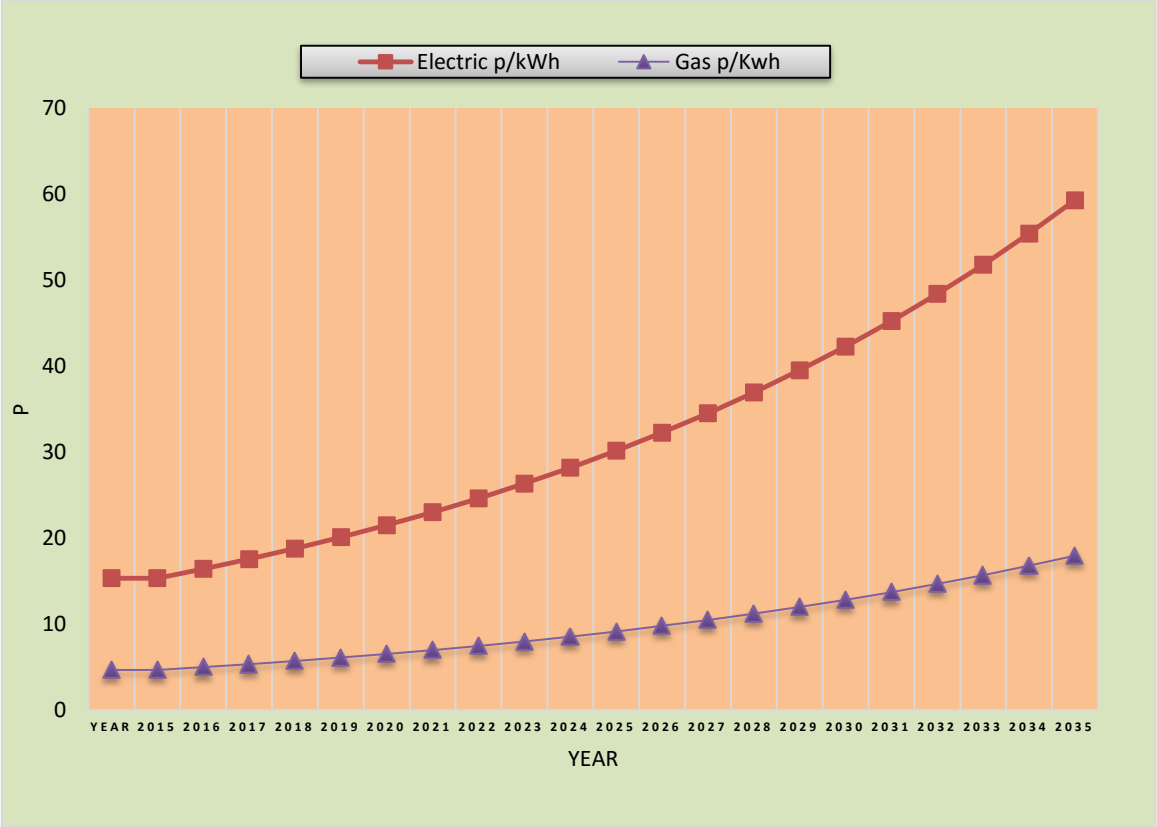


Figure 8.16: Energy Price with inflation rate of 7%

8.5.2 Capital and Running Cost for THSS

The estimation of capital cost for the THSS listed in Table 8.4. The basis for estimating this capital cost is using the construction cost of the THSS and other auxiliary equipment included in the whole system such as heat pump and in-line heater. The capital cost also included the labour cost and other cost incurred in real commercialise item such as VAT (value added tax of 20%). Hence, with 50% estimated in the reduction of mass production of this system, the total capital cost will be £5,217.10. The running cost for conventional systems based on a 24kW boiler and Table 8.5 listed all input parameter for the calculations.

Table 8.4: Capital Cost for THSS systems

Equipment	£	
THSS	4,000.00	(ETL Ltd, 2014)
Thermochemical material (Vermiculite +$CaCl_2$)	443.00	(Aydin et al., 2015b)
Piping	300.00	(Ding, 2013)
3kW Willis heater	42.00	(Willis, 2015)
3kW Heat pump	2,950.00	(Kensa Heat Pump, 2015)
water tank	185.93	(Ding, 2013)
radiator	105.38	(Ding, 2013)
Total Cost exclude VAT & labour	8,026.31	
Labour (10% of total)	802.63	
VAT (20%)	1,605.26	
Total	10,434.2	
50% of mass production	5,217.10	

Table 8.5: List of input parameters for THSS

Input parameters	**Value**	**Units**
Capital Cost	5217.10	£
Gas and electricity inflation rate	7 (Carbon, 2014)	%
Annual market discount rate	8 (Wu, 2014)	%

The estimations of running cost and Net Present Value (NPV) of THSS indicates Appendix F-1, the initial operation and maintenance (O&M) cost of £300 and annual growth of 3%. Other than that, it was assumed that the running cost incurred from the consumption of 3kW heat pump for desorption process at night–time. In this table, it can be seen that the annual running cost for THSS are £546 and gives the NPV of £-13,458.02 in 20 years of lifespans. The NPV is the present value of investment by the discounted sum of all cash flows received from the project. Therefore, the negative value indicates that the amount of money spends for the project. Furthermore, sensitivity analysis methods of the net present value (NPV) and internal rate of return (IRR) are introduced to evaluate this proposed novel system. Both NPV and IRR are primarily used in capital budgeting for companies to determine whether a

new investment or expansion opportunity is valuable. Hence, with the investment prospect, any company need to make a decision whether the investment will generate net economic profits or losses for the company regarding NPV and IRR.

8.5.3 Payback period, saving and IRR

From the estimation of the running cost spends on THSS saving, the payback period of the THSS can be calculated. This result shows that this THSS will pay for itself in approximately 7.5 years (see Figure 8.17). The 20 years of NPV are £13,458.46 (Appendix F-2) with the internal rate of return of 15.25% (see Table 8.6). This value of IRR is higher than the required rate of return (annual market discount rate, 8%), which means this system is viable to be employ in term of 20 years' system lifespan.

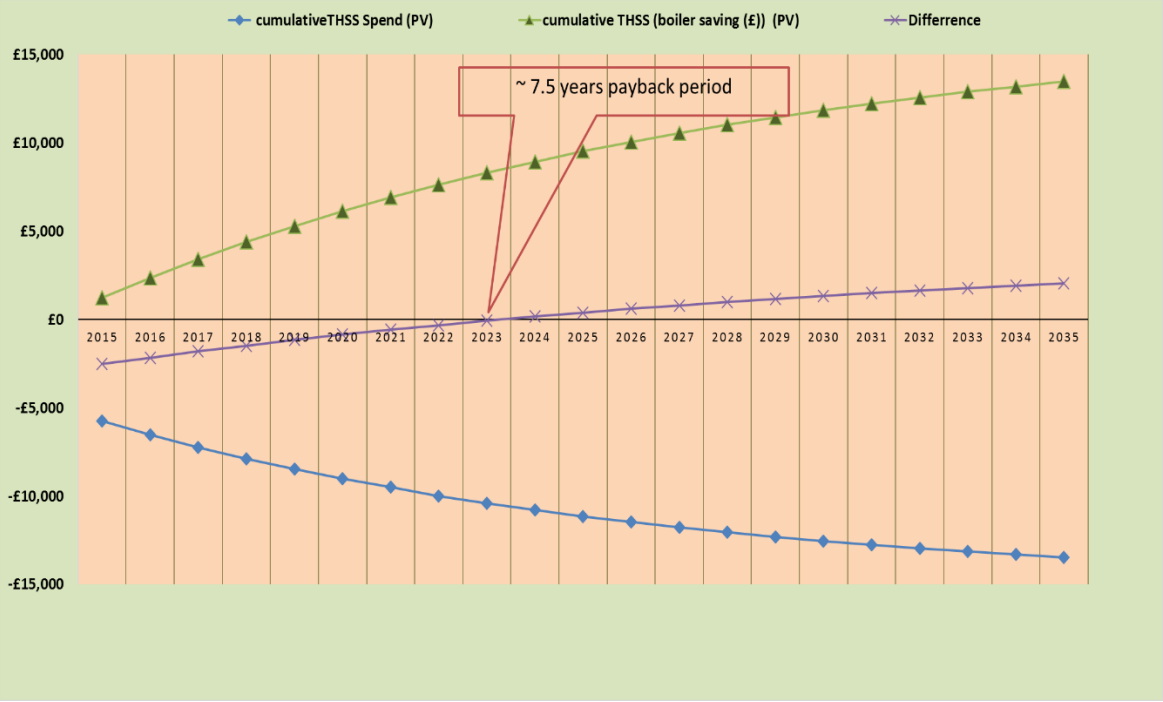


Figure 8.17: THSS spend, saved and payback period

Table 8.6: Discount rate of THSS

Discount rate	**15.25%**	For Present Value calculations	
IRR is the discount rate that produces a Present Value of zero			
20 year IRR for THSS			
	THSS Spend Present Value	THSS- Present Value	Total Present Value
	-£13,458.02	£13,458.46	£0

8.6 **Environmental analysis**

The UK has targeted to reduce carbon dioxide (CO_2) emissions by 80% below 1990 levels by 2050 (Department of Climate Change, 2015). Hence, to realise this in the future, more low-carbon technology needed to be employ. The THSS integrated with a ground heat source and operated at the off-peak period will reduce the energy consumption of a conventional boiler and hence reduce the CO_2 emission. The analysis for emission reduction was based on the UK Guidelines and reports on employing low carbon technology (Carbon, 2014). The emission factor used in this analysis are according to below equations;

$$\text{Carbon Dioxide Emission (kg} \cdot \text{ CO}_2\text{/year)} = \text{Electricity (kWh/year) x } 0.517 \quad (8.5)$$

$$\text{Carbon Dioxide Emission (kg} \cdot \text{ CO}_2\text{/year)} = \text{Gas (kWh/year) x } 0.185 \quad (8.6)$$

Figure 8.18 exhibit the cumulative emissions of THSS and Boiler in the next 20 years. From these results, it can be seen that the boiler has higher Tonnes of CO_2 emissions compared to that of THSS, which are 5648.95 tonnes CO_2-e and 3728.21 tonnes CO_2-e respectively. With the result of this, the emission will reduce 34% in 20 years of lifespans of the THSS. The reduction of emission can be improved more if the heat-pump consumption is reduced by using ground heat source which required lower energy (GSHP, 2016).



Figure 8.18: Cumulative GHG emission for THSS and Boiler in 20 years of lifespan

8.7 Conclusions of the Chapter

In this chapter, the build-up and experimental of a domestic-scale THSS analysed and discussed. The domestic-scale THSS has shown that a temperature lift from the adsorption process is 57°C from the initial temperature of 11°C. This result showed that the domestic-scale THSS has potential temperature uplift appropriate for heating purposes in the building. However, limitation occurred during the desorption which the disassociation of water particle from the hydrated composite material was not up to satisfactory level. Hence, more improvement needed to be entail to overcome this limitation. Nevertheless, the analysis was carried out based on the temperature lift and the usage of a heat pump during desorption. Therefore, by using this basis, the energy storage per unit volume calculated is

364kWh/m^3 with a corresponding COP of 0.13. The economic analysis has shown that this THSS could receive its payback in 7.5 years with IRR (Internal rate of return) of 15.25% This payback range is below ten years indicating that this system is viable to be employed in the future. Other than that, from the emissions analysis results has shown that the CO_2 emission of this systems is 3728.21 tonnes CO_2^{-e} in 20 years of its lifespans. Hence, with this will give the reduction of emissions of 34% up to the end of life of the systems. The emission can be further reduced if the systems integrate with a ground source heat pump, which consumes lesser energy compared to the conventional heat pump systems. Furthermore, an actual installation of THSS system in a new or retrofit household shall be more realistic and added reliable data in THSS research.

9. CONCLUSIONS AND FURTHER WORKS

9.1 Introduction

Thermochemical Heat Storage System has received significant interest in the last few decades to overcome the problems with high demand for cooling and heating in buildings. Furthermore, with these systems will promote more low-carbon technology to be adopted for a better environment. This thesis investigates experimentally and theoretically the potential of the different type of thermochemical materials, a small-scale Thermochemical Heat Storage Systems, a small-scale Solar Heat Storage collector and finally a domestic-scale Thermochemical Heat Storage System.

9.2 Main conclusion

In this section, the principal finding of each chapter and key points conclude the research contributions.

9.2.1 Literature Review (Chapter 2)

A detailed review concerning the Thermochemical Energy Storage technology developments and possible thermochemical materials that were currently investigated by researchers were discussed in Chapter 2. Findings from literature review showed that new composite materials are known as ‘salt inside matrix’ have high heat storage capacity, improve heat and mass transfer of chemical adsorbents, increase adsorption quantity, low desorption temperature and environmentally friendly. Most potential working pairs are of using the host matrix of silica gel, vermiculite and metal chlorides due to their potentials properties as mentioned before. Furthermore, the reviewed of mathematical simplification has found that most of the researchers employing the lumped parameter model due to its

most explicit and easy to integrate with any numerical software. Other than that, to overcome with low heat and mass transfer (HAM) in THSS, the researcher used the method of embedding the adsorbent material in the heat exchanger fins to enhance the HAM.

9.2.2 Thermochemical Material Screening, Synthesizing and Optimization (Chapter 4)

Most potential TCMs were selected for screening, synthesize, and optimize in Chapter 4. From adsorption test of using horizontal glass and metal rig, it was found that Silica Gel+$CaCl_2$ has the highest temperature uplift of 72.70°C compared molecular Sieve+$CaCl_2$ and Vermiculite +$CaCl_2$ which is 68.20°C and 67.25°C respectively. Continuity from the horizontal rig, another test has conducted using a vertical glass and metal rig. The different between the horizontal rig and the vertical rig was the installation of heat source at the adsorption pipe to use in desorption process. From these two configurations, the results showed that pressure loss were insignificant in vertical rig. Furthermore, the temperature increase during the adsorption process without repeating the vacuum pump. Two working pairs were selected for these experiments based on the temperature lift from the horizontal rig. The working pair consists of silica gel+$CaCl_2$/water and Vermiculite+$CaCl_2$/water. From this test, vermiculite+$CaCl_2$ has chosen as the potential candidate for THSS due to high-temperature lift of increased from initial of 21.46 to 48.36°C. Other than that, the temperature drop is lower compared to that of the silica gel+$CaCl_2$. Through the microscopic investigations of Environmental Scanning Electrometry Microscopic (ESEM) and Scanning Electrometry Microscopic (SEM) has found that, the TCM of using a host matrix of silica gel showing a rupturing after the hydrating process. However, no significant changes in the structure of host matrix of Vermiculite. Other than that, the host matrix of vermiculite showed larger pores compared to silica gel. Hence, the ESEM and SEM results suggested that the host matrix vermiculite has a strong structure when exposed to high temperature, and larger

pores will give an advantage on absorbing water for adsorption process. This result was defended by another investigation on pore size distribution and pore volume through Mercury Intrusion Porosimetry (MIP). From this survey, it was found that Vermiculite has a considerably large pore volume and large nominal pore size of 4.12cm^3/g and 4.0µm respectively. Other than that, from differential scanning calorimetry (DSC) had shown that vermiculite +$CaCl_2$ has a higher heat storage capacity (374 KJ/kg) compared to silica gel.

9.2.3 Performance investigation of Thermochemical Heat Storage Systems (THSS) with different type of heat source (electric, heat pump circuit using different refrigerant gases of R134a and R1234yf & solar thermal) (Chapter 5)

Numerical analysis has conducted to investigates the performance of THSS using a different kind of heat source for desorption which consisting of an electrical clamp heater, a heat pump circuits and solar thermal. Four influence factors have included in the analysis involve the heating temperature, change of mass of adsorbent material, desorption time and solar collector area. From these simulations, Q_{ads} of heat-pump circuit was higher than that of using the electric clamp. The Q_{ads} of using heat-pump circuit of ranges from 0.0009 to 1.18 kW and Q_{ads} of using electric clamp ranges from 0.02 to 0.38 kW. The COP of using heat-pump circuit of R1234yf was higher than that of the electric clamp and solar thermal. This COP ranges from 0.05 to 9.4.

9.2.4 Build up and experimental testing of a small-scale THSS (Chapter 6)

A small-scale THSS has built and tested for its performance in term of energy storage density and COP. The build-up was based on the experimental in Chapter 3 and numerical analysis from Chapter 5 of using Vermiculite+$CaCl_2$ and R134a for adsorption and desorption process. The influence factor used based on the weight ratio between Thermochemical material and water. The weight ratio used is 1:1 and 1:2. From this analysis it was found the weight ratio of 1:2 has higher temperature lift of 57.20°C to 71.10°C with

calculated heating storage capacity of 281kWh/m^3 to 474kWh/m^3 and corresponding COP of 0.53 to 1.34. Despite limitation to a small-scale, the result has shown that this TCM has the potential to be employ for THSS. Furthermore, the R134a circuit build-up using the smallest compressor that hitherto hardly found in the literature.

9.2.5 Performance investigation of Solar Heat Storage Systems (SHSS) (Chapter 7)

Another investigation involving a solar thermal energy incorporated with thermochemical heat storage has conducted numerically and experimentally. Two design options consist of air-to-air heat exchange and air to water heat exchange have numerically investigated. From the numerical results of Option 1, it was found that with a constant mass flow rate of 0.07kg/s, 5m^2 of the solar collector area, and solar intensities *(I)* of 0.5kW/m^2 efficiently would generate a heat storage for 100m^2 house with a heating temperature of 42°C. The simulation results of Option 2 suggested that with air mass flow rate of ($\dot{m}_a$=0.07 kg/s) & water mass flowrate ($\dot{m}_w$= 0.3 kg/s) & 10 kg of adsorbent material will sufficient to heat 100m^2 house with fan-coil temperature of 41°C. Other than that, the optimum time for discharge would be in the range of 5 hours. According to the experimental results 79.95 Wh thermal energy was achieved using 0.026m^3 of absorbent corresponding to 3075 Wh/m^3 energy storage density. In 2hr of desorption cycle, nearly 50% of moisture was disassociated from the hydrated composite materials. Thus, this experiment indicates that the composite material can be 50% dehydrate with an average of 850W/m^2 solar intensities. Despite of limitation on a single evacuated tube used in the experiments, this SHSC proved the potential on harnessing the solar thermal energy integrated with thermochemical energy storage.

9.2.6 Domestic-scale prototype of THSS: building up, experimental investigation, economic & environmental analysis (Chapter 8)

Lastly, in this investigation, a domestic-scale of THSS was built and tested for its performance in terms of energy storage per unit volume and COP. Using a basis of a household diurnal of 24kW and 10kg of TCM (Vermiculite+$CaCl_2$), 57°C the temperature from adsorption process achieved. With the result of this, the heat storage per unit volume calculated is 364kWh/m^3 with a corresponding COP of 1.2. Economic & environmental analysis has also investigated on this domestic scale prototype by using the inflation rate of 7% on energy price, and Single Payment present worth factor (SPPWF) method. The THSS will pay for itself in approximately 7.5 years with NPV (net present value) of £13,458.46 and the internal rate of return are 15.25%. The environmental analysis has found that 3728.21 tonnes CO_2 will reduce in 20 years of its lifespans.

9.3 Further Works

This thesis presented research efforts towards the investigation of a novel Thermochemical Heat Storage system, and it considered as a strong foundation for further work. The following is a list of the suggested future work;

- This thesis has presented Thermochemical Material Screening, Synthesizing, and Optimization. In this study, more works need to be entailed to investigate the kinetic behaviour of a novel Vermiculite+$CaCl_2$ as it was limited to find in the literature. Moreover, the measurement of water sorption was carried out by measuring weight before and after experiments by dismantling the whole systems. This method may affect the accuracy of water sorption measurements. Hence, more accurate method of the synthesising need to be entailed such as using a high accuracy machine such as Rubotherm magnetic suspension balance. The kinetic behaviour such as vapour pressure and water sorption can be measure without interfering with the prepared

sample. Moreover, to validate the heating temperature effect, more testing is required to validate against the numerical results.

- This thesis has presented the small-scale of THSS investigation, and further works are needed to have more detailed research data. The small-scale of THSS need to be reconstructed with heat-source pipe inside the adsorption section to avoid temperature loss at adsorption and desorption test. Furthermore, a method of measuring a vapour transport required to be entail to ensure the effectiveness of adsorption and desorption process.
- Similar works need to carry out in the domestic-scale of THSS system as limitation occurs on low vapour transport in the systems. Two options have recommended to overcome this problem were as follow:

    - **Option 1**

    Due to lack of disassociation of water vapour from hydrated TCM material, some further works need to investigate. One other possible piping arrangement option is to make the both section in serial connecting via a ball valve (see Figure 9.1). Other than that to overcome with low vapour transport in the THSS, an internal fan will install in the adsorption section during the construction of the system. This will create a force convection inside the heat-pipe and hence will improve mass transfer in the system. However, any leakage from the installation needs to be avoided to ensure that the system is perfect vacuum during the operations.

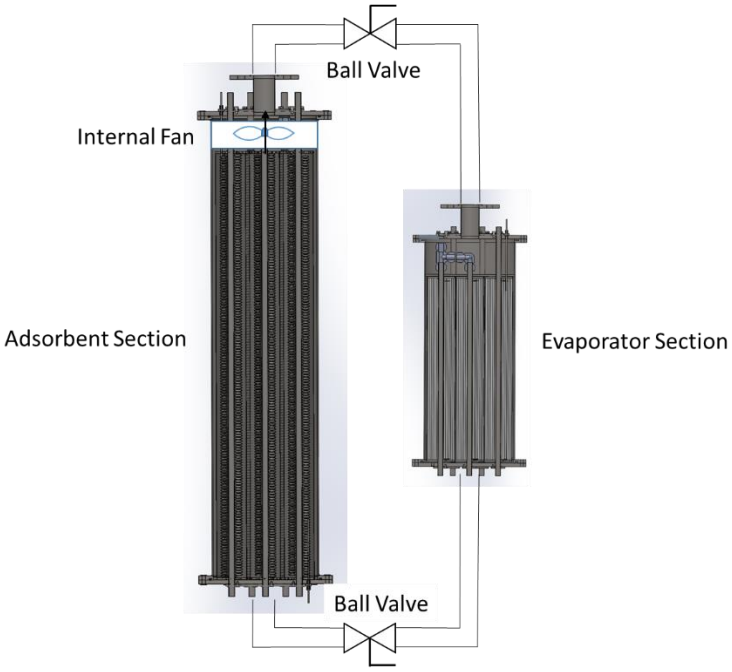


Figure 9.1: Proposed Modification to Heat Pipe, Circulate Water Vapour through Evaporator during desorption

- **Option 2**

Option 2 is by rearranging the adsorption section to be at the top of evaporator section (see Figure 9.2). This arrangement is similar with the small – scale THSS discussed in Chapter 6. As the water vapour technically lighter than air, hence, the vapour will condense easier in the evaporator section when it is saturated. Chapter 3 of this thesis has proved that 0.55% of water disassociated from the hydrated TCM materials by using this arrangement. If the hydrated TCM is effective or at least 80% of water disassociated, this will improve the THSS cyclic operating conditions. Hence, more reaction will occur in the next cycle of adsorption process and more temperature uplift in the systems.

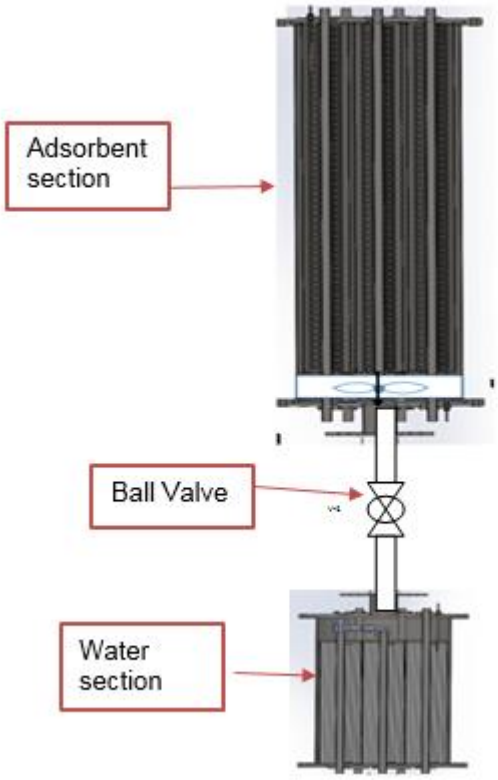


Figure 9.2: Option 2 piping arrangement

- Other than that, a heat exchanger and a fan-coil need to be included to investigate the effectiveness of heat transfer to the building. Additionally, an integration of THSS with dehumidification systems such as thermoelectric cooler (TEC) proposed by Jiang (2014) will optimise the cooling temperature receive from the evaporator section. Furthermore, a domestic-scale system required to build in the actual household to realise the performance of Thermochemical Heat Storage systems on optimising the supply and demands of heating in the buildings.

REFERENCES

Abdullah, M.O., Yii, L.P., Junaidi, E., Tambi, G., Mustapha, M.A., 2013. Electricity cost saving comparison due to tariff change and ice thermal storage (ITS) usage based on a hybrid centrifugal-ITS system for buildings: A university district cooling perspective. Energy and Buildings 67, 70–78.

Abedin, A., Rosen, M., 2011. A Critical Review of Thermochemical Energy Storage Systems. Open Renewable Energy Journal 42–46.

Abedin, A.H., Rosen, M., 2012a. Closed and open thermochemical energy storage: Energy- and exergy-based comparisons. Energy 41, 83–92.

Abedin, A.H., Rosen, M. a., 2012b. Assessment of a closed thermochemical energy storage using energy and exergy methods. Applied Energy 93, 18–23.

Abhat, A., Huy, T.Q., 1983. Heat and mass transfer considerations in a thermochemical energy storage system based on solid-gas reactions. Solar Energy 30, 93–98.

Ahmed, R., 2012. Theoretical and experimental investigation of silica gel/water for adsorption refrigeration systems. Ph.D. Thesis. University of Birmingham.

Airxchange, 2007. Use of Type A Silica Gel in Airxchange Energy Recovery Ventilation Wheels [WWW Document]. URL http://www.airxchange.com/Collateral/Documents/English-US/Use of Silica Gel Type A - Jun 2014 Final.pdf (accessed 6.12.15).

Akolekar, D.B., Kaliaguine, S., 1994. MAPO-43 molecular sieve : synthesis , characterization thermal stability. Microporous Materials 2, 137–144.

Alam, K.C.A., Saha, B.B., Akisawa, A., 2013. Adsorption cooling driven by solar collector: A case study for Tokyo solar data. Applied Thermal Engineering 50, 1603–1609.

Álvarez De Miguel, S., Gonzalez-Aguilar, J., Romero, M., Miguel, S.Á. de, Gonzalez-Aguilar, J., Romero, M., 2014. 100-Wh Multi-purpose Particle Reactor for Thermochemical Heat Storage in Concentrating Solar Power Plants. Energy Procedia 49, 676–683.

Anyanwu, E.E., Ezekwe, C.I., 2003. Design, construction and test run of a solid adsorption solar refrigerator using activated carbon/methanol, as adsorbent/adsorbate pair. Energy Conversion and Management 44, 2879–2892.

Anyanwu, E.E., Ogueke, N.V., 2005. Thermodynamic design procedure for solid adsorption solar refrigerator. Renewable Energy 30, 81–96.

Apostolakis, G.E., 2007. Engineering Risk Benefit Analysis [WWW Document]. Massachusetts Institute of Technology. URL http://ocw.mit.edu/courses/engineering-systems-division/esd-72-engineering-risk-benefit-analysis-spring-2007/lecture-notes/cba2.pdf (accessed 11.17.15).

Aristov, Yu.I. G. Resstucia, G. Cacciola, M.T., 1996. Selective Water Sorbents For Multiple Applications, 1. CaCl2 Confined In Mesopores of Silica Gel: Sorption Properties. Reaction Kinetics and Catalysis Letters 59, 325–333.

Aristov, Y., Restuccia, G., 2000. Selective water sorbents for multiple applications, 10. Energy storage ability. Reaction Kinetics and Catalysis Letters 69, 345–353.

Aristov, Y.I., 2003. Selective Water Sorbents, A new Family of Materials for Adsorption Cooling/Heating : State -Of -The -Art, in: Vminsk International Seminar “Heat Pipe, Heat Pumps, Refrigerators” September 8-11, 2003. Belarus, pp. 379–390.

Aristov, Y.I., Glaznev, I.S., Girnik, I.S., 2012. Optimization of adsorption dynamics in adsorptive chillers: Loose grains configuration. Energy 46, 484–492.

Aristov, Y.I., Restuccia, G., Cacciola, G., Parmon, V.N., 2002. A family of new working materials for solid sorption air conditioning systems. Applied Thermal Engineering 22, 191–204.

Aristov, Y.I., Restuccia, G., Tokarev, M., Buerger, H., Freni, A., 2000. Selective Water Sorbent for Multiple Applications.11 $CaCl_2$ Confined to Expanded Vermiculite. React.Kinet.Catal.Lett. 71, 377–384.

Aristov, Y.I., Sapienza, A., Ovoshchnikov, D.S., Freni, A., Restuccia, G., 2012. Reallocation of adsorption and desorption times for optimisation of cooling cycles. International Journal of Refrigeration 35, 525–531.

Aristov, Y.I., Tokarev, M.M., Freni, A., Glaznev, I.S., Restuccia, G., 2006. Kinetics of water adsorption on silica Fuji Davison RD. Microporous and Mesoporous Materials 96, 65–71.

Aristov, Y.I., Tokarev, M.M., Restuccia, G., Cacciola, G., Aristov, Yu.I. G. Resstucia, G. Cacciola, M.T., 1996. Selective Water Sorbents For Multiple Applications, 1. $CaCl_2$ Confined In Mesopores of Silica Gel: Sorption Properties. Reaction Kinetics and Catalysis Letters 59, 325–333.

Arteconi, A., Hewitt, N.J., Polonara, F., 2012. State of the art of thermal storage for demand-side management. Applied Energy 93, 371–389.

Atakan, A., Fueldner, G., Munz, G., Henninger, S., Tatlier, M., 2013. Adsorption kinetics and isotherms of zeolite coatings directly crystallized on fibrous plates for heat pump applications. Applied Thermal Engineering 58, 273–280.

Aydin, D., Casey, S.P., Riffat, S., 2015a. Numerical analysis of solar-assisted seasonal “open” thermochemical heat storage. International Journal of Low-Carbon Technologies 1–8.

Aydin, D., Casey, S.P., Riffat, S., 2015b. The latest advancements on thermochemical heat storage systems. Renewable & Sustainable Energy Reviews 41, 356–367.

Aydin, D., Casey, S.P., Riffat, S., 2014. Numerical investigation of solar thermal heat storage potential under UK climatic conditions, in: 13th International Conference on Sustainable Energy Technologies (SET2014). pp. 25–28.

Balasubramanian, G., Ghommem, M., Hajj, M.R., Wong, W.P., Tomlin, J.A., Puri, I.K., 2010. Modeling of thermochemical energy storage by salt hydrates. International Journal of

Heat and Mass Transfer 53, 5700–5706.

Balasubramanian, Ghommem, G., Hajj, M., R, M., Wong, W.P., Tomlin, J. a., Puri, I.K., 2010. Modeling of thermochemical energy storage by salt hydrates. International Journal of Heat and Mass Transfer 53, 5700–5706.

Bales, C., 2007. Laboratory prototypes of thermo-chemical and sorption storage units ,Report B3—IEA SHC Task 32, Report B3—IEA SHC Task 32. Sweden.

Bales, C., 2005. Thermal Properties of Materials for Thermo-chemical Storage of Solar Heat.

Bales, C., Gantenbein, P., Jaenig, D., Kerskes, H., Summer, K., Van Essen, M., Weber, R., 2008. Laboratory Tests of Chemical Reactions and Prototype Sorption Storage Units, A Report of IEA Solar Heating and Cooling programme - Task 32, Solar Heating & Cooling Programme.

Banker, N.D., Dutta, P., Prasad, M., Srinivasan, K., 2008. Performance studies on mechanical + adsorption hybrid compression refrigeration cycles with HFC 134a. International Journal of Refrigeration 31, 1398–1406.

Banker, N.D., Prasad, M., Dutta, P., Srinivasan, K., 2009. Activated carbon + HFC 134a based two stage thermal compression adsorption refrigeration using low grade thermal energy sources. Applied Thermal Engineering 29, 2257–2264.

Barreneche, C., Fernández, A.I., Cabeza, L.F., Cuypers, R., 2015. Thermophysical characterization and thermal cycling stability of two TCM: $CaCl_2$ and zeolite. Applied Energy 137, 726–730.

Barrett, E.P., Joyner, L.G., Halenda, P.P., 1951. The determination of pore volume and area distributions in porous substances. I. Computations from nitrogen isotherms. Journal of the American Chemical society 1896.

Barry Crittenden, 1998. Adsorption Technology & Design. Butterworth-Heinemann.

Bertsch, F., Jaehnig, D., Asenbeck, S., Kerskes, H., Drueck, H., Wagner, W., Weiss, W., 2014. Comparison of the Thermal Performance of a Solar Heating System with Open and Closed Solid Sorption Storage. Energy Procedia 48, 280–289.

BOC, 2011. R1234yf – Opteon ® YF . [WWW Document]. BOC. URL https://www.boconline.co.uk/internet.lg.lg.gbr/en/images/Opteon-R1234yf-Brochure410_124745.pdf?v=2.0 (accessed 7.22.16).

Boer, R., Haije, W.G., Veldhuis, J.B.J., Smeding, S.F., 2004. Solid-Sorption Cooling With Integrated Thermal Storage: The SWEAT Prototype, in: International Conference on Heat Powerd Cycles, Larnaca, Cyprus.

Bonaccorsi, L., Bruzzaniti, P., Calabrese, L., Freni, A., Proverbio, E., Restuccia, G., 2013a. Synthesis of SAPO-34 on graphite foams for adsorber heat exchangers. Applied Thermal Engineering 61, 848–852.

Bonaccorsi, L., Calabrese, L., Freni, A., Proverbio, E., 2013b. Hydrothermal and microwave synthesis of SAPO (CHA) zeolites on aluminium foams for heat pumping applications. Microporous and Mesoporous Materials 167, 30–37.

Bonaccorsi, L., Calabrese, L., Freni, A., Proverbio, E., Restuccia, G., 2013c. Zeolites direct synthesis on heat exchangers for adsorption heat pumps. Applied Thermal Engineering 50, 1590–1595.

Brunauer, S., Humble, P.H., Edware, T., 1936. Adsorption of Gases in Multimolecular Layers, Bureau Of Chemistry and Soils.

BS11357-4:2013, 2013. BS EN ISO 11357-4:2013 Differential Scanning Calorimeter. British Standards Institution.

Cabeza, L.F., Mehling, H., 2003. Review on thermal energy storage with phase change : materials , heat transfer analysis and applications. Appplied Thermal Engineering 23, 251–283.

Cacciola, G., Restuccia, G., 1995. Reversible adsorption heat pump: a thermodynamic model. International Journal of Refrigeration 18, 100–106.

Cacciola, G., Restuccia, G., Benthem, G.H.W. Van, van Benthem, G.H.W., 1999. Influence of the adsorber heat exchanger design on the performance of the heat pump system. Applied Thermal Engineering 19, 255–269.

Carbon, 2014. Fuel prices and carbon intensity [WWW Document]. Energy Saving Trust. URL http://www.energysavingtrust.org.uk/corporate/our-calculations (accessed 2.2.16).

Casey, S., 2013. Nano-Structure Sorbents For Rapid Response Interior Air Humidity Buffering Applications. University Of Nottingham. P.h.D. Thesis, University Of Nottingham.

Casey, S.P., Aydin, D., Riffat, S., Elvins, J., 2015. Salt impregnated desiccant matrices for “open” thermochemical energy storage—Hygrothermal cyclic behaviour and energetic analysis by physical experimentation. Energy and Buildings 92, 128–139.

Casey, S.P., Elvins, J., Riffat, S., Robinson, A., 2014. Salt impregnated desiccant matrices for “open” thermochemical energy storage—Selection, synthesis and characterisation of candidate materials. Energy and Buildings 84, 412–425.

Castell, A., Solé, C., Medrano, M., Roca, J., Cabeza, L.F., García, D., 2008. Natural convection heat transfer coefficients in phase change material (PCM) modules with external vertical fins. Applied Thermal Engineering 28, 1676–1686.

Chan, K.C.C., Chao, C.Y.H.H., Sze-To, G.N.N., Hui, K.S.S., 2012. Performance predictions for a new zeolite 13X/$CaCl_2$ composite adsorbent for adsorption cooling systems. International Journal of Heat and Mass Transfer 55, 3214–3224.

Chi, T., 1994. Adsorption Calculations and Modelling. Butterworh and Heinnemann, Newton, MA.

Cho, S.-H., Kim, J.-N., 1992. Modeling of a silica gel/water adsorption-cooling system. Energy 17, 829–839.

Cot-Gores, J., Castell, A., Cabeza, L.F., 2012. Thermochemical energy storage and conversion: A-state-of-the-art review of the experimental research under practical conditions. Renewable and Sustainable Energy Reviews 16, 5207–5224.

Critoph, R.E., 2012. Solid sorption cycles: A short history. International Journal of Refrigeration 35, 490–493.

Critoph, R.E., 1998. Forced convection adsorption cycles. Journal Applied Thermal Engineering 18, 799–807.

Crofoot, L., Harrison, S., 2012. Performance evaluation of a liquid desiccant solar air conditioning system, in: Energy Procedia. pp. 542–550.

Cyklis, P., 2014. Two stage ecological hybrid sorption–compression refrigeration cycle. International Journal of Refrigeration 48, 121–131.

Daou, K., Wang, R.Z., Xia, Z.Z., 2006. Development of a new synthesized adsorbent for refrigeration and air conditioning applications. Applied Thermal Engineering 26, 56–65.

Daou, K., Wang, R.Z., Yang, G.Z., Xia, Z.Z., 2008. Theoretical comparison of the refrigerating performances of a $CaCl_2$ impregnated composite adsorbent to those of the host silica gel. International Journal of Thermal Sciences 47, 68–75.

Darkwa, K., 1998. Thermochemical Energy Storage In Inorganic Oxides : An Experimental Evaluation. Applied Thermal Engineering 18, 387–400.

Darkwa, K., Ianakiev, A., O'Callaghan, P.W., 2006. Modelling and simulation of adsorption process in a fluidised bed thermochemical energy reactor. Applied Thermal Engineering 26, 838–845.

Darkwa, K., O'Callaghan, P.W., 1997. Green transport technology (GTT): Analytical studies of a thermochemical store for minimising energy consumption and air pollution from automobile engines. Applied Thermal Engineering. doi:10.1016/S1359-4311(97)80001-4

Dawoud, B., 2013. Water vapor adsorption kinetics on small and full scale zeolite coated adsorbers; A comparison. Applied Thermal Engineering 50, 1645–1651.

Dawoud, B., Vedder, U., Amer, E.-H., Dunne, S., 2007. Non-isothermal adsorption kinetics of water vapour into a consolidated zeolite layer. International Journal of Heat and Mass Transfer 50, 2190–2199.

DECC, 2015. Quaterly Energy price December 2015 [WWW Document]. URL /uploads/system/uploads/attachment_data/file/487856/QEP_final_Dec_15.pdf (accessed 1.26.15).

DECC, 2013. Energy Consumption in the UK. Overall Energy Consumption Factsheet [WWW Document]. DECC (Department of Energy & Climate Change). URL https://www.gov.uk/government/organisations/department-of-energy-climate-change (accessed 10.13.13).

DECC, 2011. UK Renewable Energy Roadmap. Carbon 5, 293–298.

Delgado, M., Lázaro, A., Mazo, J., Zalba, B., 2012. Review on phase change material emulsions and microencapsulated phase change material slurries: Materials, heat transfer studies and applications. Renewable and Sustainable Energy Reviews 16, 253–273.

Demir, H., Mobedi, M., Ülkü, S., 2008. A review on adsorption heat pump: Problems and solutions. Renewable and Sustainable Energy Reviews 12, 2381–2403.

Department of Climate Change, 2015. 2010 to 2015 government policy: greenhouse gas emissions [WWW Document]. URL https://www.gov.uk/government/publications/2010-to-2015-government-policy-greenhouse-gas-emissions/2010-to-2015-government-policy-greenhouse-gas-emissions (accessed 6.18.15).

Di, J., Wu, J.Y., Xia, Z.Z., Wang, R.Z., 2007. Theoretical and experimental study on characteristics of a novel silica gel–water chiller under the conditions of variable heat source temperature. International Journal of Refrigeration 30, 515–526.

Dincer, I., 2002. Thermal energy storage systems as a key technology in energy conservation. International Journal of Energy Research 26, 567–588.

Dincer, I., Rosen, M.A., 2011. Thermal Energy Storage -Systems and Applications. John Wiley & Sons, United Kingdom.

Ding, Y., 2013. Investigation of High Capacity Heat Energy Storage for Buildings Applications. PhD Thesis, University Of Nottingham.

Ding, Y., Riffat, S.B., 2012. Thermochemical energy storage technologies for building applications: a state-of-the-art review. International Journal of Low-Carbon Technologies 8, 106–116.

Duffie, J.A., Beckman, W.A., 2013. Solar Engineering of Thermal Processes: Fourth Edition, Solar Engineering of Thermal Processes: Fourth Edition. John Wiley and Sons.

Dupre Chemical, 2011. Aqueous Vermiculite Dispersion [WWW Document]. Dupré Minerals Limited. URL http://www.dupreminerals.com/en/products/vermiculite-dispersion (accessed 7.11.15).

Dyball, D.L., 2013. An Innovative Wall -Lining for Buildings Incorporatign Phase Change Materials. PhD Thesis, University Of Brighton,UK.

E.ON, 2015. E.ON [WWW Document]. URL https://www.eonenergy.com (accessed 1.26.15).

Eames, I.W., Wu, S., 2000. Experimental proof-of-concept testing of an innovative heat-powered vapour recompression-absorption refrigerator cycle. Applied Thermal Engineering 20, 721–736.

EIA, 2013. EIA Forecast [WWW Document]. URL http://www.eia.gov/forecasts/aeo/pdf/0383(2013).pdf (accessed 3.26.13).

El-Sharkawy, I.I., Saha, B.B., Koyama, S., Ng, K.C., 2006. A study on the kinetics of ethanol-activated carbon fiber: Theory and experiments. International Journal of Heat and Mass Transfer 49, 3104–3110.

Enibe, S.O., 2002. Performance of a natural circulation solar air heating system with phase change material energy storage. Renewable Energy 27, 69–86.

ETL Ltd, 2014. European Thermodynamics Ltd [WWW Document]. URL http://www.europeanthermodynamics.com/index.php/products.html (accessed

1.26.15).

Ezan, M.A., Erek, A., Dincer, I., 2011. Energy and exergy analyses of an ice-on-coil thermal energy storage system. Energy 36, 6375–6386.

Fernandez, R., Giotto, M., Pastore, H., Cardoso, D., 2002. Synthesis of characterization of MAPO-11 molecular sieves. Microporous and Mesoporous Materials 53, 135–144.

Finck, C., Henquet, E., van Soest, C., Oversloot, H., de Jong, A.-J., Cuypers, R., Spijker, H. van"t "T, 2014. Experimental Results of a 3 kWh Thermochemical Heat Storage Module for Space Heating Application. Energy Procedia 48, 320–326.

Friedli.com, 2015. Thermal Analysis [WWW Document]. URL http://www.friedli.com/research/PhD/DSC/chap3.html (accessed 3.15.15).

Fu, Y., 2014. Investigation Of Solar Assisted Heat Pump High-rise Residential Buildings. PhD Thesis, University Of Nottingham, UK.

Fujimoto, S., Bilgen, E., Ogura, H., 2002. $CaO/Ca(OH)_2$ chemical heat pump system. Energy Conversion and Management 43, 947–960.

Fujioka, K., Hatanaka, K., Hirata, Y., 2008. Composite reactants of calcium chloride combined with functional carbon materials for chemical heat pumps. Applied Thermal Engineering 28, 304–310.

Garh, H.P., Mullick, S.C., Bhargava, A.K., 1985. Solar Thermal Energy Storage. D. Reidel Publishing Company, Holland.

Ge, T.S., Dai, Y.J., Wang, R.Z., Peng, Z.Z., 2010. Experimental comparison and analysis on silica gel and polymer coated fin-tube heat exchangers. Energy 35, 2893–2900.

Giesche, H., 2006. Mercury porosimetry: A general (practical) overview. Particle and Particle Systems Characterization 23, 9–19.

Glaznev, I., Ponomarenko, I., Kirik, S., Aristov, Y., 2011. Composites $CaCl_2$/SBA-15 for adsorptive transformation of low temperature heat: Pore size effect. International Journal of Refrigeration 34, 1244–1250.

Gong, L.X., Wang, R.Z., Xia, Z.Z., Lu, Z.S., 2012. Experimental study on an adsorption chiller employing lithium chloride in silica gel and methanol. International Journal of Refrigeration 35, 1950–1957.

Gordeeva, L.G., Aristov, Y.I., 2012. Composites "salt inside porous matrix" for adsorption heat transformation: a current state-of-the-art and new trends. International Journal of Low-Carbon Technologies 7, 288–302.

Grekova, a. D., Veselovskaya, J.V., Tokarev, M.M., Krieger, T. a., Shmakov, A.N., Gordeeva, L.G., 2014. Ammonia sorption on the composites "($BaCl_2$+$BaBr_2$) inside vermiculite pores." Colloids and Surfaces A: Physicochemical and Engineering Aspects 448, 169–174.

GSHP, 2016. Ground Source Heat-Pump [WWW Document]. URL http://www.gshp.org.uk/ (accessed 1.20.16).

Hadorn, J., 2006. Solar Heating and Cooling Programme Task 32 : Advanced Storage

Concepts for Solar and Low Energy Buildings. EIA.

Hadorn, J., 2005. Thermal energy storage for solar and low energy buildings: State of the Art. Servei de Publicacions de la Universitat de Lleida. Halford, Lleida, Spain.

Hamdan, M.., Rossides, S.D., Haj Khalil, R., 2013. Thermal energy storage using thermo-chemical heat pump. Energy Conversion and Management 65, 721–724.

Hassan, H.Z., Mohamad, A. a., 2013. Thermodynamic analysis and theoretical study of a continuous operation solar-powered adsorption refrigeration system. Energy 61, 167–178.

Hauer, A., 2008. Sorption storage for solar thermal energy—possibilities and limits., in: Proceedings of Eurosun. pp. 1–8.

Hauer, A., 2007. A Sorption storage for solar thermal energy—possibilities and limits., in: Paksoy H (Ed). Thermal Energy Storage for Sustainable Energy Consumption Springer, 2007, 377–91.

Hauer, A., Fischer, F., 2011. Open Adsorption System for an Energy Efficient Dishwasher. Chemie Ingenieur Technik 83, 61–66.

He, Z.H., Huang, H.Y., Deng, L.S., Yuan, H.R., Kobayashi, N., Kubota, M., Huhetaoli, Zhao, D.D., 2014. Development of Novel Type of Two-stage Adsorption Chiller with Different Adsorbents. Energy Procedia 61, 1996–1999.

Hongois, S., Kuznik, F., Stevens, P., Roux, J.-J.J., 2011. Development and characterisation of a new MgSO4-zeolite composite for long-term thermal energy storage. Solar Energy Materials and Solar Cells 95, 1831–1837.

Hu, P., Yao, J.-J., Chen, Z.-S., 2009. Analysis for composite zeolite/foam aluminum–water mass recovery adsorption refrigeration system driven by engine exhaust heat. Energy Conversion and Management 50, 255–261.

Huang, H., Oike, T., Watanabe, F., Osaka, Y., Kobayashi, N., Hasatani, M., 2010. Development research on composite adsorbents applied in adsorption heat pump. Applied Thermal Engineering 30, 1193–1198.

Iammak, K., Wongsuwan, W., Kiatsiriroj, T., 2004. Investigation of Modular Chemical Energy Storage Performance, in: The Joint International Conference on "Sustainable Energy and Environment (SEE). Hua Hin, Thailand, pp. 504–507.

Inglezakis, V.., Poulopoulos, S.., 2006. Adsorption, ion exchange and catalysis: design of operations and environmental applications.

Inglezakis, V.., Poulopoulos, S.., Inglezakis. Vassilis; Stavros. Poulopoulo, 2006. Adsorption, ion exchange and catalysis: design of operations and environmental applications. Elsevier.

Jabbari-Hichri, A., Bennici, S., Auroux, A., 2015. Enhancing the heat storage density of silica–alumina by addition of hygroscopic salts ($CaCl_2$, $Ba(OH)_2$, and $LiNO_3$). Solar Energy Materials and Solar Cells 140, 351–360.

Jänchen, J., Ackermann, D., Weiler, E., Stach, H., Brösicke, W., 2005. Calorimetric investigation on zeolites, AlPO4's and CaCl2 impregnated attapulgite for

thermochemical storage of heat. Thermochimica Acta 434, 37–41.

Javani, N., Dincer, I., Naterer, G.F., 2012. Thermodynamic analysis of waste heat recovery for cooling systems in hybrid and electric vehicles. Energy 46, 109–116.

Jiang, L., 2014. Isothermal dehumidification with a simply thermoelectric device: concept and feasibility. International Journal of Ambient Energy 1–5.

Jiang, Y., Ge, T.S., Wang, R.Z., Hu, L.M., 2014. Experimental investigation and analysis of composite silica-gel coated fin-tube heat exchangers. International Journal of Refrigeration 1.

Katejanekarn, T., Chirarattananon, S., Kumar, S., 2009. An experimental study of a solar-regenerated liquid desiccant ventilation pre-conditioning system. Solar Energy 83, 920–933.

Kato, Y., Takahashi, R., Sekiguchi, T., Ryu, J., 2009. Study on medium-temperature chemical heat storage using mixed hydroxides. International Journal of Refrigeration 32, 661–666.

Kato, Y., Yoshizawa, Y., Kobayashi, K., Yoshizawa, Y., 1998. Durability To Repetative Reaction Of Magnesium Oxide / Water Reaction System For A Heat Pump. Applied Thermal Engineering 18, 85–92.

Kawasaki, H., Watanabe, T., Kanzawa, A., 1999. Proposal of a chemical heat pump with paraldehyde depolymerization for cooling system 19, 133–143.

Kensa Heat Pump, 2015. Kensa Heat Pump [WWW Document]. URL http://www.kensaheatpumps.com/ (accessed 1.26.15).

Khattab, N.M., Sharawy, H., Helmy, M., 2012. Development of Novel Solar Adsorption Cooling Tube. Energy Procedia 18, 709–714.

Kimseng, K., Meissel, M., 2001. Environmental Scanning Electron Microscope [WWW Document]. CALCE Electronic Products and Systems Centre, University of Maryland.

Kubota, M., Ueda, T., Fujisawa, R., Kobayashi, J., Watanabe, F., Kobayashi, N., Hasatani, M., 2008. Cooling output performance of a prototype adsorption heat pump with fin-type silica gel tube module. Applied Thermal Engineering 28, 87–93.

Kuravi, S., Trahan, J., Goswami, D.Y., Rahman, M.M., Stefanakos, E.K., 2013. Thermal energy storage technologies and systems for concentrating solar power plants. Progress in Energy and Combustion Science 39, 285–319.

Kürklü, A., Özmerzi, A., Bilgin, S., 2002. Thermal performance of water-phase change material solar collector. Renewable Energy 26, 391–399.

Lahmidi, H., Mauran, S., Goetz, V., 2006. Definition, test and simulation of a thermochemical storage process adapted to solar thermal systems. Solar Energy 80, 883–893.

Lee, K.S., 2013. Green Energy and Technology. Springer-Verlag, London.

Lee, Y., Jung, D., 2012. A brief performance comparison of R1234yf and R134a in a bench tester for automobile applications. Applied Thermal Engineering 35, 240–242.

Lele, A.F., 2015. A Thermochemical Heat Storage System for Households: Thermal Transfers Coupled to Chemical Reaction Investigations. PhD Thesis, Leuphana University of Luneburg, Germany.

Li, T., Wang, R., Kiplagat, J.K., Kang, Y., 2013. Performance analysis of an integrated energy storage and energy upgrade thermochemical solid–gas sorption system for seasonal storage of solar thermal energy. Energy 50, 454–467.

Li, T.X., Wang, R.Z., Kiplagat, J.K., Wang, L.W., 2009a. Performance study of a consolidated manganese chloride–expanded graphite compound for sorption deep-freezing processes. Applied Energy 86, 1201–1209.

Li, T.X., Wang, R.Z., Wang, L.W., Kiplagat, J.K., 2009b. Study on the heat transfer and sorption characteristics of a consolidated composite sorbent for solar-powered thermochemical cooling systems. Solar Energy 83, 1742–1755.

Li, T.X., Wang, R.Z., Yan, T., Ishugah, T.F., 2014. Integrated energy storage and energy upgrade, combined cooling and heating supply, and waste heat recovery with solid–gas thermochemical sorption heat transformer. International Journal of Heat and Mass Transfer 76, 237–246.

Li, Z.., Sumathy, K., 2000. Technology development in the solar absorption air-conditioning systems. Renewable and Sustainable Energy Reviews 4, 267–293.

Liu, H., Nagano, K., Sugiyama, D., Togawa, J., Nakamura, M., 2013. Honeycomb filters made from mesoporous composite material for an open sorption thermal energy storage system to store low-temperature industrial waste heat. International Journal of Heat and Mass Transfer 65, 471–480.

Liu, S., Riffat, S., Zhao, X., Yuan, Y., 2009. Impact of adsorbent finishing and absorbent filming on energy exchange efficiency of an air-to-air cellulose fibre heat & mass exchanger. Building and Environment 44, 1803–1809.

Louajari, M., Mimet, A., Ouammi, A., 2011. Study of the effect of finned tube adsorber on the performance of solar driven adsorption cooling machine using activated carbon–ammonia pair. Applied Energy 88, 690–698.

Lu, Y.Z., Wang, R.Z., Zhang, M., Jiangzhou, S., 2003. Adsorption cold storage system with zeolite-water working pair used for locomotive air conditioning. Energy Conversion and Management 44, 1733–1743.

Ma, X., Chen, J., Li, S., Sha, Q., Liang, A., Li, W., Zhang, J., Zheng, G., Feng, Z., 2003. Application of absorption heat transformer to recover waste heat from a synthetic rubber plant. Applied Thermal Engineering 23, 797–806.

Maggio, G., Gordeeva, L.G., Freni, A., Aristov, Y.I., Santori, G., Polonara, F., Restuccia, G., 2009. Simulation of a solid sorption ice-maker based on the novel composite sorbent “lithium chloride in silica gel pores.” Applied Thermal Engineering 29, 1714–1720.

Mauran, S., Lahmidi, H., Goetz, V., 2008. Solar heating and cooling by a thermochemical process. First experiments of a prototype storing 60kWh by a solid/gas reaction. Solar Energy 82, 623–636.

Mauran, S., Prades, P., L’Haridon, F., 1993. Heat and mass transfer in consolidated

reacting beds for thermochemical systems. Heat Recovery Systems and CHP 13, 315–319.

Medrano, M., Yilmaz, M.O., Nogués, M., Martorell, I., Roca, J., Cabeza, L.F., 2009. Experimental evaluation of commercial heat exchangers for use as PCM thermal storage systems. Applied Energy 86, 2047–2055.

Mempouo, B., 2011. Investigations of Novel Heat Pump Systems for Low Carbon Homes. PhD Thesis. University Of Nottingham.

Mettawee, E.B.S., Assassa, G.M.R., 2006. Experimental study of a compact PCM solar collector. Energy 31, 2622–2632.

Meunier, F., 1998. Solid sorption heat powered cycles for cooling and heat pumping applications. Applied Thermal Engineering 18, 715–729.

Micrometrics Instruments Corporation, 2014. Mercury Intrusion Porosimetry Theory [WWW Document]. Miromemeritics Instrument Corporation. URL http://www.micromeritics.com (accessed 5.12.15).

Miyazaki, T., Akisawa, A., Saha, B.B.B., El-Sharkawy, I.I.I., Chakraborty, A., 2009. A new cycle time allocation for enhancing the performance of two-bed adsorption chillers. International Journal of Refrigeration 32, 846–853.

Mosaffa, a. H., Infante Ferreira, C. a., Talati, F., Rosen, M. a., 2013. Thermal performance of a multiple PCM thermal storage unit for free cooling. Energy Conversion and Management 67, 1–7.

Muthukumar, P., Groll, M., 2010. Metal hydride based heating and cooling systems: A review. International Journal of Hydrogen Energy 35, 3817–3831.

Myat, A., Kim Choon, N., Thu, K., Kim, Y.-D., 2013. Experimental investigation on the optimal performance of Zeolite–water adsorption chiller. Applied Energy 102, 582–590.

N'Tsoukpoe, K.E., Liu, H., Le Pierrès, N., Luo, L., 2009. A review on long-term sorption solar energy storage. Renewable and Sustainable Energy Reviews 13, 2385–2396.

Nellis, G., Sanford, K., 2009. Heat Transfer. Cambridge University Press., New York.

Niazmand, H., Dabzadeh, I., 2012. Numerical simulation of heat and mass transfer in adsorbent beds with annular fins. International Journal of Refrigeration 35, 581–593.

Ogueke, N. V., Anyanwu, E.E., 2008. Design improvements for a collector/generator/adsorber of a solid adsorption solar refrigerator. Renewable Energy 33, 2428–2440.

Ogura, H., 2003. Efficiencies of $CaO/H_2O/Ca(OH)_2$ chemical heat pump for heat storing and heating/cooling. Energy 28, 1479–1493.

Ogura, H., Miyazaki, M., Matsuda, H., Hasatani, M., Yanadori, M., Hiramatsu, M., 1991. Experimental Study on Heat Transfer Enhancement of the Solid Reactant Particle Bed in a Chemical Heat Pump Using $Ca(OH)_2/CaO$ Reaction. Kagaku Kogaku Ronbunshu 17, 916–623.

Ouden, C.D., 1982. Thermal storage of solar energy, Solar Energy. Martinus Nijhoff

Publishers, The Haque.

Owen, M.S., Kennedy, H.E., 2009. ASHRAE, Handbook Fundamentals. The American Society of Heating, Refrigerating and Air- Conditioning Engineers.

Paksoy, H.Ö., 2007. Thermal energy storage for sustainable energy consumption - Fundamentals, Case Studies and Design. Springer, Turkey.

Pan, Q.W., Wang, R.Z., Lu, Z.S., Wang, L.W., 2014. Experimental investigation of an adsorption refrigeration prototype with the working pair of composite adsorbent-ammonia. Applied Thermal Engineering 72, 275–282.

Pérez-Lombard, L., Ortiz, J., Pout, C., 2008. A review on buildings energy consumption information. Energy and Buildings 40, 394–398.

Ponomarenko, I.V., Glaznev, I.S., Gubar, A.V., Aristov, Y.I., Kirik, S.D., 2010. Synthesis and water sorption properties of a new composite "$CaCl_2$ confined into SBA-15 pores." Microporous and Mesoporous Materials 129, 243–250.

Pons, M., Laurent, D., Meunier, F., 1996. Experimental Temperature Fronts for Adsorptive heat pump applications. Journal of Applied Thermal Engineering 16, 395–404.

Pons, M., Laurent, D., Meunier, F., 1996. Experimental temperature fronts for absorptive heat pump applications. Applied Thermal Engineering 16, 395–404.

Quoilin, S., Aumann, R., Grill, A., Schuster, A., Lemort, V., Spliethoff, H., 2011. Dynamic modeling and optimal control strategy of waste heat recovery Organic Rankine Cycles. Applied Energy 88, 2183–2190.

R.Sh.Mikhail, Guindy, N.M., S.Hanafi, 1970. Low-Temperature Dehaydration of Vermiculite. Journal of Applied Chemistry 20, 346–351.

Regin, a. F., Solanki, S.C., Saini, J.S., 2008. Heat transfer characteristics of thermal energy storage system using PCM capsules: A review. Renewable and Sustainable Energy Reviews 12, 2438–2458.

Restuccia, G., Freni, A., Russo, F., Vasta, S., 2005. Experimental investigation of a solid adsorption chiller based on a heat exchanger coated with hydrophobic zeolite. Applied Thermal Engineering 25, 1419–1428.

Restuccia, G., Freni, A., Vasta, S., Aristov, Y., 2004. Selective water sorbent for solid sorption chiller: experimental results and modelling. International Journal of Refrigeration 27, 284–293.

Riffat, S., Su, Y., Ding, Y., 2013. Thermochemical cooling system based on adsorption pumping pipe. International Journal of Low-Carbon Technologies 1–7.

Riffel, D.B., Wittstadt, U., Schmidt, F.P., Núñez, T., Belo, F. a., Leite, A.P.F.F., Ziegler, F., 2010. Transient modeling of an adsorber using finned-tube heat exchanger. International Journal of Heat and Mass Transfer 53, 1473–1482.

Ristić, A., Maučec, D., Henninger, S.K., Kaučič, V., 2012. New two-component water sorbent $CaCl_2$-$FeKIL_2$ for solar thermal energy storage. Microporous and Mesoporous Materials 164, 266–272.

Romero, R.J., Rodriguez-Martinez, A., 2008. Optimal water purification using low grade waste heat in an absorption heat transformer. Desalination 220, 506–513.

Ruthhaven, D.M., 1984. Principles of adsoprtion and adsoprtion processes. John Wiley & Sons. Inc., United State Of America.

Sadeghlu, A., Yari, M., Mahmoudi, S.M.S., Dizaji, H.B., 2014. Performance evaluation of Zeolite 13X/$CaCl_2$ two-bed adsorption refrigeration system. International Journal of Thermal Sciences 80, 76–82.

Sakoda, A., Suzuki, M., 1983. Fundamental study on solar powered adsorption cooling system. Journal of chemical engineering of Japan 17, 52–57.

Sakoda, Suzuki, 1986. Simutaneous Transport of Heat And Adsorbate In Closed Type Adsoprtion Cooling Systems Utilizing Solar Heat. ASME Transaction Vol 108.

Sami, S.M., Tribes, C., 1996. An improved model for predicting the dynamic behaviour of adsorption systems. Applied Thermal Engineering 16, 149–161.

San, J.-Y., Hsu, H.-C., 2009. Performance of a multi-bed adsorption heat pump using SWS-1L composite adsorbent and water as the working pair. Applied Thermal Engineering 29, 1606–1613.

Sanaye, S., Shirazi, A., 2013. Thermo-economic optimization of an ice thermal energy storage system for air-conditioning applications. Journal Of Energy and Buildings 60, 100–109.

Schnabel, L., Tatlier, M., Schmidt, F., Erdem-Şenatalar, A., 2010. Adsorption kinetics of zeolite coatings directly crystallized on metal supports for heat pump applications (adsorption kinetics of zeolite coatings). Applied Thermal Engineering 30, 1409–1416.

Sharma, A., Tyagi, V.V., Chen, C.R., Buddhi, D., 2009. Review on thermal energy storage with phase change materials and applications. Renewable and Sustainable Energy Reviews 13, 318–345.

Shkatulov, A., Ryu, J., Kato, Y., Aristov, Y., 2012. Composite material " Mg(OH)$_2$/vermiculite": A promising new candidate for storage of middle temperature heat. Energy 44, 1028–1034.

Srivastava, N.C., Eames, I.W., 1998. A review of adsorbents and adsorbates in solid–vapour adsorption heat pump systems. Applied Thermal Engineering 18, 707–714.

Stitou, D., Mazet, N., Mauran, S., 2012. Experimental investigation of a solid/gas thermochemical storage process for solar air-conditioning. Energy 41, 261–270.

Sur, A., Das, R.K., 2010. Review on solar adsorption refrigeration cycle. International Journal of Mechanical Engineering and Technology 1, 190–226.

Suzuki, M., Suzukl, M., Wankat, P.C., 1991. Adsorption Engineering, Reactive Polymers. Elservier Science Publishers, Japan.

Tahat, M.A., Babus'Haq, R.F., O'Callaghan, P.W., Probert, S.D., 1995. Performance of an integrated thermochemical heat pump/energy store. Thermochimica Acta 255, 39–47.

Tanashev, Y.Y., Krainov, A. V., Aristov, Y.I., 2013. Thermal conductivity of composite

sorbents “salt in porous matrix” for heat storage and transformation. Applied Thermal Engineering 61, 401–407.

Tatlıer, M., Tantekin-Ersolmaz, B., Erdem-Şenatalar, A., 1999. A novel approach to enhance heat and mass transfer in adsorption heat pumps using the zeolite–water pair. Microporous and Mesoporous Materials 27, 1–10.

Tay, N.H.S., Belusko, M., Bruno, F., 2012. Designing a PCM storage system using the effectiveness-number of transfer units method in low energy cooling of buildings. Energy and Buildings 50, 234–242.

Tay, N.H.S., Bruno, F., Belusko, M., 2013. Experimental investigation of dynamic melting in a tube-in-tank PCM system. Applied Energy 104, 137–148.

Tokarev, M.M., Veselovskaya, J.V., Yanagi, H., Aristov, Y.I.I., Tokarev, M.M., Aristov, Y.I.I., 2010. Novel ammonia sorbents “porous matrix modified by active salt” for adsorptive heat transformation: 2. Calcium chloride in ACF felt. Applied Thermal Engineering 30, 584–589.

Tso, C.Y., Chao, C.Y.H., 2012. Activated carbon, silica-gel and calcium chloride composite adsorbents for energy efficient solar adsorption cooling and dehumidification systems. International Journal of Refrigeration 35, 1626–1638.

Utley, J.I., Shorrock, L.D., 2008. Domestic energy fact file 2008 [WWW Document]. DECC (Department of Energy & Climate Change). URL https://www.gov.uk/government/organisations/department-of-energy-climate-change (accessed 1.12.13).

Utlu, Z., Aydın, D., Kıncay, O., 2014. Comprehensive thermodynamic analysis of a renewable energy sourced hybrid heating system combined with latent heat storage. Energy Conversion and Management 84, 311–325.

van Essen, V.M., Zondag, H. a., Gores, J.C., Bleijendaal, L.P.J., Bakker, M., Schuitema, R., van Helden, W.G.J., He, Z., Rindt, C.C.M., 2009. Characterization of MgSO4 Hydrate for Thermochemical Seasonal Heat Storage. Journal of Solar Energy Engineering 131, 41014.

van Essen, V.M., Zondag, H. a., Schuitema, R., van Helden, W.G.J., Rindt, C.C.M., 2008. Materials for thermochemical storage : characterization of magnesium sulfate. Proceedings Eurosun 4–9.

Vasta, S., Giacoppo, G., Barbera, O., Calabrese, L., Bonaccorsi, L., Freni, A., 2014. Innovative zeolite coatings on graphite plates for advanced adsorbers. Applied Thermal Engineering 72, 153–159.

Veselovskaya, J.V., Critoph, R.E., Thorpe, R.N., Metcalf, S., Tokarev, M.M., Aristov, Y.I., 2010. Novel ammonia sorbents “porous matrix modified by active salt” for adsorptive heat transformation: 3. Testing of “$BaCl_2$/vermiculite” composite in a lab-scale adsorption chiller. Applied Thermal Engineering 30, 1188–1192.

Veselovskaya, J. V., Tokarev, M.M., 2011. Novel ammonia sorbents “porous matrix modified by active salt” for adsorptive heat transformation: 4. Dynamics of quasi-isobaric ammonia sorption and desorption on BaCl2/vermiculite. Applied Thermal Engineering 31, 566–572.

Visscher, K., Veldhuis, J.B.J., 2005. Comparison Of Candidate Materials For Seasonal Storage Of Solar Heat Through Dynamic Simulation Of Building And Renewable Energy Systems, in: Buildings Simulations 2005 (The Ninth International Building Performance Simulation Association), Montreal August 15-18,2005. Montreal, Canada, pp. 1–11.

Voort, I.M. Van De, 2007. Characterization of a thermochemical storage material. Technische university Eidhoven. Master Thesis, Technische university Eidhoven.

Wajid, N.M., Mempouo, B., Dodo, A., Omer, S., Riffat, S.B., 2016. Experimental study of an adsorption heat storage systems for building applications. Renewable Bioresources 4, 2.

Wang, B.K., Vineyard, E.A., 2011. Adsorption Refrigeration. ASHRAE Journal.

Wang, D.C., Wang, Y.J., Zhang, J.P., Tian, X.L., Wu, J.Y., 2008. Experimental study of adsorption chiller driven by variable heat source. Energy Conversion and Management 49, 1063–1073.

Wang, D.C., Zhang, J.P., 2009. Design and performance prediction of an adsorption heat pump with multi-cooling tubes. Energy Conversion and Management 50, 1157–1162.

Wang, K., Wu, J.Y., Wang, R.Z., Wang, L.W., 2006a. Composite adsorbent of $CaCl_2$ and expanded graphite for adsorption ice maker on fishing boats. International Journal of Refrigeration 29, 199–210.

Wang, K., Wu, J.Y., Wang, R.Z., Wang, L.W., 2006b. Effective thermal conductivity of expanded graphite–CaCl2 composite adsorbent for chemical adsorption chillers. Energy Conversion and Management 47, 1902–1912.

Wang, S.G., Wang, R.Z., Li, X.R., 2005. Research and development of consolidated adsorbent for adsorption systems. Renewable Energy 30, 1425–1441.

Wang, X., Chua, H.T., 2007. Two bed silica gel-water adsorption chillers: An effectual lumped parameter model. International Journal of Refrigeration 30, 1417–1426.

Willis, 2015. Immersion Heater [WWW Document]. Willis. URL http://www.willis-renewables.com/immersion-specifications.htm (accessed 1.26.15).

Wu, H., Wang, S., Zhu, D., 2007. Effects of impregnating variables on dynamic sorption characteristics and storage properties of composite sorbent for solar heat storage. Solar Energy 81, 864–871.

Wu, H., Wang, S., Zhu, D., Ding, Y., 2009. Numerical analysis and evaluation of an open-type thermal storage system using composite sorbents. International Journal of Heat and Mass Transfer 52, 5262–5265.

Wu, L., 2014. Chapter 6 [WWW Document]. FIN3000. URL faculty.baruch.cuny.edu/lwu/3000/SGJch6.ppt (accessed 3.2.16).

Wu, S., Eames, I.W., 2000. Innovations in vapour-absorption cycles. Applied Energy. doi:10.1016/S0306-2619(99)00128-2

Yang, F., Meng, X., Deng, J., Wang, Y., Zhang, Z., 2009. Identifying heat and mass transfer characteristics of metal hydride reactor during adsorption: Improved formulation about

parameter analysis. International Journal of Hydrogen Energy 34, 1852–1861.

Yong, L., Sumathy, K., 2002. Review of mathematical investigation on the closed adsorption heat pump and cooling systems. Jourlnal Renewable and Sustainable Energy Reviews 6, 305–337.

Yu, N., Wang, R.Z., Lu, Z.S., Wang, L.W., 2014. Development and characterization of silica gel-LiCl composite sorbents for thermal energy storage. Chemical Engineering Science 111, 73–84.

Yu, N., Wang, R.Z., Wang, L.W., 2013. Sorption thermal storage for solar energy. Progress in Energy and Combustion Science 39, 489–514.

Yukitaka, K., 2007. Chemical energy conversion technologies for efficient energy use, in: Paksoy H, Thermal Energy Storage for Sustainable Energy Consumption. Springer.

Zajaczkowski, B., Królicki, Z., Jeżowski, A., 2010. New type of sorption composite for chemical heat pump and refrigeration systems. Applied Thermal Engineering 30, 1455–1460.

Zettl, B., Englmair, G., Somitsch, W., 2015. An Open Sorption Heat Storage Concept and Materials for Building Heat Supply. Energy Procedia 73, 297–304.

Zhang, G., Wang, D.C., Zhang, J.P., Han, Y.P., Sun, W., 2011. Simulation of operating characteristics of the silica gel–water adsorption chiller powered by solar energy. Journal of Solar Energy 85, 1469–1478.

Zhang, Y., Lin, K., Jiang, Y., Zhou, G., 2008. Thermal storage and nonlinear heat-transfer characteristics of PCM wallboard. Energy and Buildings 40, 1771–1779.

Zheng, X., Wang, L.W., Wang, R.Z., Ge, T.S., Ishugah, T.F., 2014. Thermal conductivity, pore structure and adsorption performance of compact composite silica gel. International Journal of Heat and Mass Transfer 68, 435–443.

Zhong, Y., 2006. Studies on equilibrium and dynamic characteristics of new adsorption pairs. PhD Thesis. University Of Warwick.

Zhu, D., Wu, H., Wang, S., 2006. Experimental study on composite silica gel supported CaCl2 sorbent for low grade heat storage. International Journal of Thermal Sciences 45, 804–813.

Ziegler, F., Grossman, G., 1996. Heat-transfer enhancement by additives 19, 301–309.

Zilio, C., Brown, J.S., Schiochet, G., Cavallini, A., 2011. The refrigerant R1234yf in air conditioning systems. Journal of Energy 36, 6110–6120.

Zondag, H., Kikkert, B., Smeding, S., Boer, R. de, Bakker, M., 2013. Prototype thermochemical heat storage with open reactor system. Applied Energy 109, 360–365.

APPENDICES

AI: Photographs of experimental apparatus

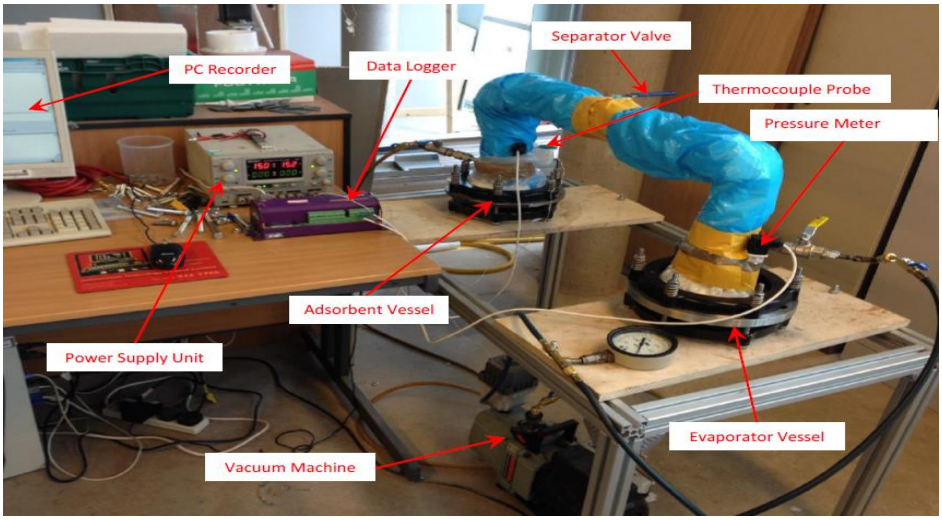


Figure A-1: A photo is showing a Horizontal Metal and Glass Rig for the adsorption test.

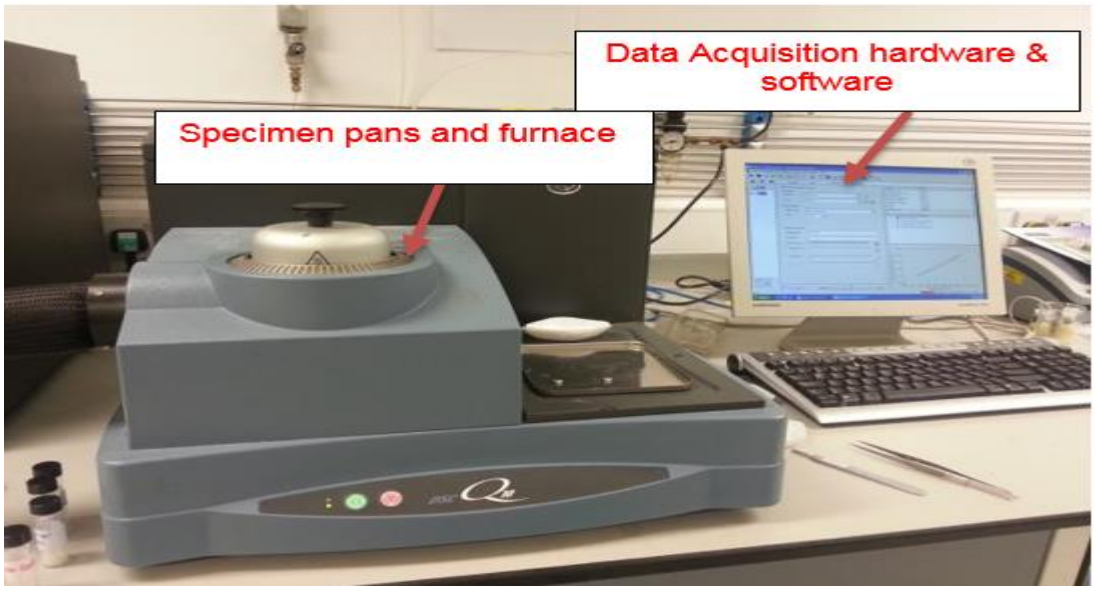


Figure A-2: Differential Scanning Calorimeter (DSC TA Q10) for measurement of specific heat of the specimen

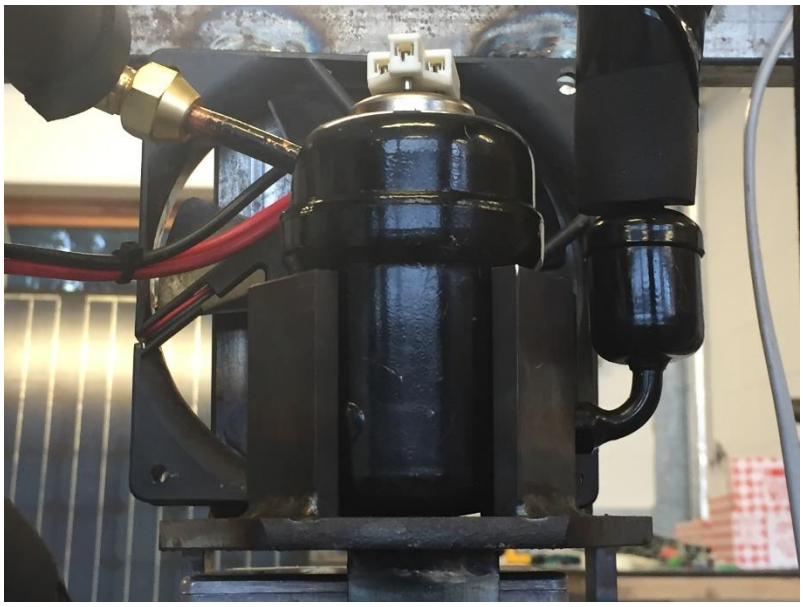


Figure A-3: Greatcool Miniature Compressor

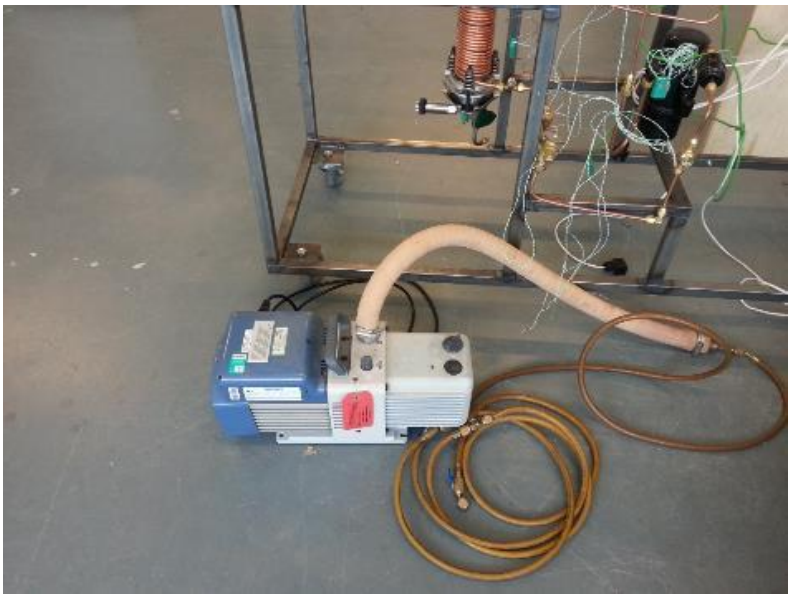


Figure A-4: Vacuum Pump used in Chapter 6



Figure A-5: Data Taker DT500 used in Chapter 6

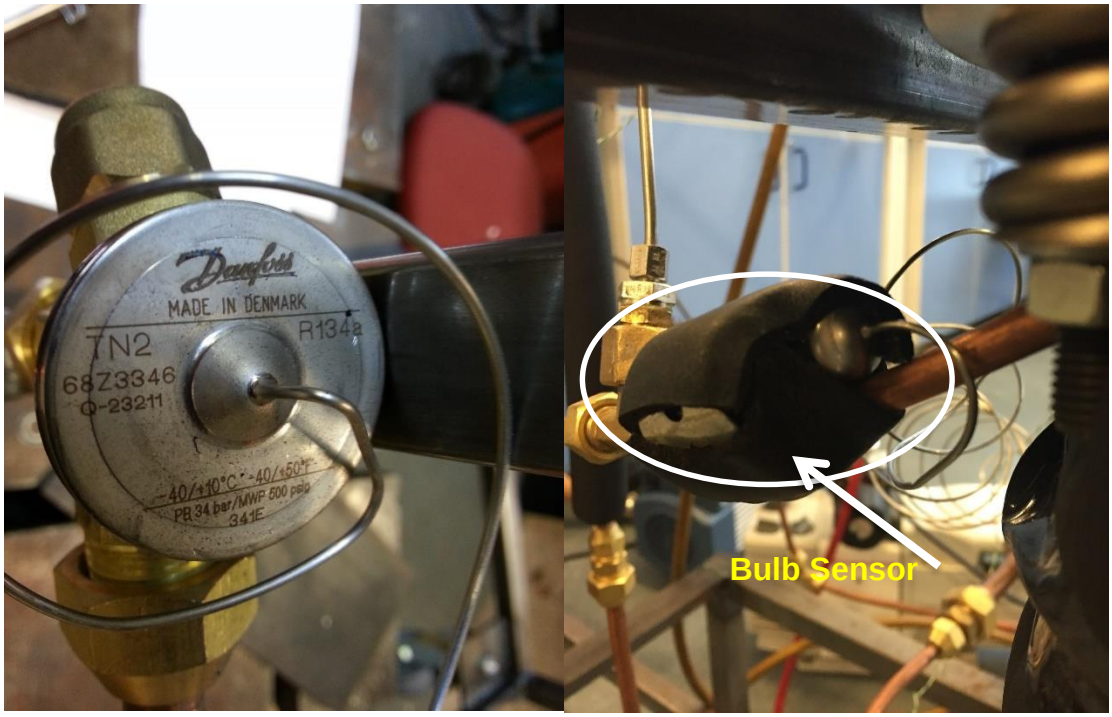


Figure A-6: Thermostatic Expansion Valve (left) with bulb temperature sensor (right)



Figure A-7: Refrigerant receiver, AIRMENDER, capacity of 1.5 litres



Figure A-8: Liquid Line Filter Drier



Figure A-9: Sight Glass

Appendix B: Calculation on Sample volume (MIP) for Chapter 3

Penetrometer + sample (g) = 60.8605

Sample (g) =0.3832

Penetrometer +sample +Hg (g) = 139.9389

Mass of mercury = 139.9389 g-60.8605 g=79.0784g

Hence = $V = m/\rho$ = 79.0784/13.8340=5.8429 mL

Bulk sample volume = 6.6259g-5.8429g=0.783mL

Bulk density = bulk mass/bulk volume = 0.3832/0.783=0.489g/cc

Appendix C: Compressor Specifications for Chapter 6

1. Specification

1.1 Basic parameters

Compressor Type	Hermetic rotary compressor motor
Use refrigerant	R134a
Lubricating oil • Oil amount (ml)	POE 68 • 40ml
The total mass (including oil)	700g
Excluded volume	1.9cm³/rev
Motor Type	Brushless DC Motor
Speed range	1800-6000rpm
Voltage	DC 24V
Current Range	Max 12A

1.2 Performance

Category	Test conditions for air conditioning			
	3000rpm	3600rpm	4500rpm	5100rpm
Refrigerating capacity (W)	245	305	375	425
The input power (W)	85	100	120	135
COP (W/W)	2.90	3.05	3.10	3.15

Appendix D: Specification of Rotary Vane Vacuum Pumps (Source: http://www.coleparmer.co.uk) for Chapter 6

Specifications	
Free air capacity	6.1 (173) cfm (L/min)
Max vacuum	1 x 10^{-4} (1.3 x 10^{-4}) Torr (mbar)
Dimensions	19 3/8"L x 6 ½"W x 9 ¾"H
Power (VAC/Hz)	115/230 (50/60)
Hp	0.5
Brand	Cole-Palmer
Product Type	Rotary Vane Vacuum Pumps

Appendix E: 3kW Heat Pump Specification (Kensa Heat Pump, 2015) for Chapter 6

Phase	**Single**
Nominal thermal kW rating	3
Power consumption	0.8kW
Co-efficient of Performance*	4.15
Max flow temperature °C	65
Electrical values at B0/W35	
Rated voltage	220 - 240V / 50 - 60 Hz
Power supply rating amps	13
Rated current (max) amps	7
Typical running currently at B0/W35 amps	4
Starting current amps	30
Acoustic performance	47dBA
Refrigerant circuit	
Process medium	R134a
Fill volume kg	0.7
Compressor type	Reciprocal
Dimensions	
H X W X L (mm)	530 x 475 x 370
Nominal weight kg	60

Appendix F: Economic and Environmental Analysis

Table F-1: Estimate of THSS running cost and NPV

THSS (HEAT PUMP) Note: THSS electric consumption when running = 3.0 kw (3 Kw heat pump)

Assumptions:

1. Operating cost growth= 3%
2. Initial (O&M) cost= 300
3. All currency in British pound
4. The heat pump run for the desorption at night time

Month	Jan	Feb	Mar	Apr	May	Jun	Jul	Aug	Sep	Oct	Nov	Dec		
	1	1	1	1	1	1	1	1	1	1	1	1		
Days	31	28	31	30	31	30	31	31	30	31	30	31		
Hours per day	7	7	7	7	7	7	7	7	7	7	7	7	Total	
Resultant hours	217	196	217	210	217	210	217	217	210	217	210	217	2555	
kWh	651	588	651	630	651	630	651	651	630	651	630	651	7,665	
Tonnes Co^2-e	303.996	303.996	336.567	325.710	336.567	325.710	336.567	336.567	325.710	336.567	325.710	336.567	3,930.2	Emitted
£/kwh (2015)(night)	£0.07	£0.07	£0.07	£0.07	£0.07	£0.07	£0.07	£0.07	£0.07	£0.07	£0.07	£0.07		
Electricity Spend	£46.35	£41.87	£46.35	£44.86	£46.35	£44.86	£46.35	£46.35	£44.86	£46.35	£44.86	£46.35	£545.75	

Year	2015	2016	2017	2018	2019	2020	2021	2022	2023	2024	2025	2026	2027	2028	2029	2030	2031	2032	2033	2034	2035
Capital cost (£)	(5,217.00)	-	-	-	-	-	-	-	-	-	-	-	-	-	-	-	-	-	-	-	-
O&M cost(£)	-	-£300	-£309	-£318	-£328	-£338	-£348	-£358	-£369	-£380	-£391	-£403	-£415	-£428	-£441	-£454	-£467	-£481	-£496	-£511	-£526
Electricity spend	-£546	-£584	-£625	-£669	-£715	-£765	-£819	-£876	-£938	-£1,003	-£1,074	-£1,149	-£1,229	-£1,315	-£1,407	-£1,506	-£1,611	-£1,724	-£1,845	-£1,974	-£2,112
Total spend	-£5,763	-£884	-£934	-£987	-£1,043	-£1,103	-£1,167	-£1,235	-£1,307	-£1,383	-£1,465	-£1,552	-£1,644	-£1,743	-£1,848	-£1,960	-£2,079	-£2,205	-£2,340	-£2,484	-£2,638

Present Value using The SPPWF (Single Payment Present Worth Factor) Method

Year	2015	2016	2017	2018	2019	2020	2021	2022	2023	2024	2025	2026	2027	2028	2029	2030	2031	2032	2033	2034	2035	
(n) Year	0	1	2	3	4	5	6	7	8	9	10	11	12	13	14	15	16	17	18	19	20	
Discount Rate (=*i*)	15%	15%	15%	15%	15%	15%	15%	15%	15%	15%	15%	15%	15%	15%	15%	15%	15%	15%	15%	15%	15%	
(P/F,i%,n)	1	0.868	0.753	0.653	0.567	0.492	0.427	0.370	0.321	0.279	0.242	0.210	0.182	0.158	0.137	0.119	0.103	0.090	0.078	0.067	0.059	
Future Value in £	-£5,763	-$883.95	-$933.83	-$986.83	-$1,043.18	-$1,103.09	-$1,166.80	-$1,306.66	-$1,306.66	-$1,383.37	-$1,465.00	-$1,551.89	-$1,644.40	-$1,742.90	-$1,847.79	-$1,959.51	-$2,078.53	-$2,205.33	-$2,340.45	-$2,484.44	-$2,637.92	NPV in 20 years
Present value in £	-$5,762.75	-$767.02	-$703.11	-$644.73	-$591.39	-$542.63	-$498.04	-$483.96	-$419.94	-$385.78	-$354.50	-$325.85	-$299.60	-$275.54	-$253.48	-$233.25	-$214.69	-$197.65	-$182.01	-$167.65	-$154.46	**-$13,458.02**

Table F-2: Estimate of THSS saving cost and NPV

THSS (BOILER GAS SAVING)

heating demand **24** kW

Assumptions:

Winter : 3 hour peak + 5 hours off peak

Summer : 3 hours peak +3 hours off peak

	JAN	FEB	MAR	APR	MAY	JUN	JUL	AUG	SEP	OCT	NOV	DEC	
Total days	31	28	31	30	31	30	31	31	30	31	30	31	
Peak hours	93	84	93	90	93	90	93	93	90	93	90	93	
Off Peak hours	155	140	155	150	93	90	93	93	90	155	150	155	
Total hours	279	252	248	240	186	180	186	186	180	248	270	279	**2,734**
kWh generated peak	2,232	2,016	2,232	2,160	2,232	2,160	2,232	2,232	2,160	2,232	2,160	2,232	
kWh generated off peak	3,720	3,360	3,720	3,600	2,232	2,160	2,232	2,232	2,160	3,720	3,600	3,720	
Total kWh generated	5952	5376	5952	5760	4464	4320	4464	4464	4320	5952	5760	5952	62736
p/kWh (2015) -	4.64	4.64	4.64	4.64	4.64	4.64	4.64	4.64	4.64	4.64	4.64	4.64	Total
Total Gas Saved	**£103.56**	**£93.54**	**£103.56**	**£100.22**	**£103.56**	**£100.22**	**£103.56**	**£103.56**	**£100.22**	**£103.56**	**£100.22**	**£103.56**	**£1,219.39**

Year	2015	2016	2017	2018	2019	2020	2021	2022	2023	2024	2025	2026	2027	2028	2029	2030	2031	2032	2033	2034	2035	
																						Total gas saved in 20 years
gas saved	£1,219.39	£1,304.75	£1,396.08	£1,493.81	£1,598.37	£1,710.26	£1,829.98	£1,958.08	£2,095.14	£2,241.80	£2,398.73	£2,566.64	£2,746.30	£2,938.55	£3,144.24	£3,364.34	£3,599.84	£3,851.83	£4,121.46	£4,409.96	£4,718.66	$54,708.24

Present Value using The SPPWF (Single Payment Present Worth Factor) Method

Year	2014	2015	2016	2017	2018	2019	2020	2021	2022	2023	2024	2025	2026	2027	2028	2029	2030	2031	2032	2033	2034	
(n) Year	0	1	2	3	4	5	6	7	8	9	10	11	12	13	14	15	16	17	18	19	20	
Discount Rate (=i)	15.25%	15.25%	15.25%	15.25%	15.25%	15.25%	15.25%	15.25%	15.25%	15.25%	15.25%	15.25%	15.25%	15.25%	15.25%	15.25%	15.25%	15.25%	15.25%	15.25%	15.25%	
(P/F,i%,n)	1	0.868	0.753	0.653	0.567	0.492	0.427	0.370	0.321	0.279	0.242	0.210	0.182	0.158	0.137	0.119	0.103	0.090	0.078	0.067	0.059	
Future Value in £	£1,219.39	£1,304.75	£1,396.08	£1,493.81	£1,598.37	£1,710.26	£1,829.98	£1,958.08	£2,095.14	£2,241.80	£2,398.73	£2,566.64	£2,746.30	£2,938.55	£3,144.24	£3,364.34	£3,599.84	£3,851.83	£4,121.46	£4,409.96	£4,718.66	**NPV in 20 years**
Present value in £	£1,219.39	£1,132.15	£1,051.15	£975.95	£906.13	£841.30	£781.11	£725.23	£673.34	£625.17	£580.44	£538.92	£500.36	£464.56	£431.33	£400.47	£371.82	£345.22	£320.52	£297.59	£276.30	£13,458.46